To the Graduate Council:

I am submitting herewith a thesis written by Jeora Melik-Baghdassarians-Fard entitled "Evaluation of Multivariate Autoregressive Time Series Models and their Application to Reactor Noise Analysis." I recommend that it be accepted in partial fulfillment of the requirements for a Master of Science, with a major in Nuclear Engineering.

T. W. Kerlin, Major Professor

We have read this thesis
and recommend its acceptance:

Accepted for the Council:

Vice Chancellor
Graduate Studies and Research

EVALUATION OF MULTIVARIATE AUTOREGRESSIVE TIME SERIES MODELS AND THEIR APPLICATION TO REACTOR NOISE ANALYSIS

A Thesis

Presented for the

Master of Science

Degree

The University of Tennessee, Knoxville

Jeora Melik-Baghdassarians-Fard

August 1980

3044851

ACKNOWLEDGEMENTS

The author expresses deep appreciation to Dr. T. W. Kerlin and Dr. B. R. Upadhyaya who served as advisors through the research; their guidance, interest and encouragement is genuinely appreciated.

I would like to thank Dr. P. F. Pasqua for making available the educational opportunity in the form of a research assistantship and Dr. M. Kitamura who provided helpful comments throughout this research.

I would like also to thank Mrs. Sara Hansen for patiently typing the draft and final copy of this thesis.

ABSTRACT

The multivariate autoregressive (MAR) time series model is investigated to determine its usefulness for representing continuous random signals. This is achieved by determining the best criterion of fit, an estimate of the total number of sample points of signals and the choice of sampling interval. Furthermore, the MAR model procedures are employed to investigate the effect of nonstationarity of the data. The autoregressive (AR) time series model is statistically evaluated to compare the error in the AR spectrum with the error estimates of Fourier transform (FFT) method. Moreover, the error in the AR spectrum is calculated using an empirical procedure. Finally, the MAR model procedures are used as a diagnostic tool to derive cause-effect relationship among process variables from the St. Lucie nuclear power plant.

It is determined that the MAR model can adequately represent noisy continuous signals including periodic processes. Proper analysis must be carried out for signals with wide dynamic ranges.

TABLE OF CONTENTS

CHAPTER		PAGE
1.	INTRODUCTION	1
	Purpose of this Work	1
	Prior Related Work	1
	Scope of the Study	2
	Organization of the Thesis	3
2.	THEORETICAL CONSIDERATIONS OF THE DISCRETE FOURIER TRANSFORM	5
	Sampling Theorem	5
	Discrete Fourier Transform	6
	Power Spectrum	7
	Frequency Response	8
	Coherence Function	9
3.	RANDOM PROCESS REPRESENTATION USING TIME SERIES MODELS	10
	Time Series Models	10
4.	THEORETICAL CONSIDERATIONS OF TIME SERIES MODELS	13
	Multivariate Autoregressive Model	13
	Parameter Estimation	14
	Equivalence of Yule-Walker Equations and the Least-Squares Method	17
	Estimation of Noise Covariance Matrix	18
	Model Order Determination	19
	Power Spectral Matrix	21
	Closed Loop Input-Output Relationship	24
	Open Loop Input-Output Relationship	25
	Signal Contribution Ratio	25
	Relationship Between Coherence Function and the Signal Contribution Ratios	26
5.	VALIDATION OF DECOMPOSITION	29
6.	DETERMINATION OF ERROR IN THE POWER SPECTRUM	32
	Error Evaluation of FFT Power Spectrum	32
	Error Evaluation of the AR Spectrum	32
7.	APPLICATION OF EMPIRICAL MODELING TO REACTOR NOISE ANALYSIS	36

CHAPTER PAGE

Introduction 36
Correlation Analysis 37
Fast Fourier Transform Analysis. 38
MAR Modeling of PWR Noise Signals 39
Summary of the Results of MAR Modeling 51

8. UNCERTAINTY IN THE AR AUTOPOWER SPECTRUM. 53

Comparison of Error in the AR Power Spectrum with that of FFT. 53
Empirical Investigation of the AR Models. 56

9. DIAGNOSTIC ANALYSIS. 65

Introduction 65
Cause-Effect Relation at 4.5×10^{-2} Hertz 65

10. CONCLUSIONS AND RECOMMENDATIONS. 68

Summary and Conclusions 68
Recommendations 69

LIST OF REFERENCES 70

APPENDICES 73

APPENDIX A. DESCRIPTION OF THE ALGORITHMS EMPLOYED FOR THE EMPIRICAL EVALUATION OF THE AR MODELS . . . 74

APPENDIX B. DESCRIPTION OF ALGORITHMS EMPLOYED FOR MAR MODELING 76

APPENDIX C. DESCRIPTION OF THE ALGORITHM FOR CORRELATION ANALYSIS 79

APPENDIX D. DEFINITION OF STATIONARITY 81

APPENDIX E. LIST OF FIGURES 83

VITA 233

LIST OF TABLES

TABLE		PAGE
1.	Comparison of Optimal Orders Predicted by AIC and BPC for Two and Four Variables (m)	40
2.	Comparison of the Actual Variance Reduction Ratios with the Preselected Theoretical One	43
3.	Comparison of the Model Parameters A_{21}, A_{31} Relating Primary Pressure to Feed Flow and Cold Leg Temperature for Cases 1 and 2.	47
4.	Noise Covariance Matrices Eigenvalues and Eigenvectors for Various Pairs of Signals	50
5.	Comparison of the Calculated and the Determined Standard Deviation for a Second Order AR Model . . .	57
6.	Frequency of Occurrence of Optimal Orders of Case (1) .	59
7.	Frequency of Occurrence of Optimal Orders of Case (2) .	60
8.	Frequency of Occurrence of Optimal Orders of Case (3) .	61
9.	Frequency of Occurrence of Optimal Orders of Case (4) .	62
10.	Frequency of Occurrence of Optimal Orders of Case (5) .	64

LIST OF FIGURES

FIGURE		PAGE
1.	Closed Loop Input-Output Relation for Four Variables.	84
2.	Closed Loop Block Diagram for Two Variables.	85
3.	Open Loop Input-Output Block Diagram	85
4.	Autocorrelation of Primary Pressure (A)	86
5.	Autocorrelation of Primary Pressure (B)	87
6.	Autocorrelation of Primary Pressure (C)	88
7.	Autocorrelation of Cold Leg Temperature	89
8.	Autocorrelation of Feed Water Flow Rate	90
9.	Autocorrelation of Power	91
10.	Cross-Correlation of Primary Pressure Versus Cold Leg Temperature	92
11.	Cross-Correlation of Primary Pressure Versus Power	93
12.	Cross-Correlation of Primary Pressure Versus Feed Water Flow Rate	94
13.	Cross-Correlation of Cold Leg Temperature Versus Feed Water Flow Rate.	95
14.	Power Spectrum of Primary Pressure (FFT).	96
15.	Power Spectrum of Cold Leg Temperature (FFT)	97
16.	Power Spectrum of Feed Water Flow Rate (FFT)	98
17.	Power Spectrum of Power (FFT)	99
18.	Coherence of Cold Leg Temperature Versus Primary Pressure (FFT).	100
19.	Coherence of Feed Water Flow Rate Versus Primary Pressure (FFT).	101
20.	Coherence of Power Versus Primary Pressure (FFT)	102

FIGURE PAGE

21. Coherence of Cold Leg Temperature Versus Feed Water Flow Rate (FFT) 103

22. Coherence of Power Versus Cold Leg Temperature (FFT) . . . 104

23. Coherence of Power Versus Feed Water Flow Rate (FFT) . . . 105

24. Plot of $N\alpha$ Versus N (A) 106

25. Plot of $N\alpha$ Versus N (B) 107

26. Predicted Optimal Order for Four Variables ($\Delta t=3$) 108

27. Predicted Optimal Order for Three Variables 109

28. Predicted Optimal Order for Two Variables 110

29. Predicted Optimal Order for Four Variables ($\Delta t=2$) 111

30. Power Spectrum of Primary Pressure (Case 1) 112

31. Power Spectrum of Cold Leg Temperature (Case 1) 113

32. Power Spectrum of Feed Water Flow Rate (Case 1) 114

33. Power Spectrum of Power (Case 1) 115

34. Power Spectrum of Primary Pressure (Case 2) 116

35. Power Spectrum of Cold Leg Temperature (Case 2) 117

36. Power Spectrum of Feed Water Flow Rate (Case 2) 118

37. Power Spectrum of Power (Case 2) 119

38. Signal Contribution Ratio from Source One to Cold Leg Temperature (Case 1) 120

39. Signal Contribution Ratio from Source One to Feed Water Flow Rate (Case 1) 121

40. Signal Contribution Ratio from Source Two to Cold Leg Temperature (Case 1) 122

41. Signal Contribution Ratio from Source Three to Feed Water Flow Rate (Case 1) 123

42. Coherence of Primary Pressure Versus Cold Leg Temperature (Case 1) 124

FIGURE PAGE

43. Coherence of Primary Pressure Versus Feed Water Flow Rate (Case 1) 125

44. Signal Contribution Ratio from Source One to Cold Leg Temperature (Case 2) 126

45. Signal Contribution Ratio from Source One to Feed Water Flow Rate (Case 2) 127

46. Signal Contribution Ratio from Source Three to Feed Water Flow Rate (Case 2) 128

47. Signal Contribution Ratio from Source Two to Cold Leg Temperature (Case 2) 129

48. Coherence of Primary Pressure Versus Cold Leg Temperature (Case 2) 130

49. Coherence of Primary Pressure Versus Feed Water Flow Rate (Case 2) 131

50. Signal Contribution Ratio from Source One to Primary Pressure (A) 132

51. Signal Contribution Ratio from Source Two to Cold Leg Temperature (A) 133

52. Signal Contribution Ratio from Source One to Cold Leg Temperature 134

53. Power Spectrum Component of Cold Leg Temperature from Source One 135

54. Power Spectrum Component of Primary Pressure from Source Two. 136

55. Signal Contribution Ratio from Source Two to Primary Pressure. 137

56. Signal Contribution Ratio from Source One to Primary Pressure (B) 138

57. Signal Contribution Ratio from Source Three to Primary Pressure. 139

58. Power Sectrum Component of Primary Pressure from Source Three 140

59. Signal Contribution Ratio from Source One to Feed Water Flow Rate 141

FIGURE PAGE

60. Power Spectrum Component of Feed Water Flow Rate from Source One 142

61. Signal Contribution Ratio from Source Three to Feed Water Flow Rate (A) 143

62. Signal Contribution Ratio from Source One to Primary Pressure (C) 144

63. Signal Contribution Ratio from Source Four to Primary Pressure. 145

64. Power Spectrum Component of Primary Pressure from Source Four. 146

65. Signal Contribution Ratio from Source One to Power 147

66. Power Spectrum Component of Power from Source One 148

67. Signal Contribution Ratio from Source Four to Power (A) 149

68. Signal Contribution Ratio from Source Three to Feed Water Flow Rate (B) 150

69. Signal Contribution Ratio from Source Two to Cold Leg Temperature (B). 151

70. Power Spectrum Component of Feed Water Flow Rate from Source Two 152

71. Power Spectrum Component of Cold Leg Temperature from Source Three 153

72. Signal Contribution Ratio from Source Two to Feed Water Flow Rate 154

73. Signal Contribution Ratio from Source Three to Cold Leg Temperature 155

74. Signal Contribution Ratio from Source Two to Cold Leg Temperature (C) 156

75. Power Spectrum Component of Power from Source Two 157

76. Signal Contribution Ratio from Source Four to Cold Leg Temperature 158

77. Signal Contribution Ratio from Source Two to Power 159

FIGURE PAGE

78. Power Spectrum Component of Cold Leg Temperature from Source Four 160

79. Signal Contribution Ratio from Source Four to Power (B) 161

80. Power Spectrum of Primary Pressure (MAR). 162

81. Power Spectrum of Cold Leg Temperature (MAR) 163

82. Power Spectrum of Feed Water Flow Rate (MAR) 164

83. Power Spectrum of Power (MAR) 165

84. Coherence of Primary Pressure Versus Cold Leg Temperature (MAR). 166

85. Coherence of Primary Pressure Versus Feed Water Flow Rate (MAR) 167

86. Coherence of Primary Pressure Versus Power (MAR) 168

87. Coherence of Cold Leg Temperature Versus Feed Water Flow Rate (MAR) 169

88. Coherence of Cold Leg Temperature Versus Power (MAR). 170

89. Coherence of Feed Water Flow Rate Versus Power (MAR). 171

90. Normalized Power Spectrum of Primary Pressure (FFT) 172

91. Normalized Power Spectrum of Primary Pressure (AR) 173

92. Error Spectrum of Primary Pressure (FFT). 174

93. Error Spectrum of Primary Pressure (AR) 175

94. Power Spectrum of Primary Pressure (Order 2) 176

95. Normalized Power Spectrum of Primary Pressure (Order 2). . . . 177

96. Error Spectrum of Primary Pressure (Order 2) 178

97. Average Power Spectrum of Case (1) for Order 9. 179

98. Average Power Spectrum of Case (2) for Order 9. 180

99. Normalized Standard Deviation of Power Spectrum of Case (1) for Order 9. 181

FIGURE PAGE

100. Normalized Standard Deviation of Power Spectrum of Case (2) for Order 9. 182

101. Average Power Spectrum of Case (3) for Order 9. 183

102. Average Power Spectrum of Case (4) for Order 9. 184

103. Normalized Standard Deviation of Power Spectrum of Case (3) for Order 9. 185

104. Normalized Standard Deivation of Power Spectrum of Case (4) for Order 9. 186

105. Average Power Spectrum of Case (5) for Order 9. 187

106. Normalized Standard Deviation of Power Spectrum of Case (5) for Order 9. 188

107. Average Power Spectrum of Case (1) for Order 2. 189

108. Average Power Spectrum of Case (1) for Order 4. 190

109. Normalized Standard Deviation of Power Spectrum of Case (1) for Order 2. 191

110. Normalized Standard Deviation of Power Spectrum of Case (1) for Order 4. 192

111. Average Power Spectrum of Case (1) for Order 15 193

112. Normalized Standard Deviation of Power Spectrum of Case (1) for Order 15 194

113. Signal Contribution Ratio from Source One to Primary Pressure (Order 23) 195

114. Signal Contribution Ratio from Source Two to Primary Pressure (Order 23) 196

115. Signal Contribution Ratio from Source Three to Primary Pressure (Order 23) 197

116. Signal Contribution Ratio from Source Four to Primary Pressure (Order 23) 198

117. Signal Contribution Ratio from Source One to Cold Leg Temperature (Order 23) 199

118. Signal Contribution Ratio from Source Two to Cold Leg Temperature (Order 23) 200

FIGURE PAGE

119. Signal Contribution Ratio from Source Three to Cold Leg Temperature (Order 23) 201

120. Signal Contribution Ratio from Source Four to Cold Leg Temperature (Order 23) 202

121. Signal Contribution Ratio from Source One to Feed Water Flow Rate (Order 23) 203

122. Signal Contribution Ratio from Source Two to Feed Water Flow Rate (Order 23) 204

123. Signal Contribution Ratio from Source Three to Feed Water Flow Rate (Order 23). 205

124. Signal Contribution Ratio from Source Four to Feed Water Flow Rate (Order 23). 206

125. Signal Contribution Ratio from Source One to Power (Order 23) 207

126. Signal Contribution Ratio from Source Two to Power (Order 23) 208

127. Signal Contribution Ratio from Source Three to Power (Order 23) 209

128. Signal Contribution Ratio from Source Four to Power (Order 23) 210

129. Closed Loop Input-Output Relation 211

130. Open Loop Frequency Response of Primary Pressure Versus Cold Leg Temperature. 213

131. Open Loop Frequency Response of Cold Leg Temperature Versus Primary Pressure. 214

132. Phase Relation of Primary Pressure Versus Cold Leg Temperature. 215

133. Open Loop Frequency Response of Primary Pressure Versus Feed Water Flow Rate 216

134. Open Loop Frequency Response of Feed Water Flow Rate Versus Primary Pressure. 217

135. Phase Relation of Primary Pressure Versus Feed Water Flow Rate 218

FIGURE PAGE

136. Open Loop Frequency Response of Primary Pressure Versus Power 219

137. Open Loop Frequency Response of Power Versus Primary Pressure 220

138. Phase Relation of Primary Pressure Versus Power. 221

139. Open Loop Frequency Response of Cold Leg Temperature Versus Feed Water Flow Rate. 222

140. Open Loop Frequency Response of Feed Water Flow Rate Versus Cold Leg Temperature. 223

141. Phase Relation of Cold Leg Temperature Versus Feed Water Flow Rate. 224

142. Open Loop Frequency Response of Cold Leg Temperature Versus Power 225

143. Open Loop Frequency Response of Power Versus Cold Leg Temperature 226

144. Phase Relation of Cold Leg Temperature Versus Power 227

145. Open Loop Frequency Response of Feed Water Flow Rate Versus Power 228

146. Open Loop Frequency Response of Power Versus Feed Water Flow Rate. 229

147. Phase Relation of Feed Water Flow Rate Versus Power 230

148. Frequency Response of Feed Water Flow Rate Due to 10% Increase in Inlet Temperature 231

149. Power Spectrum of Feed Water Flow Rate (Order 23) 232

CHAPTER 1

INTRODUCTION

1.1 Purpose of this Work

The research presented in this thesis is a combination of experimental and theoretical investigation of the multivariate autoregressive (MAR) time series models. Included are demonstrations using St. Lucie pressurized water reactor (PWR) power plant data. The objectives of the investigation are: (1) determination of the best criterion of fit, (2) determination of an estimate of the total number of sample points, (3) determination of the sampling interval, (4) investigation of the effect of nonstationarity of data, (5) verification of the assumption of mutual independence of the driving forces, (6) comparison of the MAR model autopower spectra with those of fast Fourier transform, (7) statistical and empirical evaluation of the autoregressive (AR) time series model, (8) diagnostic analysis of the St. Lucie PWR power plant data.

1.2 Prior Related Work

The multivariate autoregressive time series models for random data representation have been investigated and applied as a diagnostic tool to study the dynamics of boiling water reactors (8-10). The special case of the MAR models, univariate autoregressive models have also been investigated and found useful for determining the resistance temperature detectors time constants (11, 21). The AR models have been a subject of detailed statistical evaluation including investigation of the

effects of parameters such as sampling interval and the total data record length on the AR models (22). There is a need to perform more comprehensive investigation of the parameters affecting the MAR procedures or to investigate the effect of nonstationarity of the data on the procedures. Numerous publications of theoretical developments related to the MAR model procedures will be referenced at appropriate places in the thesis.

1.3 Scope of the Study

An important problem in parametric model fitting of time series is the determination of the optimal model. An observational comparison is made between Akaike's information criterion (AIC) and Bayes' probability criterion (BPC) to determine the better of the two for optimal model prediction. The mathematical definition of the AIC is used in a theoretical study to determine an estimate of the total number of sample points for a given number of variables (m) and a desired theoretical variance reduction (α). An empirical relation referred to as the condition of optimality is derived using the dynamic range of variables determined from cross-correlation analysis. The condition furnishes information concerning: (1) choice of sampling interval, (2) efficient model, (3) sufficiency of the desired theoretical variance reduction ratio. The effect of nonstationarity of data is investigated by applying the MAR model procedures both to stationary and nonstationary portions of data. The results are compared and differences discussed. The decomposition of the power spectral density is achieved by assuming that the noise covariance matrix Q is diagonal. The validity of the decomposition is checked by replacing Q with an exact diagonal matrix

obtained from an orthogonal transformation. The resulting exact decomposition is then compared with that obtained from the assumption of diagonality of Q. The MAR model autopower spectra are compared with those obtained from the FFT to reemphasize the usefulness of the model in representing actual plant data. The AR model is statistically evaluated by determining the uncertainty in the AR model power spectrum and comparing to that obtained by the FFT. This is done to show that the error in the AR spectrum is smaller than that of FFT for a given period of data. The empirical error analysis is carried out by determining the average power spectrum from the power spectra of a number of cases (equal data points) and then evaluating the error.

Finally, the MAR model procedures are used as a diagnostic tool to derive cause-effect relations for the St. Lucie power plant data.

1.4 Organization of the Thesis

Chapter 2 introduces a brief account of theoretical aspects of the discrete Fourier transform (DFT). Chapter 3 is devoted to the discussion of different forms of time series models. Chapter 4 contains the mathematical and theoretical developments of the MAR model procedures. Chapter 5 introduces the mathematical developments of an orthogonal transformation. Chapter 6 presents the mathematical aspects of the error evaluation in FFT power spectra and in the AR model power spectrum. Chapter 7 is the applications chapter. It is divided into three major sections following the introduction dealing with: (1) correlation analysis, (2) FFT analysis, (3) MAR modeling of PWR noise signals. Section three is divided into six subsections dealing with: (1) comparison of AIC and BPC, (2) estimate of sample size, (3) bound on order, (4) effect of nonstationarity of data, (5) the MAR model

validation, (6) comparison of MAR model spectra with those of FFT. Chapter 8 presents the results of the error evaluation for FFT and AR model power spectra. Chapter 9 contains the diagnostic analysis of St. Lucie PWR noise data. Chapter 10 contains the conclusions which can be reached from this research and recommendations for future related work.

CHAPTER 2

THEORETICAL CONSIDERATIONS OF THE DISCRETE FOURIER TRANSFORM

The calculation of Fourier transforms on a digital computer requires the numerical evaluation of Fourier integrals. Any method for approximating the integrals using data obtained at discrete points is called (1) a discrete Fourier transform (DFT). This chapter introduces a brief account of the theoretical aspects of the DFT.

2.1 Sampling Theorem

If the maximum frequency content of a continuous signal is F_{max}, then the sampling frequency F_s must be such that $F_s \geq 2F_{max}$. This is necessary to obtain proper representation of the original signal. If Δt is the sampling interval then, $F_{max} \leq \frac{1}{2\Delta t}$ where

$$F_N = \frac{1}{2\Delta t} , \tag{2.1}$$

is defined as the Nyquist frequency (1). If an input signal is sampled for a time period of T, with a sampling interval of Δt, then the number of sample points is given (1) by

$$N = \frac{T}{\Delta t} , \tag{2.2}$$

where T is referred (2) to as the "time window." Substituting Equation (2.2) into Equation (2.1) yields

$$F_N = \frac{N}{2}\frac{1}{T} = \frac{N}{2}\ \Delta f \tag{2.3}$$

where Δf is the separation of harmonic frequencies in the frequency

domain and N is the number of data points representing the sampled signal. If F_N is the maximum frequency present in the input signal, then the Fourier transform of these $\frac{N}{2}$ frequencies gives a complete spectral representation (1) of the signal. Combining Equations (2.1), (2.2) and (2.3) one obtains the following relations:

$$\Delta f = \frac{1}{N \cdot \Delta t} = \frac{1}{T} \quad . \tag{2.4}$$

By definition (1)

$$\text{sampling rate} = SR = \frac{1}{\Delta t} \text{ (samples per unit time)},$$

thus

$$\Delta f = \frac{SR}{N} \ . \tag{2.5}$$

2.2 Discrete Fourier Transform

The continuous Fourier coefficient X'(f) of a periodic function X(t) is defined (1) by

$$X'(f) = \frac{1}{T} \int_0^T X(t)\, e^{-2\pi i f t} dt, \tag{2.6}$$

where T is the period and $i \triangleq \sqrt{-1}$ is the imaginary operator. The most common method for calculating the DFT is to approximate the above integral (1) by

$$\frac{1}{T} \int_0^T X(t) e^{-2\pi i f t} dt \cong \frac{1}{T} \sum_{n=0}^{N-1} X_n e^{-2\pi i f n \Delta t} \Delta t, \tag{2.7}$$

where X_n is the nth sample of X(t), N is the number of sample points and Δt is the sampling interval. Since, $N = \frac{T}{\Delta f}$ and $T = \frac{1}{\Delta f}$ (Δf being the separation of harmonic frequencies) and taking the product $f = m\Delta f$ where m is a positive integer number, it follows from Equation (2.7) that

$$X(m\Delta f) = \frac{1}{N} \sum_{n=0}^{N-1} X_n e^{-2\pi i \frac{mn}{N}} , \qquad (2.8)$$

where $X(m\Delta f)$ is the DFT approximation to $X'(m\Delta f)$. It is shown (1) that the inverse DFT of the above equation is given by

$$X_n = \sum_{m=0}^{N-1} X(m\Delta f) e^{2\pi i \frac{mn}{N}} \qquad (2.9)$$

2.3 Power Spectrum

The average power associated with X_n, the nth sample over a time span T is defined (1) by

$$\overline{P}_x = \frac{1}{N} \sum_{n=0}^{N-1} X_n^2 , \qquad (2.10)$$

where subscript x refers to the sampled signal X_n. Replacing X_n in Equation (2.10) by its inverse DFT (Equation 2.9), and rearranging, yields

$$\overline{P}_x = \sum_{m=0}^{N-1} X(m\Delta f) \left(\frac{1}{N} \sum_{n=0}^{N-1} X_n e^{2\pi i \frac{mn}{N}}\right) \qquad (2.11)$$

The term in the parenthesis of Equation (2.11) is the complex conjugate of Equation (2.8), that is

$$\overline{P}_x = \sum_{m=0}^{N-1} X(m\Delta f) X^*(m\Delta f), \qquad (2.12)$$

where the * denotes the complex conjugate. The term within the summation sign can be expressed as:

$$P_x(m\Delta f) = X(m\Delta f) X^*(m\Delta f) , \qquad (2.13)$$

where $P_x(m\Delta f)$ is called (1) the mth harmonic autopower spectrum of the sampled signal X_n.

Similarly, when a pair of signals, X_n and Y_n are being considered, the associated average power is defined (1) by

$$\overline{P}_{xy} = \frac{1}{N} \sum_{n=0}^{N-1} X_n Y_n , \tag{2.14}$$

Replacing Y_n in Equation (2.14) by its inverse DFT and rearranging, yields

$$\overline{P}_{xy} = \sum_{m=0}^{N-1} Y(m\Delta f) \left(\frac{1}{N} \sum_{n=0}^{N-1} X_n e^{2\pi i \frac{mn}{N}}\right). \tag{2.15}$$

The term in the parenthesis of Equation (2.15) is the complex conjugate of Equation (2.8), that is

$$\overline{P}_{xy} = \sum_{m=0}^{N-1} X^*(m\Delta f)\ Y(m\Delta f). \tag{2.16}$$

The term within the summation can be expressed as

$$P_{xy}(m\Delta f) = X^*(m\Delta f)\ Y(m\Delta f), \tag{2.17}$$

where $P_{xy}(m\Delta f)$ is called (1) the mth harmonic cross power spectrum of the sampled signals X_n and Y_n. Unlike the autopower spectrum the cross power spectrum, in general, is a complex quantity.

2.4 Frequency Response

In classical control theory, the transfer function is defined as the ratio of the Fourier transform of the system output to that of the input. In random data analysis with $X(m\Delta f)$ as the input and $Y(m\Delta f)$ as the corresponding system response, the transfer function $H(m\Delta f)$, is given by (1,2) by

$$H(m\Delta f) = \frac{P_{xy}(m\Delta f)}{P_x(m\Delta f)} \quad . \tag{2.18}$$

Since $H(m\Delta f)$ is a complex number, it has a magnitude and a phase given by

$$| H(m\Delta f) | = \frac{| P_{xy}(m\Delta f) |}{P_x(m\Delta f)} \quad , \tag{2.19}$$

and

$$\phi = \tan^{-1} \frac{Im[P_{xy}(m\Delta f)]}{Re[P_{xy}(m\Delta f)]} \quad , \tag{2.20}$$

where Im(*) and Re(*) denote the imaginary and real parts.

2.5 Coherence Function

The coherence function (γ^2) for the mth harmonic is defined (1,2) as follows:

$$\gamma^2(m\Delta f) = \frac{| P_{xy}(m\Delta f) |^2}{P_x(m\Delta f)\ P_y(m\Delta f)} \quad . \tag{2.21}$$

It can be readily shown (2) that $0 \leq \gamma^2(m\Delta f) \leq 1$. When the coherence is equal to zero at a particular harmonic, X(t) and Y(t) are said to be statistically independent at that frequency. Furthermore, γ^2 equal to unity indicates linearity between X(t) and Y(t). If the coherence function is greater than zero but less than unity one or more of the three possible situations exist (2).

a. Extraneous noise is present in the measurement.

b. The system relating X(t) to Y(t) is nonlinear.

c. Y(t) is an output due to an input X(t) as well as to other inputs.

CHAPTER 3

RANDOM PROCESS REPRESENTATION USING TIME SERIES MODELS

This chapter is devoted to the overview of time series models. The most general form is discussed first stating all the assumptions involved in the development of the time series models.

3.1 Time Series Models

Let $\underline{y}(t)$ and $\underline{u}(t)$ represent the m dimensional output and known input of a system. It is assumed that $\underline{y}(t)$ (in practice $\underline{y}(t)$ should be replaced by $\underline{y}(t) - \hat{\underline{y}}$, where $\hat{\underline{y}}$ is the mean value of $\underline{y}(t)$), admits (5) the following autoregressive representation:

$$\underline{y}(t) = \sum_{J=1}^{\infty} A_J \underline{y}(t-J) + \sum_{J=1}^{\infty} B_J \underline{v}(t-J) + \underline{v}(t) + \sum_{J=1}^{\infty} C_J \underline{u}(t-J), \quad (3.1)$$

where A_J, B_J, C_J are (mxm) dimensional matrices and $\underline{v}(t)$ is a random (mx1) vector satisfying (5) the relations

$$E\{\underline{v}(t)\} = 0$$

$$E\{\underline{v}(t)\underline{y}^T(t-m)\} = 0 \quad \text{for } m > 1 \quad (3.2)$$

$$E\{\underline{v}(t)\underline{v}^T(m)\} = Q\delta_{mt},$$

where E and T represent the expectation operator and the matrix transpose respectively, and Q is the random source covariance matrix. The delta function δ_{mt} is unity for m=t and is zero for m≠t. A special case of Equation (3.1) is the multivariate Mixed Autoregressive Moving Average representation (15,11), (ARMA), defined by

$$\underline{y}(t) = \sum_{J=1}^{\infty} A_J \underline{y}(t-J) + \underline{v}(t) + \sum_{I=1}^{\infty} B_J \underline{v}(t-J). \quad (3.3)$$

In practice Equation (3.3) is finite and the summation limits must be appropriately determined. Indeed with the introduction of criterion of fit (7,16), the fitting of a model to time series became quite practical. Especially its application to multivariate time series (5) was found very useful in developing computer control of stochastic system (6). A parsimonious (parsimony relates to choosing the best model with least number of parameters (7,11))use of parameters is often derived with finite orders as follows:

$$\underline{y}(t) = \sum_{J=1}^{p} A_J \underline{y}(t-J) + \underline{v}(t) + \sum_{J=1}^{q} B_J \underline{v}(t-J). \tag{3.4}$$

The summation limits p and q as well as parameters $\{A_J, B_J\}$ are adjusted to fit the data. Furthermore, the parameters are chosen such that the model is invertible (20,11), that is, the random source sequence, $\underline{v}(t)$, can be completely determined from knowledge of the observed output sequence $\underline{y}(t)$, i.e.,

$$\underline{v}(t) = (I + \sum_{J=1}^{q} B_J D^J)^{-1} (I - \sum_{J=1}^{p} A_J D^J)\underline{y}(t) , \tag{3.5}$$

where D is the backward shift operator,

$$D^J \underline{v}(k) = \underline{v}(k-J). \tag{3.6}$$

The linear process (3.4) is shown (20,11) to be invertible if the roots of the equation

$$| I + \sum_{J=1}^{q} B_J D^J | = 0 \tag{3.7}$$

lie outside the unit circle.

Many special cases of ARMA process are obtained as follows:

Univariate ARMA process:

$$y(t) = \sum_{J=1}^{p} a_J y(t-J) + v(t) + \sum_{J=1}^{q} b_J\, v(t-J) \qquad (3.8)$$

Multivariate Autoregressive (MAR) process:

$$\underline{y}(t) = \sum_{J=1}^{p} A_J \underline{y}(t-J) + \underline{v}(t) \qquad (3.9)$$

Univariate Autoregressive (AR) process:

$$y(t) = \sum_{J=1}^{p} a_J y(t-J) + v(t) \qquad (3.10)$$

Univariate Moving Average (MA) process:

$$y(t) = \sum_{J=1}^{p} b_J\, v(t-J) + v(t) \qquad (3.11)$$

The special cases of importance in nuclear power plant applications are the ARMA (3.8), MAR (3.9) and the AR (3.10) processes. In both AR and MAR processes only the present value of the random source(s) is used and it is assumed that the present observation(s) is a linear combination of past observations plus an uncorrelated random source, $\underline{v}(t)$, independent of $\underline{y}(k)$ for $k < t$.

The univariate AR models have been used successfully for response time testing of resistance temperature detectors (RTDs) from operational data, without disturbing the reactor system (Upadhyaya and Kerlin (11)). Further work has been carried out by Wu, et al. (21) for identification of the time constants of RTDs and pressure sensors.

The multivariate autoregressive (MAR) model, the subject of investigation in this thesis, is a relatively new noise analysis technique introduced by Fukunishi (8) for diagnostic analysis of boiling water reactors (BWRs). Further work has been carried out by Kitamura et al. (9) and Upadhyaya (10) with applications to BWRs.

CHAPTER 4

THEORETICAL CONSIDERATIONS OF TIME SERIES MODELS

This chapter introduces the theoretical and mathematical aspects of the multivariate autoregressive (MAR) model. The topics include MAR model description, estimation of the noise covariance matrix, model order determination, power spectral matrix, closed loop transfer functions, open loop transfer functions and the signal contribution ratios.

4.1 Multivariate Autoregressive Model

To quote James W. Allen (22) "An autoregressive (AR) model is a linear prediction model, i.e., given the history of a discrete variable $y(j)$ for $j=0,.....,t$, the AR model estimates or predicts a value of $y(t+n)$ for $n>0$." The quoted definition applies also to MAR models, i.e., the predicted value of $y(t)$ can be written as:

$$\hat{\underline{y}}(t) = \sum_{J=1}^{p} A_J \, \underline{y}(t-J), \tag{4.1}$$

where the symbol $\hat{}$ denotes the one-step predicted value and $\{A_J, J=1, ..., p\}$ are (mxm) dimensional parameter matrices to be determined. The difference between the actual and the predicted value is defined (22) as

$$\underline{v}(t) = \underline{y}(t) - \hat{\underline{y}}(t) \tag{4.2}$$

or using Equation (4.1)

$$\underline{v}(t) = \underline{y}(t) - \sum_{J=1}^{p} A_J \, \underline{y}(t-J), \tag{4.3}$$

where p is the MAR model order, which can be thought of as a measure of the memory of events past in time. $\underline{v}(t)$ is referred to as the innovation

process (15) of $\underline{y}(t)$ at the time t and it is required of $\underline{v}(t)$ to satisfy the following conditions:

$$E\{\underline{v}(t)\} = \underline{0} \ , \tag{4.4}$$

and

$$E\{v(t)\ v^T(t+k)\} = Q\ \delta_k \tag{4.5}$$

where Q denotes an (mxm) dimensional matrix and T represents the matrix transpose. Equation (4.5) indicates that the noise covariance matrix, Q, has the characteristics of an impulse function, that is the noise signals $\underline{v}(t)$ is an uncorrelated random process. Thus in acoustic term it is required of $\underline{v}(t)$ to represent sources of white noise.

In practice, a basic test of the model validation is the verification of the whiteness of driving sources.

4.2 Parameter Estimation

Multiplying both sides of Equation (4.3) by $\underline{y}^T(t-k)$, taking the expected values, and rearranging, yields

$$E\{\underline{y}(t)\underline{y}^T(t-k)\} = \sum_{J=1}^{p} A_J\ E\{\underline{y}(t-J)\underline{y}(^T(t-k)\} \tag{4.6}$$

Defining the correlation matrix at lag k(18) as

$$C(k) = E\{\underline{y}(t)\underline{y}^T(t-k)\}, \tag{4.7}$$

and substituting in Equation (4.6), yields

$$C(k) = \sum_{J=1}^{p} A_J\ C(k-J), \quad k=1, \ldots, p. \tag{4.8}$$

The set of Equations (4.7) is called (17) the Yule-Walker equations in honor of the authors who originally presented this technique for univariate analysis. The correlation matrices satisfy the following properties (17):

$$C(-k) = C^T(k), \tag{4.9}$$

and

$$C_{iJ}(-k) = C_{Ji}(k), \tag{4.10}$$

where C_{iJ} represent the iJ-th element of C. Taking the transpose of Equation (4.8) gives

$$C^T(k) = \sum_{J=1}^{P} C^T(k-J)A_J^T \ , \ k>0 \tag{4.11}$$

The set of equations (4.11) can be written in matrix notation (17) as follows:

$$\overline{C} = P\overline{A} \tag{4.12}$$

$$P = \begin{bmatrix} C(0) & C(1) & C(-p+1) \\ C(+1) & C(0) & C(-p+2) \\ \cdot & \cdot & \cdot \\ \cdot & \cdot & \cdot \\ \cdot & \cdot & \cdot \\ C(p-1) & C(p-2) & C(0) \end{bmatrix}, \tag{4.13}$$

$$\overline{C} = \begin{bmatrix} C^T(1) \\ C^T(2) \\ \cdot \\ \cdot \\ \cdot \\ C^T(p) \end{bmatrix}, \tag{4.14}$$

and

$$\overline{A} = \begin{bmatrix} A_1^T \\ A_2^T \\ \cdot \\ \cdot \\ \cdot \\ A_p^T \end{bmatrix}, \tag{4.15}$$

where P is an (mnxmn) block Toeplitz matrix (19), (a square matrix p is a Toeplitz matrix if $p_{iJ} = p_{i-J}$) and where $\bar{A}$ is an (mnxm) rectangular matrix. The correlation matrix C(k) has the form

$$C(k) = \begin{bmatrix} C_{11}(k) & C_{12}(k) & \cdot & \cdot & C_{1m}(k) \\ \cdot & \cdot & \cdot & \cdot & \cdot \\ \cdot & \cdot & \cdot & \cdot & \cdot \\ \cdot & \cdot & \cdot & \cdot & \cdot \\ C_{m1}(k) & C_{m2}(k) & \cdot & \cdot & C_{mm}(k) \end{bmatrix} \tag{4.16}$$

where the elements $C_{iJ}(k)$ for $\{\underline{y}(\ ),\ \ = 1,\ldots,N\}$ are computed numerically (17) as

$$C_{iJ}(k) = \frac{1}{N} \sum_{\ell=1}^{N-k} y_i(\ell+k)\, y_J(\ell)\ , \tag{4.17}$$

for k=0, 1, ..., p and i, j=1, ..., m. With the above definitions an estimate of the parameter set is then given (17) by

$$\bar{A} = P^{-1}\, \bar{C}, \tag{4.18}$$

where P^{-1} is the matrix inverse of P.

4.3 Equivalence of Yule-Walker Equations and the Least-Squares Method

The parameter matrices can also be determined by the linear least-squares method (11), by multiplying Equation (4.3) by $v^T(t)$ and by differentiating the resultant scalar with respect to A_k and setting the result to zero, i.e., let

$$\frac{\partial}{\partial A_k} \{ \sum_{t=1}^{N} [(y^T(t) - \sum_{J=1}^{P} \underline{y}^T(t-J)A_J^T)(\underline{y}(t) - \sum_{m=1}^{P} Am\ \underline{y}(t-m))\} = 0 \tag{4.19}$$

where N is the total number of data points. The above equation reduces (11) to

$$\sum_{t=1}^{N} \underline{y}(t-k)\underline{y}^T(t) = \sum_{t=1}^{N} \sum_{J=1}^{P} \underline{y}(t-k)\underline{y}^T(t-J)A_J^T \cdot \tag{4.20}$$

Dividing both sides of Equation (4.20) by N and taking the limit as N tends to infinity, yields

$$C(-k) = \sum_{J=1}^{p} C(J-k)\, A_J^T , \tag{4.21}$$

or using Equation (4.10),

$$C^T(k) = \sum_{J=1}^{p} C^T(k-J)\, A_J^T. \tag{4.22}$$

Set of Equations (4.22) is identical to that of Yule-Walker Equations (4.11).

4.4 Estimation of Noise Covariance Matrix

Multiplying Equation (4.3) by $\underline{y}^T(t)$ and taking the expected value, yields

$$E\{\underline{v}(t)\underline{y}^T((t)\} = E\{\underline{y}(t)\underline{y}^T(t)\} - \sum_{J=1}^{p} A_J E\{\underline{y}(t-J)\underline{y}^T(t)\} \tag{4.23}$$

with the following definitions (17):

$$E[\underline{v}(t)\underline{v}(t)^T] = E[\underline{v}(t)\underline{y}^T(t)] = Q \tag{4.24}$$

and

$$E\{\underline{y}(t)\underline{y}^T(t)\} = C(0), \tag{4.25}$$

Equation (4.23) simplifies to

$$Q = C(0) - \sum_{J=1}^{p} A_J C^T(J) \cdot \tag{4.26}$$

Here C(0) is the correlation matrix at lag zero and Q is the noise covariance matrix.

4.5 Model Order Determination

One important problem in parametric model fitting of time series is the determination of the model order, p. Two methods for model order determination are discussed in the following two subsections.

4.5.1 Akaike's information criterion. Akaike's information criterion (16), (AIC), is based on computing the value of the maximum logarithmic likelihood function. The likelihood of a function is $p(\underline{y}^N|\theta)$, the joint probability density function of $\underline{y}^N$ given θ. The maximum likelihood principle is to take as $\hat{\theta}$, that value which maximizes the probability of the measurements $\underline{y}^N$. Thus with $\hat{\theta}$ as the conditional maximum likelihood estimate of θ, it is shown (7) that

$$E\{\ell np(\underline{y}^N \mid \theta)\} = \ell np(\underline{y}^N \mid \hat{\theta}) - (n+1)m^2, \tag{4.27}$$

where $(n+1)m^2$ is the number of independently adjustable parameters to get $\hat{\theta}$. If the likelihood function of the measurement is assumed to be normal with zero mean and a variance of Q, then

$$P(\underline{y}^N \mid \hat{\theta}) = \{(2\pi)^m \mid Q \mid\}^{-N/2} \exp\{-\frac{1}{2} \sum_{n=1}^{N} \underline{v}^T(n) Q^{-1} \underline{v}(n)\}, \tag{4.28}$$

where $|Q|$ denotes the determinant of Q. The logarithm of the likelihood (Equation 4.28) is given (4) by

$$L = \frac{N}{2} m \ell n 2\pi - \frac{N}{2} \ell n \mid Q \mid - \frac{N}{2} tr\,(C_o Q^{-1}), \tag{4.29}$$

where L denotes $\ell n\, p(\underline{y}^N|\hat{\theta})$, tr denotes the trace (trace of a matrix is equal to the sum of the diagonal elements of that matrix) and

$$C_o = \frac{1}{N} \sum_{n=1}^{N} \underline{v}(n)\, \underline{v}^T(n) \tag{4.30}$$

It is shown (4) that $C_o = Q$ gives the maximum value of L, i.e.,

$$L_{max} = -\frac{N}{2} m \ell n 2\Pi - \frac{N}{2} m - \frac{N}{2} \ell n \left| Q \right| . \tag{4.31}$$

Substituting Equation (4.31) into Equation (4.27) and denoting $E\{\ell np\ (\underline{y}^N|\theta^*)\}$ by L_1, yields

$$L_1 = -(\frac{N}{2} m \ell n 2\Pi + \frac{N}{2} m + m^2) - \frac{N}{2} \ell n \left| Q \right| - m^2 n. \tag{4.32}$$

Since the term in the parentheses is constant and not a function of model order one can rewrite Equation (4.32) as

$$L_2 = -\frac{N}{2} \ell n \left| Q \right| - m^2 n. \tag{4.33}$$

Multiplication of the above equation by 2, yields

$$AIC(n) = -N \ell n \left| Q \right| - 2m^2 n, \tag{4.34}$$

where $AIC(n) = 2L_2$.

Thus from Equation (4.34) the optimal order is n=p such that AIC(p) has the largest numerical value than for any other order n.

4.5.2 Bayes' probability criterion. The Bayes' probability criterion (7), (BPC), is derived such that, the probability of error in selecting an optimal model is minimized. The BPC is given (11) by

$$BPC(n) = -N \ell n \left| Q_n \right| - m^2 n \left[\ell nN + \ell n \frac{\left| C(o) \right|}{\left| Q_n \right|} - 1 \right] . \tag{4.35}$$

The optimal order is n=p such that BPC(p) has a larger value than for any other order.

4.6 Power Spectral Matrix

Expanding Equation (4.3), page 13 yields

$$\underline{v}(t) = \underline{y}(t) - A_1\underline{y}(t-1) \ldots A_p\underline{y}(t-p) \ , \tag{4.36}$$

where $\underline{y}(t)$ is an (mx1) dimensional observation vector from which the mean values are already subtracted. Another expression of Equation (4.36) is given (8) by

$$\{I - A_1D, \ldots - A_pD^p\}\ \underline{y}(t) = \underline{v}(t), \tag{4.37}$$

or

$$A(D)\underline{y}(t) = \underline{v}(t), \tag{4.38}$$

where I is an mxm identity and D is a backward shift operator,

$$D^J\underline{y}(t) = \underline{y}(t-J), \quad D^0=1, \ J=0, \ \ldots, \ P. \tag{4.39}$$

The measurable variable, $\underline{y}(t)$, in Equation (4.38) is interpreted (8) as the output of the linear system, $A^{-1}(D)$, whose inputs are the uncorrelated residual disturbances, $\underline{v}(t)$. The Fourier transform of Equation (4.36) is given by (8)

$$A(f)\underline{y}(f) = \underline{v}(f), \tag{4.40}$$

with

$$A(f) = A(D) = I - \sum_{J=1}^{p} A_J e^{-2\Pi ifJ\Delta t} \ , \tag{4.41}$$

Since $\underline{y}(f)$ is interpreted as the output of linear system $A^{-1}(f)$, then

$$\underline{y}(f) = A^{-1}(f)\underline{v}(f) \ , \tag{4.42}$$

where $A^{-1}(f)$ is the matrix inverse of A(f). Multiplying Equation (4.42) by the transpose complex conjugate from each side of the equation and taking the expected value, yields

$$S(f) = \Delta t A^{-1}(f) Q A^{-1}(f)^*, \tag{4.43}$$

where * denotes a complex conjugate transpose and where S(f) is an (mxm) dimensional spectral matrix, defined (17) by

$$S(f) = \begin{bmatrix} S_{11}(f) & S_{12}(f) & \cdot & \cdot & \cdot & S_{1m}(f) \\ S_{21}(f) & S_{22}(f) & \cdot & \cdot & \cdot & S_{2m}(f) \\ \cdot & \cdot & & & & \cdot \\ \cdot & \cdot & & & & \cdot \\ \cdot & \cdot & & & & \cdot \\ S_{m1}(f) & S_{m2}(f) & \cdot & \cdot & \cdot & S_{mm}(f) \end{bmatrix} \tag{4.44}$$

The diagonal elements $S_{ii}(f)$ (real), i=1, ..., m are autopower spectra and the off-diagonal elements (complex quantities) $S_{iJ}(f)$, $i \neq J$ for i as the output and J as the input, J=1, ..., n, represent the cross power spectra.

4.6.1 Autopower spectrum. If it is assumed (8) that the input disturbances are mutually independent, then the off-diagonal elements of the noise covariance matrix are neglected. In this situation one obtains an estimate of the power spectra (8) for each measured signal from Equation (4.43):

$$S_{ii}(f) = \sum_{J=1}^{m} \left| A^{-1}(f)_{iJ} \right|^2 q_{JJ}, \quad i=1, \ldots, m \tag{4.45}$$

where $S_{kk}(f)$ and q_{kk} for k=1, ..., m are the diagonal elements of S(f) and Q matrices, and where $|A^{-1}(f)_{iJ}|^2$ is the norm of the iJ-th element of $A^{-1}(f)$ matrix. This representation of the power spectrum is called (8) the spectral decomposition, i.e., the spectrum is decomposed into m components, each one being contributed from the corresponding noise source, indicated by the variance term q_{kk}.

4.6.2 Cross power spectrum. The cross power spectrum of signal i as the output and J as the input is defined (8) (neglecting the off-diagonal elements of Q) by

$$S_{iJ}(f) = \sum_{k=1}^{m} A^{-1}(f)_{ik} A^{-1}(f)^{*}_{Jk} q_{kk}, \qquad i \neq J, \tag{4.46}$$

where i=1, ..., m and J=1, ..., m. Since $S_{iJ}(f)$ is a complex number it has a magnitude of $|S_{iJ}(f)|$ and a phase angle defined (17) by

$$\phi_{iJ}(f) = \tan^{-1}\left\{ \frac{\mathrm{Im}[S_{iJ}(f)]}{\mathrm{Re}[S_{iJ}(f)]} \right\}, \tag{4.47}$$

where Im(x) and Re(x) denote the imaginary and real components of $S_{iJ}(f)$ respectively.

4.6.3 Coherence function. The coherence ($\gamma^2_{iJ}(f)$) is defined (2) by

$$\gamma^2_{iJ}(f) = \frac{|S_{iJ}(f)|^2}{S_{ii}(f) S_{JJ}(f)}. \tag{4.48}$$

The coherence has a maximum value of unity and a minimum value of zero (2). If the coherence is less than unity, one or more of the three possible situations exist.

a. Extraneous noise is present in the measurement.

b. The system relating i to J is not linear.

c. y_i is an output due to an input y_j as well as to other inputs.

4.7 Closed Loop Input-Output Relationship

The MAR model closed loop input-output relationship for the Jth of m variables (Figure 1*) is defined (9) by

$$y_J(f) = \sum_{k=1}^{m} \{A^{-1}(f)\}_{Jk} \quad v_k(f), \tag{4.49}$$

where $A^{-1}(f)_{Jk}$ are the Jk-th elements of the $A^{-1}(f)$ matrix. The closed loop transfer function (9), $G_{Jk}(f)$, is defined as:

$$G_{Jk}(f) = \frac{y_J(f)}{v_k(f)} = A^{-1}_{Jk}(f). \tag{4.50}$$

Figure 2 represents the closed loop block diagram for two variables. The closed loop transfer functions for such a system (9) are given by

$$G_{12} = \frac{y_1(f)}{v_2(f)} = \frac{A_{12}/A_{11}A_{22}}{1 - \frac{A_{12}}{A_{11}}\frac{A_{21}}{A_{22}}}, \tag{4.51}$$

and

$$G_{21} = \frac{y_2(f)}{v_2(f)} = \frac{A_{21}/A_{11}A_{22}}{1 - \frac{A_{12}}{A_{11}}\frac{A_{21}}{A_{22}}} \tag{4.52}$$

where A_{iJ} are the ij-th elements of A(f) matrix. The closed loop transfer function G_{12} and G_{21}, give the overall input-output relations for the feedback system considered.

---

*All figures are in Appendix E, page 83.

4.8 Open Loop Input-Output Relationship

The open loop input-output relation (17) between the ith variable as output and the Jth one as input (Figure 3) is defined by

$$y_i(f) = H_{iJ}(f)\, y_J(f) \qquad i \neq J,\ i, J = 1, \ldots, m \tag{4.53}$$

where $H_{iJ}(f)$ is the open loop transfer function (9) defined as follows:

$$H_{iJ}(f) = \frac{A_{iJ}(f)}{A_{ii}(f)} \tag{4.54}$$

The open loop transfer functions for two variables (Figure 3) are given (9) by

$$H_{12}(f) = \frac{-A_{12}}{A_{11}}(f), \tag{4.55}$$

and

$$H_{21}(f) = -\frac{A_{21}(f)}{A_{22}(f)} \tag{4.56}$$

The open loop transfer function give the input-output relationships among the measurable variables and are useful in the determination of cause-effect relationships.

4.9 Signal Contribution Ratio

The decomposition of the spectral density leads to an important interpretation (8) of the components of the power spectrum. Equation (4.45) can be written in the form

$$1 = \sum_{k=1}^{m} \frac{\left| A^{-1}(f)_{ik} \right|^2}{S_{ii}(f)} q_{kk}, \quad i = 1, \ldots, m. \tag{4.57}$$

There are m components in the summation and each component is defined as follows:

$$SCR_{ik} = \frac{|A^{-1}(f)_{ik}|^2}{S_{ii}(f)} q_{kk}, \quad i=1, \ldots, m, \quad k-1, \ldots, m. \tag{4.58}$$

SCR_{ik} indicates signal contribution ratio (8). Using Equation (4.57) and Equation (4.58) it can be readily shown that

$$\sum_{k=1}^{m} SCR_{ik} = 1, \quad i=1, \ldots, m. \tag{4.59}$$

The SCR_{ik} is interpreted (8) as the contribution of the kth noise source to the signal power of the ith variable. An important property of the SCR is that SCR_{iJ} is in general not equal to SCR_{Ji}.

$$SCR_{iJ} = \frac{|A^{-1}(f)_{iJ}|^2}{S_{ii}(f)} q_{JJ}, \tag{4.60}$$

and

$$SCR_{Ji} = \frac{|A^{-1}(f)_{Ji}|^2}{S_{JJ}(f)} q_{ii}. \tag{4.61}$$

The directional preference of SCR is an important tool for the determination of cause-effect relations of a process and can be used to obtain a flow graph of signals under consideration.

4.10 Relationship Between Coherence Function and the Signal Contribution Ratios

This section presents the mathematical developments for relating signal contribution ratios to the coherence functions. The decomposed cross power spectrum for x_1 as the input and x_2 as the output is given by

$$S_{12} = \sum_{k=1}^{2} A^{-1}(f)_{1k} A^{-1}(f)^*_{2k} q_{kk}. \tag{4.62}$$

Dividing Equation (4.62) by $\sqrt{S_{11}(f)S_{22}(f)}$, yields

$$\frac{S_{12}(f)}{\sqrt{S_{11}(f)S_{22}(f)}} = \sum_{k=1}^{2} A^{-1}(f)_{1k}\sqrt{\frac{q_{kk}}{S_{11}(f)}}\, A^{-1}(f)^{*}_{2k}\sqrt{\frac{q_{kk}}{S_{22}(f)}}\,, \qquad (4.63)$$

where $S_{11}(f)$ and $S_{22}(f)$ are the autopower spectra of x_1 and x_2. Using the following definitions of

$$R_{1k}(f) = A^{-1}(f)_{1k}\sqrt{\frac{q_{kk}}{S_{11}(f)}} \qquad (4.64)$$

and

$$R^{*}_{2k}(f) = A^{-1}(f)^{*}_{2k}\sqrt{\frac{q_{kk}}{S_{22}(f)}} \qquad (4.65)$$

Equation (4.64) reduces to

$$\frac{S_{12}(f)}{\sqrt{S_{11}(f)S_{22}(f)}} = \sum_{k=1}^{2} R_{1k}(f)R^{*}_{2k}(f), \qquad (4.66)$$

where R_{1k} and R_{2k} are the complex signal contribution ratios and where

$$|R_{11}|^2 + |R_{12}|^2 = 1\,, \qquad (4.67)$$

and

$$|R_{21}|^2 + |R_{22}|^2 = 1. \qquad (4.68)$$

Since by definition $\gamma^2_{12} = \frac{|S_{12}(f)|^2}{S_{11}(f)S_{22}(f)}$, then from Equation (4.66) it follows that

$$\gamma^2_{12} = |R_{11}(f)R^{*}_{21}(f) + R_{12}(f)R^{*}_{22}(f)|^2 \qquad (4.69)$$

In a situation where the feedback effect from signal x_2 to signal x_1 is negligible, i.e., where $R_{12} = 0$, Equation (4.69) reduces to

$$\gamma_{12}^2 = | R_{11}(f) R_{21}^*(f) |^2 , \tag{4.71}$$

or

$$\gamma_{12}^2 = | R_{11}(f) |^2 | R_{21}(f) |^2 . \tag{4.72}$$

Since, $R_{11}(f)^2 = 1$, Equation (4.72) reduces to

$$\gamma_{12}^2 = | R_{21}(f) |^2 \tag{4.73}$$

or

$$1 - \gamma_{12}^2 = 1 - | R_{21}(f) |^2 = | R_{22}(f) |^2 . \tag{4.73}$$

Thus in situations where $0 < \gamma_{12}^2 < 1$, $|R_{21}(f)|^2$ represents the contribution from signal x_1 to signal x_2 and $|R_{22}(f)|^2$ represents the contribution to signal x_2 from its own source.

CHAPTER 5

VALIDATION OF DECOMPOSITION

The mathematical developments leading to the decomposition of the spectral density and the derivation of the signal contribution ratios (SCR) have made use of the fundamental assumption of mutual independence of the driving forces. That is, it is assumed that

$$E\{v_i(t)v_J(t)\} = 0, \text{ for all } i \neq J, \tag{5.1}$$

where subscripts i and J represent the ith and the Jth elements of the noise vector $\underline{v}$.

Thus, as a direct consequence of Equation (5.1) the noise covariance matrix, Q, is assumed to be a diagonal matrix in the spectral decomposition analysis. This assumption may not necessarily hold, for the driving forces may be correlated. The validity of the assumption can be tested by making use of orthogonal transformation. That is, the symmetric noise covariance matrix, Q, in Equation (4.45), page 22, is replaced by an actual diagonal matrix W (17) defined by

$$W = L^T Q L, \tag{5.2}$$

where L is a non-singular matrix whose elements are the normalized eigenvectors of the Q matrix ($L^T = L^{-1}$).

The eigenvectors of the Q matrix are determined by solving for the roots of the equation

$$\det(Q - \lambda I) = 0, \tag{5.3}$$

where det denotes the determinant. Once the eigenvalues are obtained the corresponding eigenvectors are calculated as follows:

$$Q\,\underline{x}_k = \lambda_k\,\underline{x}_k, \qquad k=1, \ldots, m, \tag{5.4}$$

where $\underline{x}_k$ is the eigenvector corresponding to the eigenvalue λ_k. The matrix L is then defined by

$$L = (\{\hat{\underline{x}}_1\}, \ldots, \{\hat{\underline{x}}_m\}), \tag{5.5}$$

where $\{.\}$ is an mxl dimensional vector and $\hat{}$ represents the normalized vectors, i.e.,

$$\{\hat{\underline{x}}_k\} = \frac{1}{||\underline{x}_k||}\,\{\underline{x}_k\}, \tag{5.6}$$

where $||\underline{x}_k|| = (\sum_{i=1}^{m} \underline{x}_{ki}^2)^{1/2}$. The diagonal matrix W is then defined by

$$W = (\{\hat{\underline{x}}_1\} \ldots \{\hat{\underline{x}}_m\})^T\; Q(\{\hat{x}_1\} \ldots \{\hat{x}_m\}), \tag{5.7}$$

where W is an (mxm) diagonal matrix. Replacing Q in Equation (4.43) page 22, yields

$$S(f) = A^{-1}(f)\, L^{T^{-1}} W L^{-1} A^{-1}(f)^* \Delta t, \tag{5.8}$$

or

$$S(f) = B^{-1}(f) W B^{-1}(f)^*, \tag{5.9}$$

where S(f) is the spectral matrix and where

$$B^{-1}(f) = A^{-1}(f)\, L^{T^{-1}}. \tag{5.10}$$

The autopower spectra and the signal contribution ratios are then defined by

$$S_{ii}(f) = \sum_{J=1}^{m} |B^{-1}(f)_{iJ}|^2\, W_{JJ}, \quad i=1, \ldots, m \tag{5.11}$$

and

$$SCR_{iJ} = \frac{|B^{-1}(f)_{iJ}|^2}{S_{ii}(f)}\, W_{JJ}, \tag{5.12}$$

where W_{JJ} for J=1, ..., m are the eigenvalues of Q matrix. The assumption of mutual independence of the driving forces is justifiable if the results of Equations (5.11) and (5.12) agree with those of Equation (4.45) page 22, and Equation (4.58) page 26.

Practical applications of the procedures explained in this chapter are further discussed in Section (7.4.5), page 49.

CHAPTER 6

DETERMINATION OF ERROR IN THE POWER SPECTRUM

In the following two sections the uncertainties in the fast Fourier transform (FFT) power spectrum and that of the univariate autoregressive (AR) model are discussed. The AR model is considered because of its relative simplicity compared to MAR model, for evaluating the AR spectrum.

6.1 Error Evaluation of FFT Power Spectrum

In reference 2, it is shown that the uncertainty in the FFT power spectrum is proportional to $\frac{1}{\sqrt{m}}$ where m is the number of blocks used in FFT averaging process and that the standard error, i.e., the standard deviation is defined by

$$\sigma(\hat{G}_x(f)) = \frac{\hat{G}_x(f)}{\sqrt{m}} , \tag{6.1}$$

where subscript x refers to the sampled signal x, which is assumed to have zero mean. In the derivation of the above equation it is assumed that the frequency resolution, Δf, is sufficiently small so that the spectrum is constant over the bandwidth Δf and that $\hat{G}(f)$ is an unbiased estimate of G(f).

6.2 Error Evaluation of the AR Spectrum

The estimate $\hat{p}_x(f)$ of the power spectrum $p_x(f)$ is given (18) by

$$\hat{p}_x(f) = \frac{s^2(p)}{\left| 1 - \sum_{J=1}^{p} \hat{a}_J \, e^{-2\pi i f J \Delta t} \right|^2} \tag{6.2}$$

where

$$s^2(p) = C(0) - \sum_{J=1}^{p} \hat{a}_J C(J). \tag{6.3}$$

The coefficients $\{\hat{a}_1, \ldots, \hat{a}_p\}$ are calculated as follows:

$$C(\ell) = \sum_{J=1}^{p} a_J\, C(\ell-J), \quad \ell=1, \ldots, p, \tag{6.4}$$

where the correlation functions $C(\ell)$ are obtained (18) from the following equation:

$$C(\ell) = \frac{1}{N} \sum_{n=1}^{N-\ell} x(\ell+n)x(n), \tag{6.5}$$

where it is assumed that $x(n)$, $n=1, \ldots, N$, is stationary and ergodic. With the following definitions

$$A_p = 1 - \sum_{J=1}^{p} a_J\, e^{-2\Pi i f J \Delta t}, \tag{6.6}$$

and

$$\hat{A}_p = 1 - \sum_{J=1}^{p} \hat{a}_J e^{-2\Pi i f j \Delta t}, \tag{6.7}$$

the difference between the estimate and the actual value of the spectrum (18) is defined by

$$\begin{aligned} \Delta P_x(f) &= \hat{P}_x(f) - P_x(f) \\ &= \frac{\Delta s^2 \left| A_p(f) \right|^2 - \Delta \left| A_p(f) \right|^2 \sigma^2}{\left| A_p(f) \right|^2 \left| \hat{A}_p(f) \right|^2}, \end{aligned} \tag{6.8}$$

Under the present assumption the process x(n) is strictly stationary and ergodic and as N tends to infinity, $s^2(p)$ and $\hat{A}_p(f)$ converge (18) to σ^2 and $A_p(f)$. In reference 18 it is shown that the limiting distribution of $\sqrt{N}\ \Delta s^2(p)$ and $\sqrt{N}\ \Delta|\hat{A}_p(f)|^2$, is identical to that of $\sqrt{N}\ \nabla S^2(p)$ and $\sqrt{N}\ \nabla|A_p(f)|^2$, where $\nabla s^2(p) = \bar{v}^2 - \sigma^2$,

$\nabla|A_p(f)|^2 = A_p(f)\Delta A_p^*(f) + A_p^*(f)\Delta A_p$, $\bar{V}^2 = \frac{1}{N}\sum_{n=1}^{N} v^2(n)$,

$\Delta A_p(f) = \sum_{J=1}^{P} \Delta a_J e^{-2\pi i f J \Delta t}$ and that the limiting distribution of $\sqrt{N\Delta p_x(f)}$ is identical to that of $Q_N(f)$ which is defined by

$$Q_N(f) = \sqrt{N}\left\{\frac{\nabla s^2(p)}{\sigma^2} - \frac{\nabla|A_p(f)|^2}{|A_p(f)|^2}\right\} P_x(f) \tag{6.9}$$

Furthermore, it is shown (18) that $\sqrt{N}\ \frac{\Delta Px}{P_x}$ has a limiting distribution with a variance composed of two components. One is due to the relative variation in $s^2(p)$, i.e., $NE\left(\frac{\nabla s^2(p)}{\sigma^2}\right)^2 = \frac{3\sigma^4}{\sigma^4} - 1$ for a Gaussian noise. The second component (18) of the limit distribution is defined by

$$E_\infty\left\{N\frac{(\nabla|A_p(f)|^2)^2}{|A_p(f)|^4}\right\} = 4p_x^2(f)\sum_{k=0}^{p-1}[R_e(C_k(f)]^2, \tag{6.10}$$

where $E_\infty\{.\}$ denotes the expectation in the limiting distribution of the quantity within parenthesis, and Re(x) denotes the real part. The limiting distribution of $\sqrt{N}\ \frac{\Delta px}{p_x}$ is then determined (18) by combining the two components, i.e.,

$$E_\infty\left\{N\left(\frac{\Delta P_x}{P_x}\right)^2\right\} = \left(\frac{E(v^4)}{(E(v^2))^2} - 1\right) + 4p_x^2(f)\sum_{k=0}^{p-1}[R_e\ C_k(f)]^2, \tag{6.11}$$

where

$$C_k(f) = \frac{A_p(f)}{\sqrt{s^2(p)}}\ \frac{A_k(f)}{\sqrt{s^2(k)}}\ \exp\{2\pi i(k+1)f\Delta t\}, \tag{6.12}$$

and

$$A_k(f) = 1 - \sum_{m=1}^{k} a_m \exp\{-2\pi i m f \Delta t\}. \tag{6.13}$$

For the evaluation of the variance of $\hat{p}_x(f)$ one has only to retain (18) the second term in Equation (6.11), i.e.,

$$\mathrm{VAR}(\hat{p}_x(f)) = \frac{1}{N} p_x'^2(f) \left(4p_x^2(f) \sum_{k=0}^{p-1} [R_e C_k(f)]^2\right), \tag{6.14}$$

or

$$\sigma(\hat{p}_x(f)) = p_x'(f) \left\{\frac{4}{N} p_x^2(f) \sum_{k=0}^{p-1} [R_e\, C_k(f)]^2\right\}^{1/2} \tag{6.15}$$

where $\sigma(\hat{p}_x)$ is the standard deviation and $p_x'(f)$ is the normalized (i.e., spectrum divided by its area) nondimensional spectrum.

Using Equation (6.15) it is shown (18,22) that the uncertainty in the AR spectrum is smaller than that of FFT. Additional example of use of Equation (6.15) is illustrated in Chapter 8, page 53.

CHAPTER 7

APPLICATION OF EMPIRICAL MODELING TO REACTOR NOISE ANALYSIS

7.1 Introduction

The random signals analyzed are obtained from the St. Lucie pressurized water reactor (PWR) power plant. The following recorded signals are (at 95% of full power) on the magnetic tape. (1) reactor coolant pressure, (2) hot leg temperature, (3) cold leg temperature, (4) steam generator feedwater flow rate, (5) northeast ex-core neutron flux detector response, (6) southwest ex-core neutron flux detector response, (7) reactor core pressure drop and (8) pressure drop across the primary loop pump.

An initial low frequency (f_N = .512 Hertz) spectral analysis was performed by implementing a fast Fourier transform code to identify (in terms of high values of coherences) the signals that are correlated with one another. These were identified as: (1) reactor coolant pressure, (2) cold leg temperature, (3) steam generator feed water flow rate, (4) northeast neutron detector response, (5) southwest neutron detector response. However, only the first four signals were considered for further studies. Furthermore, an examination of the raw data revealed that all of the four except the feed flow exhibited pseudo-periodic behavior and only the initial 7000 seconds of data were identified as stationary (Appendix D).

The multivariate autoregressive (MAR) model procedures are applied to the four stated signals by implementing various computer codes (Appendix B). The PWR data are initially used to evaluate the MAR

model procedures such as determination for the best criterion of fit, investigation of the stated assumption, and determination of the proper choices of sample points and sampling interval. Moreover, the MAR model procedures are applied to both stationary and nonstationary portions of data and the differences are discussed.

The results of various investigations are presented in three major categories of: (1) correlation analysis, (2) FFT analysis and (3) MAR model analysis.

7.2 Correlation Analysis

The correlation analysis was carried out by implementing a computer code (Appendix C) for a lag interval of one second and 7500 seconds of data. The purpose of the analysis was to determine: (1) the nature of the autocorrelation functions, e.g., Markovian (exponential decay) or periodic and (2) the dynamic range of the various pairs of signals.

Figures 4 through 9 show the plots of the autocorrelation functions of reactor coolant pressure, cold leg temperature, feed flow rate and northeast neutron flux detector response respectively. The autocorrelation of the reactor coolant pressure (Figures 4-6) is damped oscillatory followed by a periodic behavior. The period is estimated to be about 106 seconds. The autocorrelation of cold leg temperature (Figure 7) suggests the presence of a periodic component of an estimated period of about 22 seconds. The autocorrelation of feed flow rate (Figure 8) exhibits a periodic behavior with an estimated period of 114 seconds.

The results of the cross-correlation analysis (Figures 10-13) suggest high correlation between: (1) reactor coolant pressure and

cold leg temperature (Figure 10), (2) reactor coolant pressure and northeast neutron detector response (Figure 11), (3) reactor coolant pressure and feed flow rate (Figure 12), (4) cold leg temperature and feed flow rate (Figure 13), at about 70 seconds of the first 100 seconds lag interval. The importance of a knowledge of the dynamic range of variables is further discussed in subsection 7.4.3.

7.3 Fast Fourier Transform Analysis

The low frequency (f_N = .512 Hertz) spectral analysis is performed by implementing a fast Fourier transform (FFT) code (1) using a sampling interval of .976 seconds and a total record length of 20,000 seconds, which covers both stationary and nonstationary portions of data. The signals considered are: (1) reactor coolant pressure (RCP), (2) cold leg temperature (CLDL), (3) feed flow rate (FDFL), (4) northeast neutron flux detector response (power).

Figures 14 through 17 present the plots of autopower spectra (PSD) from the FFT analysis. The PSDs' of RCP (Figure 14) and FDFL (Figure 16) exhibit spikes at about 9×10^{-3} Hertz. These spikes roughly correspond to the periods estimated from the autocorrelation plots of RCP (Figures 4 through 6) and FDFL (Figure 8). Consistent spikes are also exhibited in all the PSDs' at about 4.5×10^{-2} Hertz. The spike in the cold leg PSD (Figure 15) at this frequency roughly corresponds to the period estimated from CLDL autocorrelation plot (Figure 7). Furthermore, an examination of the plots of coherence function (Figures 18 through 23) suggest that the signals are highly correlated at 4.5×10^{-2} Hertz and that negligible correlation exists between FDFL and RCP (Figure 19) at 9×10^{-3} Hertz. The latter observation is rather

surprising, for one would expect to observe high coherence in view of the fact that both RCP and FDFL spectra exhibit significant spikes at this frequency. The absence of high coherence at 9 X 10^{-3} Hertz is due to inclusion of the nonstationary portion of data which is further discussed in subsection 7.4.4.

7.4 MAR Modeling of PWR Noise Signals

The results of various studies are divided into six categories. These are: (1) comparison of AIC and BPC for model order determination, (2) proper choice of sample points (N), (3) bound on order, (4) effect of nonstationarity of data, (5) decomposition validation, (6) comparison of MAR model PSDs' with those of FFT.

7.4.1 Comparison of AIC and BPC. Observations suggested that of the two available criteria for optimal model order selection, Akaike's information criterion (AIC) was the better of the two. The Bayes' probability criterion (BPC) consistently underestimated optimal orders (this conclusion was based on a comparison of PSDs' obtained from optimal models predicted by AIC and BPC with those of FFT) when compared to those obtained by AIC.

Table 1 presents a comparison of the optimal orders predicted by AIC and BPC for two and four variables (m) and sampling intervals of 1, 2, and 3 seconds. In all cases the optimal orders predicted by BPC are considerably lower than those of AIC. The results also indicate that for a fixed sampling interval (Δt) higher optimal orders are predicted by both criteria as the total data points are increased.

From the observations presented in Table 1, the AIC is adopted as the standard criterion for the optimal order selection.

TABLE 1

COMPARISON OF OPTIMAL ORDERS PREDICTED BY AIC AND BPC FOR TWO AND FOUR VARIABLES (m)

	Predicted Optimal Order by AIC	Predicted Optimal Order by BPC
$\Delta t = 1$ $N = 18432$ $m = 4$	24	10
$\Delta t = 1$ $N = 1560$ $m = 4$	10	2
$\Delta t = 1$ $N = 5760$ $m = 2$	22	15
$\Delta t = 2$ $N = 2880$ $m = 2$	13	7
$\Delta t = 3$ $N = 6144$ $m = 4$	23	8
$\Delta t = 3$ $N = 1536$ $m = 4$	9	2

7.4.2 Estimate of sample size. The difference in Akaike's information criterion (AIC) for orders p and p+1 is defined by

$$\Delta AIC = AIC(p+1) - AIC(p) = N \ell n \frac{|Q_p|}{|Q_{p+1}|} - 2m^2, \qquad (7.1)$$

where $|Q_p|$ and $|Q_{p+1}|$ are the determinants of the noise covariance matrices for orders p and p+1. In general, $|Q_p|$ is greater than $|Q_{p+1}|$, consequently $\ell n \frac{Q_p}{|Q_{p+1}|}$, defined as the variance reduction ratio (25) is always a positive number less than unity. Furthermore, it is postulated that ΔAIC will be negative, that is, $N \ell n \frac{|Q_p|}{|Q_{p+1}|}$ is less than $2m^2$. An important relation is obtained by rearranging Equation (7.1) as follows:

$$N = \frac{2m^2}{\ell n \frac{|Q_p|}{|Q_{p+1}|}} \left(1 - \frac{|\Delta AIC|}{2m^2}\right), \qquad (7.2)$$

or

$$N = \frac{2m^2}{\alpha} \left(1 - \frac{|\Delta AIC|}{2m^2}\right), \qquad (7.3)$$

where α is the variance reduction ratio. Equation (7.3) suggests that for a given m and α the maximum value of N is obtained when ΔAIC is identically zero, i.e.,

$$N_{max} = \frac{2m^2}{\alpha}. \qquad (7.4)$$

The above equation indicates that the maximum value of N is fixed for a given m and a desired α and that if N sample points (corresponding to a given α) are used for m=1, then the required sample points to achieve the same value of α for 2, 3, and 4 variables are 4N, 9N and 16N respectively.

Since α is not known a priori then desired theoretical values must be assigned to it. This is best illustrated by plotting N α versus

N (Figures 24-25) for various values of α and N. The straight lines represent the numerical values of $2m^2$ for m=1,...,4 and the point of intersection of the curve and the straight line is defined by Equation (7.4). For instance, for α = .1% and m = 3 (Figure 25), the weighted variance reduction ratio ($N\alpha$) represented by BC is considered significant (alog BC AIC(p) > AIC(p+1) and that represented by CD insignificant (CD represents the region of importance for m = 4). This suggests that the required sample points must be greater than 8,000 but less than or equal to 18,000. To check the constancy of α along BC a variance reduction of .33% is chosen which limits the range of sample points from a minimum of 5,400 to a maximum of 9,600. Two runs were made, one using 6,144 sample points (Δt=2) and another using 9,216 points. The actual variance reduction ratio for the former case was α = .34% and for the latter .3%, with optimal orders of 25. The plots also indicate that for fixed m larger values of N are required for smaller variance reduction ratios. For example, for α = 1.% and m=4 a maximum of 3,200 sample points are required, whereas to achieve a reduction of .1%, a maximum of 32,000 sample points are needed.

In practical application, the noise covariance matrix Q and hence the determinant is determined statistically and though the actual variance reduction ratio, α, may not be equal to that of preselected theoretical value, the presented theoretical investigation is still useful in the determination of an estimate of N. Practical applications of this study are illustrated in Table 2 for 4, 3 and 2 variables (m) and a theoretical variance reduction of .5%.

7.4.3 Bound on order. Since the MAR model procedures make use of the correlation functions for the estimation of the parameter

TABLE 2

COMPARISON OF THE ACTUAL VARIANCE REDUCTION RATIOS WITH THE PRESELECTED THEORETICAL ONE

Number of Variables (m)	Maximum Sample Points N_{max}	Actual Sample Points	Theoretical Variance Reduction Ratio	Actual Variance Reduction Ratio
4	6400	6144	.5%*	.47%
3	3600	3584	.5%	.5%
2	1600	1600	.5%	.3%
4	1024	1024	3.1%	2.5%

*α of .5% is chosen because data is limited to 19200 seconds.

matrices and the noise covariance matrix, then a prior knowledge of the dynamic range of signals is imperative and will provide an insight into the proper choice of sampling interval (Δt). From the cross correlation plots (Section 7.2, page 37) the bound on order is defined by

$$p \cdot \Delta t \geq T, \tag{7.5}$$

where p is the optimal order and T ($\tilde{=}$ 70 seconds) is the maximum lag time determined from cross correlation analysis. Equation (7.5) suggests that the total time span represented by the product of the optimal order and the sampling interval must be equal to or greater than 70 seconds. It is important to note that Equation (7.5) does not fix the optimal order p but rather Δt and the "efficient" order n_e defined as follows:

$$n_e \times \Delta t = 70 . \tag{7.6}$$

Moreover, the total sample points N or α must be chosen such that Equation (7.6) is satisfied. Though this does not fix the value of α it may indicate that the failure to satisfy Equation (7.6) is an indication of the insufficiency of a preselected α.

Thus to determine the proper value of α and the sampling interval (Δt) the presented theoretical discussions are applied to 4, 3, and 2 variable MAR model procedures. With a maximum order of 24, from Equation (7.5) a sampling interval of 3 seconds is chosen, such that 70 seconds falls within the time span represented by the product of the maximum order and Δt. A variance reduction of 0.5% is chosen which limited the maximum sample points for 4, 3, and 2 variables to 6400, 3600, and 1600 respectively. Equation (7.5) suggests that with this choice of Δt at least an optimal order of 23 must be predicted by AIC if .5% theoretical variance reduction is sufficient.

Figures 26 through 28 represent the results of this investigation. The optimal order predicted by AIC for 4 (Figure 26) and 2 (Figure 28) variables are 23 with a total time span of 69 seconds. The predicted optimal order for m=3 (Figure 27) is 24 and it is worth mentioning that the numerical values of AIC for orders 23 and 24 are exactly identical and equal to 30134 with $|Q_{23}| = .19876 \times 10^{-3}$ and $|Q_{24}| = .19777 \times 10^{-3}$. Substituting the latter two numbers in Equation (7.1) yields, $\Delta AIC = AIC(24) - AIC(23) = -.104$. This suggests that AIC for order 23 is greater than that of order 24 by a value of .104 indicating that order 23 would have been the predicted optimal order had one used a better precision for the evaluation of AIC. Finally, limiting the maximum order to 36, from Equation (7.5) a sampling interval of 2 seconds

is chosen. A theoretical variance reduction of .33% is selected which limited the maximum sample points to 9600. If the selected theoretical variance reduction is sufficient then at least an optimal order of 35 must be predicted. The predicted optimal order by AIC (Figure 29) is 25 which means a theoretical variance reduction of .33% is insufficient for Δt=2 seconds, that is N must be greater than 9600. Since the length of the digitized data is limited to 19,200 seconds a sampling interval of 2 seconds can not be used effectively.

Thus, Equation (7.6) provides the following information (T = 70 seconds, data limited to 19200 seconds):

1. The choice of sampling interval is 3 seconds.
2. The efficient model order is 23.
3. Theoretical variance reduction of 0.5%, i.e., N=6400 for Δt=3 is sufficient for the MAR model procedures.

Equation (7.5) suggests that the MAR model procedures are best suitable for signals with comparable dynamic range. It is imperative to note that Equation (7.6) is only useful in situations where the cross correlation functions exhibit clear maxima.

7.4.4 Effect of non-stationarity of data. The effect of non-stationarity of data is investigated by comparing the autopower spectra (APS), signal contribution ratios (SCR) and coherences obtained from two separate cases using four variables, 512 points per block and a sampling interval of one second. The variables considered are: (1) reactor coolant pressure (RCP), (2) cold leg temperature (CLDL), (3) steam generator feed flow rate (FDFL) and (4) northeast neutron detector

response (power). The total data lengths used for cases 1 and 2 are T_1 = 1536 and T_2 = 18432 seconds respectively.

Figures 30 through 49 represent the results of cases 1 and 2 for identical optimal orders of 24. The autopower spectra of RCP, CLDL and power for case 1 (Figure 30, 31, 33) closely match with those of case 2 (Figures 34, 35, 37) but those of FDFL (Figure 32, 36) exhibit major differences at frequencies less than 4×10^{-2} Hertz. An examination of signal contribution ratio (SCR) plots (Figure 38-41) for case 1 indicates significant contributions, in the frequency range of 9×10^{-3} Hertz to 2×10^{-2} Hertz, from RCP noise source to FDFL and CLDL which are completely absent for case 2 (Figure 44-47). Similar observations are made by comparing the coherences for case 1 (Figures 42-43) with those of case 2 (Figures 48-49). In general significant differences are observed for frequencies less than 4.5×10^{-2} Hertz, whereas the results are identical at 4.5×10^{-2} Hertz. A comparison of the parameter matrices (Table 3) indicate significantly higher calculated values of A_{21} and A_{31} for case 1, where A_{iJ} are the iJth elements of the parameter matrices relating RCP to CLDL and FDFL respectively. This suggests that the stationary portion of the data possesses vital low frequency information which is not shared by the rest of data. The conclusion from this investigation is that the low frequency information exhibited in case 1 is completely removed by utilizing a larger number of blocks in case 2, which covers both stationary and nonstationary portions of data. An equally important observation made from this study is the unique ability of the MAR model procedures to reproduce data with relatively much smaller number of sample points (case 1). This conclusion is based on the close matching of autopower spectra of RCP, CLDL and power for frequency range of 10^{-3} - 10^{-1} Hertz and of the SCR for $f > 2 \times 10^{-2}$ Hertz.

TABLE 3

COMPARISON OF THE MODEL PARAMETERS A_{21}, A_{31} RELATING PRIMARY PRESSURE TO FEED FLOW AND COLD LEG TEMPERATURE FOR CASES 1 AND 2

MAR Matrix	Case 1 (A_{21}, A_{31})	Case 2 (A_{21}, A_{31})
1	$.4558 \times 10^{-2}$ .1666	$.293 \times 10^{-1}$ $.4235 \times 10^{-1}$
2	$.6545 \times 10^{-1}$ -.141	$.9273 \times 10^{-2}$ $.502 \times 10^{-1}$
3	-.1246 .1004	$-.6376 \times 10^{-1}$ $-.4997 \times 10^{-1}$
4	$.5113 \times 10^{-1}$ $-.5548 \times 10^{-1}$	$.7884 \times 10^{-2}$ $.4137 \times 10^{-1}$
5	$.1834 \times 10^{-2}$ $-.1816 \times 10^{-1}$	$.2731 \times 10^{-1}$ $-.7609 \times 10^{-1}$
6	$.2948 \times 10^{-1}$ $.7119 \times 10^{-2}$	$.127 \times 10^{-1}$ $.773 \times 10^{-1}$
7	$-.1202 \times 10^{-1}$ -.1173	$-.5526 \times 10^{-2}$ $-.8352 \times 10^{-1}$
8	$.1237 \times 10^{-2}$ .1138	$-.4106 \times 10^{-2}$ $.1422 \times 10^{-1}$
9	$-.7153 \times 10^{-2}$ -.1607	$-.1055 \times 10^{-1}$ $-.1383 \times 10^{-1}$
10	$-.5361 \times 10^{-2}$ $.2508 \times 10^{-1}$	$.5626 \times 10^{-2}$ $.1034 \times 10^{-1}$
11	$.1056 \times 10^{-1}$ $-.4411 \times 10^{-2}$	$-.6139 \times 10^{-2}$ $-.8117 \times 10^{-1}$
12	$-.3542 \times 10^{-1}$ .1898	$-.6241 \times 10^{-2}$ $.6118 \times 10^{-1}$
13	$.1304 \times 10^{-1}$ -.149	$.9695 \times 10^{-3}$ $-.5075 \times 10^{-1}$

TABLE 3 (continued)

MAR Matrix	Case 1 (A_{21}, A_{31})	Case 2 (A_{21}, A_{31})
14	$-.1352 \times 10^{-1}$ $.2202 \times 10^{-1}$	$.4538 \times 10^{-2}$ $.6580 \times 10^{-1}$
15	$.4684 \times 10^{-1}$ $-.461 \times 10^{-1}$	$.4538 \times 10^{-2}$ $.4365 \times 10^{-1}$
16	$-.2242 \times 10^{-1}$ $.176 \times 10^{-1}$	$.5244 \times 10^{-2}$ $.3218 \times 10^{-1}$
17	$-.5752 \times 10^{-2}$ $.7706 \times 10^{-1}$	$-.1199 \times 10^{-2}$ $.2601 \times 10^{-1}$
18	$-.4458 \times 10^{-2}$ $-.1354$	$-.1043 \times 10^{-1}$ $.5400 \times 10^{-1}$
19	$.4276 \times 10^{-2}$ $.7834 \times 10^{-1}$	$.4631 \times 10^{-2}$ $-.7543 \times 10^{-1}$
20	$-.1815 \times 10^{-1}$ $.6937 \times 10^{-1}$	$.1762 \times 10^{-2}$ $.5769 \times 10^{-1}$
21	$-.5774 \times 10^{-2}$ $-.3369 \times 10^{-1}$	$-.1645 \times 10^{-2}$ $.6801 \times 10^{-2}$
22	$.3425 \times 10^{-1}$ $-.217 \times 10^{-2}$	$.6195 \times 10^{-1}$ $.2551 \times 10^{-1}$
23	$.8607 \times 10^{-2}$ $.5944 \times 10^{-1}$	$.1603 \times 10^{-2}$ $-.3329 \times 10^{-1}$
24	$-.1576 \times 10^{-1}$ $-.4048 \times 10^{-1}$	$.1117 \times 10^{-2}$ $-.3329 \times 10^{-1}$

7.4.5 Decomposition validation. The assumption of the mutual independence of the driving forces is investigated using two variables at a time and a sampling interval of three seconds. The variables considered are: (1) reactor coolant pressure (RCP), (2) cold leg temperature (CLDL), (3) feed flow rate (FDFL) and (4) northeast detector response (power).

Figures 50 through 79 represent the plots of the signal contribution ratio (SCR) and the autopower spectral components (APSD). The dotted and the solid lines represent signal contribution ratios obtained from Equations (5.11), page 30 and (4.45), page 22 respectively. As the results indicate the difference between the dotted and the solid lines for the SCR are negligible but there are some insignificant differences in the APSD's of (2, 1) the contribution of the driving force of RCP to CLDL (Figure 53) and (4, 1) the contribution of the driving force of RCP to power (Figure 66). Moreover, a (2 X 2) diagonal matrix will have eigenvalues equal to the diagonal elements with corresponding eigenvectors of $\{1, 0\}$ and $\{0, 1\}$. A comparison of the eigenvalues of noise covariance matrix, Q, with its diagonal elements for various pairs of signals (Table 4) indicates that the eigenvalues are almost identical to the diagonal elements and that the matrix L (Equation 5.5) whose elements are the normalized eigenvectors of Q, has diagonal elements close to unity with very small off diagonal elements suggesting insignificant correlation between the noise sources.

Thus the conclusion from this investigation is that the assumption of mutual independence of the noise sources is indeed justified.

7.4.6 Comparison of the MAR model autopower spectra with those of FFT. A comparison of the auto power spectra of FFT for a sampling interval of .976 seconds and a total period of 20,000 seconds, is made

TABLE 4

NOISE COVARIANCE MATRICES EIGENVALUES AND EIGENVECTORS
FOR VARIOUS PAIRS OF SIGNALS

	Noise Covariance Matrix		Eigenvalues (λ_1, λ_2)		Corresponding Eigenvectors (normalized)	
cold leg temperature versus power	.012813	-.001648	.012754,	.35853	.99872	.050493
	-.0011648	.35794			.050493	.99872
cold leg temperature versus feed flow rate	.013102	.0019877	.013087,	.28077	.99997	+.007425
	.0019877	.28076			-.007425	.99997
reactor coolant pressure versus cold leg temperature	.059792	.0030019	.059983,	.012537	.99799	-.063399
	.0030019	.012728			.063399	.99799
reactor coolant pressure versus power	.056065	-.0012337	.056138,	.035278	.99824	.059247
	-.0012337	.03535			-.059247	.99824

with those of MAR model for a sampling interval of one second and a total period of 18432 seconds to demonstrate the usefulness of the MAR model procedures in representing actual plant data.

A visual comparison of the MAR model spectra (Figures 34-37) with those of FFT analysis (Figures 14-17) suggest that though the general shape of the power spectral density are the same and that the MAR model spectra clearly exhibit the spikes at 4.5×10^{-2} Hertz in all four spectra and at 9×10^{-3} Hertz in the spectrum of the reactor coolant pressure (Figure 34), higher model orders are required for a better matching, especially for frequencies less than 4×10^{-2} Hertz. The cause of the mismatch, according to Equation (7.6), page 43, is the improper choice of sampling interval (Δt) for the MAR model procedures. Moreover it is shown (Section 7.4.3) that the proper choice of sampling interval for the MAR model procedures is three seconds. Though the choice of Δt leads to a loss of high frequency information, it is not regarded as significant, for the frequency range of interest is less than 10^{-1} Hertz. A visual comparison of the MAR model spectra (Figures 80-83) for a sampling interval of three seconds (total period of 18,432 seconds) and a predicted optimal order of 23, with those of FFT (Figures 14-17) not only confirms that a better matching is achieved but also supports the choice of t determined from Section (7.4.3).
A further indication as to the proper choice of $\Delta t = 3$ seconds is the matching of the MAR model coherences (Figures 84-89) with those of FFT (Figures 18-23).

7.5 Summary of the Results of MAR Modeling

The conclusions derived form the investigations presented in this chapter are summarized as follows: (1) AIC is a better criterion than

BPC for optimal order selection, (2) if AIC is chosen as the criterion of optimal order selection then Equation (7.4, page 41) or Figures (24-25) may be used to determine an estimate of the total number of sample points, (3) Equation (7.6), page 43, provides information concerning the choice of sampling interval (Δt) and the sufficiency of a preselected theoretical variance reduction ratio, (4) the assumption of the mutual independence of the driving forces is justified.

CHAPTER 8

UNCERTAINTY IN THE AR AUTOPOWER SPECTRUM

8.1 Comparison of Error in the AR Power Spectrum with that of FFT

The univariate autoregressive (UAR) model is statistically evaluated to determine whether the statistical uncertainty in the UAR model spectrum is smaller than that of FFT. The UAR Model is chosen because of its relative simplicity compared to the multivariate autoregressive (MAR) model. This study is carried out using the reactor coolant pressure signal, 512 sample points per block, a sampling interval of one second (corresponding to a Nyquist frequency of .5 Hertz) and a total period of 16,384 seconds (32 blocks).

Figures 90 and 91 present the normalized auto power spectra (i.e., autopower spectrum divided by its area, hence a nondimensional quantity) via FFT (FFTPSD) and predicted 29th order UAR model (UARPSD) respectively. It should be noted that, in general, the magnitude of the UARPSD is greater than that of the FFTPSD, especially for frequencies less than 10^{-2} Hertz. A comparison of the error spectra (Figures 92 and 93), that is, the spectra of the standard deviation in the FFTPSD and UARPSD respectively, indicate that the uncertainty in the UARPSD is indeed smaller than that of FFTPSD, though not so obvious because of the difference in the plotting scales. For instance, the uncertainty in the FFTPSD (Figure 92) at 2×10^{-3} and 7×10^{-3} Hertz are 15 and 16% compared to 7 and 10% in the UARPSD (Figure 93). Similarly the uncertainty in the FFTPSD (Figure 92) at 4.5×10^{-2} and 9×10^{-2} Hertz are about 16 and 16% compared to 8 and 6% in the UARPSD.

To verify the algorithm for the evaluation of the AR error PSD the second order model is considered. From Equation (6.12), page 34, $C_k(f)$ for a second order AR model is defined by:

$$C_k(f) = \frac{A_2}{\sqrt{s^2(2)}} \frac{A_k}{s^2(k)} \exp\{2\pi i(k+1)f\} \tag{8.1}$$

and the variance of PSD, $P_x(f)$ from Equation (6.14), page 35 is:

$$VAR(\hat{p}) = p_x'^2(f)\{\frac{4}{N} p_x^2(f) \sum_{k=0}^{1} [R_e C_k(f)]^2\} \tag{8.2}$$

The above equation can be rewritten as:

$$VAR(\hat{p}) = p_x'^2(f)\{\frac{4}{N} p_x^2(f)[(ReC_0(f))^2 + (ReC_1(f))^2]. \tag{8.3}$$

Using Equation (8.1) it follows that

$$C_0(f) = \frac{1}{\sqrt{s^2(2)s^2(0)}} A_2 A_0 e^{2\pi i f} \quad , \tag{8.4}$$

where $A_0 = 1$, $s^2(0)$ is the variance of the signal and $A_2(f)$ (Equation 6.6, page 33) is given by:

$$A_2 = 1 - \sum_{J=1}^{2} a_J e^{-2\pi i f J}. \tag{8.5}$$

Expanding Equation (8.5) and substituting in Equation (8.4), yields

$$C_0(f) = \frac{1}{\sqrt{s^2(2)s^2(0)}} (1 - a_1 e^{-2\pi i f} - a_{2e}^{-4\pi i f}) e^{2\pi i f}. \tag{8.6}$$

or

$$ReC_0(f) = \frac{1}{\sqrt{s^2(2)s^2(0)}} (\cos 2\pi f - a_1 - a_2 \cos 2\pi f), \tag{8.7}$$

or

$$[R_e C_0(f)]^2 = \frac{1}{s^2(2)s^2(0)} (\cos 2\pi f - a_1 - a_2 \cos 2\pi f)^2. \tag{8.8}$$

Similarly using Equation (8.1) it follows that

$$C_1(f) = \frac{A_2 A_1}{\sqrt{s^2(2)s^2(1)}} e^{4\pi i f} \tag{8.9}$$

where A_1 from Equation (6.13), page 35 is defined by:

$$A_1(f) = 1 - a_1' e^{-2\pi f}, \tag{8.10}$$

where a_1 is the coefficient corresponding to the first order AR model. Substituting Equations (8.5) and (8.10) in Equation (8.9) yields

$$C_1(f) = \frac{1}{\sqrt{s^2(2)(s^2(1))}} \{(1-a_1 e^{-2\pi i f} - a_2 e^{-4\pi i f}) (1 - a_1' e^{-2\pi i f}) e^{4\pi i f}\} \tag{8.11}$$

or

$$C_1(f) = \frac{1}{\sqrt{s^2(2)s^2(1)}} \{(1 - a_1 e^{-2\pi i f} - a_2 e^{-4\pi i f})(e^{4\pi i f} - a_1' e^{2\pi i f})\} \tag{8.12}$$

Since, the terms in the parenthesis reduces to

$$L = e^{4\pi i f} - a_1 e^{2\pi i f} - a_2 - a_1' e^{2\pi i f} + a_1 a_1 + a_1' a_2 e^{-2\pi i f}, \tag{8.13}$$

it follows that

$$R_e C_1(f) = \frac{1}{\sqrt{s^2(2)s^2(1)}} [\cos 4\pi f - a_2 + a_1' a_1 - (a_1 + a_1' - a_1 a_2)\cos 2\pi f] \tag{8.14}$$

or

$$(R_e C_1(f))^2 = \frac{1}{s^2(2)s^2(1)} [\cos 4\pi f - a_2 + a_1' a_1 - (a_1' + a_1' - a_1 a_2)\cos 2\pi f]^2 \tag{8.15}$$

substituting Equations (8.8) and (8.15) in Equation (8.3) and taking the square root, yields

$$\sigma(\hat{p}) = p_x'(f) \left\{ \frac{4p_x^2}{Ns^2(2)} \left[\frac{1}{s^2(0)} (\cos 2\pi f - a_1 - a_2 \cos 2\pi f)^2 \right. \right.$$

$$\left. \left. + \frac{1}{s^2(1)} [\cos 4\pi f - a_2 + a_1' a_1 - (a_1 + a_1' - a_1' a_2)\cos 2\pi f]^2 \right] \right\}^{1/2} \tag{8.16}$$

where $\sigma(\hat{p})$ is the standard deviation of $p_x(f)$. The standard deviation is calculated from Equation (8.16) using the autopower spectrum (Figure 94), normalized spectrum (Figure 95) and $s^2(0) = .483$, $a_1' = .98$, $s^2(1) = .0126$, $s^2(2) = .0121$, $a_1 = 1.4$ and $a_2 = -.42$. The calculated standard deviations are shown in Table 5. The calculated values match closely with the 2nd order AR error spectrum (Figure 96).

Thus the conclusion from this investigation is that the uncertainty in the UARPSD is smaller than that of FFTPSD but it is quite time consuming to calculate, especially if the error analysis is to be performed for each estimate.

8.2 Empirical Investigation of the AR Models

In random data analysis, generally the total data length under consideration is divided into a number of blocks, each block representing one period. However, different portions of the data (keeping total length constant) may yield different optimal orders. This difference in the optimal orders may be attributed to statistical fluctuations from one period to another. Thus the purpose is to determine the best analysis procedure for the estimation of the power spectrum. That is, to determine the best combination (for the cases to be considered) of sample size per block and the number of blocks for the estimation of the power spectrum. The investigation is carried out by implementing UNIVAR and SPEAR2 computer codes (Appendix A) and using 1536 seconds (30720 data points) of a BWR data.

TABLE 5

COMPARISON OF THE CALCULATED AND THE DETERMINED STANDARD DEVIATION FOR A SECOND ORDER AR MODEL

Frequency Hertz	Calculated Standard Deviation (From Equation 8.16)	Standard Deviation (From Figure 96)
2.0×10^{-3}	0.08	0.07
7.0×10^{-3}	1.5×10^{-2}	1.2×10^{-2}
1.2×10^{-2}	3.2×10^{-3}	4.0×10^{-3}
8.0×10^{-2}	4×10^{-5}	5.0×10^{-5}
0.1	2.6×10^{-5}	2.2×10^{-5}
0.5	3.1×10^{-7}	3.5×10^{-7}

To determine the effect of block averaging, two cases of interest are considered. Case (1) consists of 512 points per block, one block per case and a maximum of 60 cases. Case (2) consists of 512 points per block, two blocks per case and a maximum of 30 cases. Tables 6 and 7 present the frequency of occurrence of the optimal orders for cases (1) and (2), respectively. The optimal orders presented in Table 6 vary from a minimum of 4 to a maximum of 9, whereas those of case (2) vary from a minimum of 8 to a maximum of 10. This reduction in the range of the optimal orders for the latter case is an indication of superiority of case (2) to that of case (1). A comparison of average power spectra (for order 9) and the normalized standard deviation (standard deviation divided by the average power spectrum) for cases (1) and (2), Figures 97-100, confirm the above conclusion.

To determine the effect of sample size per block the following cases are considered. Case (3) consists of 1024 sample points per block, 2 blocks per case and a maximum of 15 cases. Case (4) consists of 256 points per block, 2 blocks per case and a maximum of 60 cases. Tables 8 and 9 present the frequency of occurrence of optimal orders for cases (3) and (4), respectively. The range of the optimal orders for case (4) vary from a minimum of 4 to a maximum of 9, whereas those of case (3) vary from a minimum of 9 to a maximum of 10. A comparison of the average power spectra (order 9) and the normalized standard deviations, Figures 101-104, indicate superiority (smaller range of optimal orders and smaller value of standard deviation) of case (3) to that of case (4). Moreover, a comparison is made between case (3) and case (5). The latter case consists of 512 points per block, 4 blocks per case and a maximum of 15 cases. The frequency of occurrence of the optimal orders is

TABLE 6

FREQUENCY OF OCCURRENCE OF OPTIMAL ORDERS OF CASE (1)

Optimal Order (p)	Frequency of Occurrence N=512, NB=1, NCMX=60
1	0
2	0
3	0
4	11
5	10
6	3
7	5
8	12
9	14
10	2
11	1
12	0
13	1
14	0
15	1

TABLE 7

FREQUENCY OF OCCURRENCE OF OPTIMAL ORDERS OF CASE (2)

Optimal Order (p)	Frequency of Occurrence N=512, NB=2, NCMX=30
1	0
2	0
3	0
4	0
5	2
6	1
7	1
8	7
9	11
10	5
11	0
12	2
13	0
14	1
15	0

TABLE 8

FREQUENCY OF OCCURRENCE OF OPTIMAL ORDERS OF CASE (3)

Optimal Order (p)	Frequency of Occurrence N=1024, NB=2, NCMX=15
1	0
2	0
3	0
4	0
5	0
6	0
7	0
8	1
9	7
10	4
11	1
12	1
13	0
14	0
15	1

TABLE 9

FREQUENCY OF OCCURRENCE OF OPTIMAL ORDERS OF CASE (4)

Optimal Order (p)	Frequency of Occurrence N=256, NB=2, NCMX=60
1	0
2	0
3	0
4	8
5	20
6	10
7	1
8	11
9	8
10	2
11	0
12	0
13	0
14	0
15	0

in Table 10. A comparison of the average power spectra and the normalized standard deviations, Figures 105-106, indicate that both cases have equal standard deviations up to 1 Hertz. However, case (3) has a standard deviation smaller than that of case (5) in the frequency range of 1 to 10 Hertz.

Further investigations are carried out using the results of case (1). A comparison of the average power spectra for optimal orders of 4 (frequency of occurrence, 11) and optimal order of 2 (frequency of occurrence, 0), Figures 107-110, indicate that the standard deviation of the power spectrum for order 4 is smaller than that of order 2 except at frequencies above 7 Hertz. A similar comparison for orders 9 and 15, Figures 111-112, indicate that for order 9, the spectrum has a smaller standard deviation up to 2 Hertz, and that the standard deviations are about equal in the range of 2 to 10 Hertz.

The conclusions that can be drawn from this investigation are as follows: 1) block averaging per case is superior to that of single block per case (the average spectrum obtained by block averaging has a smaller standard deviation). The choise of sample points per block is important with case (3) representing the best of the considered cases (the least standard deviation). 2) Average power spectra have larger standard deviations for orders with the least frequency of occurrence, for frequencies less than 1 Hertz.

TABLE 10

FREQUENCY OF OCCURRENCE OF OPTIMAL ORDERS OF CASE (5)

Optimal Order (p)	Frequency of Occurrence N=512, NB=4, NCMX=15
1	0
2	0
3	0
4	0
5	0
6	1
7	0
8	1
9	8
10	2
11	2
12	1
13	0
14	0
15	0

CHAPTER 9

DIAGNOSTIC ANALYSIS

9.1 Introduction

This chapter presents the diagnostic analysis of St. Lucie nuclear power plant noise data using the results of the multivariate autoregressive (MAR) model procedure. The discussion and conclusion presented in the following section are based on the signal contribution ratio (SCR) and the frequency response plots of four plant signals (1) reactor coolant pressure (RCP), (2) cold leg temperature (CLDL), (3) steam generator feed flow rate (FDFL), and (4) northeast neutron detector response (power). Because of the nonstationarity of the data which has led to inconsistent observations (Section 7.4.4, page 45) for various lengths of data, a cause-effect diagnostic analysis is rather difficult and may not even be valid. However, it is shown (Section 7.4.4, page 45) that for various lengths of data results of the MAR model fitting are identical at about 4.5×10^{-2} Hertz. Thus an effort is made to derive cause-effect relation at this frequency. Furthermore, according to the studies presented in Chapter 7 results of the MAR model fitting to be considered for this study are those for a sampling interval of three seconds and total record length of 18,432 seconds with a predicted optimal order of 23. Since this length of data includes the nonstationary portion of data, the results considered, are for a sampling interval of three seconds and a total record length of 3,072 seconds (Figures 113-147).

9.2 Cause-Effect Relation at 4.5×10^{-2} Hertz

Figure (129) represents a summary of the closed loop input-output relation with the corresponding approximate percent contributions (calculated from signal contribution ratio plots Figures 113-128 from each

source to the measurable signals. As Figures (113-128) indicate the RCP is a significant contributor to the fluctuations in the CLDL (Figure 129b), FDFL (Figure 129c) and power (Figure 129d). This observation physically is implausible, for the pressurized water reactors (PWRs) are designed to operate at constant primary pressure with negligible feedback effects due to the pressure coefficient of reactivity. This indeed is supported by the open-loop frequency response plots (Figures 136-137) which clearly indicate that power is a cause of the fluctuations in the RCP and that the feedback effect due to primary pressure changes is negligible (Figure 137). However, the phase relation (Figure 138) suggests that RCP leads power by 270° which can be interpreted as -90°, that is, power leading RCP. Since the steam generator is coupled to the reactor via "hot" and "cold" legs, then a plausible way to cause fluctuations in FDFL is to induce fluctuations in the hot leg temperature (unmeasured variable) due to fluctuations in the reactor power. This is also supported by the open-loop frequency response and phase plots (Figures 145-146). The plots indicate the power is a cause of fluctuations in FDFL and that power leads the FDFL (Figure 147). Moreover, perturbations in the CLDL can lead to fluctuations in FDFL via power with feedback effects from FDFL to CLDL. The open-loop frequency response plots for CLDL versus power (Figures 142-143) and the phase $\triangleq$ -180° (Figure 144) fail to indicate the cause-effect relation whereas the open-loop frequency response plots (Figures 130-131) clearly indicate that CLDL is a cause of fluctuations in RCP. However, the phase relation (Figure 132) suggests that RCP leads CLDL by about 90°. Furthermore, Figures (139-140) indicate negligible feedback effects from FDFL to CLDL. If we think of CLDL as the output of the system (steam

generator), then it can be perturbed by one of the following variables: (1) steam flow rate (unmeasured), (2) feed water flow rate, (3) hot leg temperature (unmeasured), (4) feed water flow temperature (unmeasured), the most plausible of which are: (1) steam flow rate, (2) feed flow rate. In short, representing the steam generator by one variable is quite inadequate and at least, in addition to FDFL, the steam flow rate should have been considered in the cause-effect study. The open-loop frequency response plots for the RCP versus FDFL (Figures 133 through 134) indicate that RCP is a cause of fluctation in FDFL. This is not physically plausible (the pressurizer (23) and the reactor control system (23) will not tolerate such a behavior) and the cause of the FDFL fluctuations must be due to an unmeasured variable, e.g., steam flow rate or hot leg temperature.

The steam generator "three element controller" (23) can also be responsible for fluctuations in FDFL. This is illustrated in Figure 148, obtained from steam generator physical model (24) for 10 percent increase in the steam generator inlet temperature. The plateau of FDFL frequency response plot (Figure 148) corresponds to about 3×10^{-2} Hertz which is fairly close to the spike observed in the FDFL spectrum (Figure 149) at about 2.7×10^{-2} Hertz. This suggests that the cause of fluctuations in FDFL represented by a spike at 4.5×10^{-2} Hertz, is probably not the controller but rather due to an unmeasured variable.

With the results presented, determination of a conclusive cause-effect relation is impossible, however, an important conclusion derived from this investigation is that the incorrect choice of combination of variables and the inadequate representation of a complex system such as a reactor coupled with the steam generator, does lead to incorrect results and interpretation of data.

CHAPTER 10

CONCLUSIONS AND RECOMMENDATIONS

10.1 Summary and Conclusions

The purpose of this thesis is to present an experimental and theoretical investigation of the MAR model procedures to determine its usefulness for analysis of noisy, continuous signals. The conclusion from this study is that MAR modeling is indeed a useful tool in the field of noise analysis and is recommended to be used in conjunction with correlation analysis. However, problems may be encountered with signals having large dynamic range.

The major conclusions dealing with the specifics of MAR modeling are:

(1) The combination of signals for the analysis should be determined from cross-correlation analysis.

(2) If AIC is used as the criterion for optimal order selection then Equation (7.4), page 41 can be used to determine an estimate of the total number of sample points.

(3) Equation (7.6), page 43 not only provides an insight into the choice of the sampling interval but also furnishes information about the sufficiency of a preselected theoretical variance reduction ratio and the efficient model order.

(4) The error in AR power spectrum is smaller than that of FFT, but it is time consuming to calculate this, especially if the error analysis is to be performed for each estimate.

(5) The standard deviation of the AR spectrum obtained empirically decreases with block averaging per case and increasing number of sample points per block. The standard deviation increases with optimal orders having the least frequency of occurrence.

(6) The choice of the combination of variables for the diagnostic analysis was based on the plots of coherence function obtained from FFT analysis. However, investigation of the effect of nonstationarity of data using MAR modeling indicated that information provided by the coherence functions could be misleading. The choice of the combination of variables should be determined from cross-correlation analysis.

10.2 Recommendations

The recommendations for future work are:

(1) Determination of the proper choice of sampling interval in situations where the cross-correlation does not exhibit clear maxima.

(2) Determination of the sufficiency of the choice of theoretical variance reduction ratio independent of the procedures explained in Section (7.4.3), page 42. This is indeed important since it will lead to significant reduction in computation time for optimal order selection.

(3) Further investigation and verification of Equation (7.5), page 43.

LIST OF REFERENCES

LIST OF REFERENCES

1. Kerlin, T. W., Frequency Response Testing in Nuclear Reactors, Academic Press, New York, 1974.

2. Bendat, J. S., and A. G. Piersol, Random Data: Analysis and Measurement Procedures, Wiley-Interscience, New York, 1971.

3. Box, G. E., and G. M. Jenkins, Time Series Analysis Forecasting and Control, Holden Day, San Francisco, 1970.

4. Akaike, H., "Maximum Likelihood Identification of Gaussian Autoregressive Moving Average Models," Biometrika, 60, 2, p. 225, 1973.

5. Akaike, H., "Autoregressive Model Fitting for Control," Ann. Inst. State. Mat., Tokyo, Vol. 23, p. 163, 1971.

6. Otomo, T., T. Nakagawa, and H. Akaike, "Statistical Approach to Computer Control of Cement Rotary Kilns," Automatica 8, p. 35, 1972.

7. Kashyap, R. L. and A. R. Rao, Dynamic Stochastic Models from Emperical Data, Academic Press, New York, 1976.

8. Fukunishi, K., "Diagnostic Analysis of a Nuclear Power Plant Using Multivariate Autoregressive Process," Nucl. Sci. Eng. 68, 215 (February 1977).

9. Kitamura, M., et al., "Identification of BWR Dynamics from Autoregressive Analysis of Multivariable Experiments," prog. in Nucl. Energy, Vol. 1, p. 231, 1977.

10. Upadhyaya, B. R., "Multivariate Analysis of Neutron Noise Signals for Parameter Estimation in BWR," Trans. Am. Nucl. Soc., 30, p. 745, 1978.

11. Upadhyaya, B. R., and T. W. Kerlin, "Response Time Testing of Temperature Sensors using a Noise Analysis Method," Trans. Am. Nucl. Soc., 26, p. 445, 1977.

12. Upadhyaya, B. R., and T. W. Kerlin, "In-Site Response Time Testing of Platinum Resistance Thermometers," EPRI NP-834 Project 503-3 (July 1978).

13. Kaveh, M., and G. R. Cooper, "An Empirical Investigation of the Properties of the Autoregressive Spectral Estimator," IEEE. Trans. Inf. Theory, IT-22, p. 313, May 1976.

14. Gelb, et al., Applied Optimal Estimation, MIT Press, Cambridge, Massachusetts, 1974.

15. Findley, D. F. (Editor), Applied Time Series Analysis, Academic Press, New York, 1978.

16. Akaike, H. "A New Look at the Statistical Model Identification," IEEE. Trans. Aut. Contr. AC-19 (6), p. 716, December 1974.

17. Upadhyaya, B. R., M. Kitamura, and T. W. Kerlin, "Multivariate Signal Analysis Algorithms for Process Monitoring and Parameter Estimation in Nuclear Reactors," Annal. of Nucl. Energy, Pergamon Press, Vol. 7, p. 1-11, 1980.

18. Akaike, H. "Power Spectrum Estimation through Autoregression Model Fitting," Ann. Inst. Stat. Mar., Vol. 21, p. 407, 1969.

19. Grenander, U. and G. Szego, Toeplitz Forms and their Applications, Univ. of California Press, Berkeley, 1958.

20. Akaike, H., "On the Use of a Lienar Model for the Identification of Feedback Systems," Ann. Stat. Math., 20, p. 425, 1968.

21. Wu, S. M. and et al., "The Determination of Time Constants of Reactor Pressure and Temperature Sensors: The Dynamic Data System," Nucl. Sci. and Eng. 72, p. 84, 1979.

22. Allen, J. W., "An Evaluation of the Autoregressive Time Series Model for Analysis of a Continuous Noise Signal," Ph.D. dissertation, Univ. of Tennessee, Knoxville, TN (June 1978).

23. Kerlin, T. W., "Lecture Notes," Nucl. Eng. Dept., Univ. of Tennessee , Knoxville.

24. Freeles, J., "An Investigation of High Order and Low Order Dynamic Modeling of a Complete Pressurized Water Reactor Nuclear Power Plant," M. S. Thesis, Univ. of Tennessee, Knoxville, TN (June 1979).

25. Kitamura, M., "Private communication." Nuclear Engineering Department, Univ. of Tennessee , Knoxville (1979).

APPENDICES

APPENDIX A

DESCRIPTION OF THE ALGORITHMS EMPLOYED FOR THE EMPIRICAL EVALUATION OF THE AR MODELS

Programs UNIVAR and SPEAR2 are written by M. Kitamura of The Nuclear Engineering Department of The University of Tennessee, Knoxville. Program UNIVAR calculates, correlation functions, regression coefficients and the optimal orders for each case. Program SPEAR2 calculates the average spectrum and the standard deviation as follows:

$$\bar{p}(f) = \frac{1}{N} \sum_{i=1}^{N} P_i(f), \tag{A.1}$$

and

$$\sigma(p(f)) = \frac{1}{N} \sum_{i=1}^{N} (P_i(f) - \bar{p}(f))^2, \tag{A.2}$$

where N is the number of cases and $p_i(f)$ is the estimate of the spectrum for the ith case.

APPENDIX B

DESCRIPTION OF ALGORITHMS EMPLOYED FOR MAR MODELING

There are two computer code packages available for MAR modeling of random data. The first code package written by Dr. Upadhyaya of the Nuclear Engineering Department of The University of Tennessee, Knoxville, consists of three programs. These are: (1) ARMULT, (2) ARMLT1 and (3) ARMLT2. Program ARMULT calculates the correlation functions, regression coefficients, noise covariance matrices and finally determines the optimal order. Program ARMLT1 transforms the model from the time domain into the frequency domain and determines and plots: (1) autopower spectra, (2) cross power spectra, (3) coherence and (4) signal contribution ratios. Program ARMLT2 determines the open-loop and the closed-loop transfer functions. The program also calculates the diagonal matrix W (Eq. 5.7, page 30) and determines the auto power spectra (Eq. 5.11, page 30) and signal contribution ratio (Eq. 5.12, page 30) derived from exact decomposition.

The second code package written by Dr. Kitamura of the Nuclear Engineering Department of The University of Tennessee, Knoxville, consists of three programs. These are: (1) MARCO7, (2) ARCOEF and (3) FRDOM7. Program MARCO7 calculates and stores the correlation functions. Program ARCOEF7 calculates the regression coefficients, noise covariance matrix and determines the optimal model order. Program FRDOM7 transforms the model from the time domain to the frequency domain and determines: (1) power spectra, (2) cross power spectra, (3) coherence and (4) signal contribution ratio.

Programs ARMULT and ARMLT1 are limited to a maximum of four variables and limited to a maximum order of 12 for four variable analysis. Programs MARCO7, ARCOEF7, and FRDOM7 are limited to a maximum of seven variables and a maximum order of 24 for seven variable analysis. However, the maximum order is limited to 49 for four variable analysis.

APPENDIX C

DESCRIPTION OF THE ALGORITHM FOR CORRELATION ANALYSIS

Program CORFUN written by B. R. Upadhyaya computes the auto-correlation functions $C_{xx}(t)$, $C_{yy}(t)$ of two signals x and y and their cross-correlation functions $C_{xy}(t)$, $C_{yx}(t)$ for $0 < t \ll 200$.

The correlation functions are calculated as follows:

$$C_{xx}(m) = \frac{1}{N-m} \sum_{i=1}^{N-m} (x_i - x)(x_{i+m} - x), \quad m=0, \ldots, 200, \tag{C.1}$$

$$C_{yy}(m) = \frac{1}{N-m} \sum_{i=1}^{N-m} (y_i - y)(y_{i+m} - y), \quad m=0, \ldots, 200, \tag{C.2}$$

$$C_{xy}(m) = \frac{1}{N-m} \sum_{i=1}^{N-m} (x_i - x)(y_{i+m} - y), \quad m=0, \ldots, 200, \tag{C.3}$$

where

$$x = \frac{1}{N-m} \sum_{i=1}^{N} x_i, \tag{C.4}$$

and

$$y = \frac{1}{N-m} \sum_{i=1}^{N} y_i \tag{C.5}$$

APPENDIX D

DEFINITION OF STATIONARITY

A random process $x(t)$ is said to be stationary, if the mean value $\mu(t_1)$ and the autocorrelation function $R(t_1, t_1 + \tau)$ are invariant. with respect to time. That is, $x(t)$ is stationary if

$$\mu(t_1) = \mu = \lim_{N \to \infty} \frac{1}{N} \sum_{k=1}^{N} x_k(t_1) , \qquad (D.1)$$

and

$$R(t_1, t_{1+\tau}) = R(t) = \lim_{N \to \infty} \frac{1}{N} \sum_{k=1}^{N} x_k(t_1) x_k(t_1 + \tau) \qquad (D.2)$$

APPENDIX E

LIST OF FIGURES

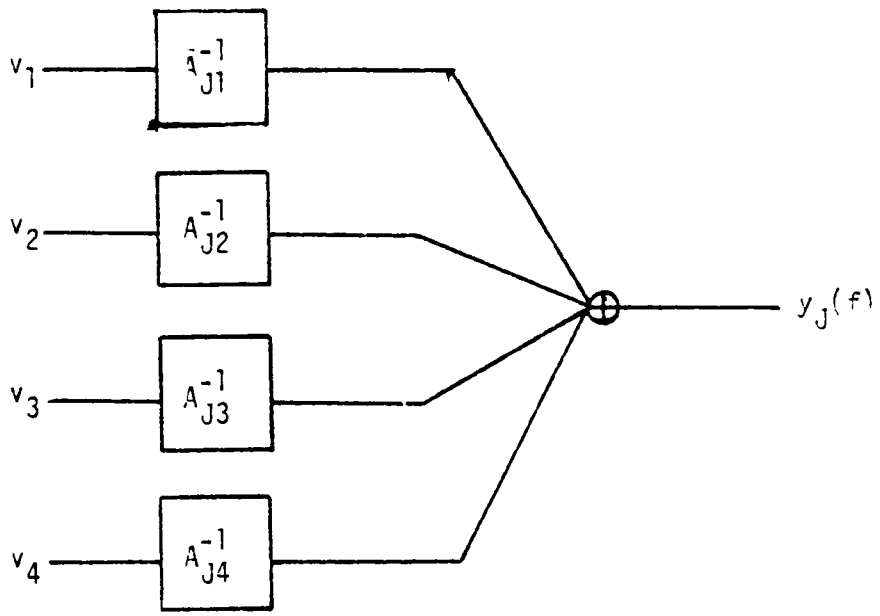


Figure 1. Closed Loop Input-Output Relation for Four Variables.

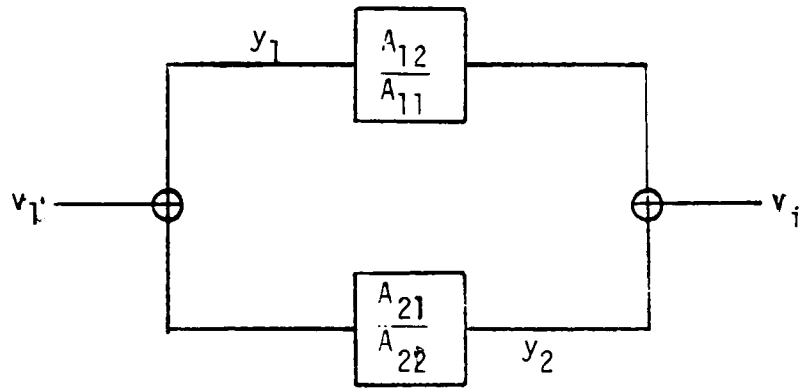


Figure 2. Closed Loop Block Diagram for Two Variables.

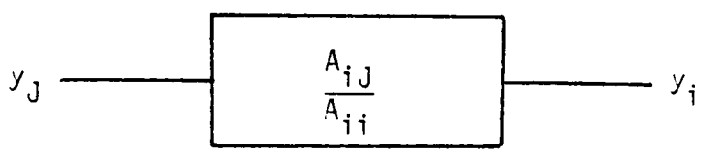


Figure 3. Open Loop Input-Output Block Diagram.

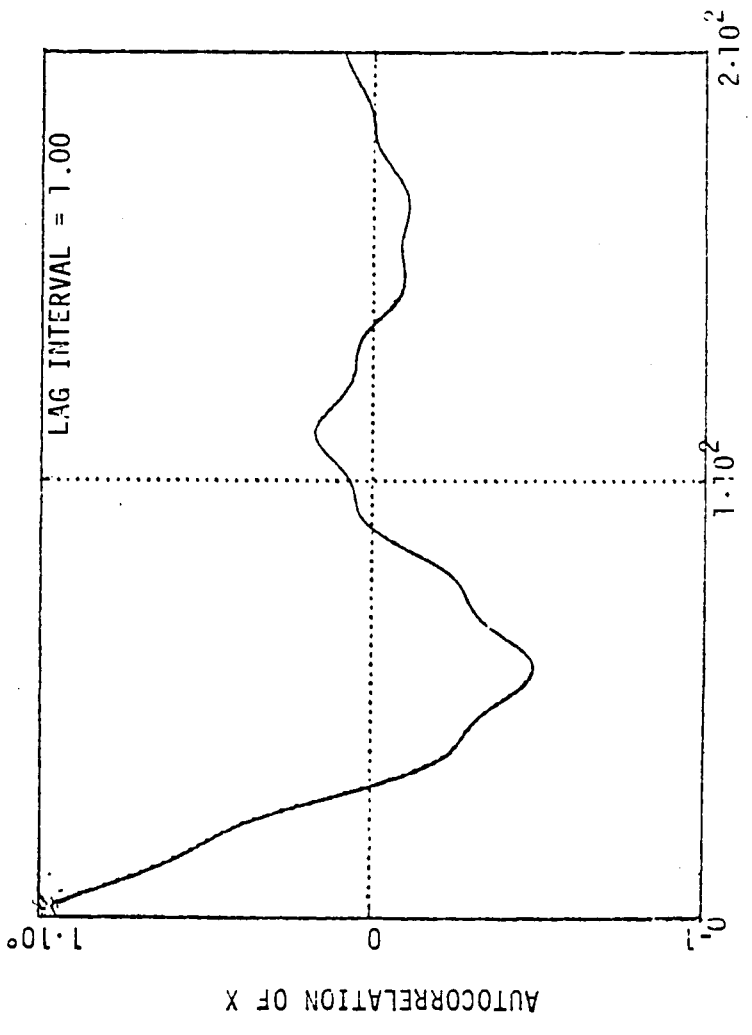


Figure 4. Autocorrelation of Primary Pressure(A).

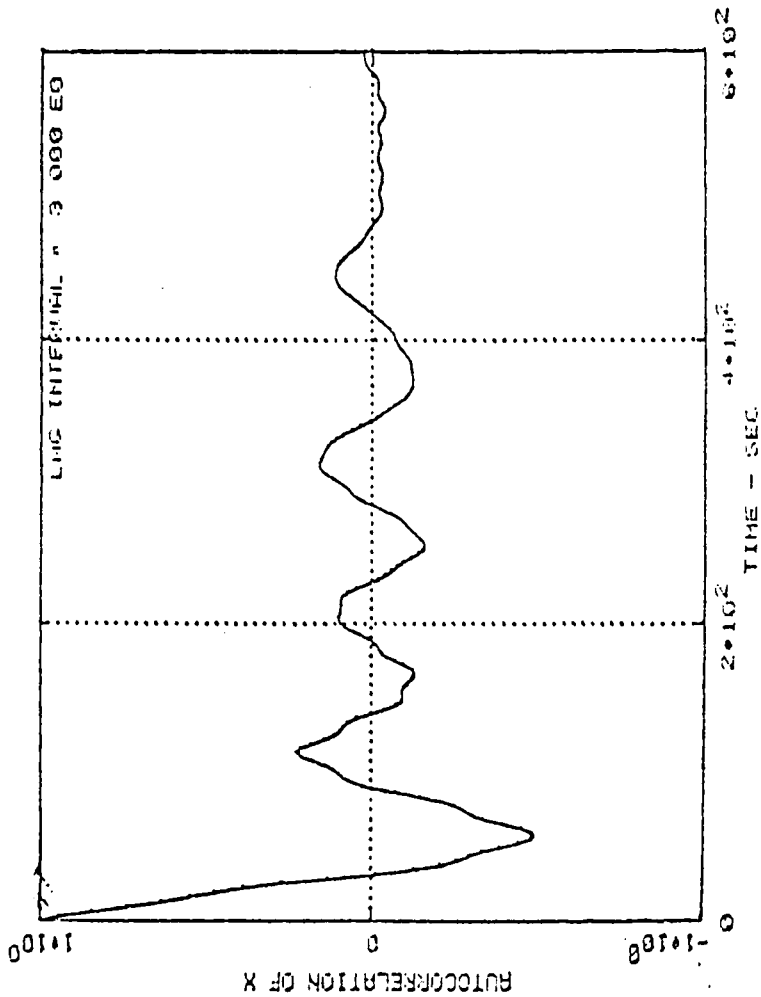


Figure 5. Autocorrelation of Primary Pressure(B).

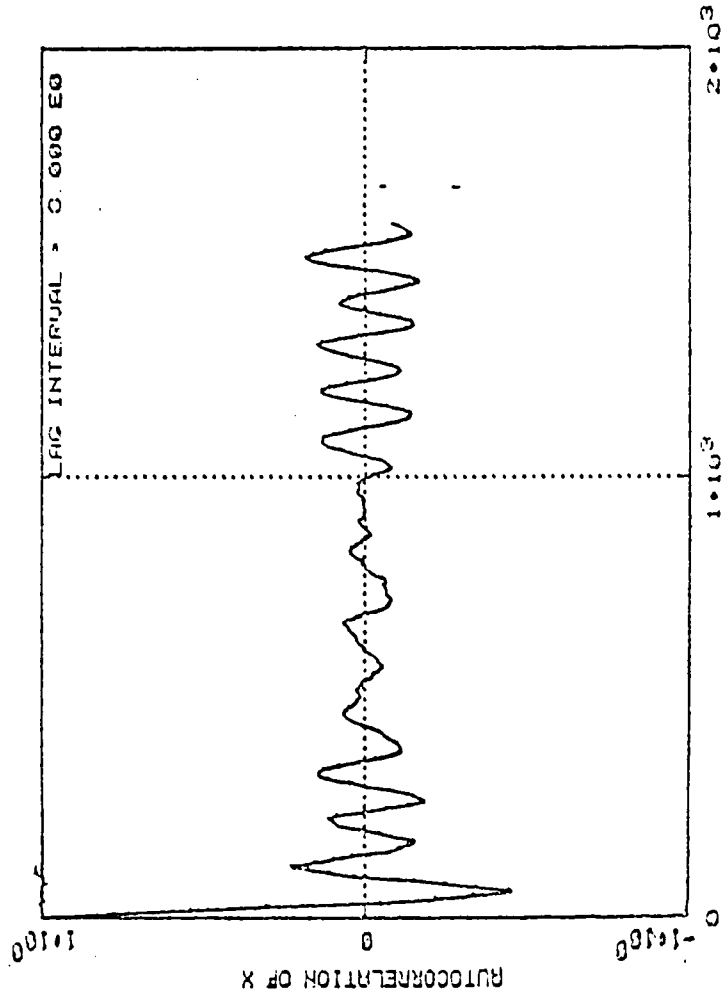


Figure 6. Autocorrelation of Primary Pressure(C).

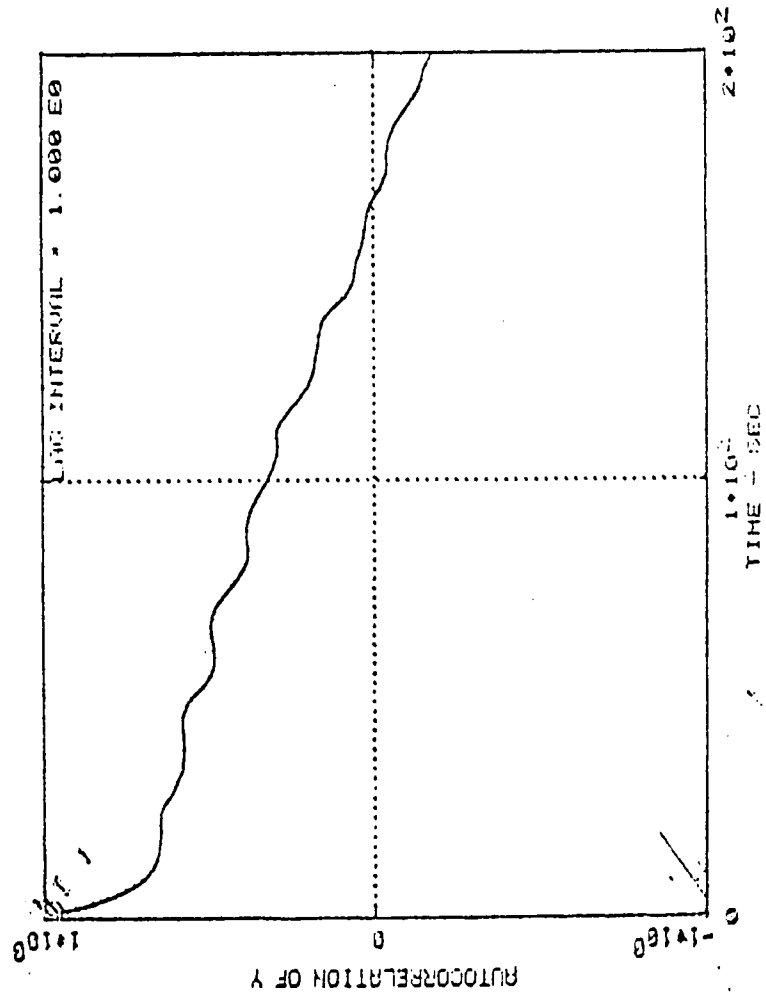


Figure 7. Autocorrelation of Cold Leg Temperature

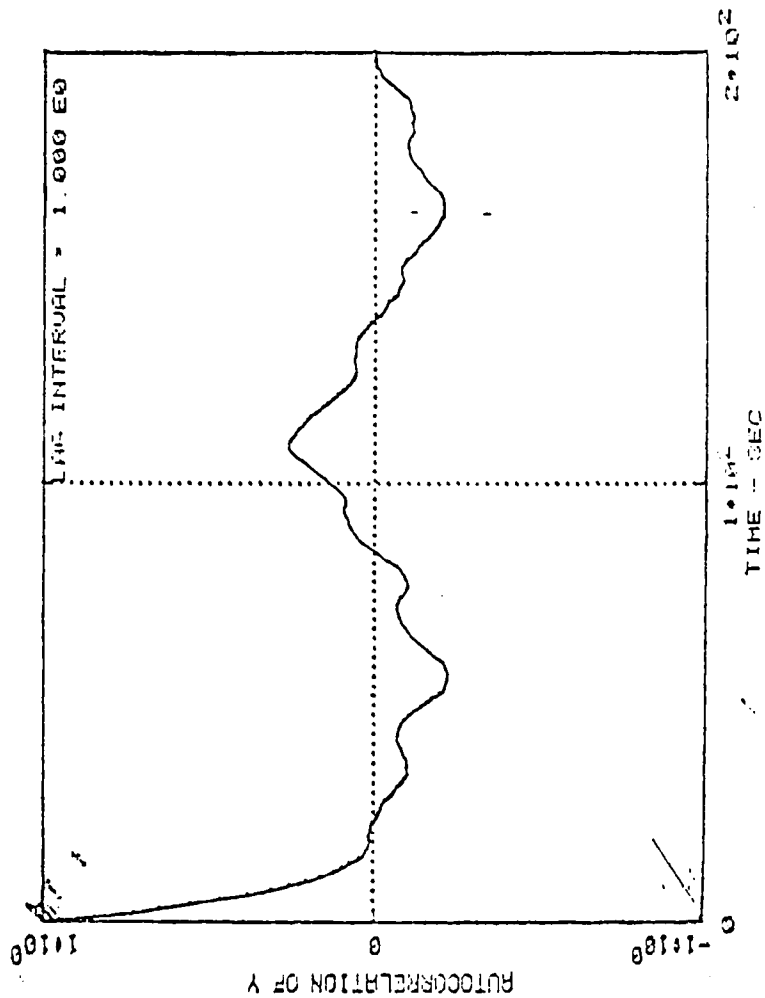


Figure 8. Autocorrelation of Feed Water Flow Rate.

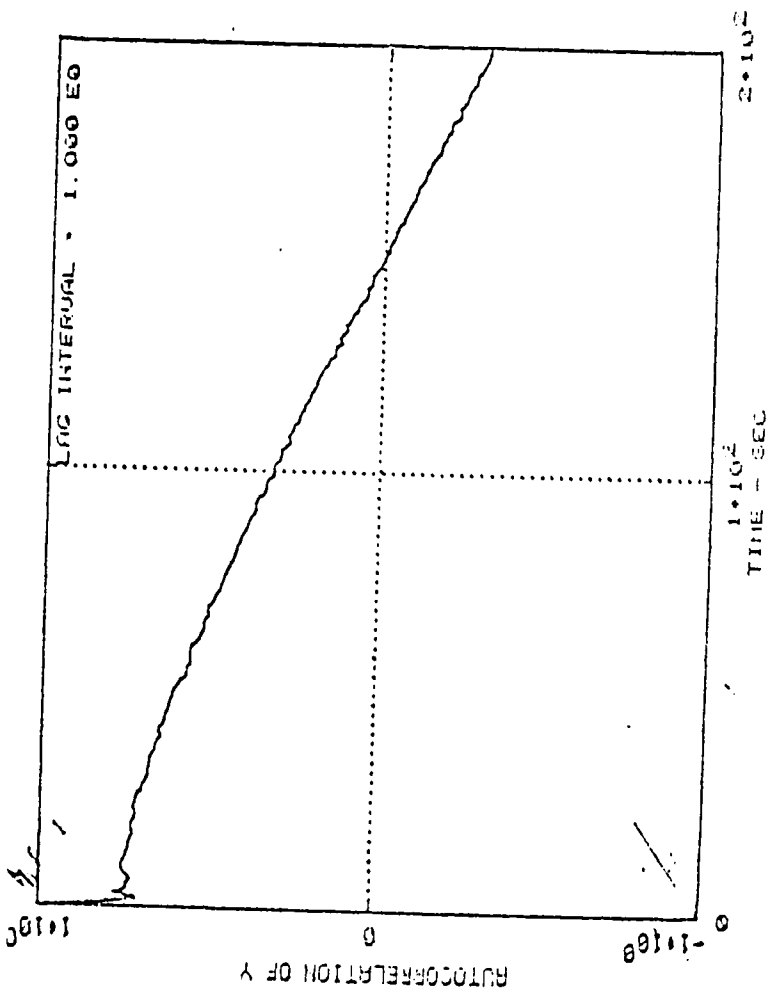


Figure 3. Autocorrelation of Power.

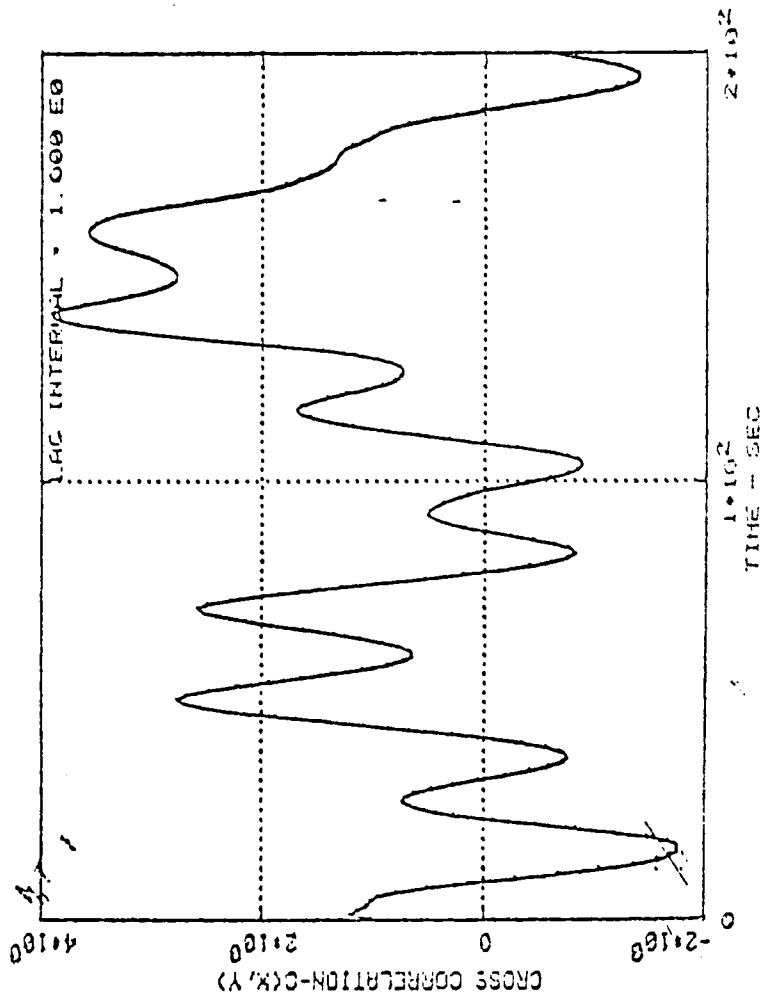


Figure 10. Cross-Correlation of Primary Pressure Versus Cold Leg Temperature

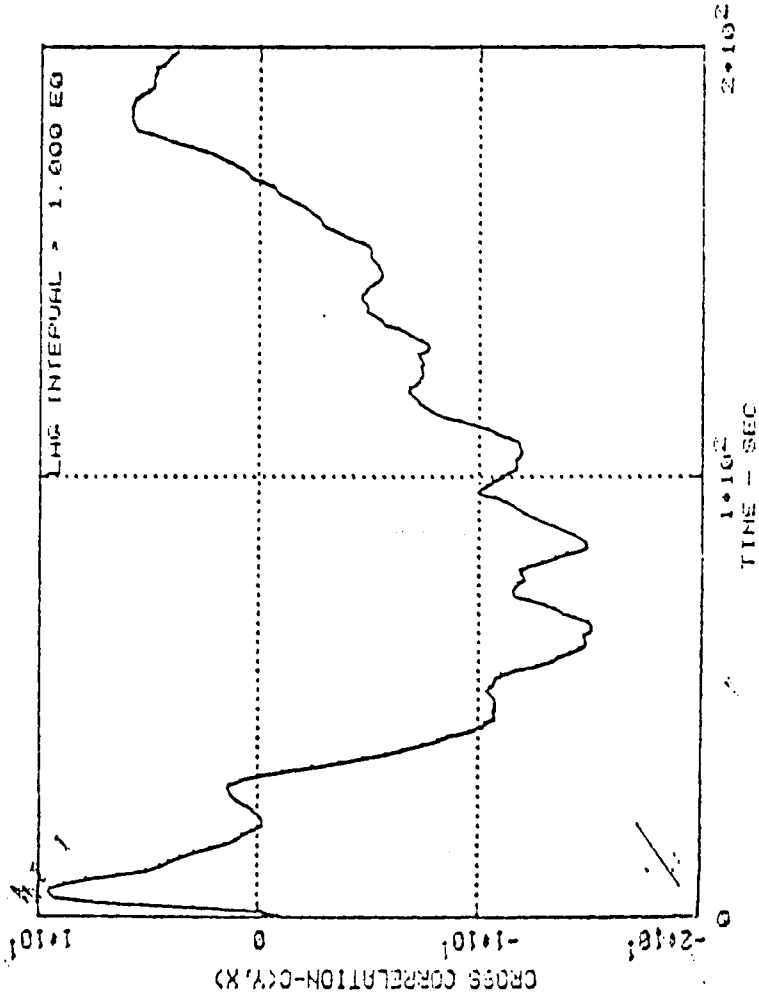


Figure 11. Cross-Correlation of Primary Pressure Versus Power.

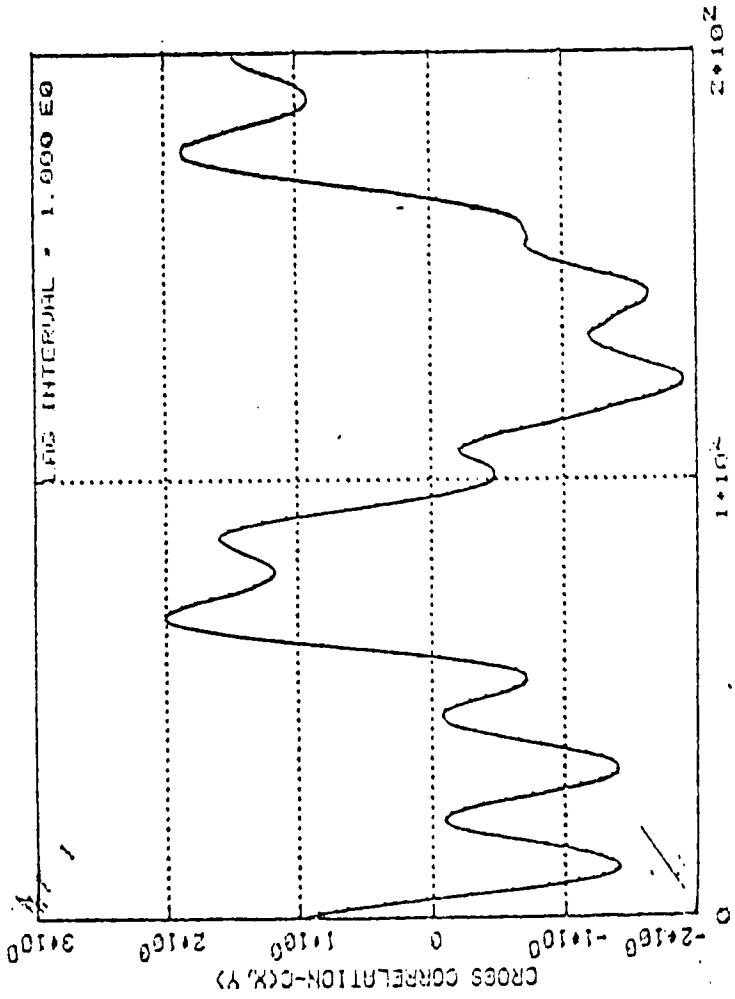


Figure 12. Cross-Correlation of Primary Pressure Versus Feed Water Flow Rate.

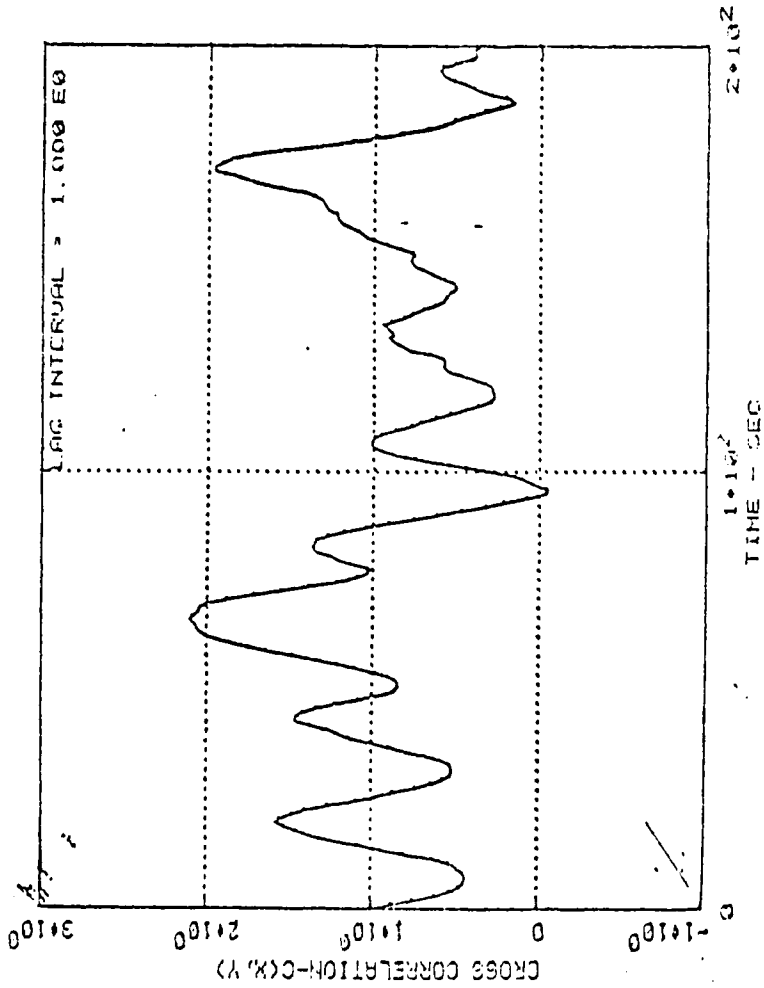


Figure 13. Cross-Correlation of Cold Leg Temperature Versus Feed Water Flow Rate.

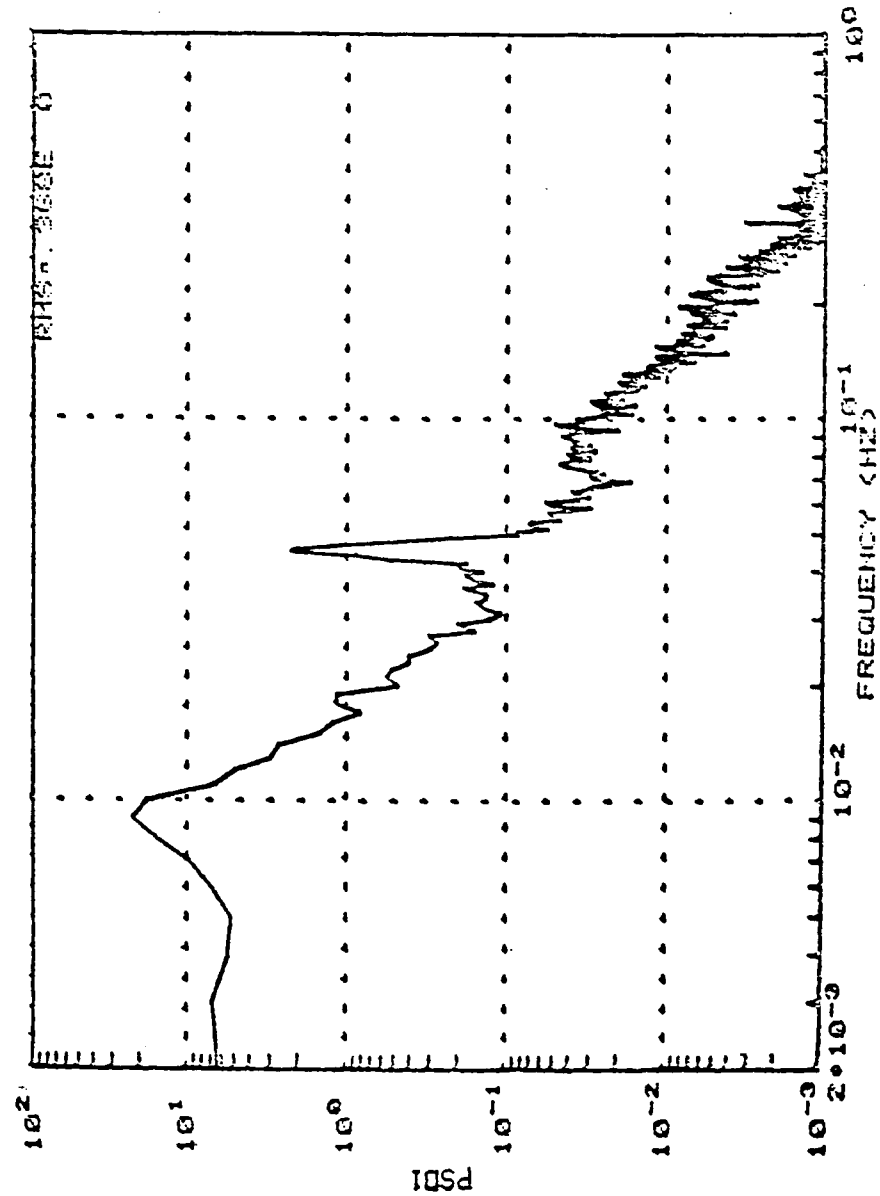


Figure 14. Power Spectrum of Primary Pressure (FFT).

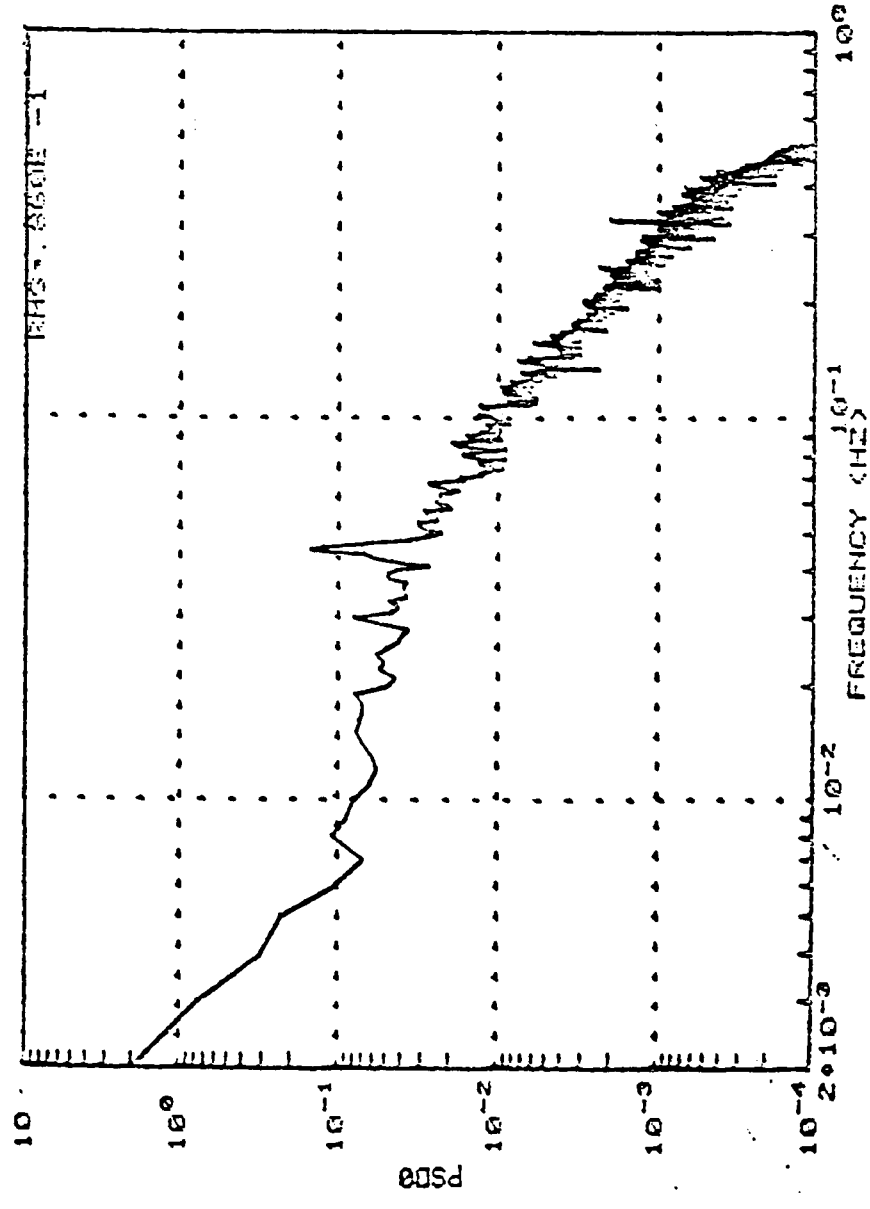


Figure 15. Power Spectrum of Cold Leg Temperature (FFT).

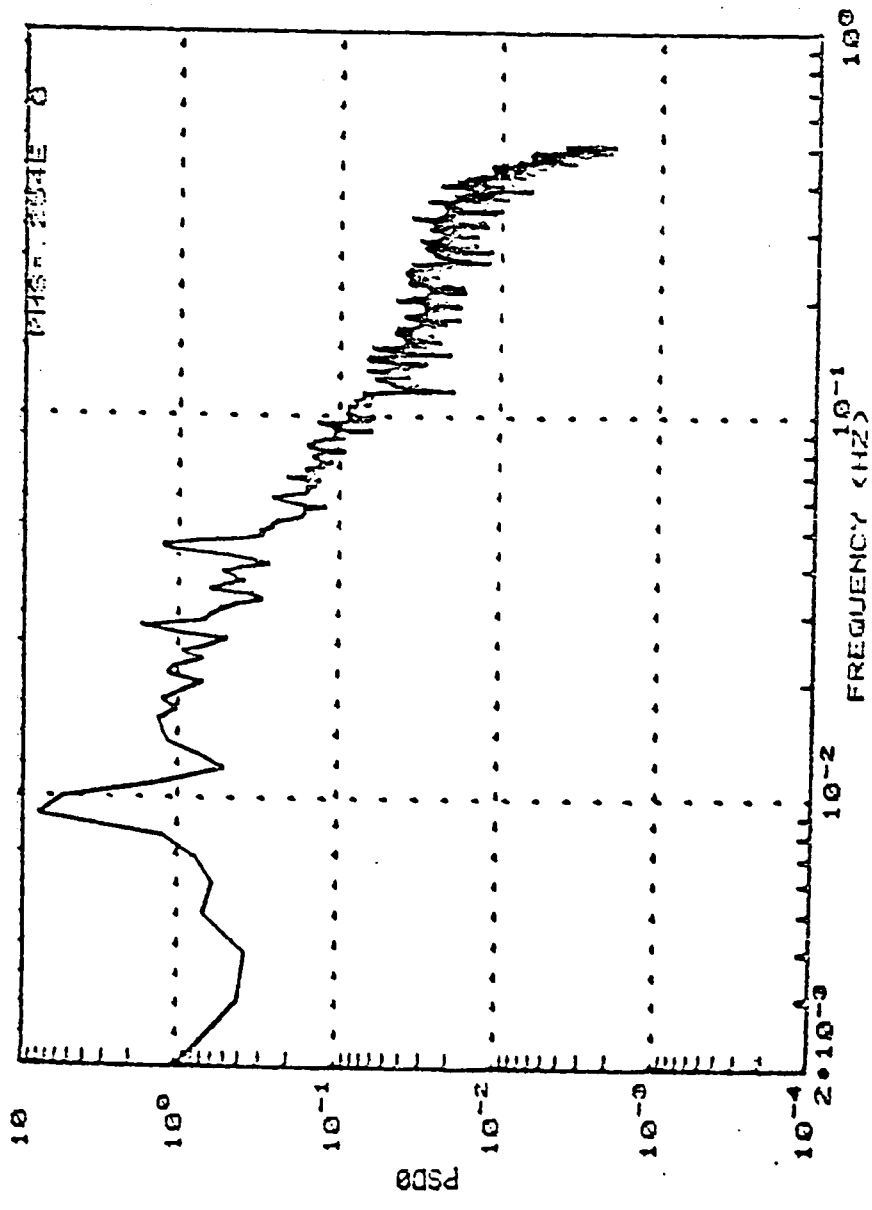


Figure 16. Power Spectrum of Feed Water Flow Rate (FFT).

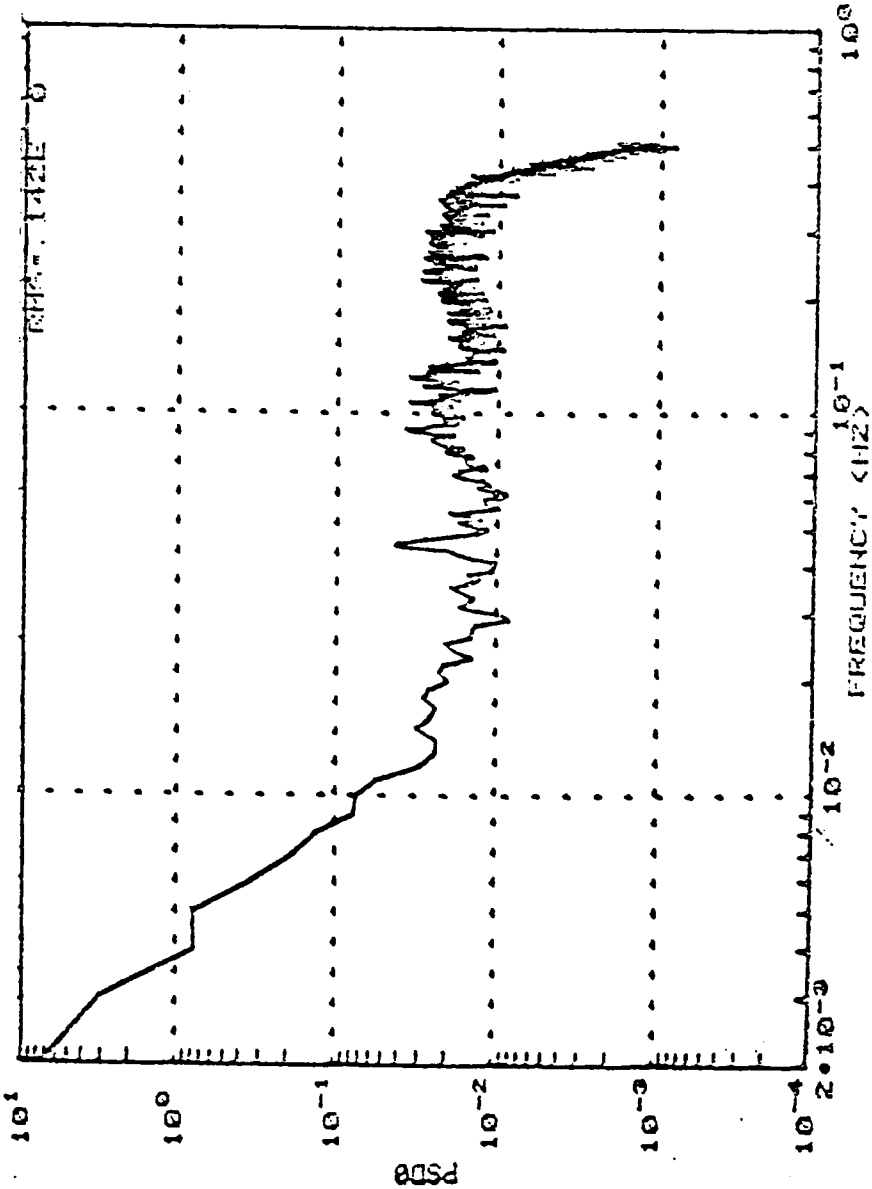


Figure 17. Power Spectrum of Power (FFT).

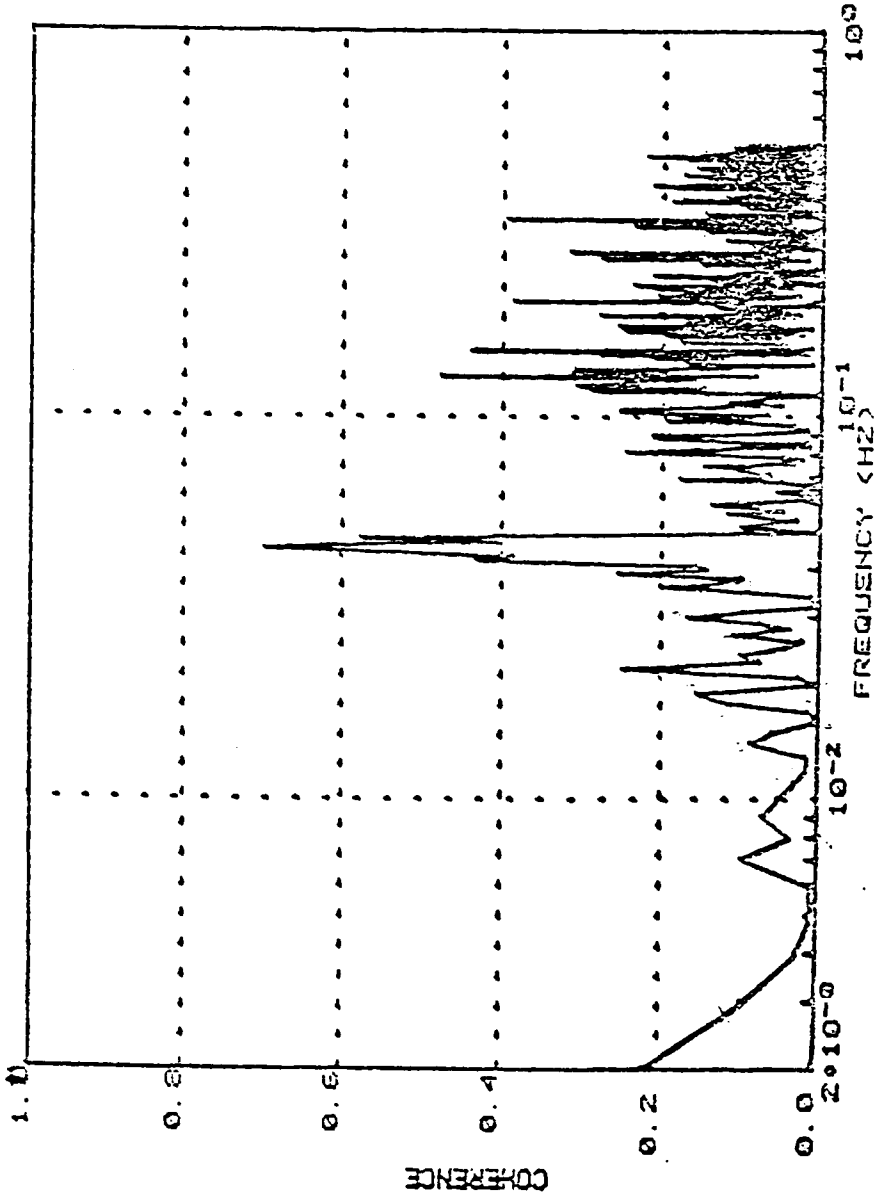


Figure 18. Coherence of Cold Leg Temperature Versus Primary Pressure (FFT).

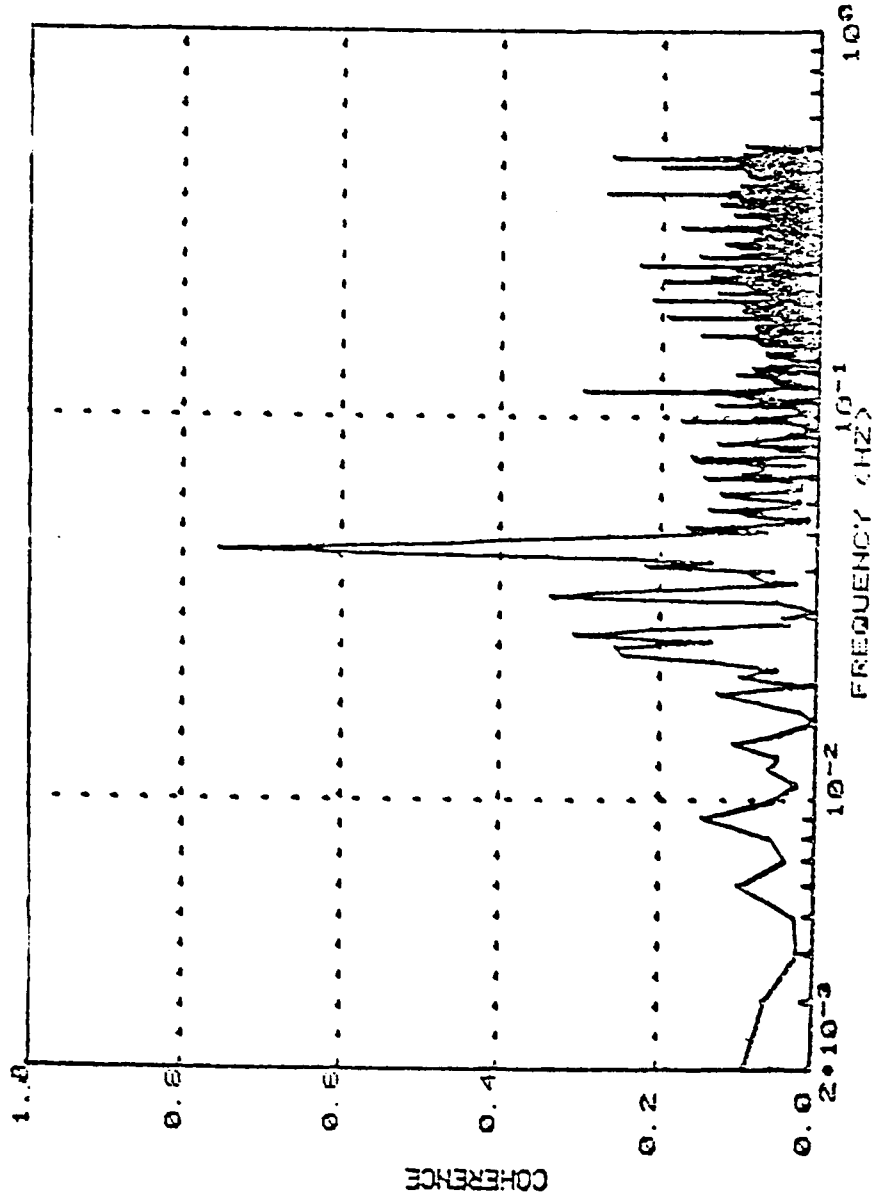


Figure 19. Coherence of Feed Water Flow Rate Versus Primary Pressure. (FFT).

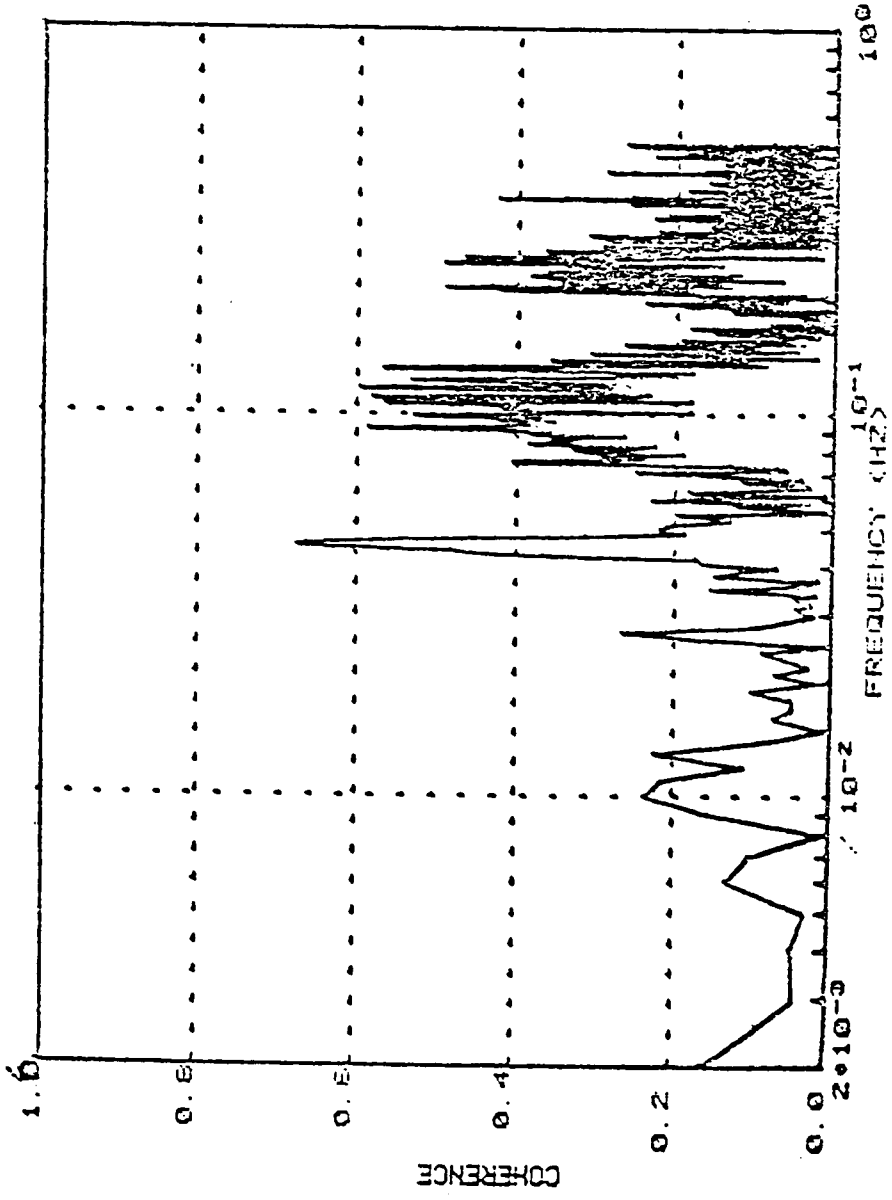


Figure 20. Coherence of Power Versus Primary Pressure (FFT).

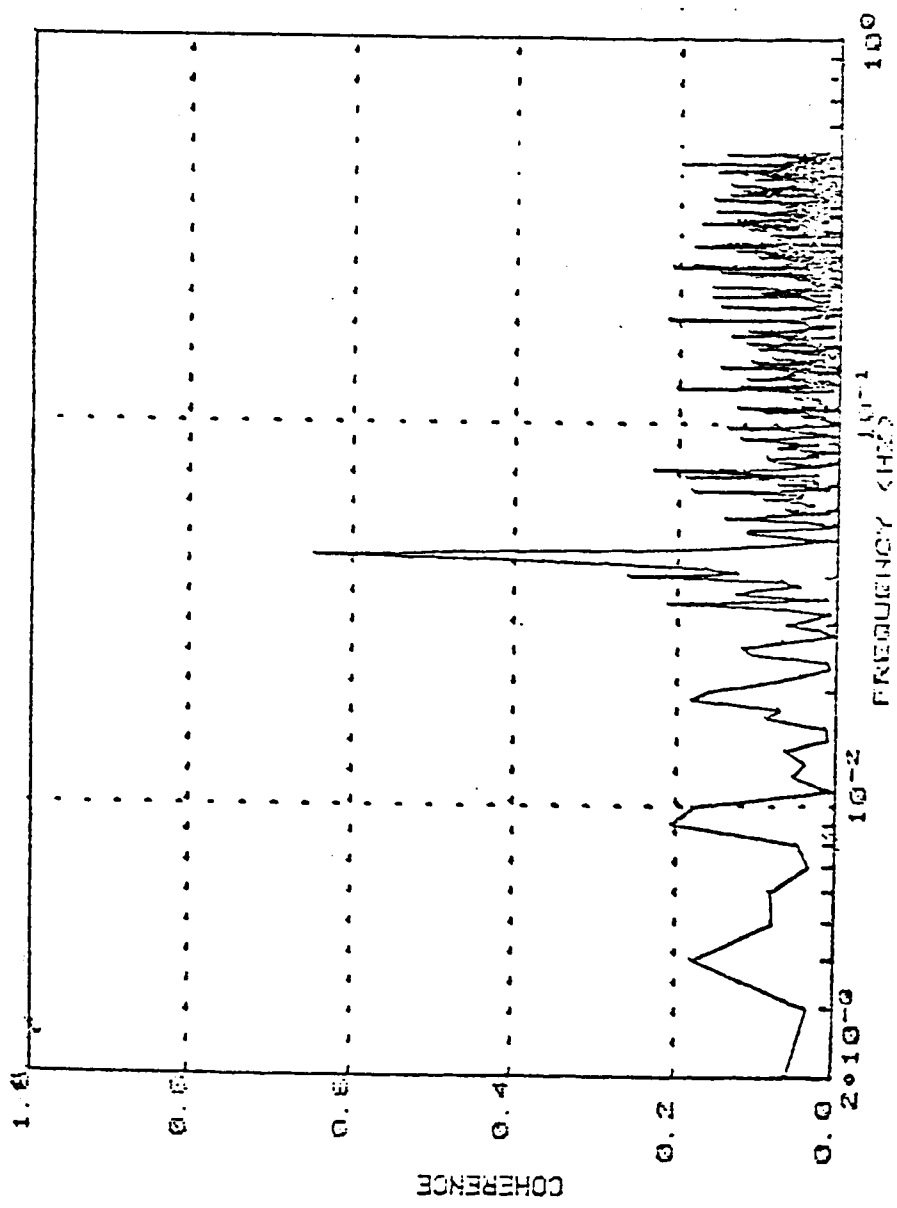


Figure 21. Coherence of Cold Leg Temperature Versus Feed Water Flow Rate (FFT).

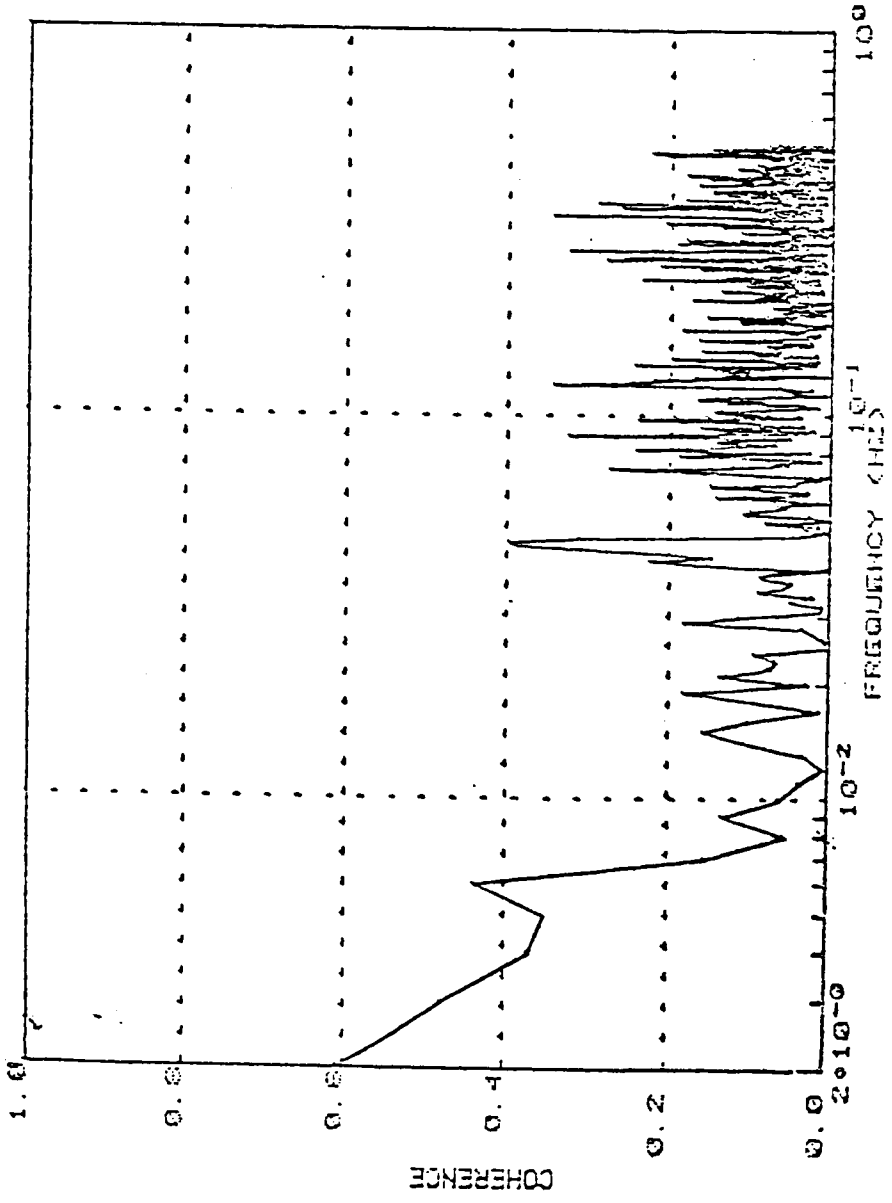


Figure 22. Coherence of Power Versus Cold Leg Temperature (FFT).

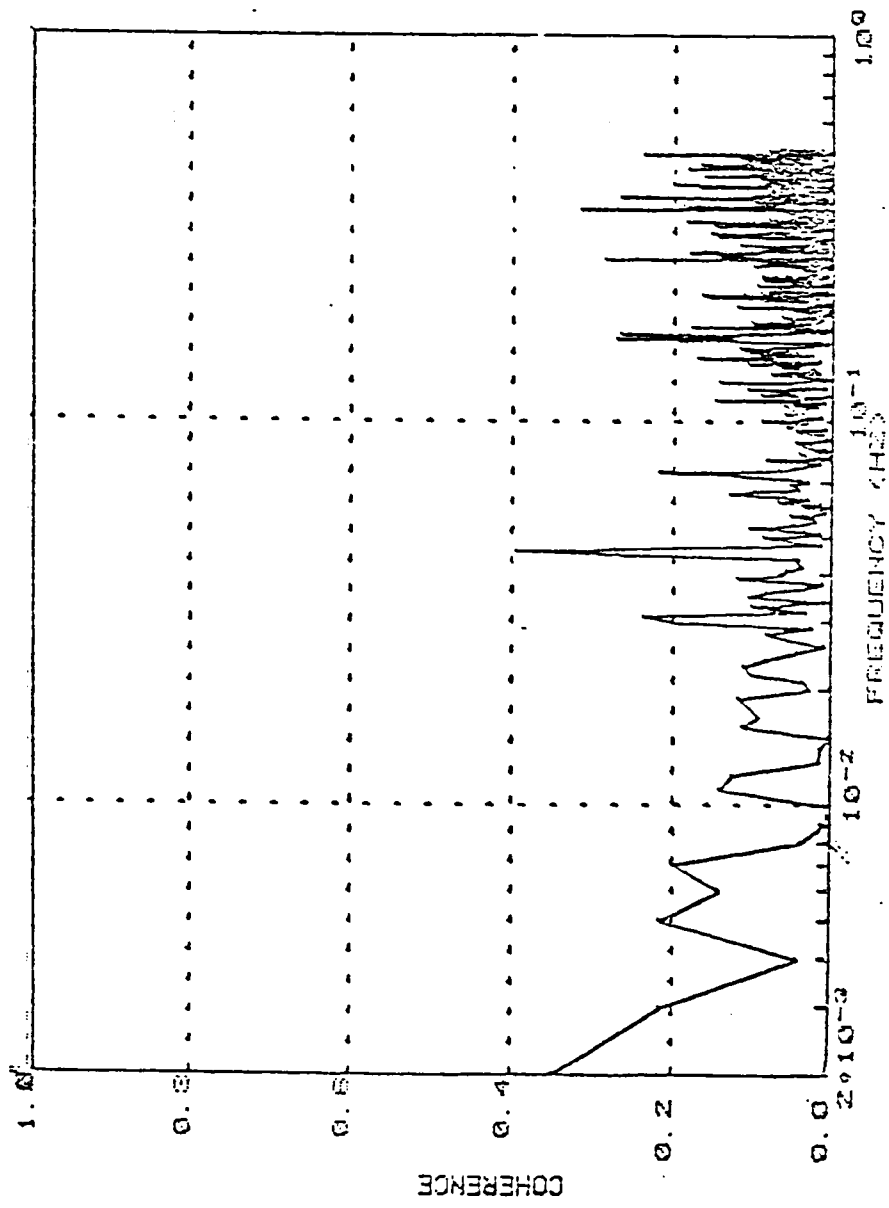


Figure 23. Coherence of Power Versus Feed Water Flow Rate (FFT).

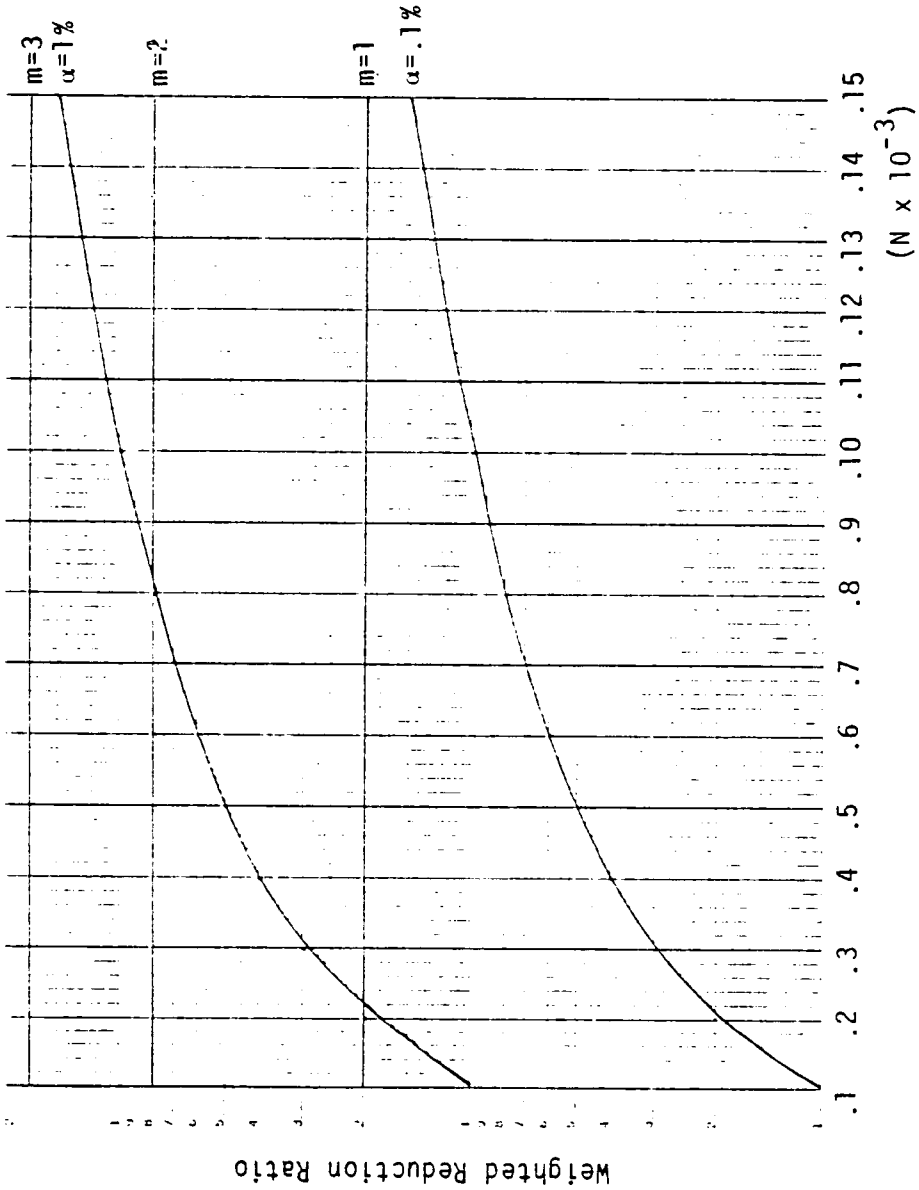


Figure 24. Plot of Nα versus N. (A).

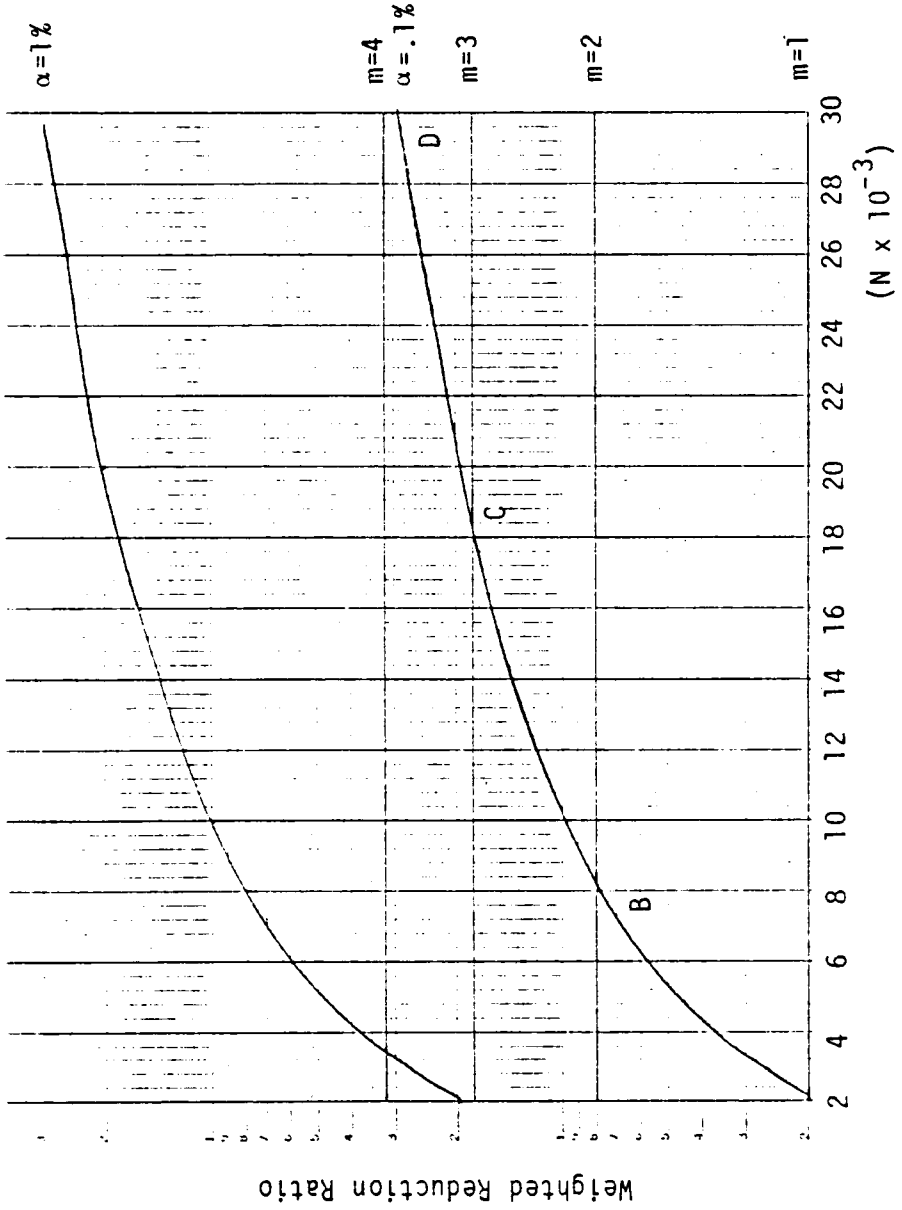


Figure 25. Plot of Nα Versus N (B).

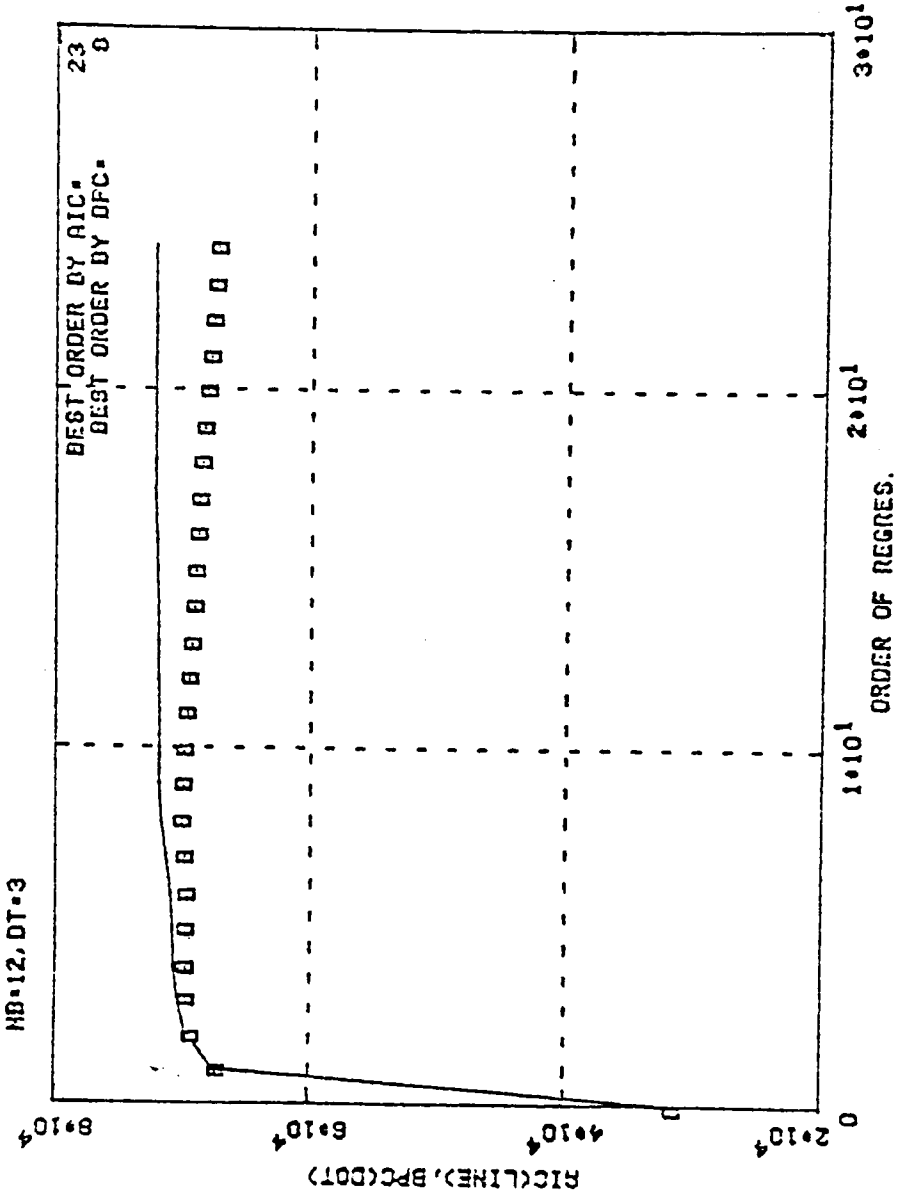


Figure 26. Predicted Optimal Order for Four Variables ($\Delta t=3$).

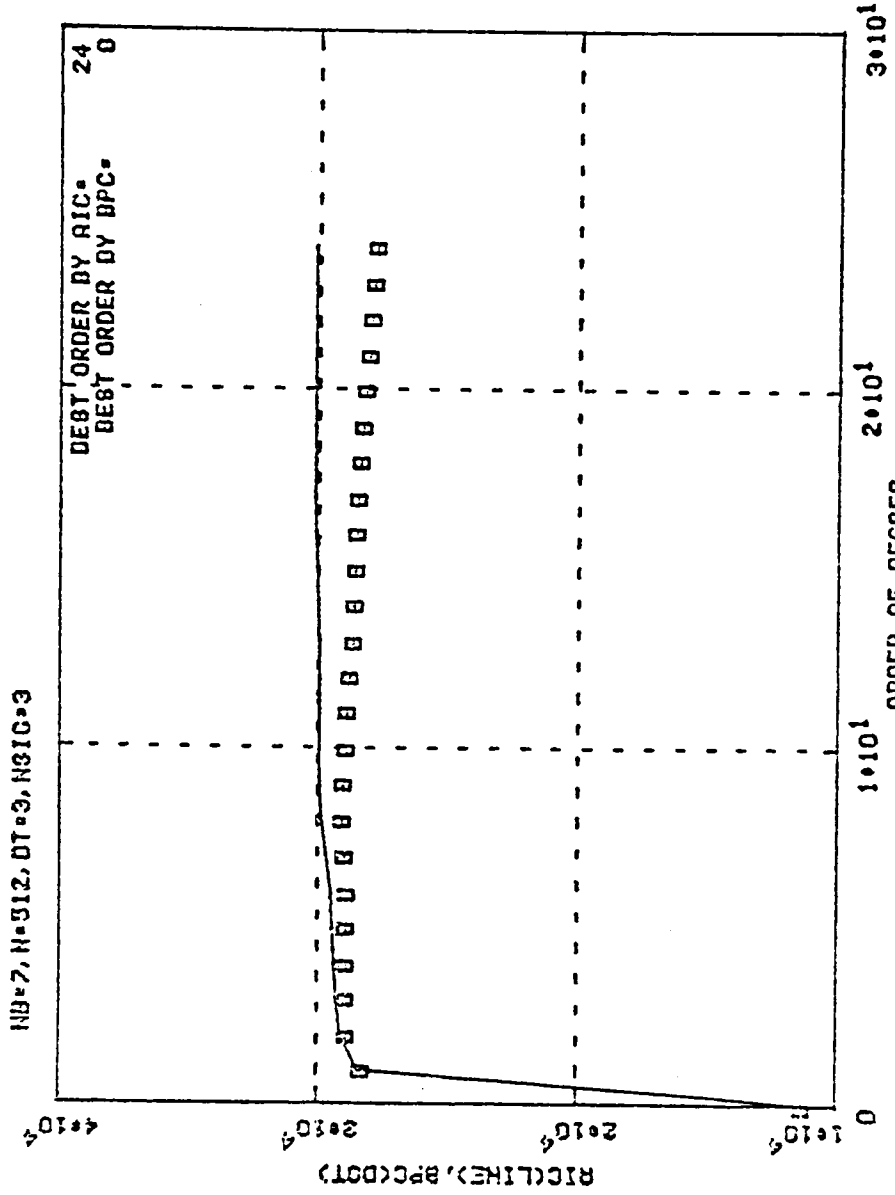


Figure 27. Predicted Optimal Order for Three Variables.

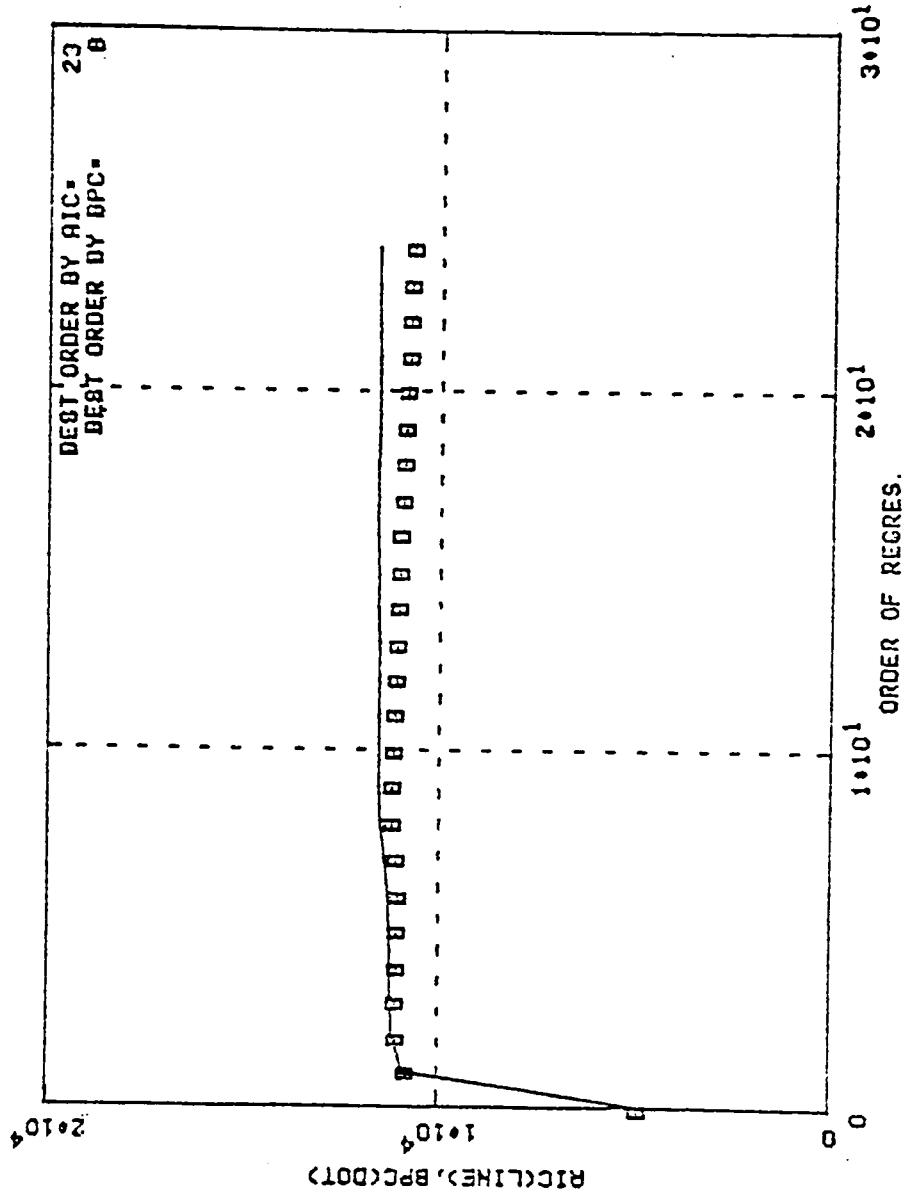


Figure 28. Predicted Optimal Order for Two Variables.

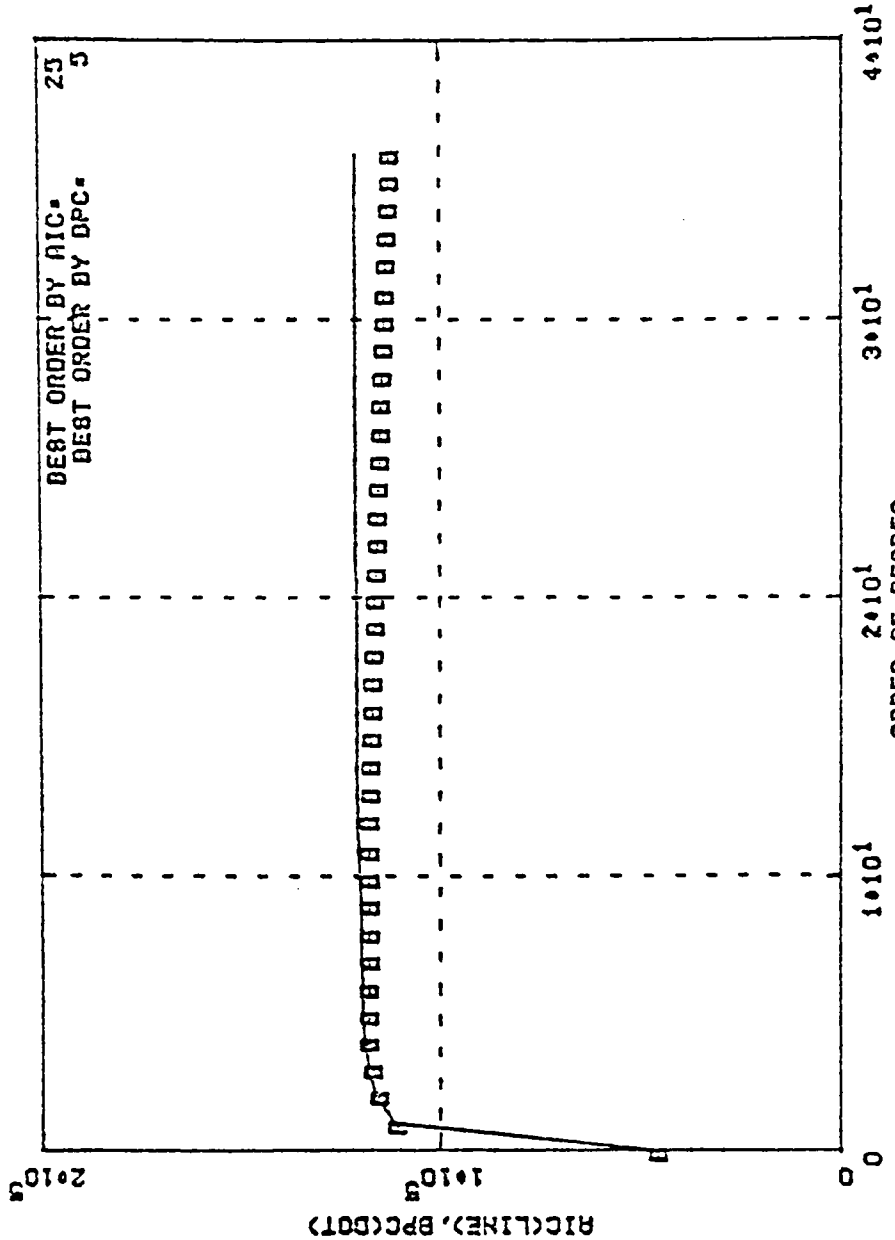


Figure 29. Predicted Optimal Order for Four Variables ($\Delta t=2$).

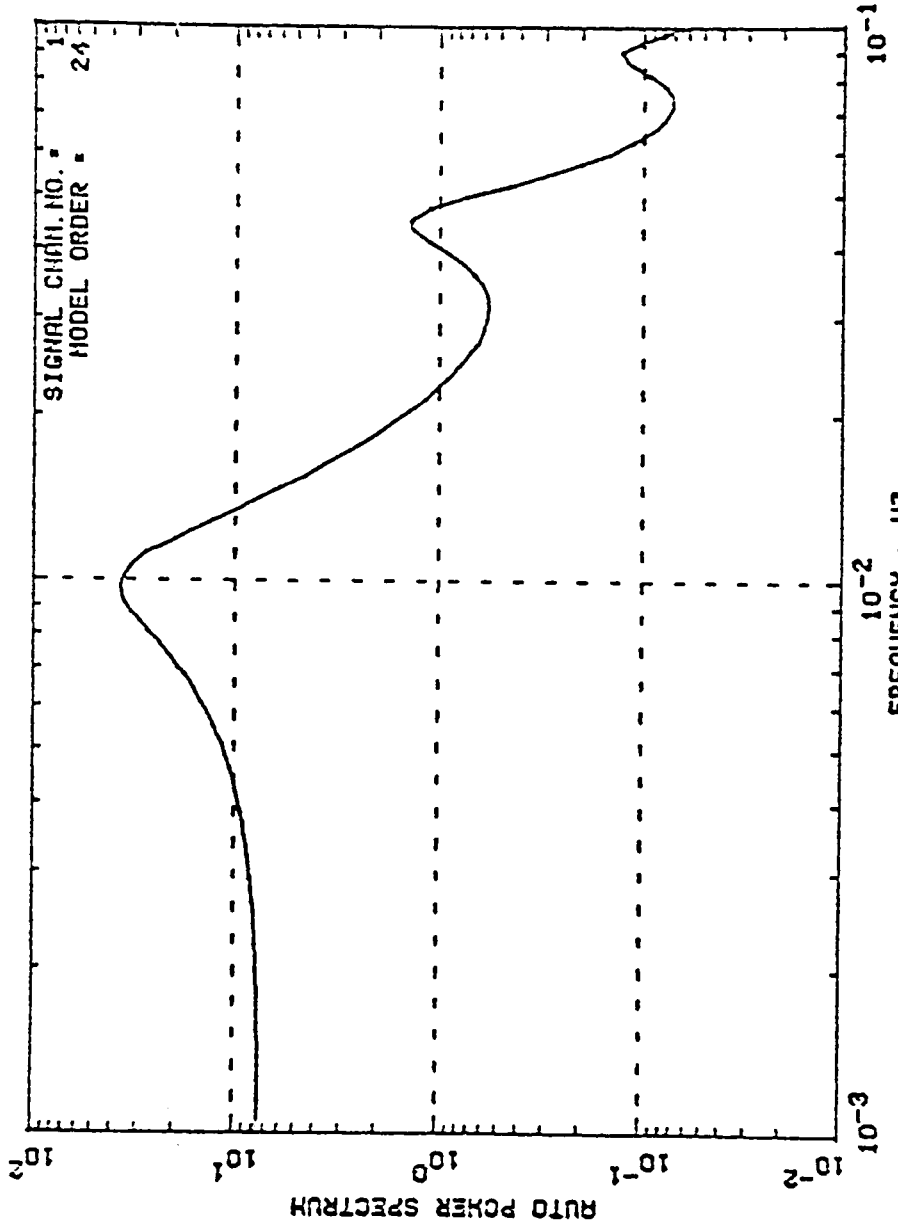


Figure 30. Power Spectrum of Primary Pressure (Case 1).

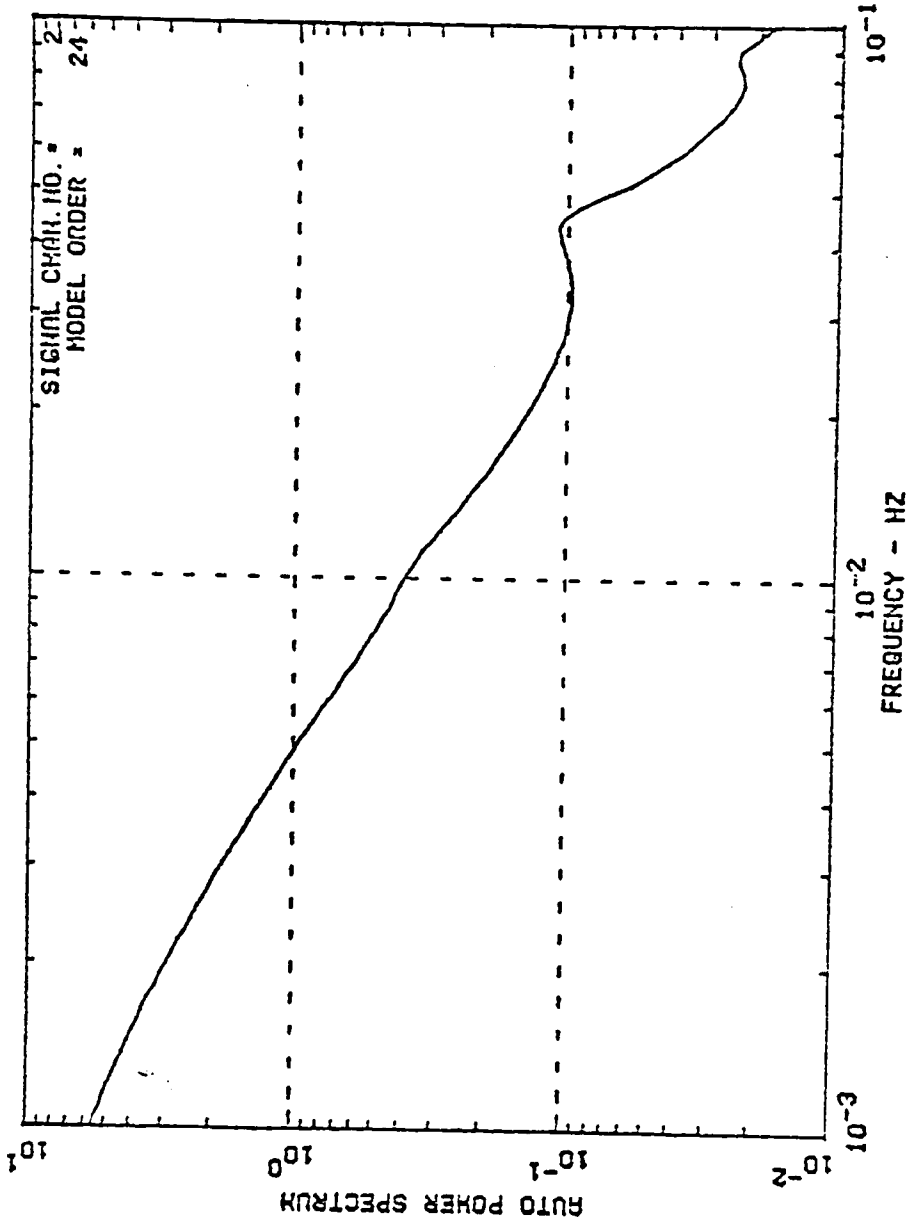


Figure 31. Power Spectrum of Cold Leg Temperature (Case 1).

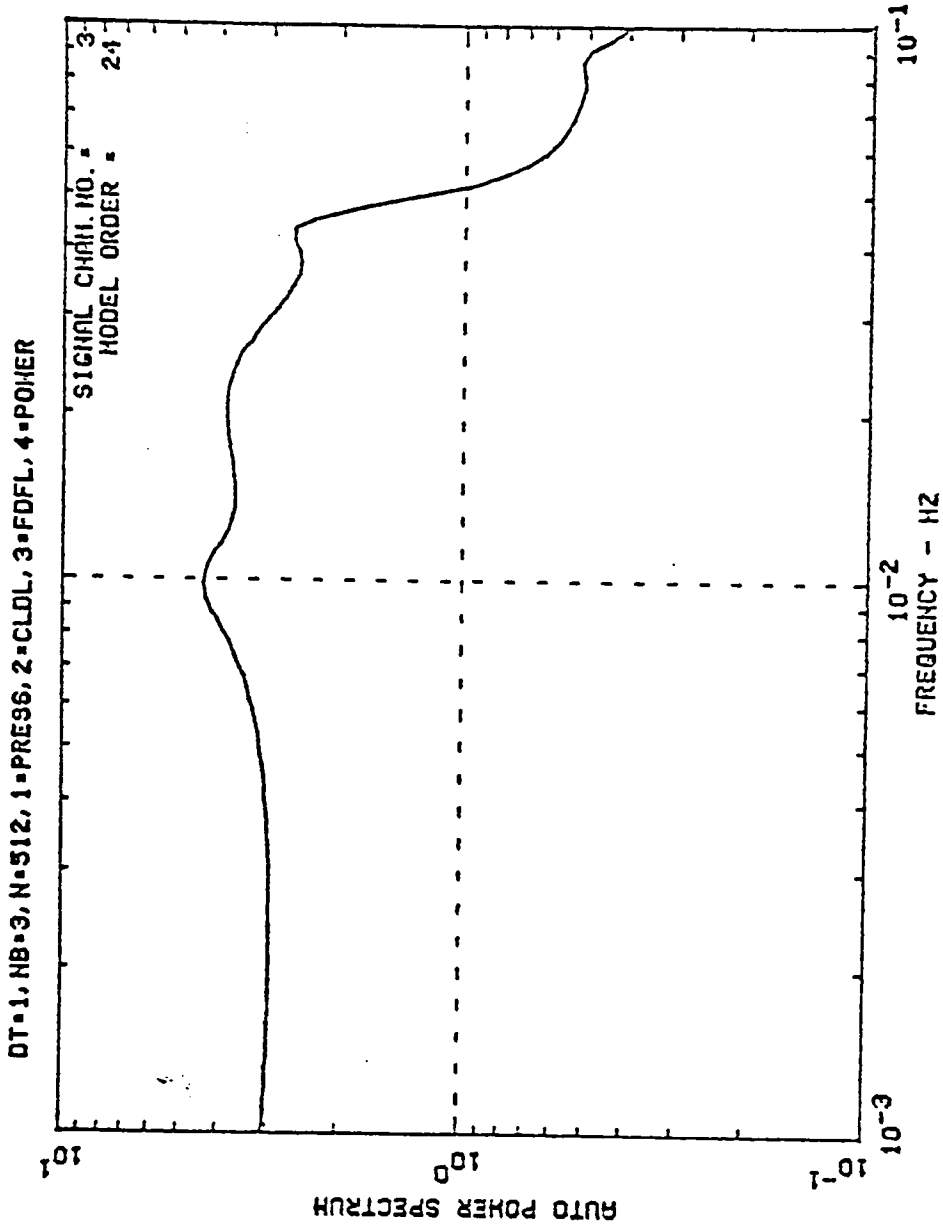


Figure 32. Power Spectrum of Feed Water Flow Rate (Case 1).

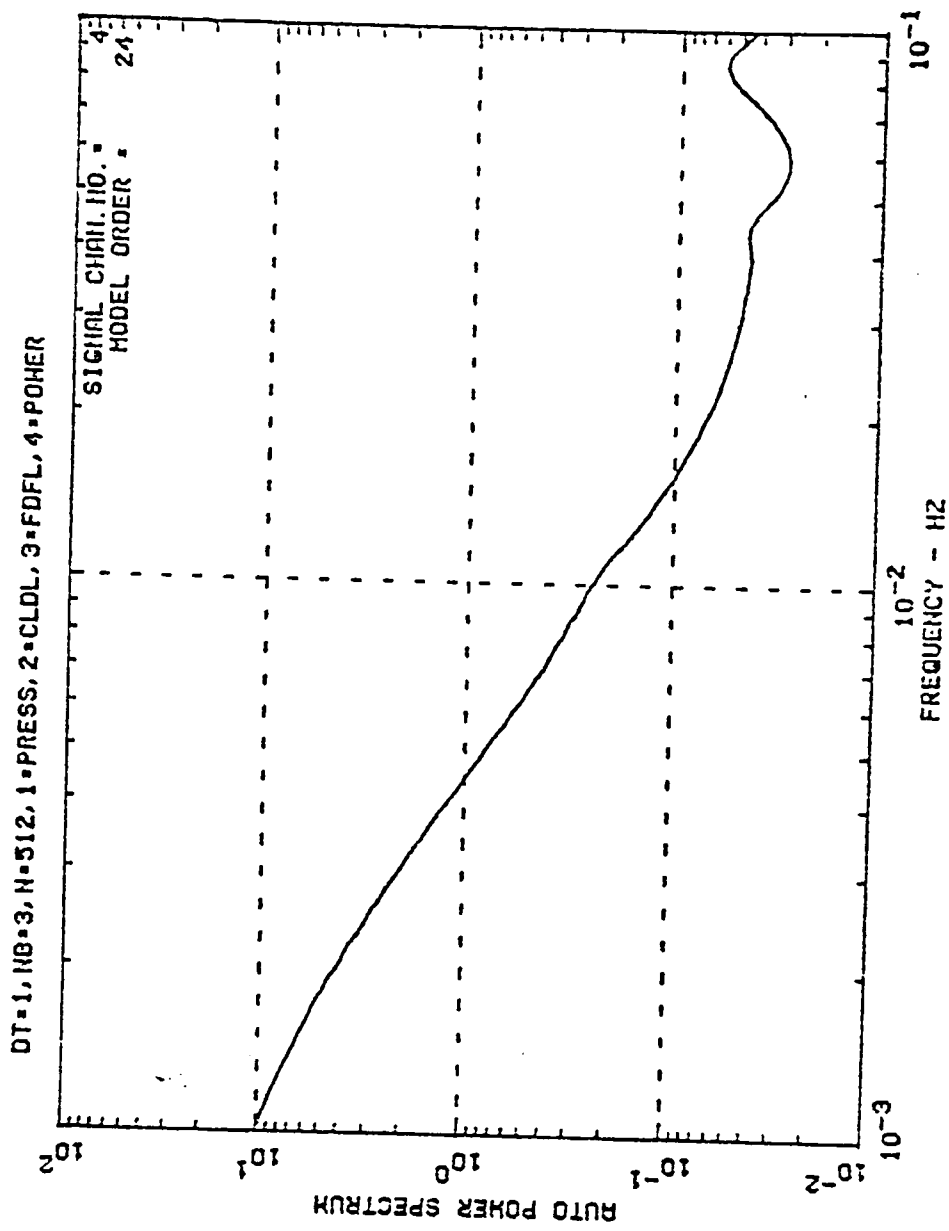


Figure 33. Power Spectrum of Power (Case 1).

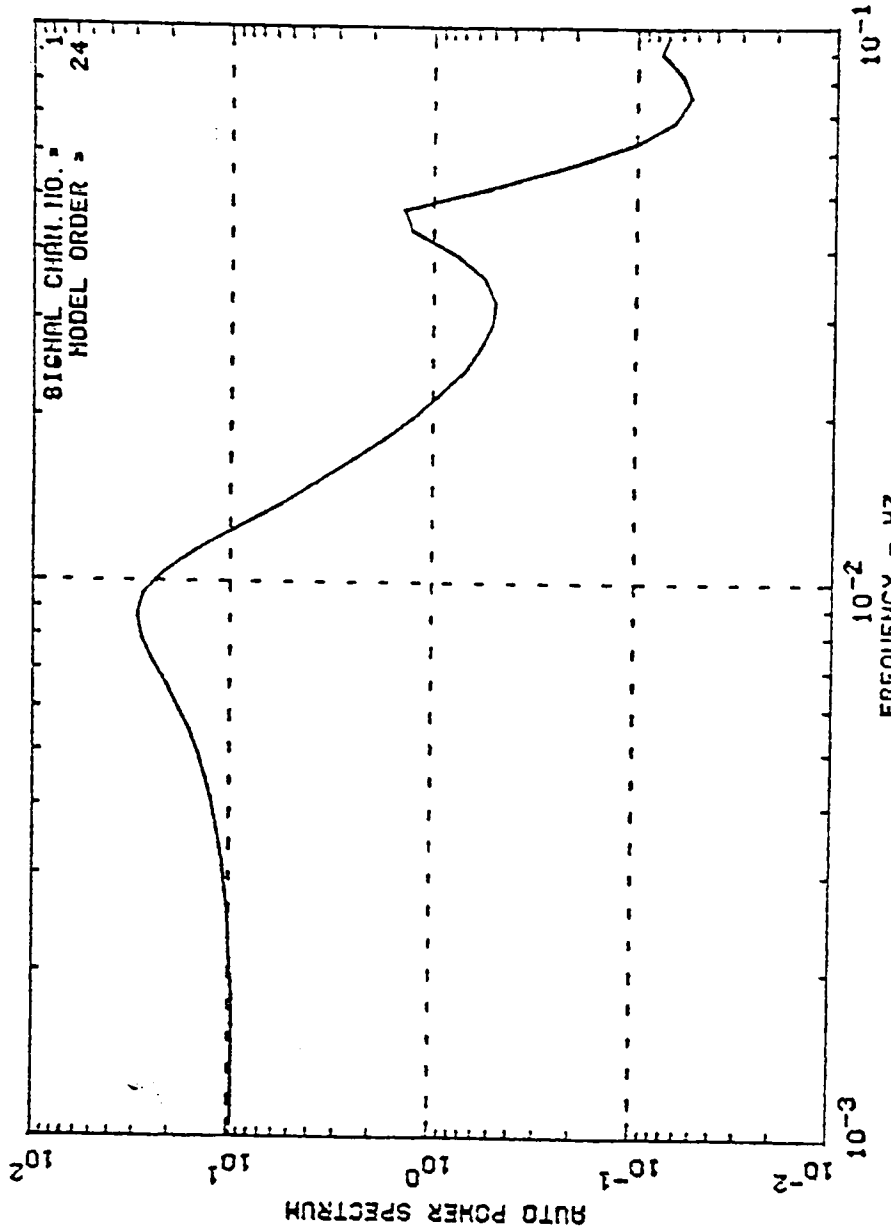


Figure 34. Power Spectrum of Primary Pressure (Case 2).

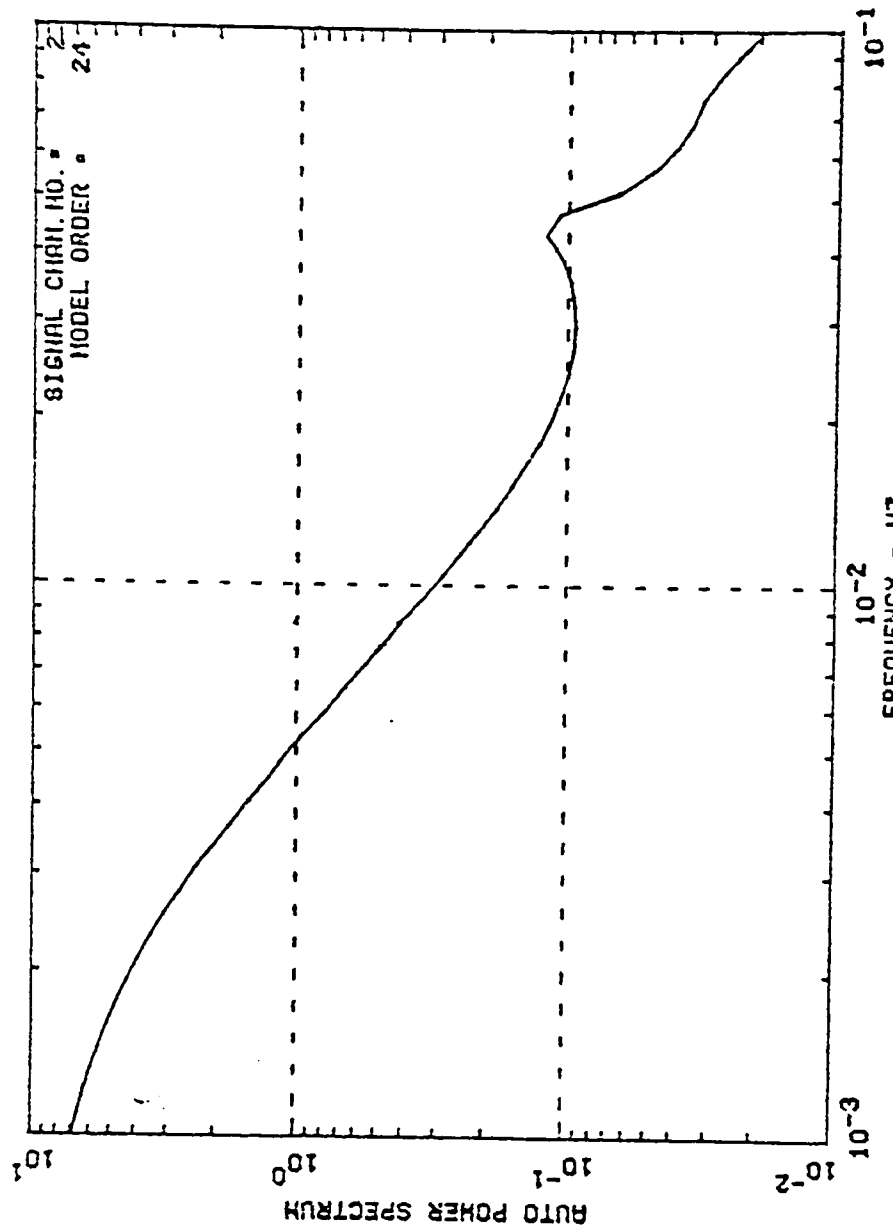


Figure 35. Power Spectrum of Cold Leg Temperature (Case 2).

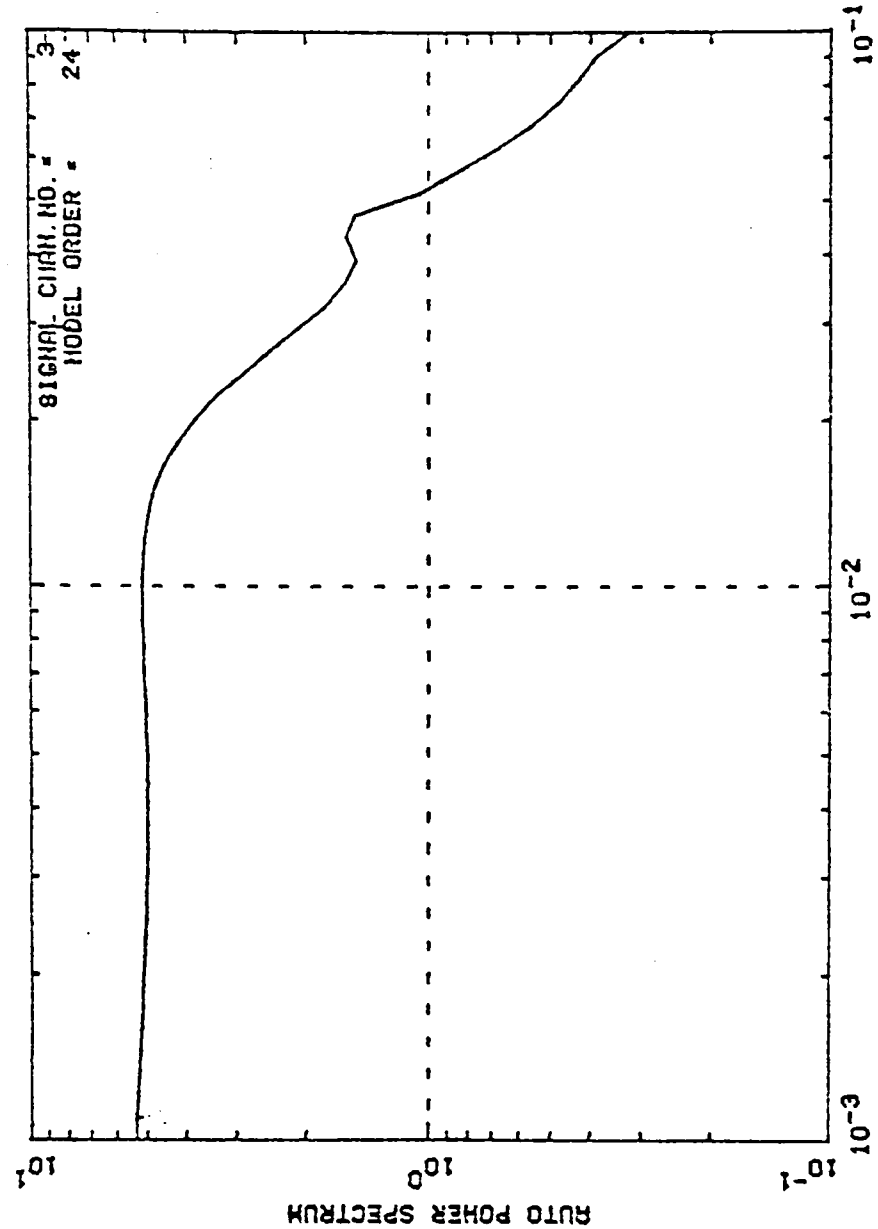


Figure 36. Power Spectrum of Feed Water Flow Rate (Case 2).

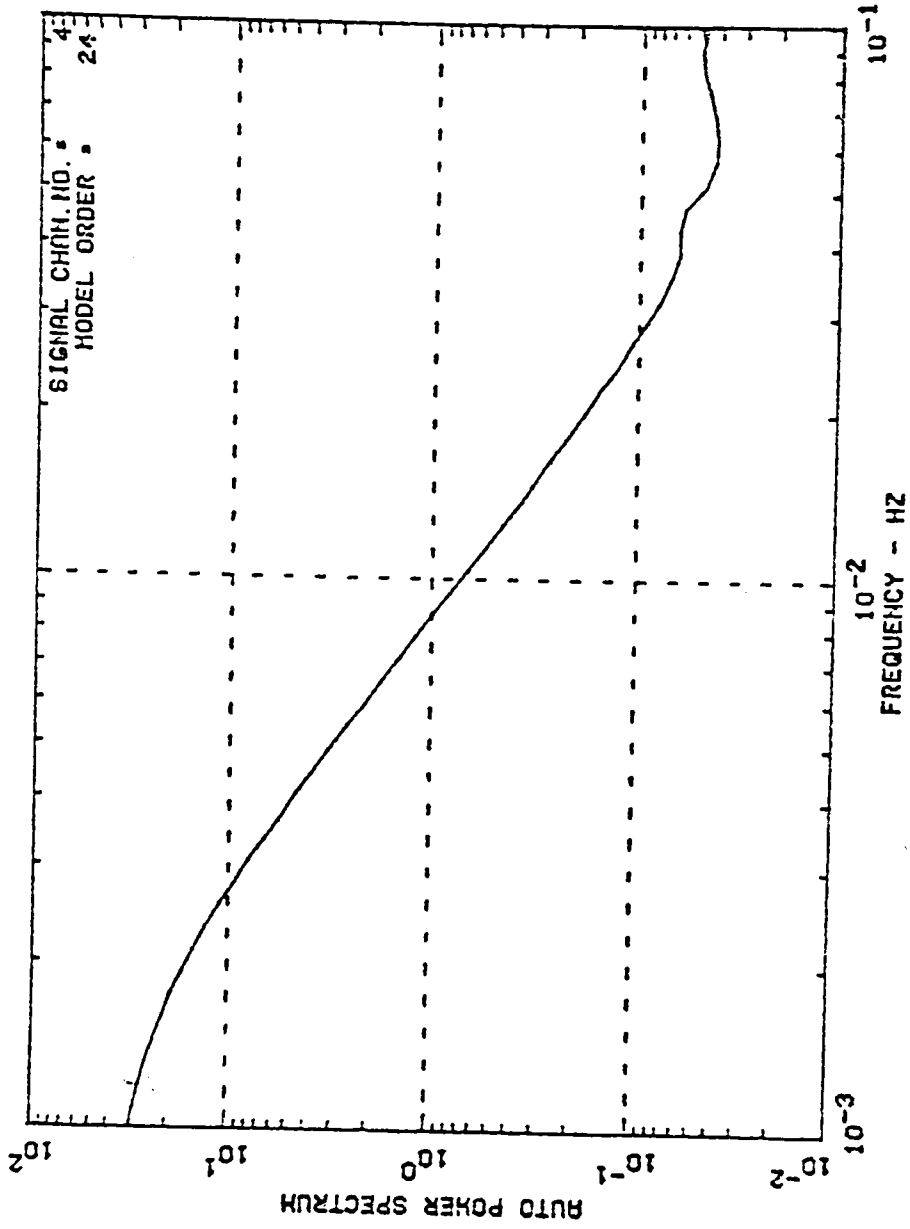


Figure 37. Power Spectrum of Power (Case 2).

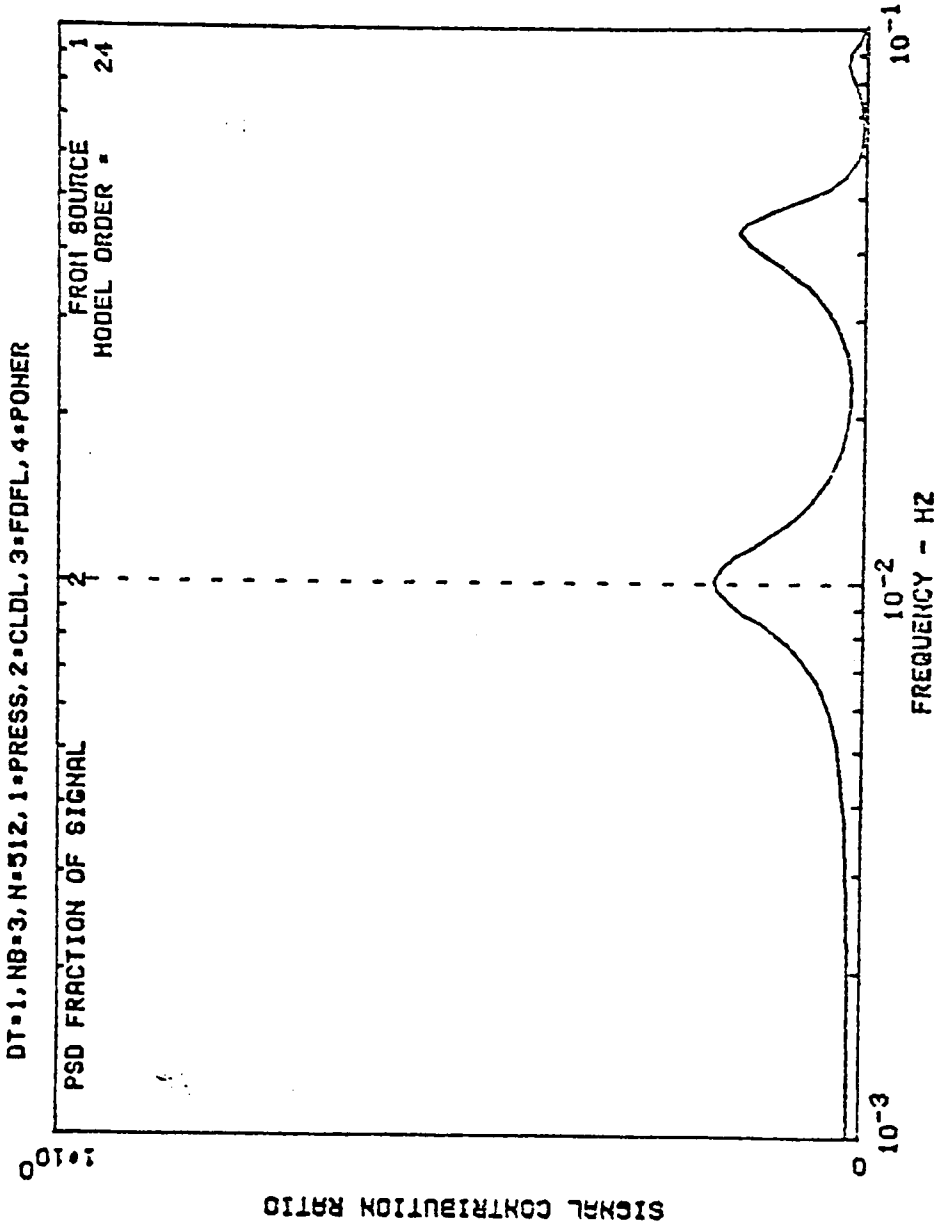


Figure 38. Signal Contribution Ratio from Source One to Cold Leg Temperature (Case 1).

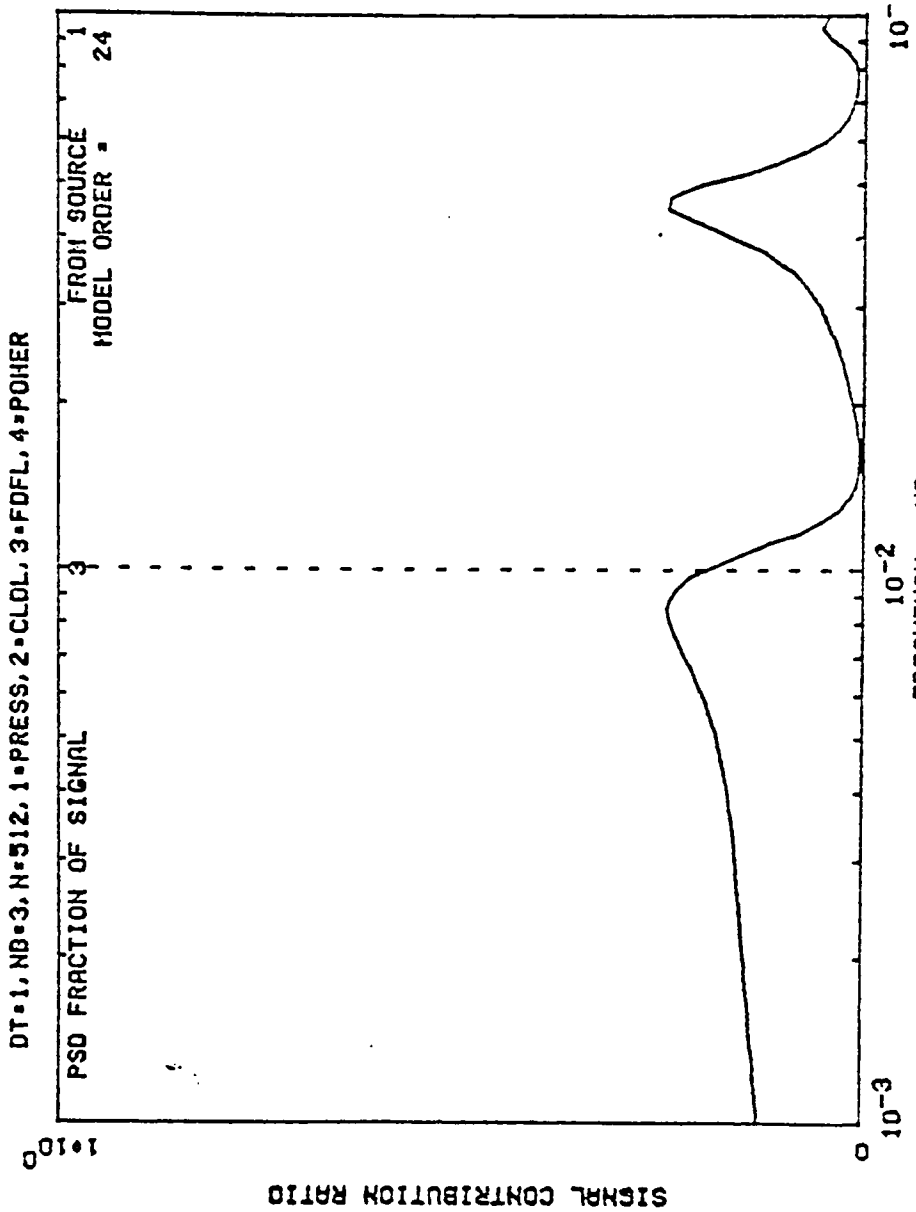


Figure 39. Signal Contribution Ratio from Source One to Feed Water Flow Rate.(Case 1).

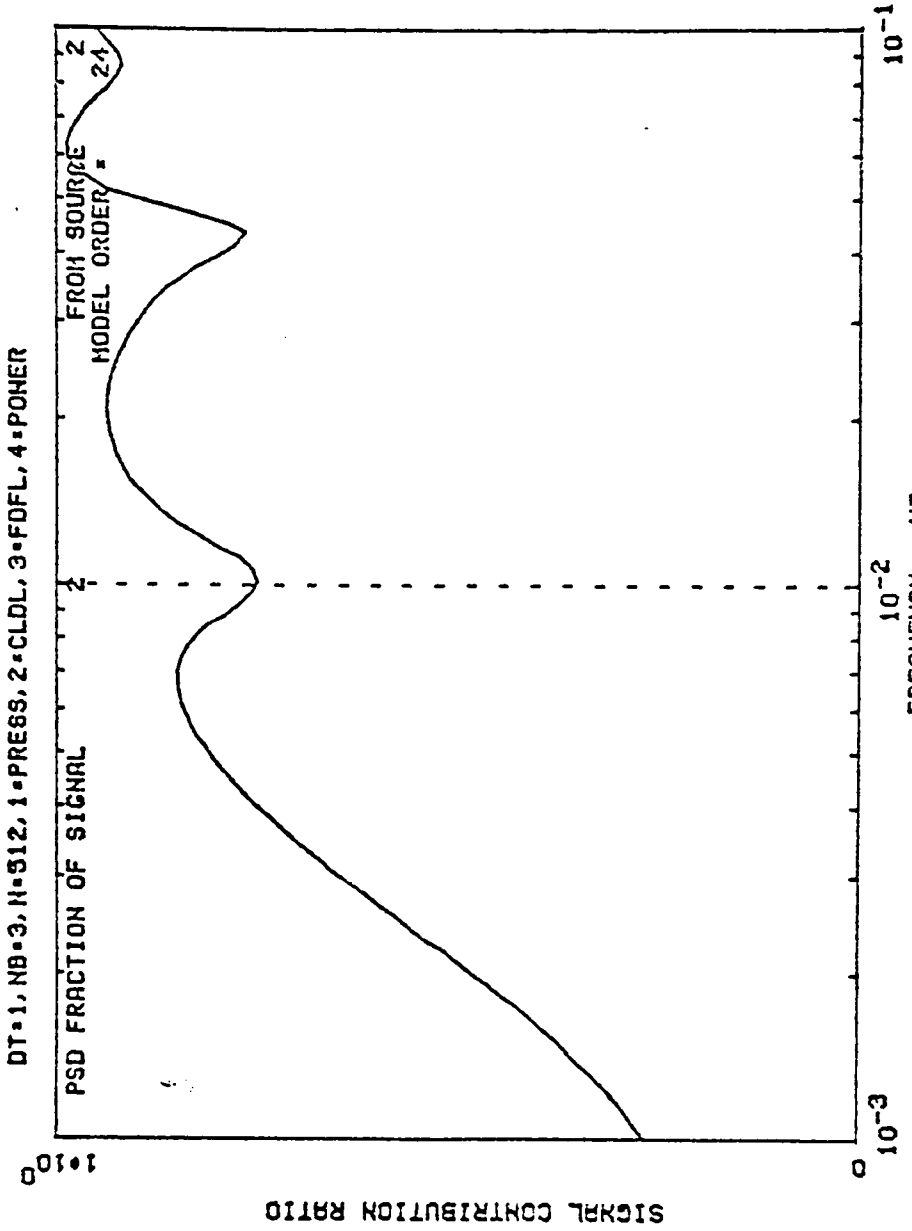


Figure 40. Signal Contribution Ratio from Source Two to Cold Leg Temperature (Case 1).

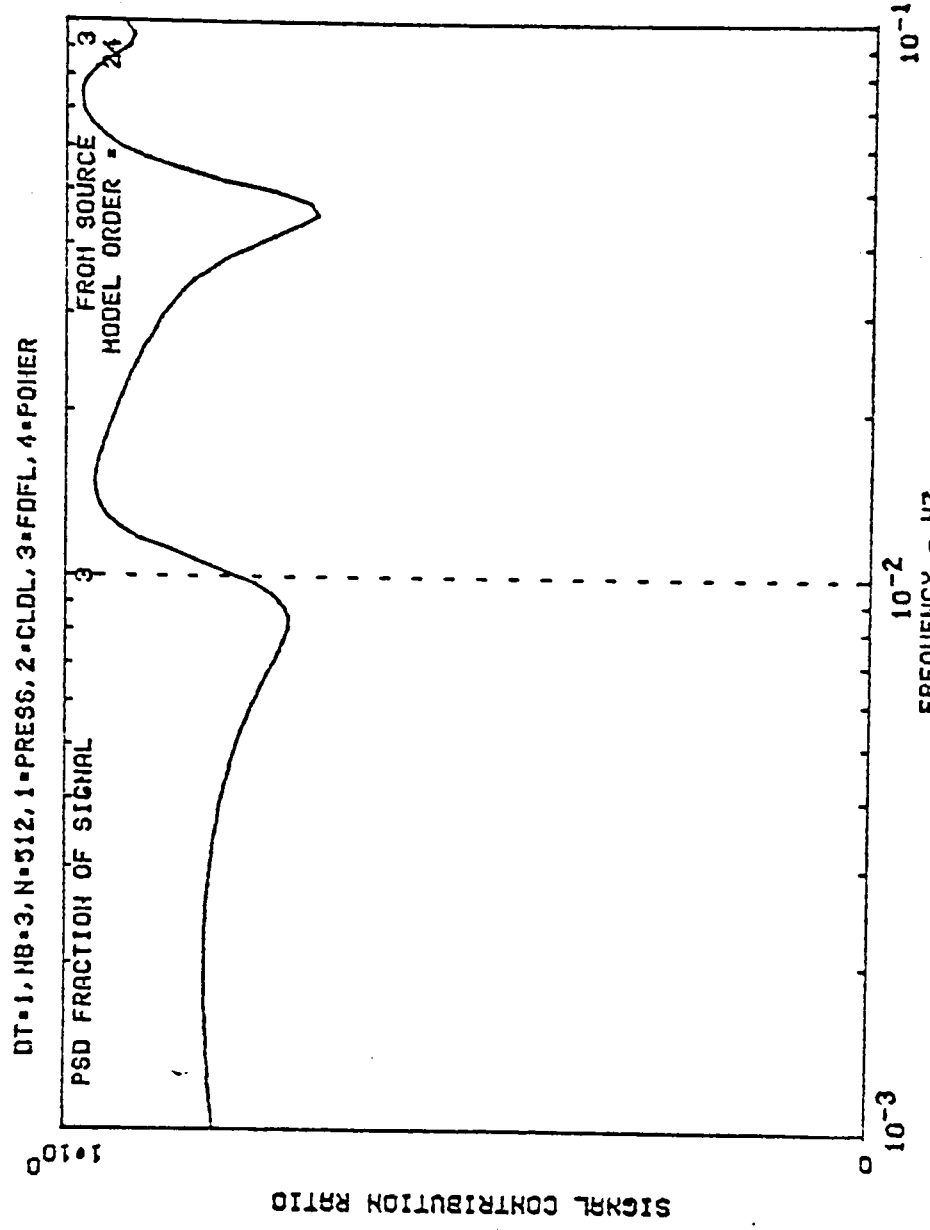


Figure 41. Signal Contribution Ratio from Source Three to Feed Water Flow Rate (Case 1).

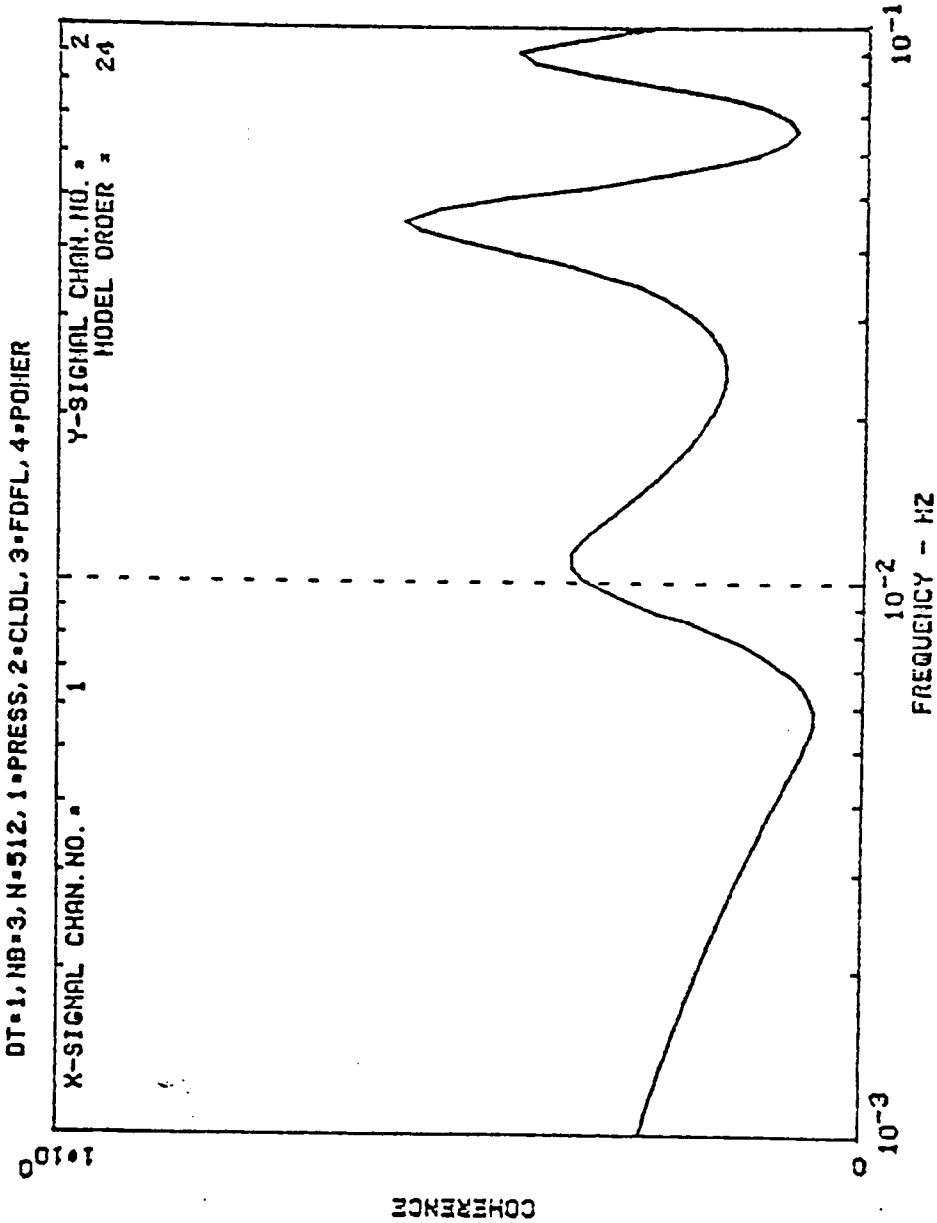


Figure 42. Coherence of Primary Pressure Versus Cold Leg Temperature (Case 1).

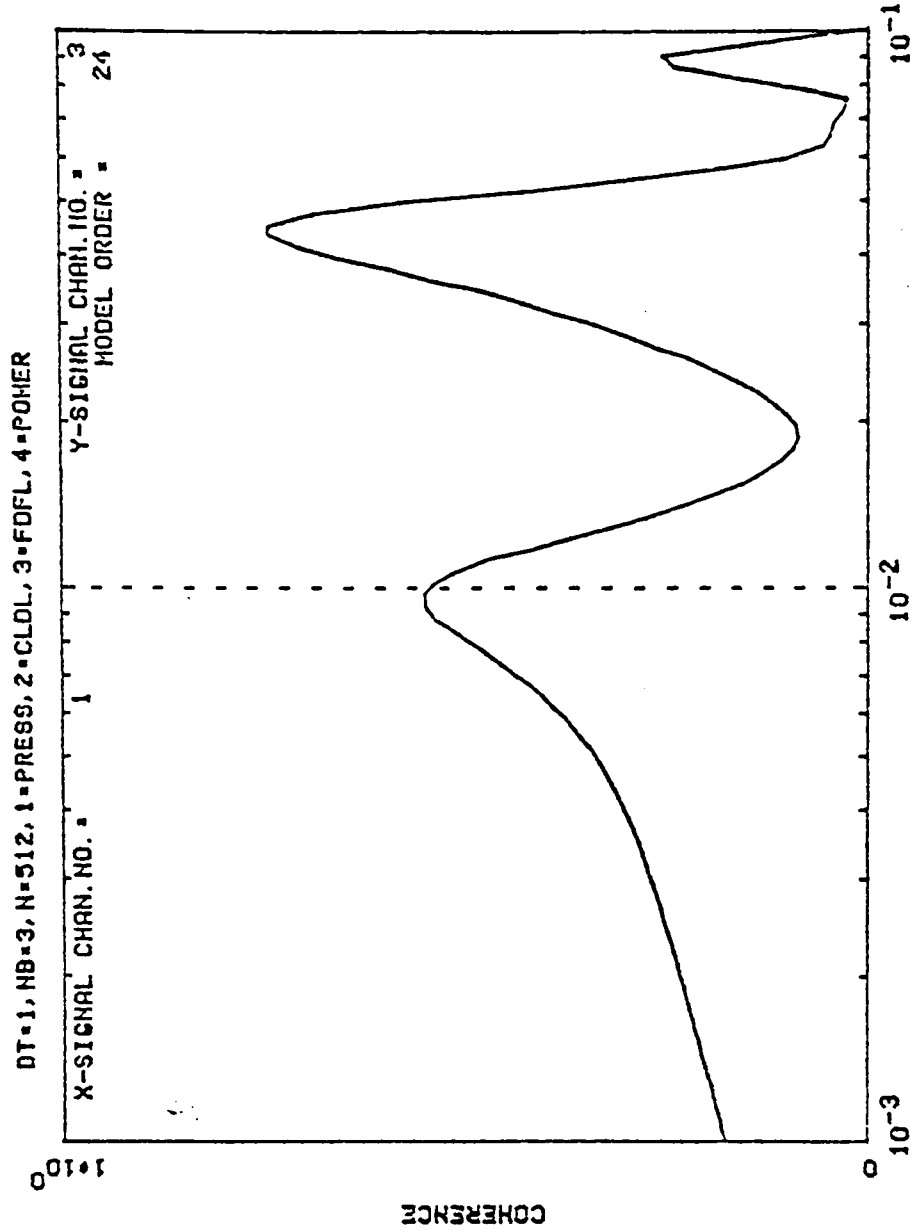


Figure 43. Coherence of Primary Pressure Versus Feed Water Flow Rate (Case 1).

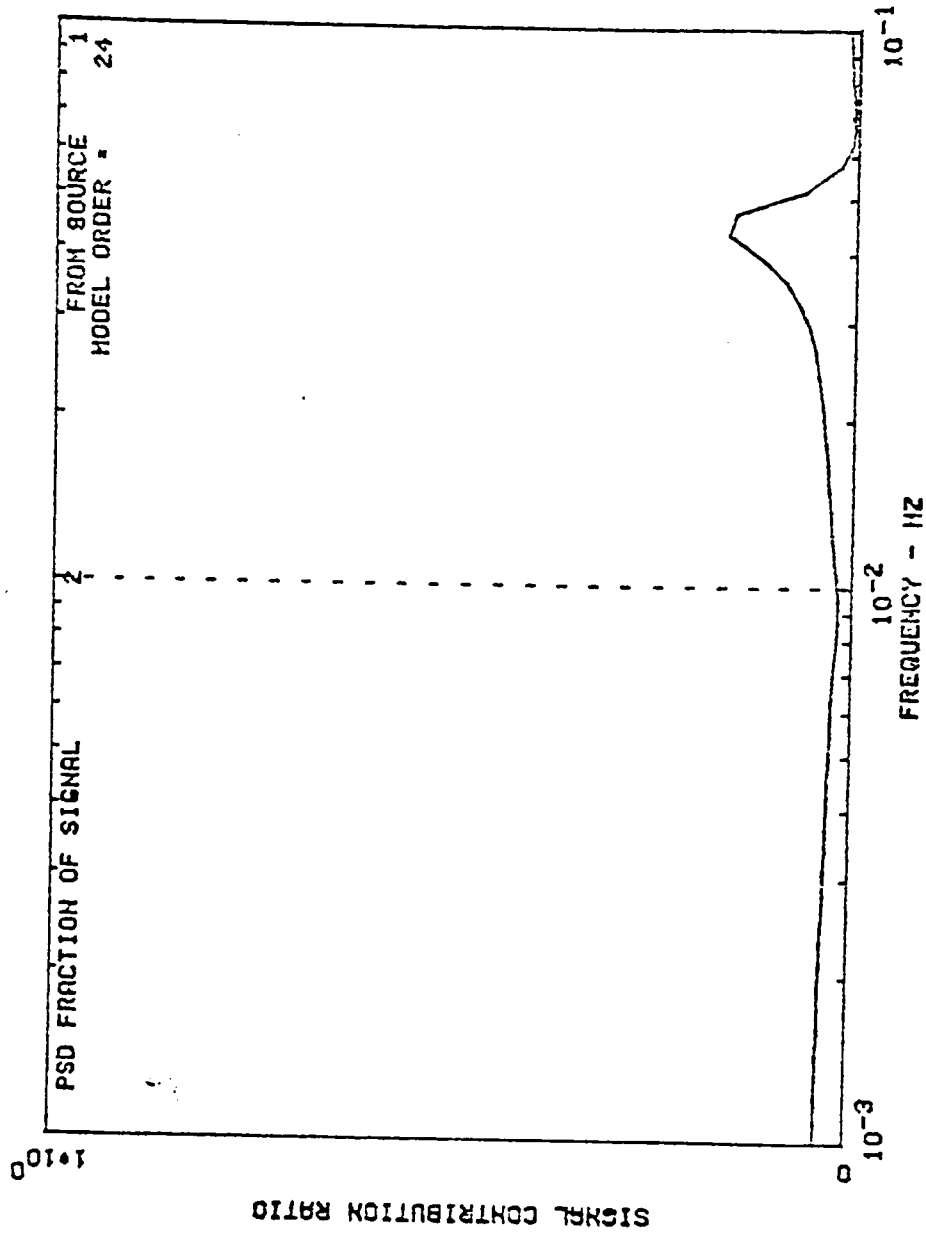


Figure 44. Signal Contribution Ratio from Source One to Cold Leg Temperature (Case 2).

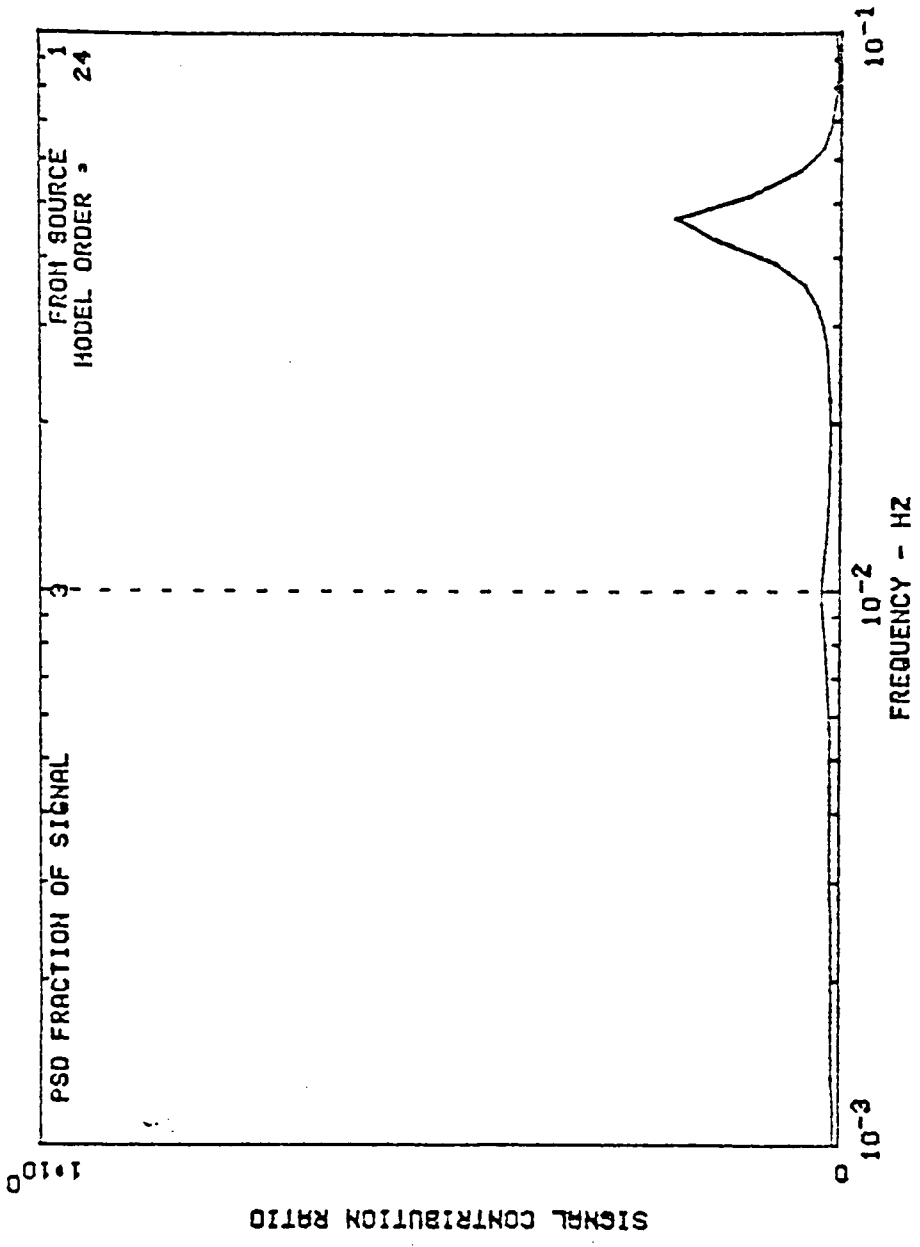


Figure 45. Signal Contribution Ratio from Source One to Feed Water Flow Rate (Case 2).

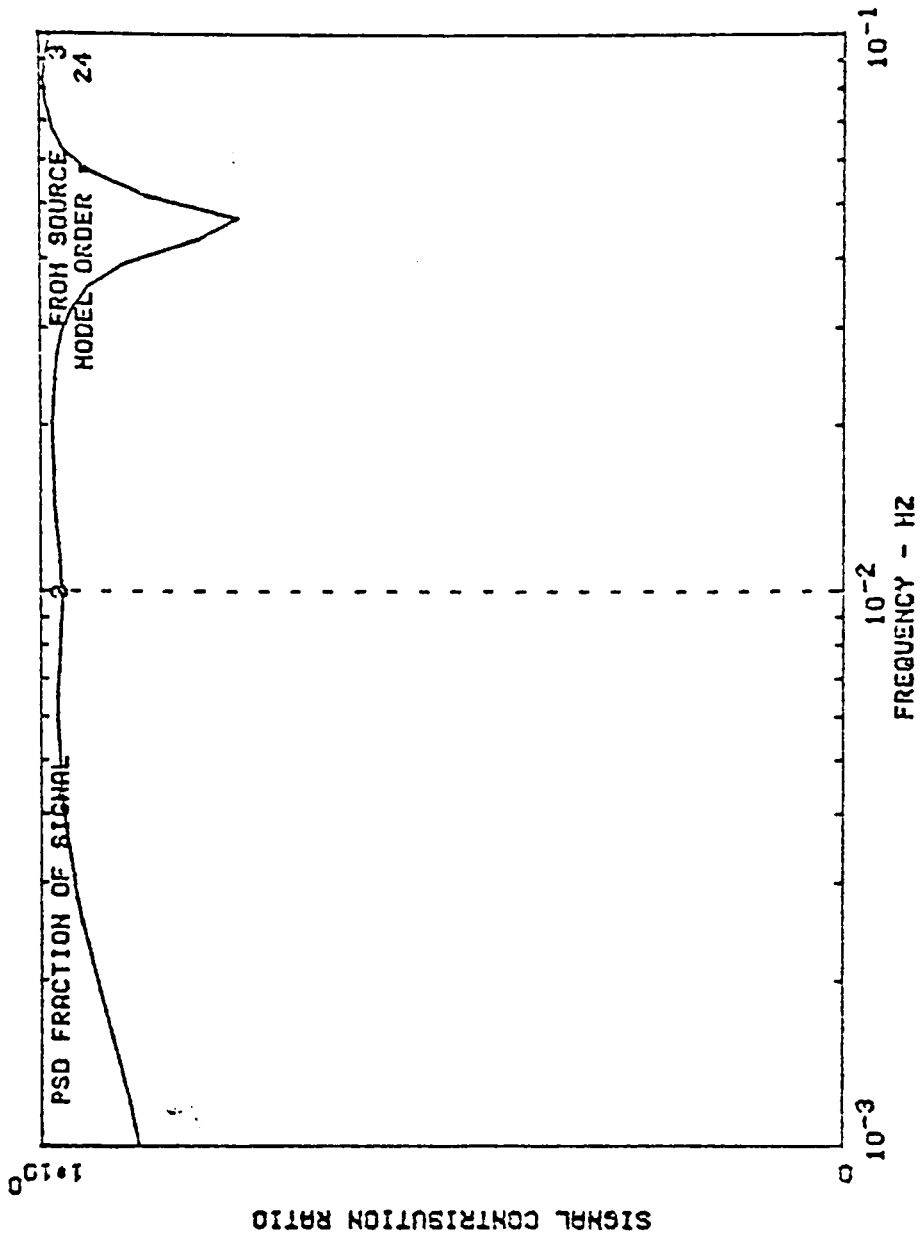


Figure 46. Signal Contribution Ratio from Source Three to Feed Water Flow Rate (Case 2).

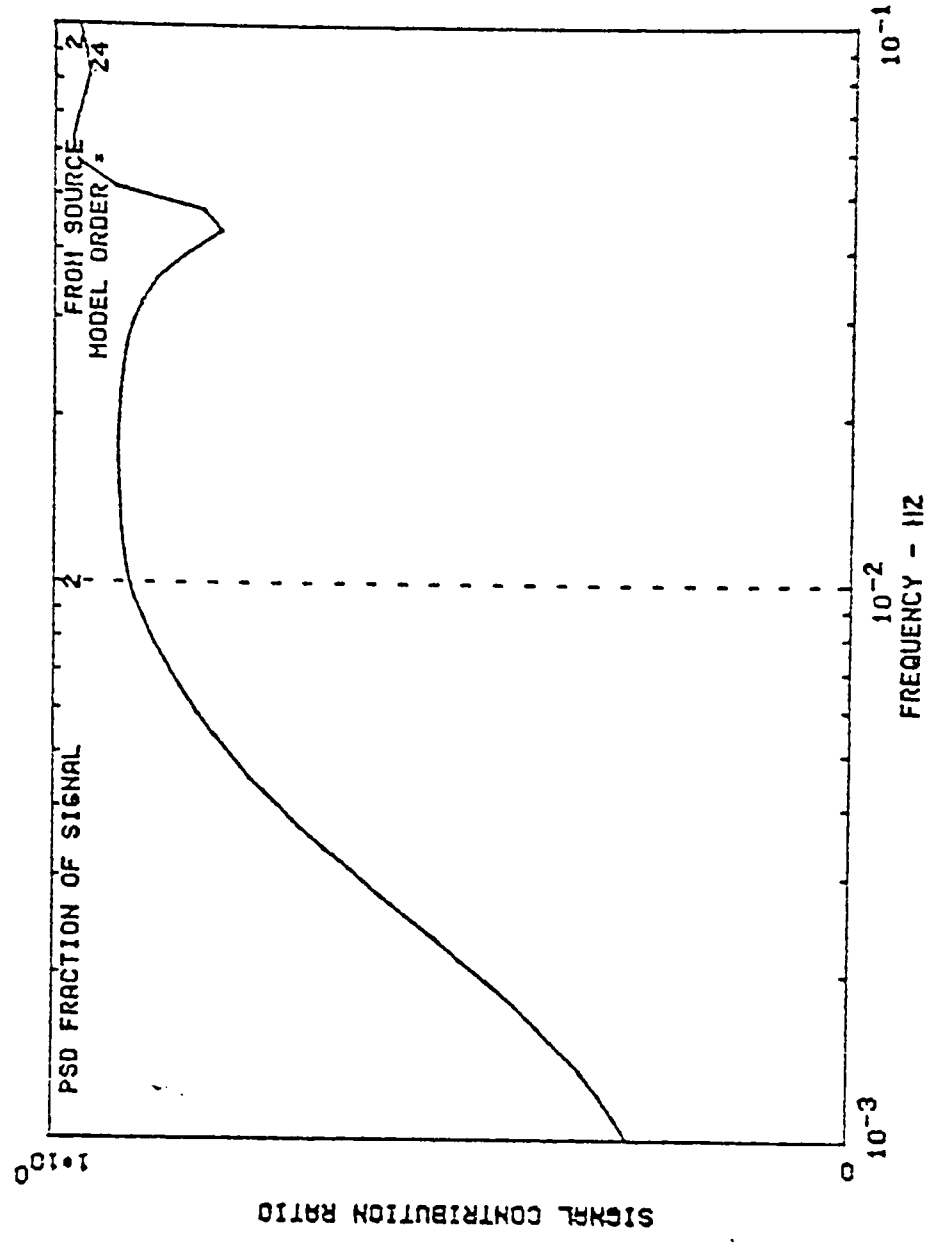


Figure 47. Signal Contribution Ratio from Source Two to Cold Leg Temperature (Case 2).

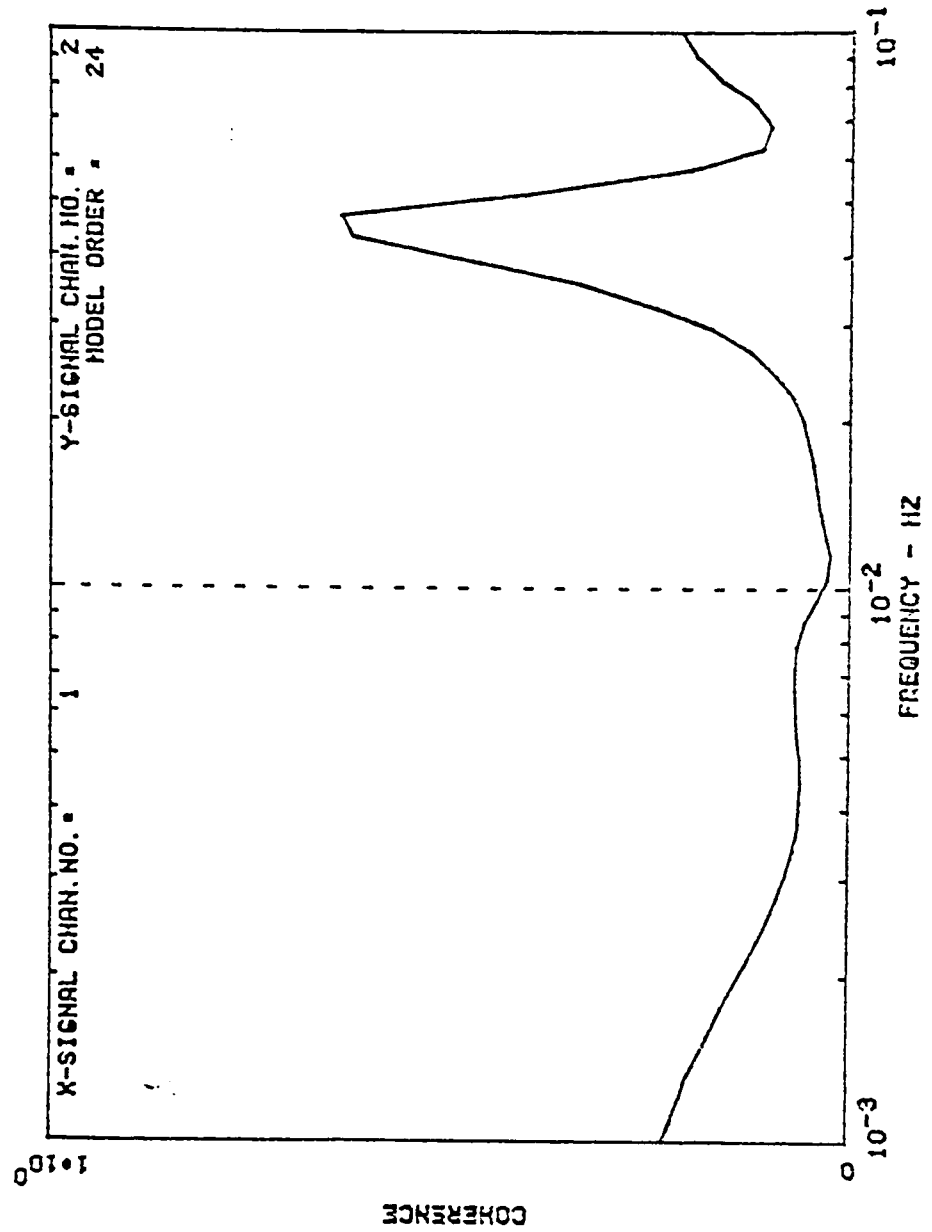


Figure 48 Coherence of Primary Pressure Versus Cold Leg Temperature (Case 2).

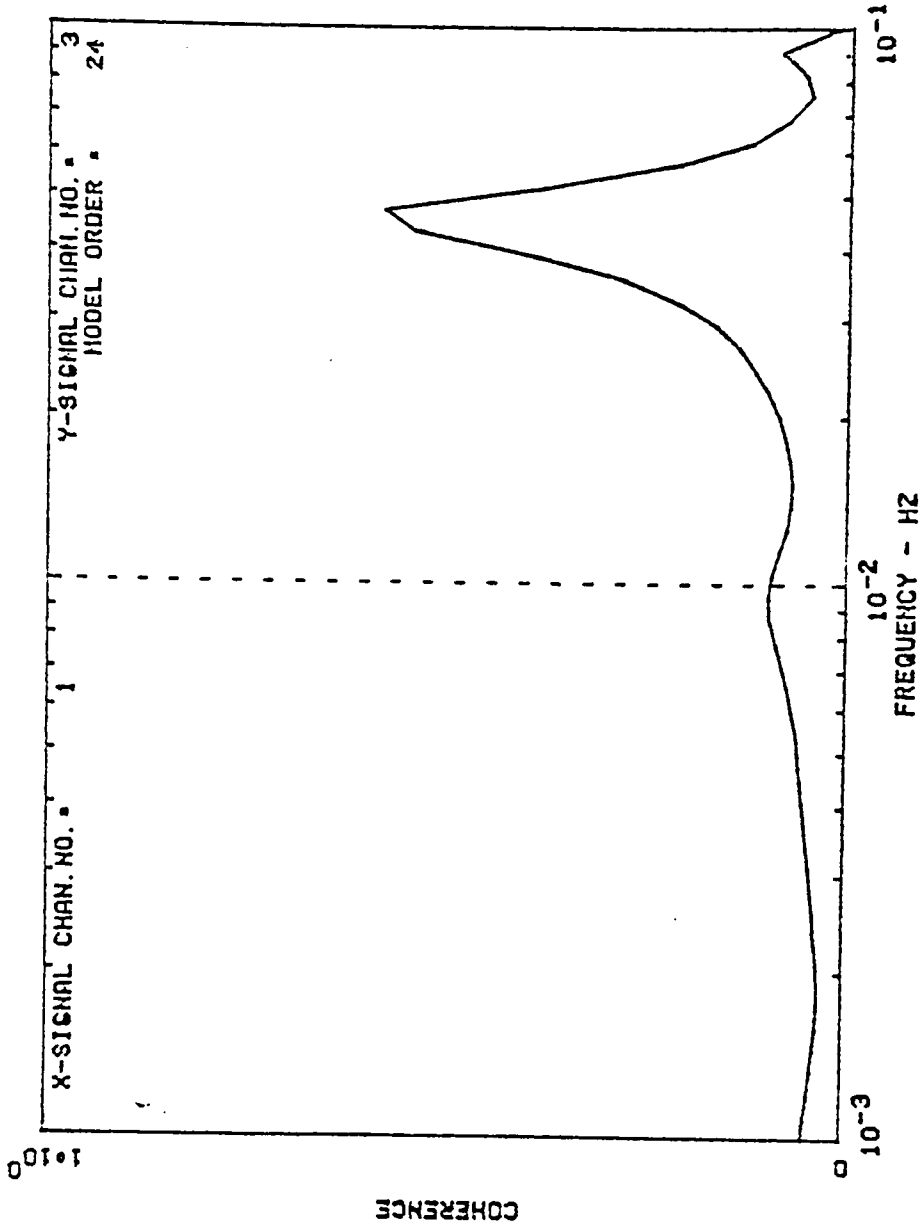


Figure 49. Coherence of Primary Pressure Versus Feed Water Flow Rate. (Case 2).

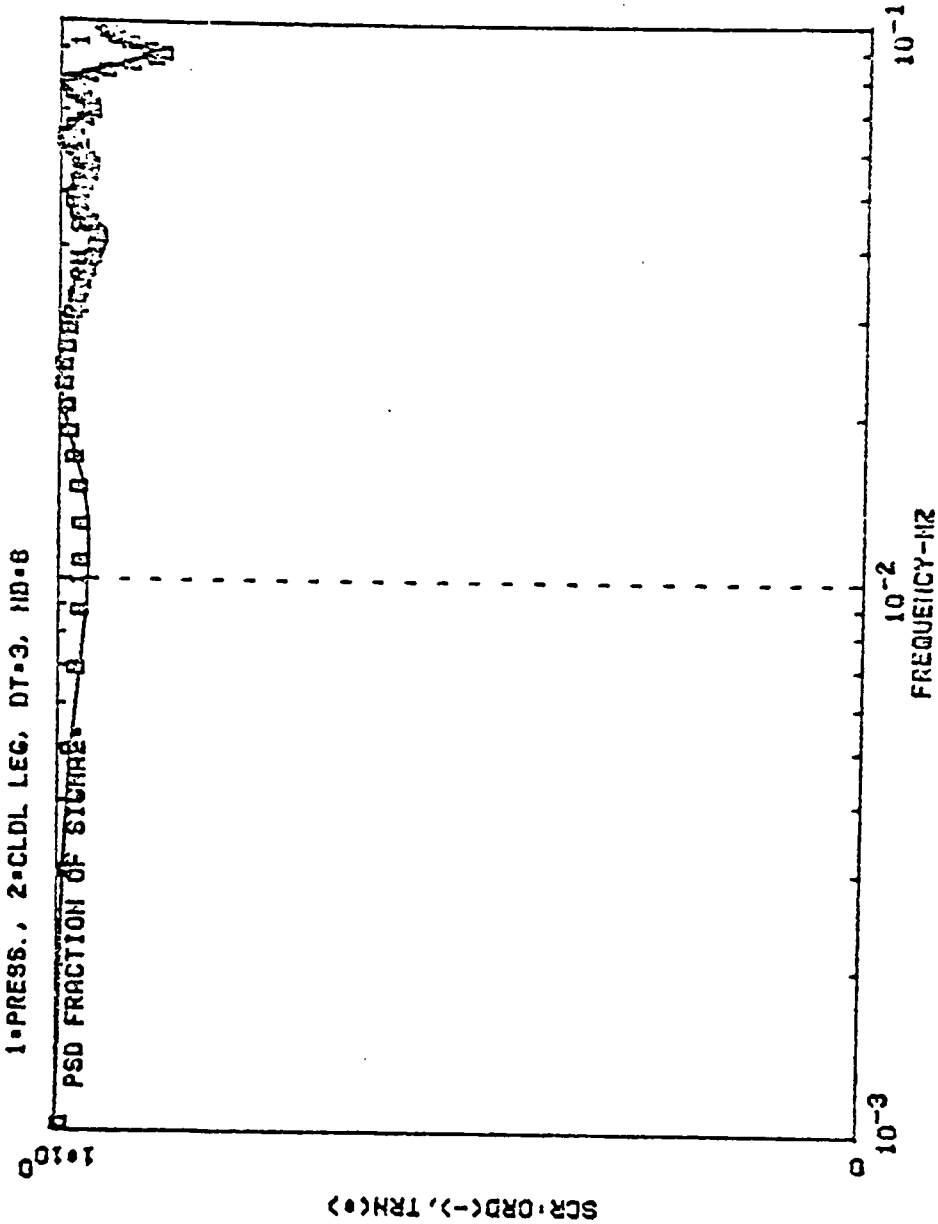


Figure 50. Signal Contribution Ratio From Source One to Primary Pressure. (A)

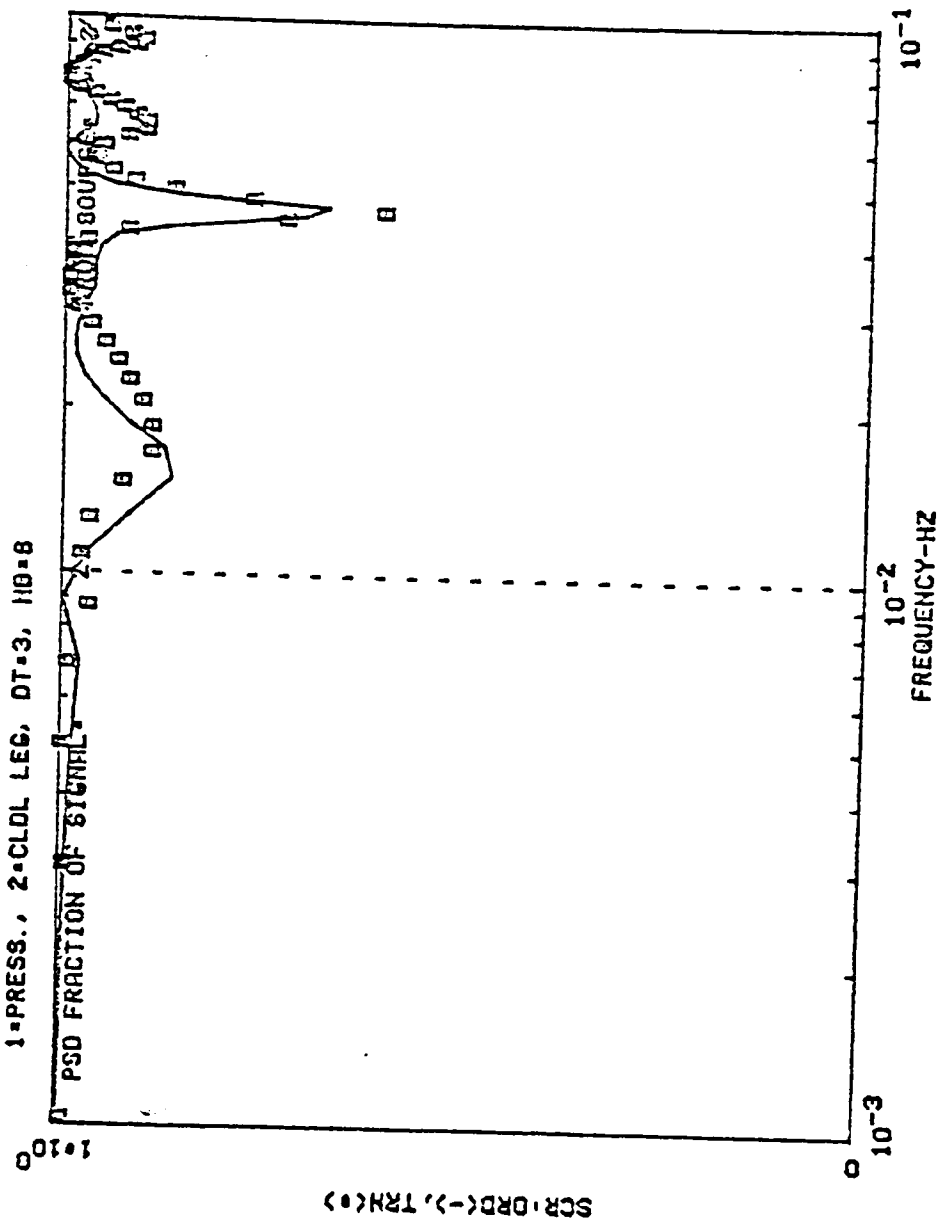


Figure 51. Signal Contribution Ratio from Source Two to Cold Leg Temperature. (A).

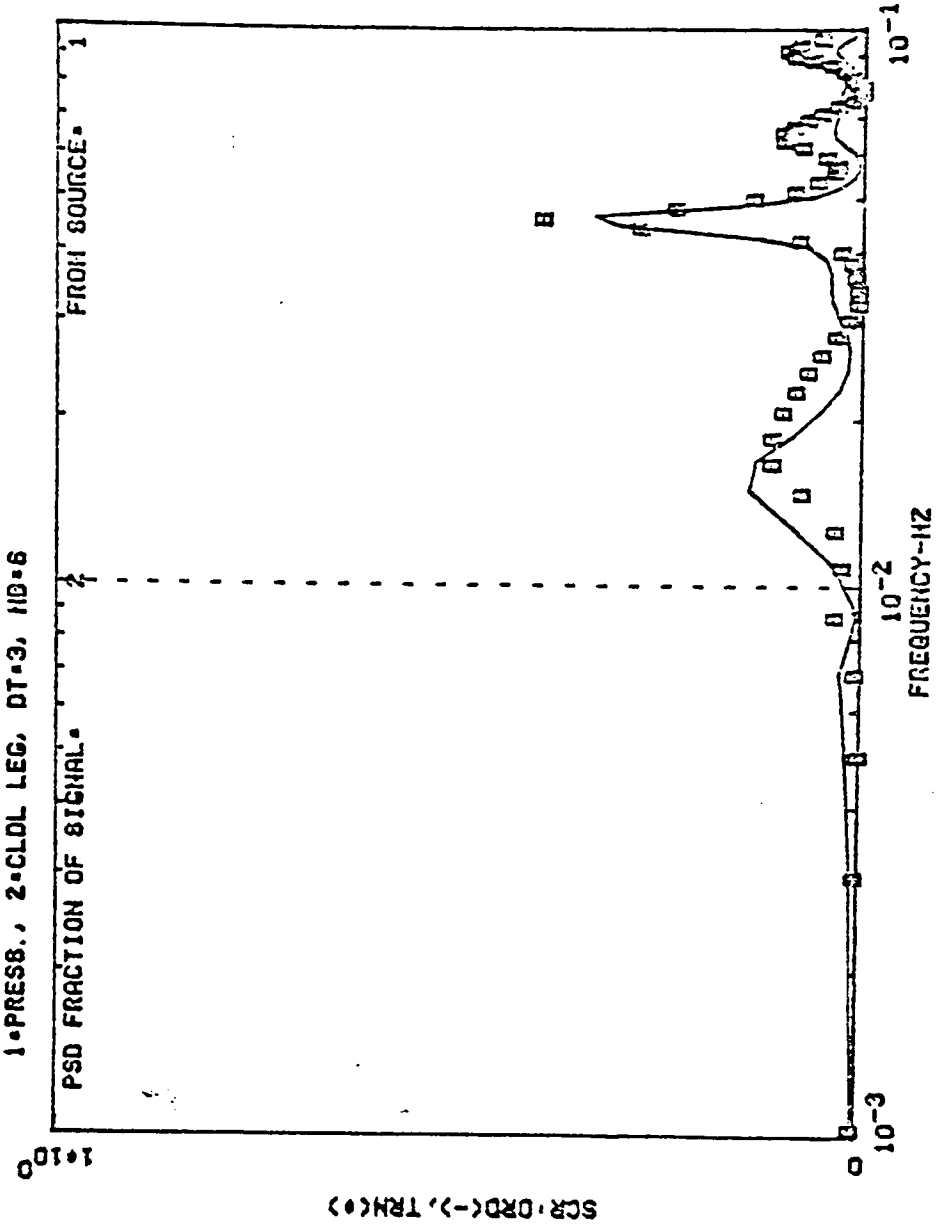


Figure 52. Signal Contribution Ratio from Source One to Cold Leg Temperature.

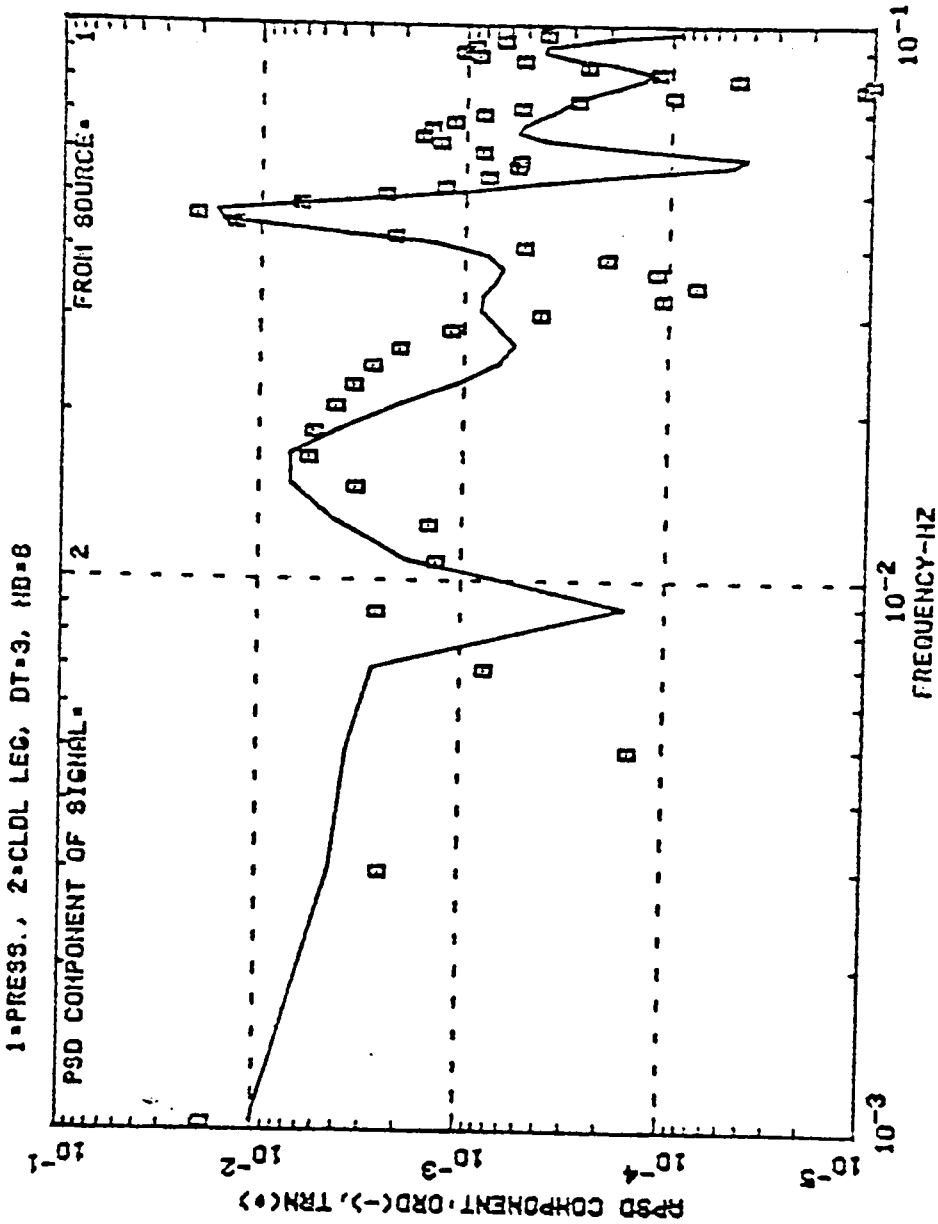


Figure 53. Power Spectrum Component of Cold Leg Temperature from Source One.

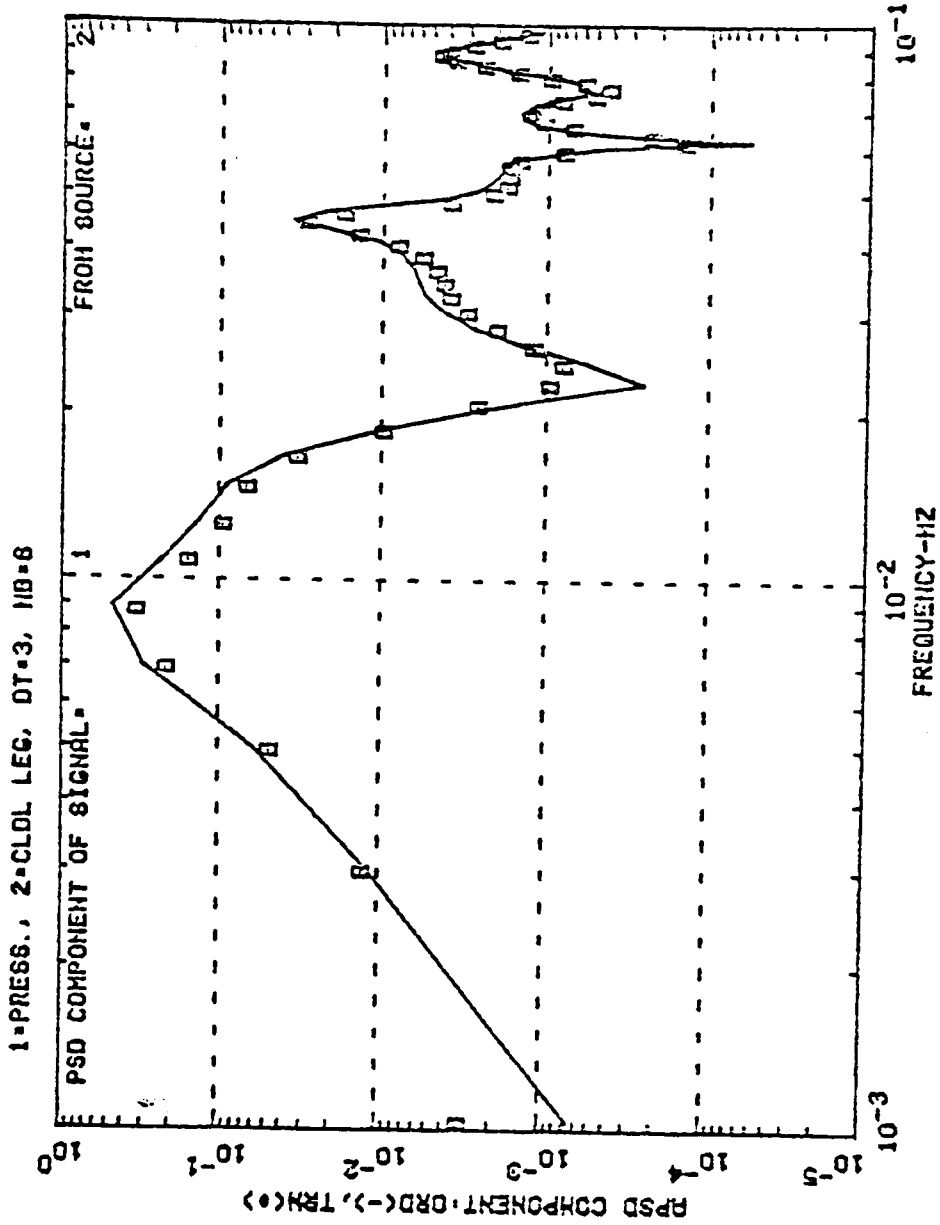


Figure 54. Power Spectrum Component of Primary Pressure from Source Two.

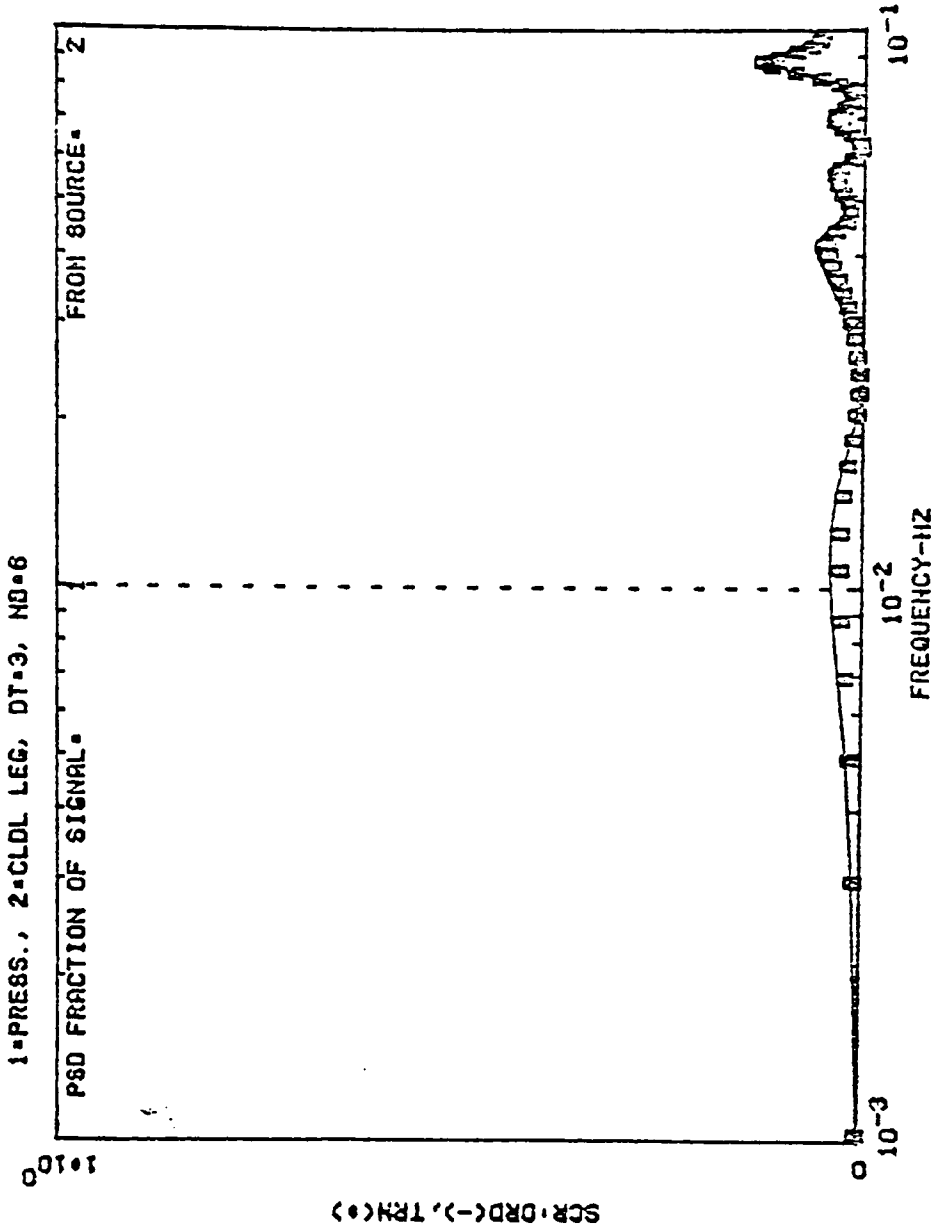


Figure 55. Signal Contribution Ratio from Source Two to Primary Pressure.

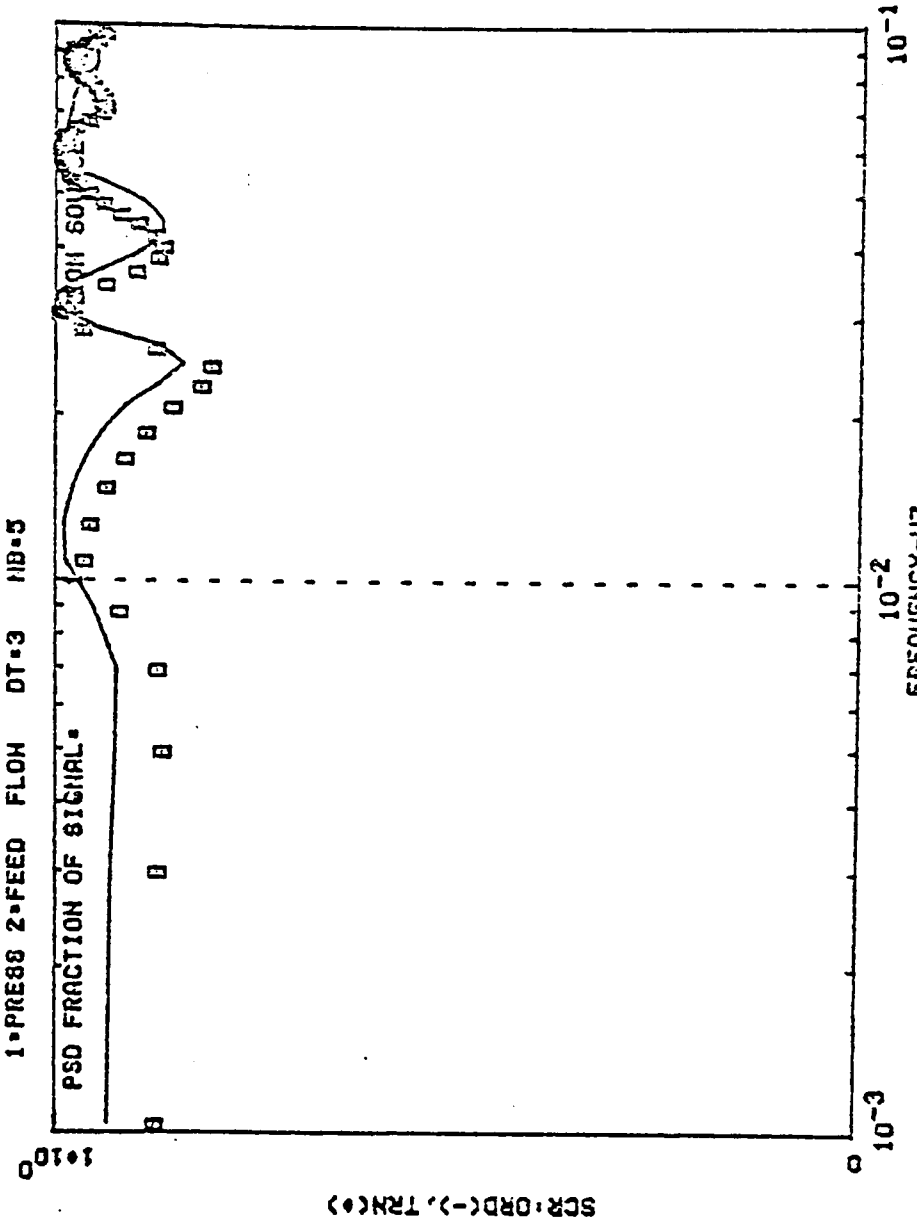


Figure 56. Signal Contribution Ratio from Source One to Primary Pressure. (B)

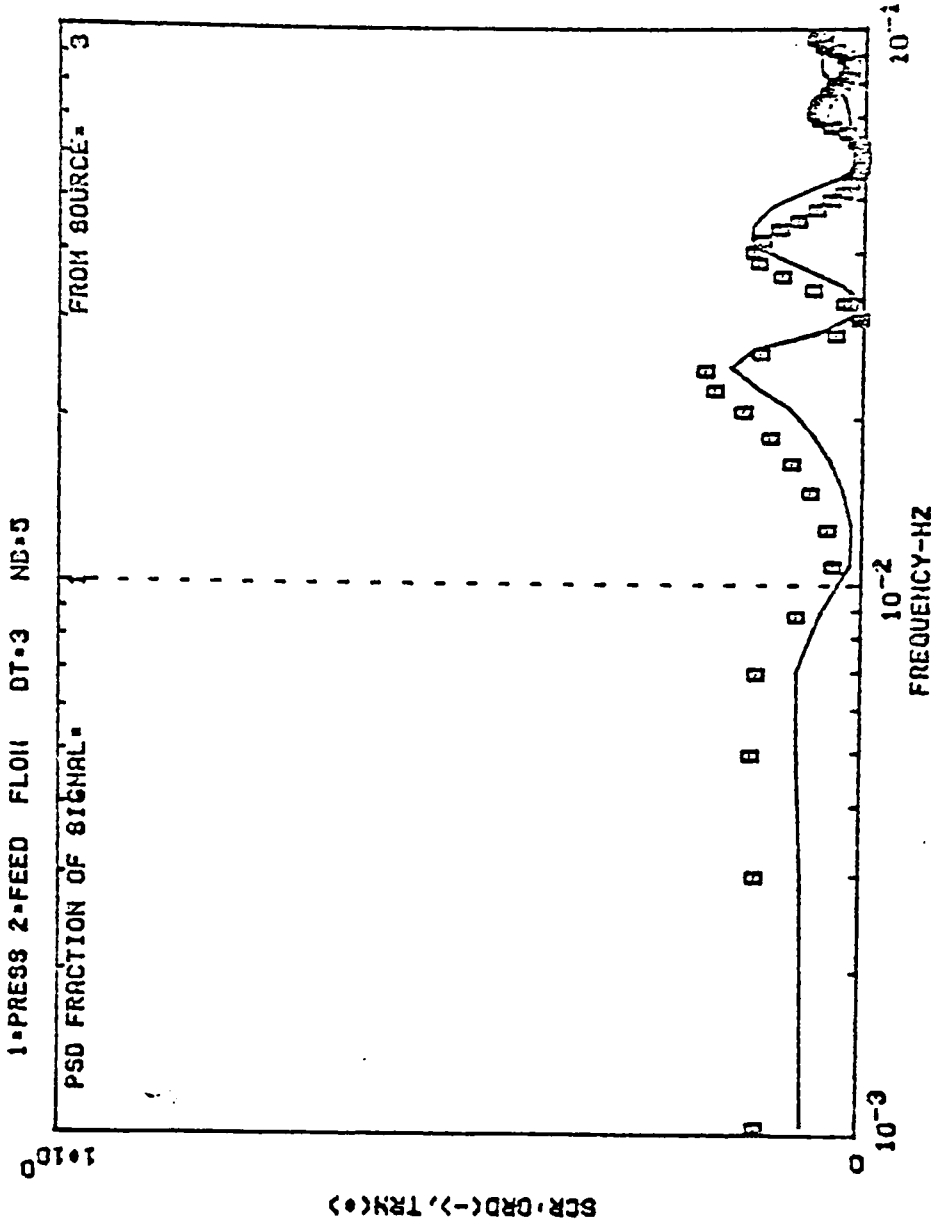


Figure 57. Signal Contribution Ratio from Source Three to Primary Pressure.

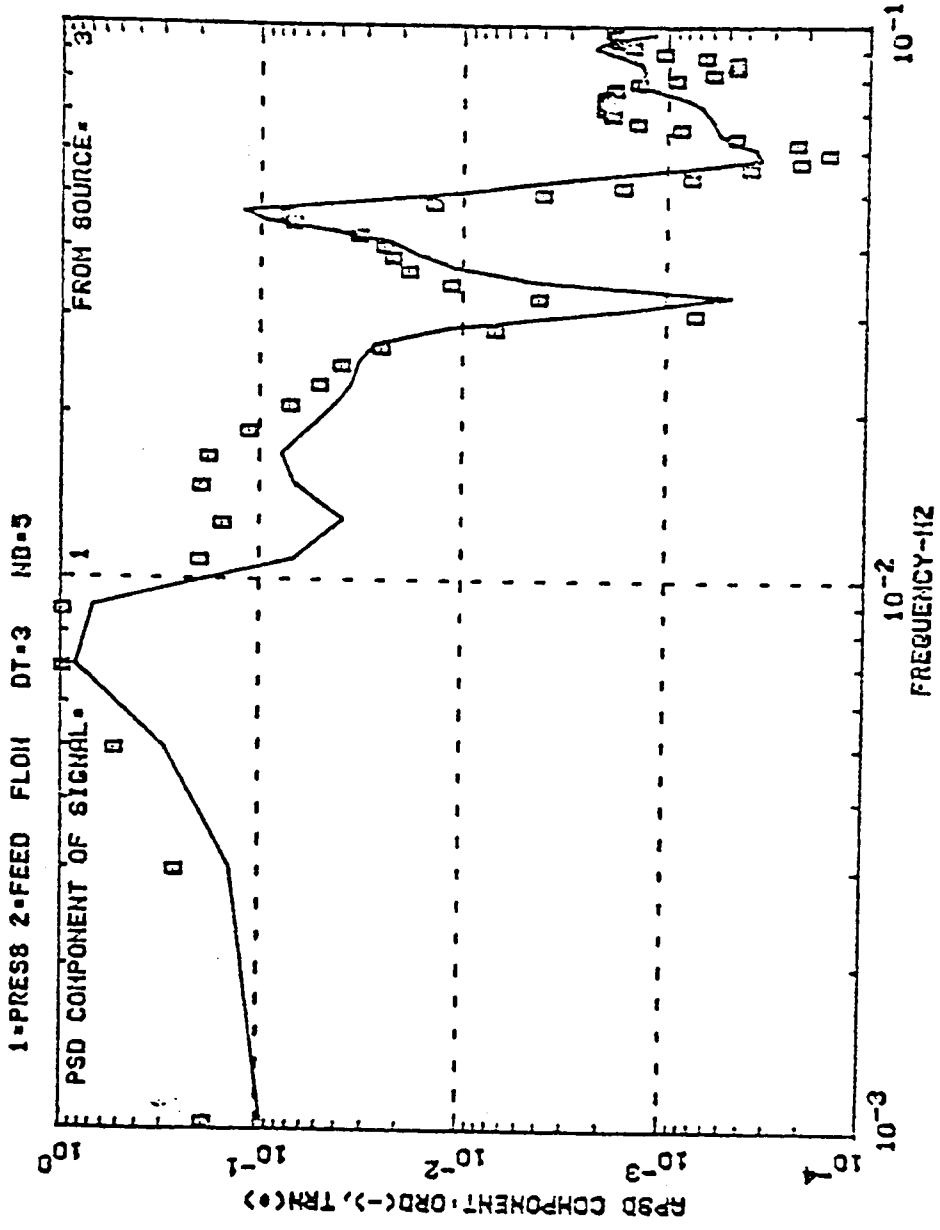


Figure 58. Power Spectrum Component of Primary Pressure from Source Three.

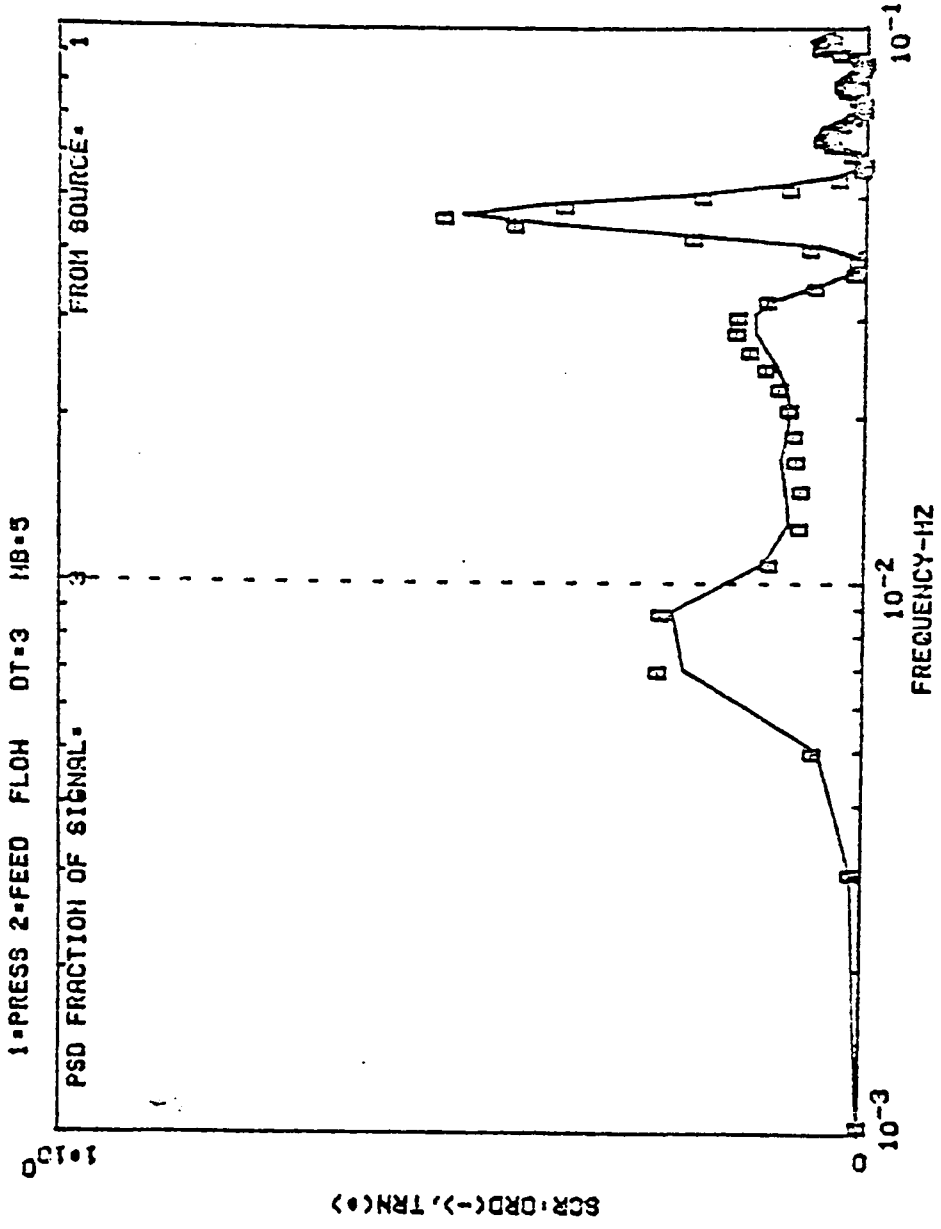


Figure 59. Signal Contribution Ratio from Source One to Feed Water Flow Rate.

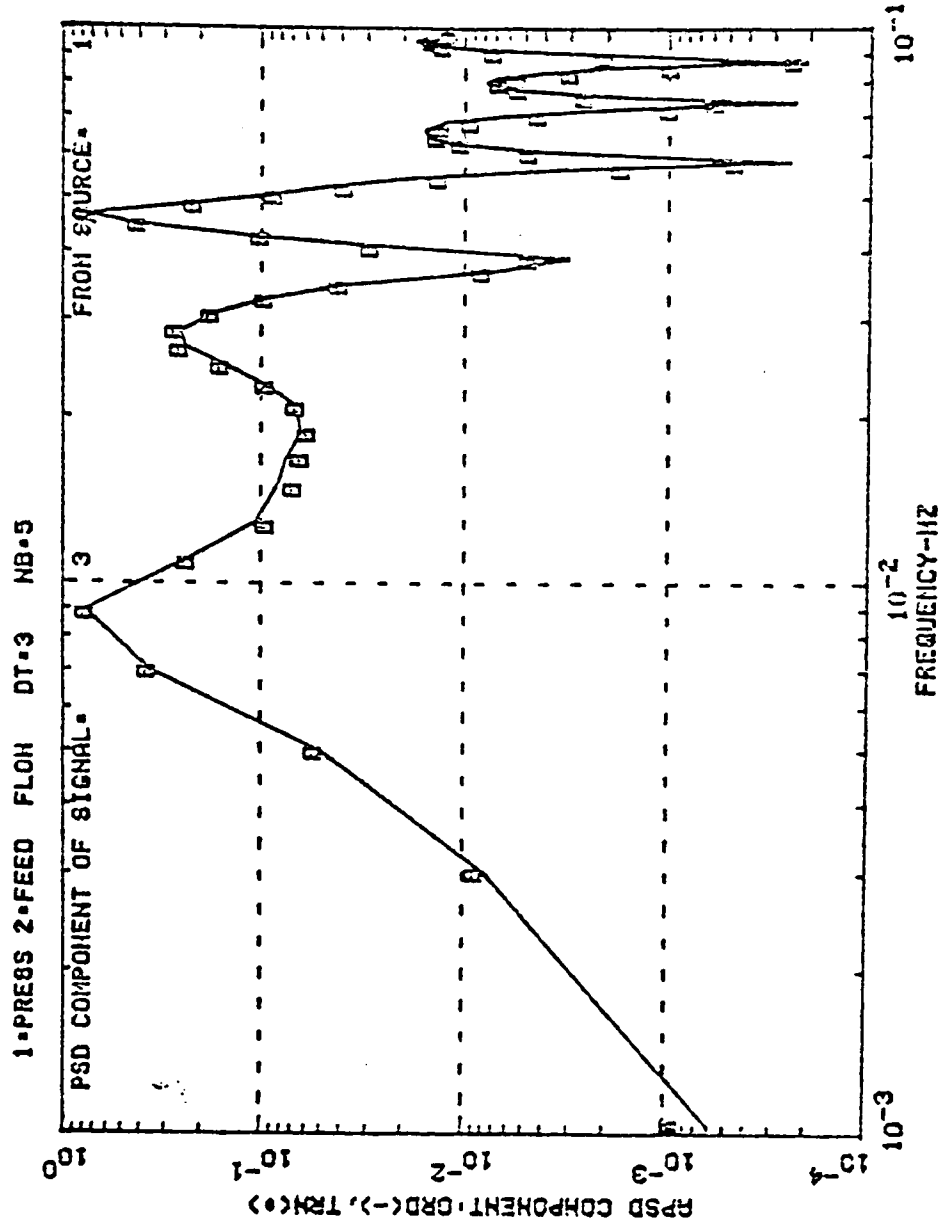


Figure 60. Power Spectrum Component of Feed Water Flow Rate from Source One.

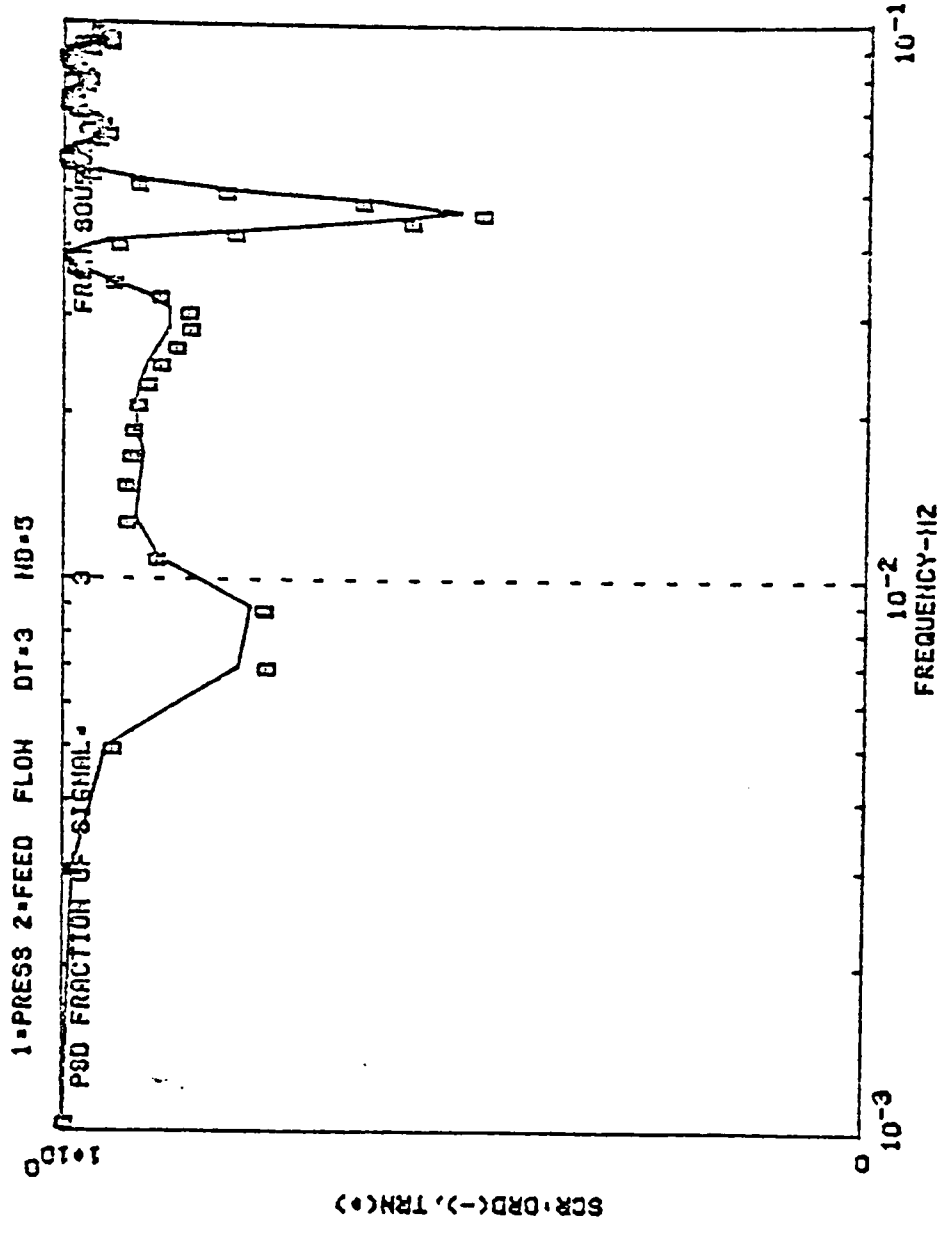


Figure 61. Signal Contribution Ratio from Source Three to Feed Water Flow Rate. (A)

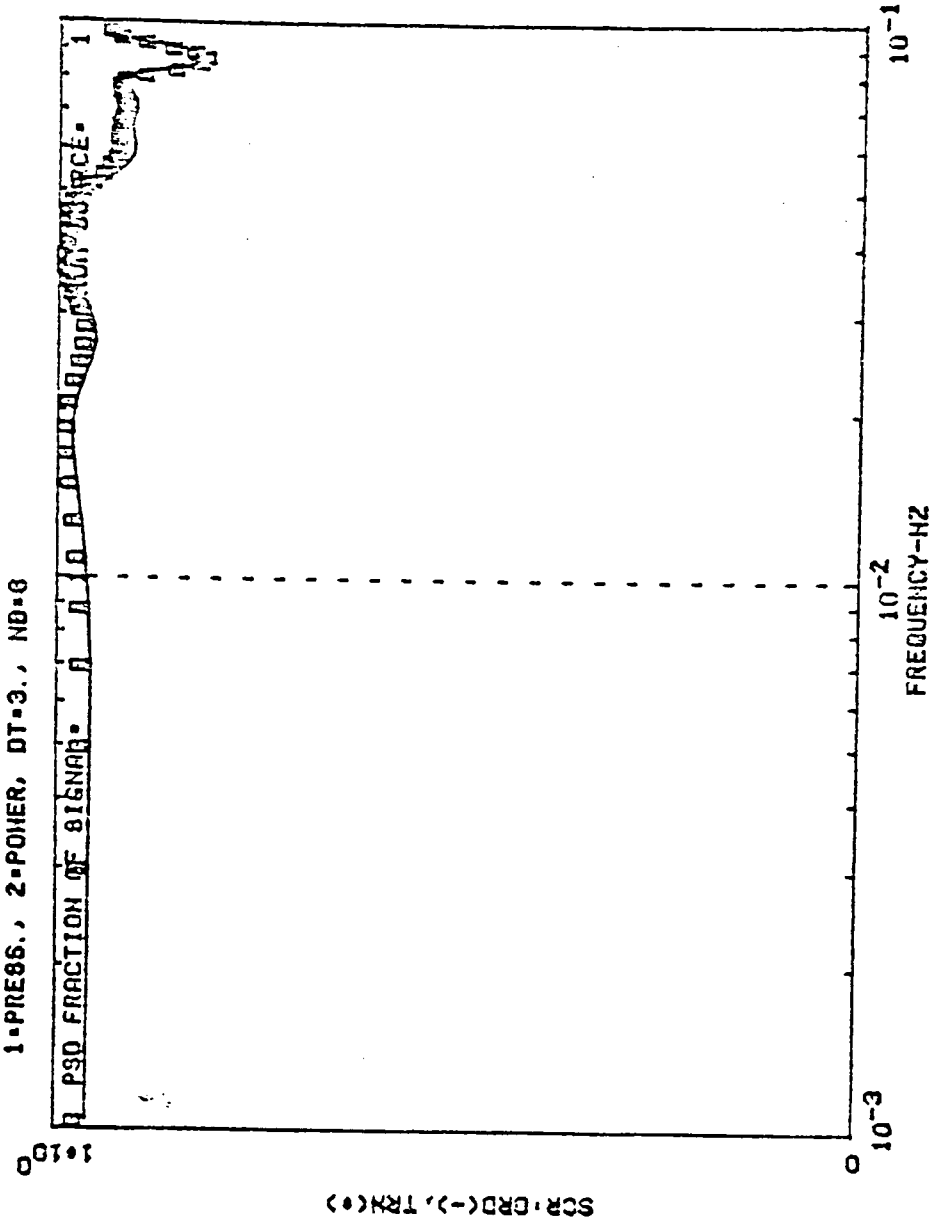


Figure 62. Signal Contribution Ratio from Source One to Primary Pressure. (C)

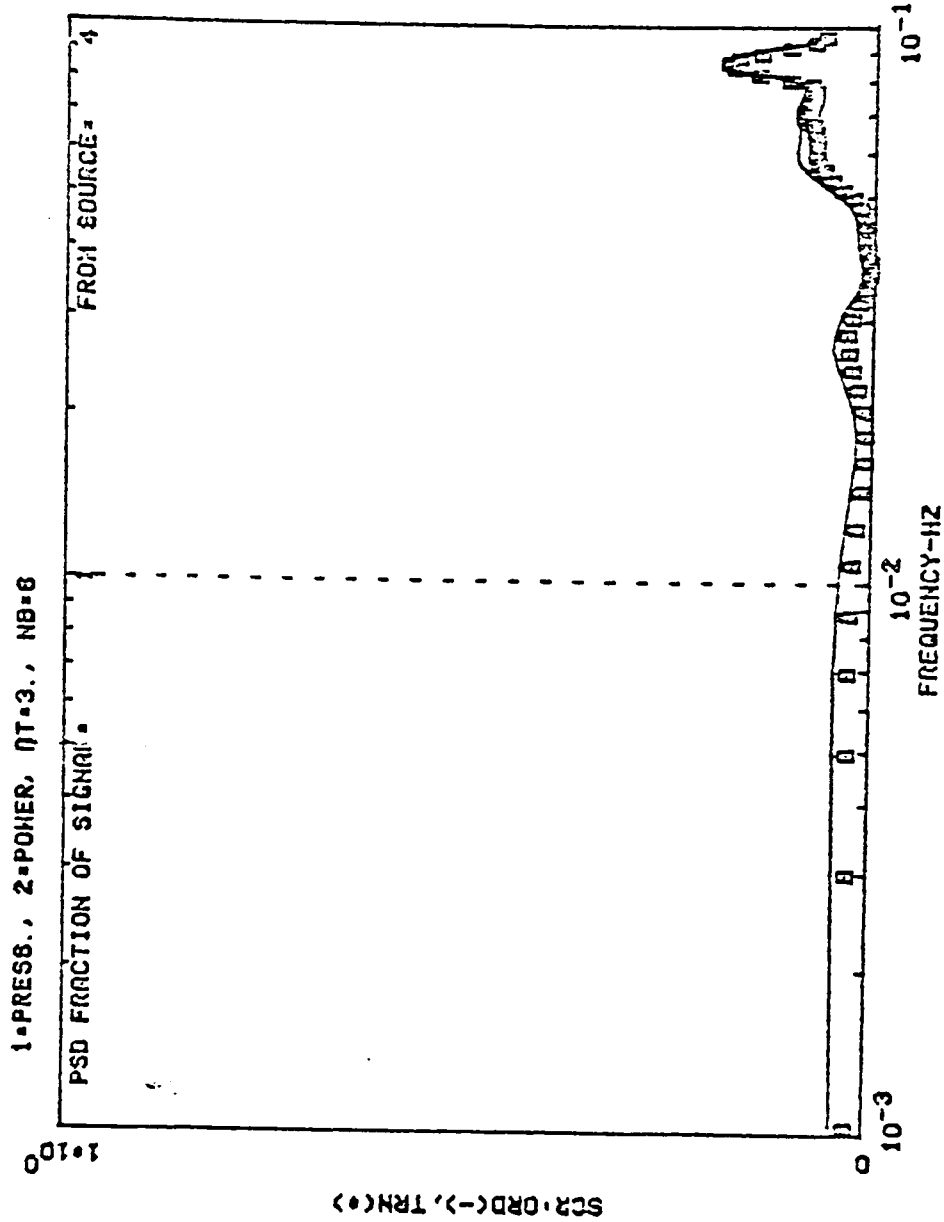


Figure 63. Signal Contribution Ratio from Source Four to Primary Pressure.

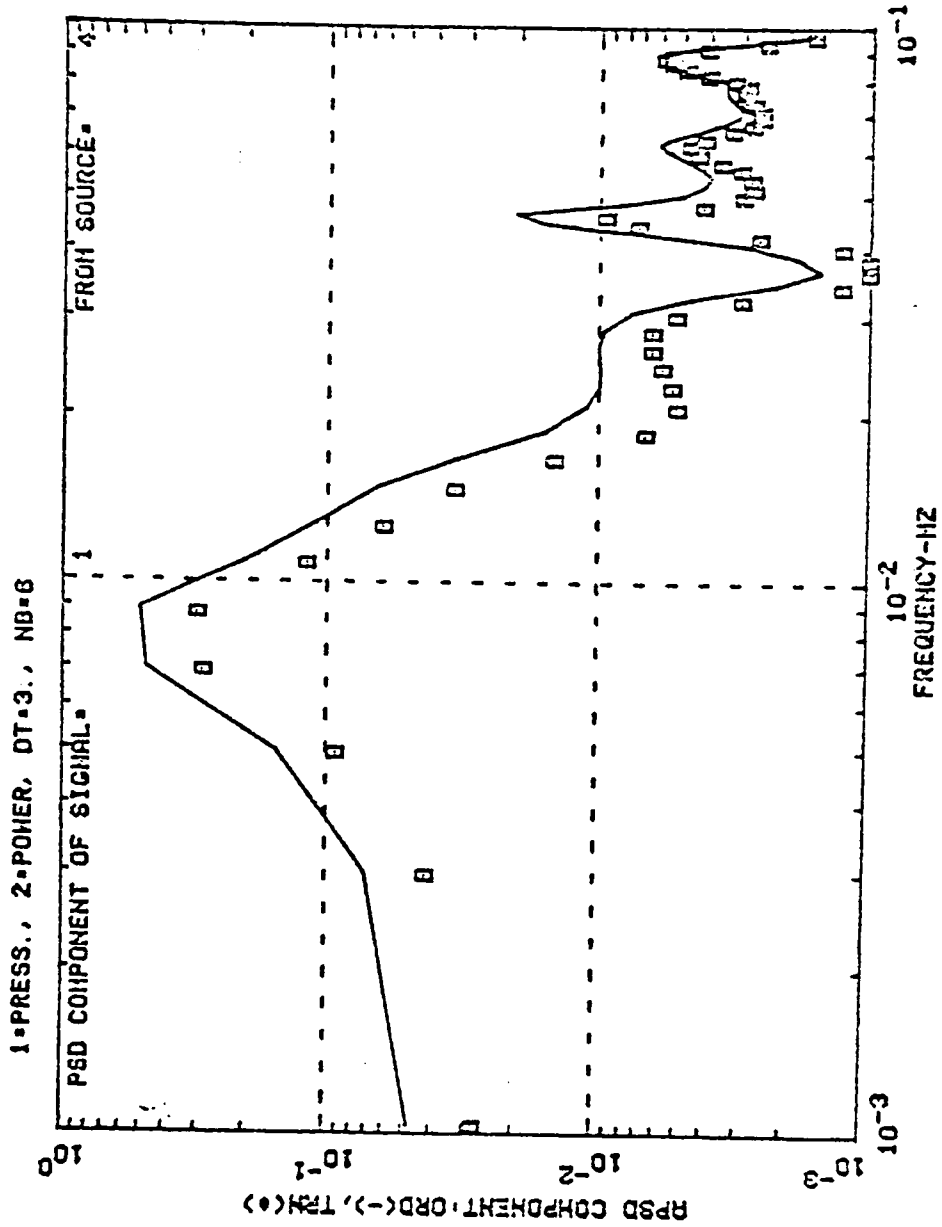


Figure 64. Power Spectrum Component of Primary Pressure from Source Four.

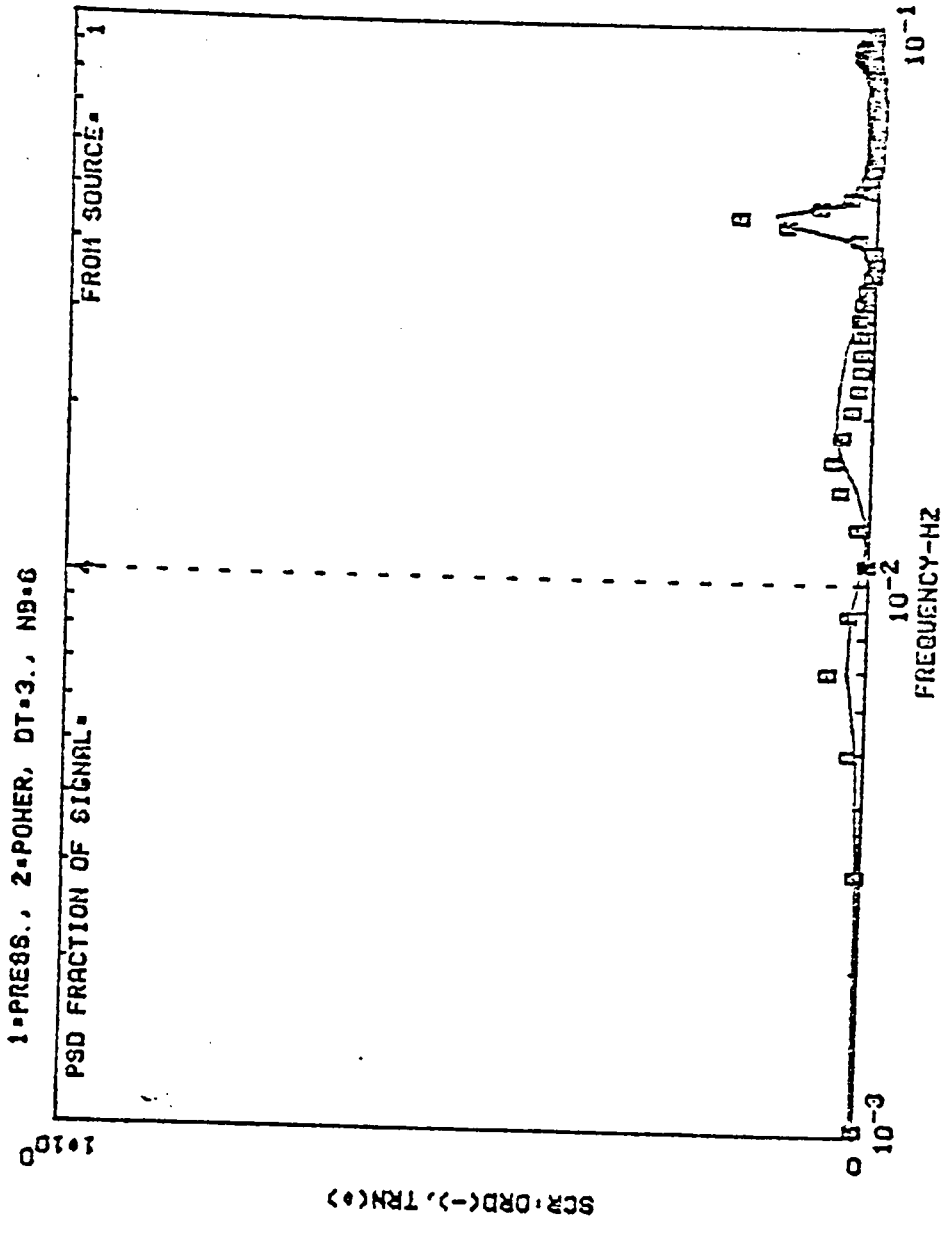


Figure 65. Signal Contribution Ratio from Source One to Power.

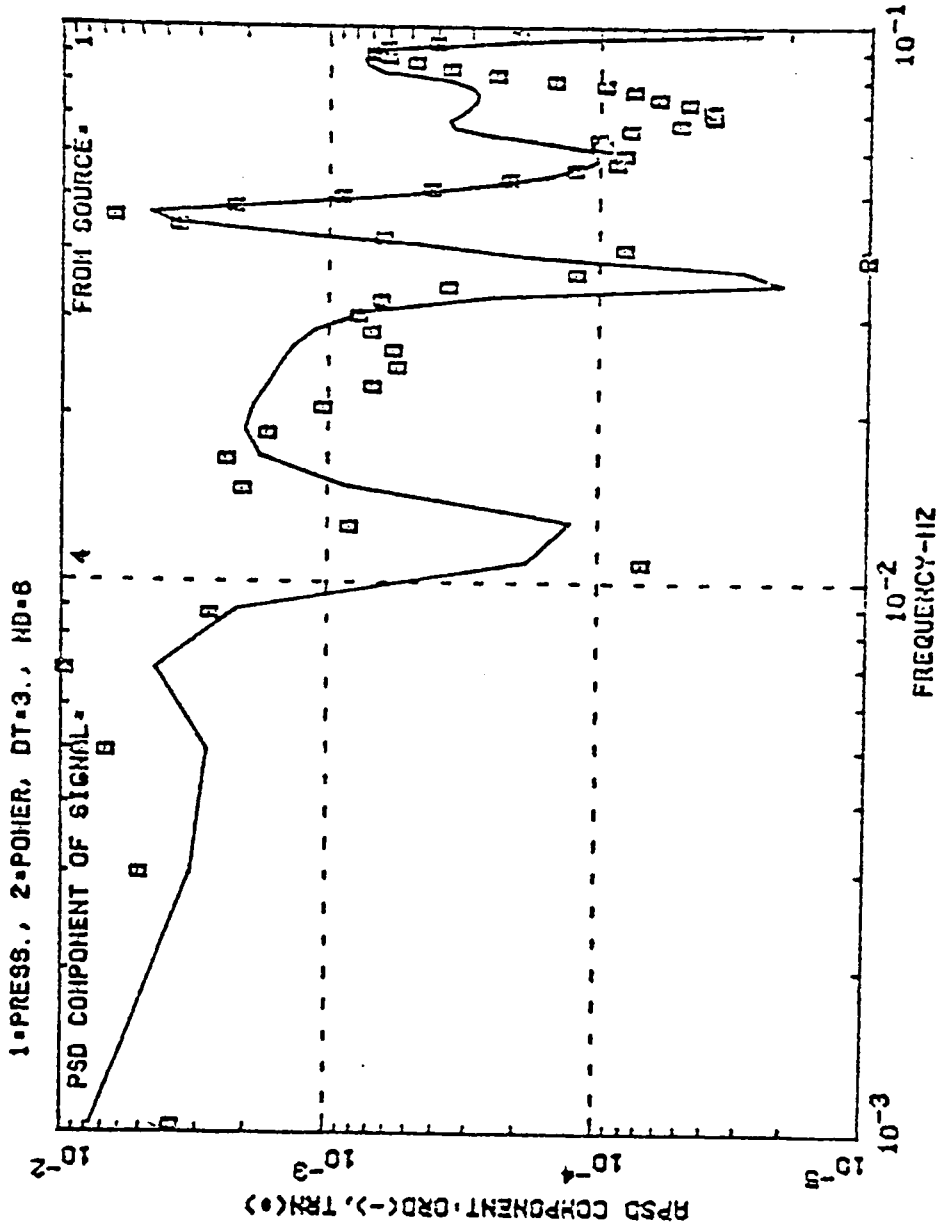


Figure 66. Power Spectrum Component of Power from Source One.

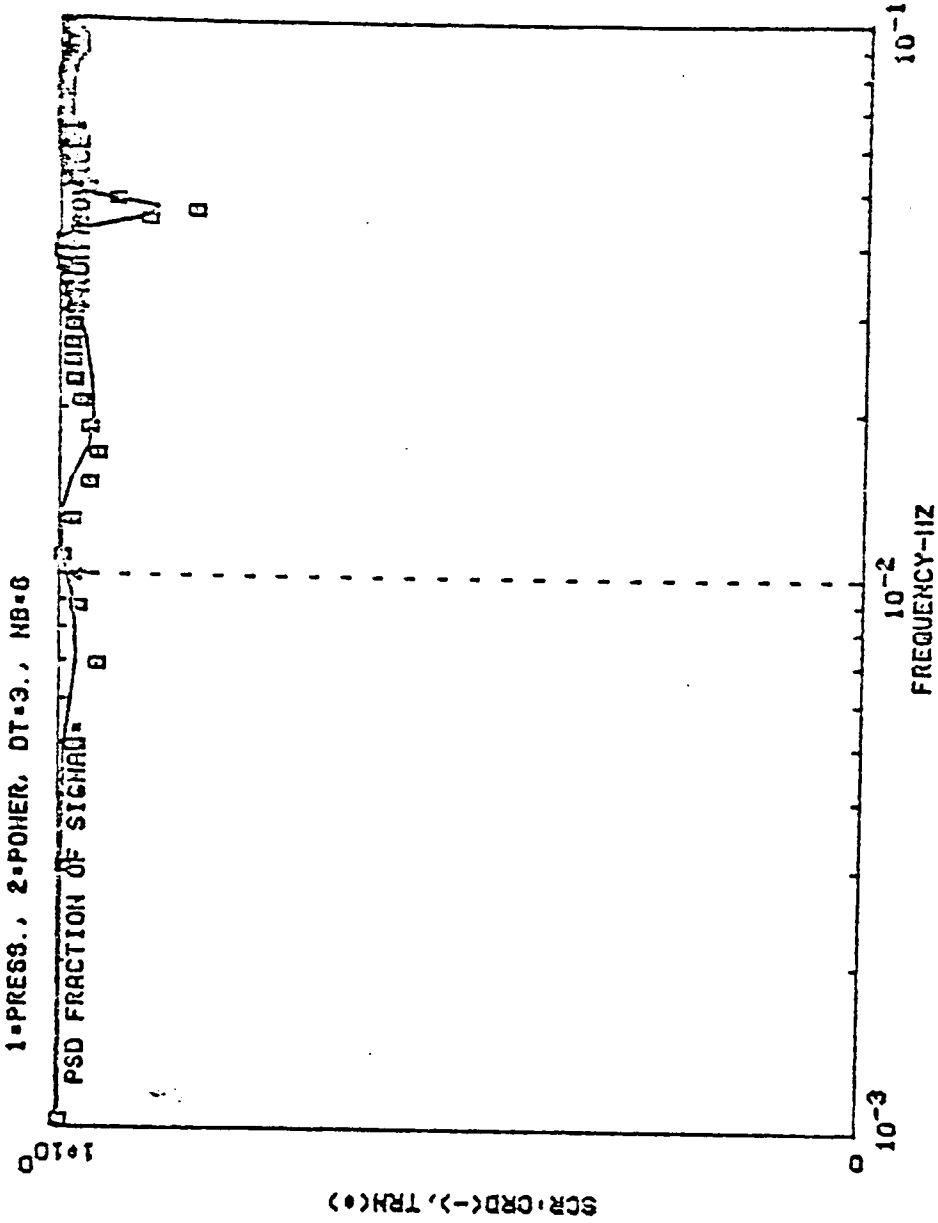


Figure 67. Signal Contribution Ratio from Source Four to Power. (A)

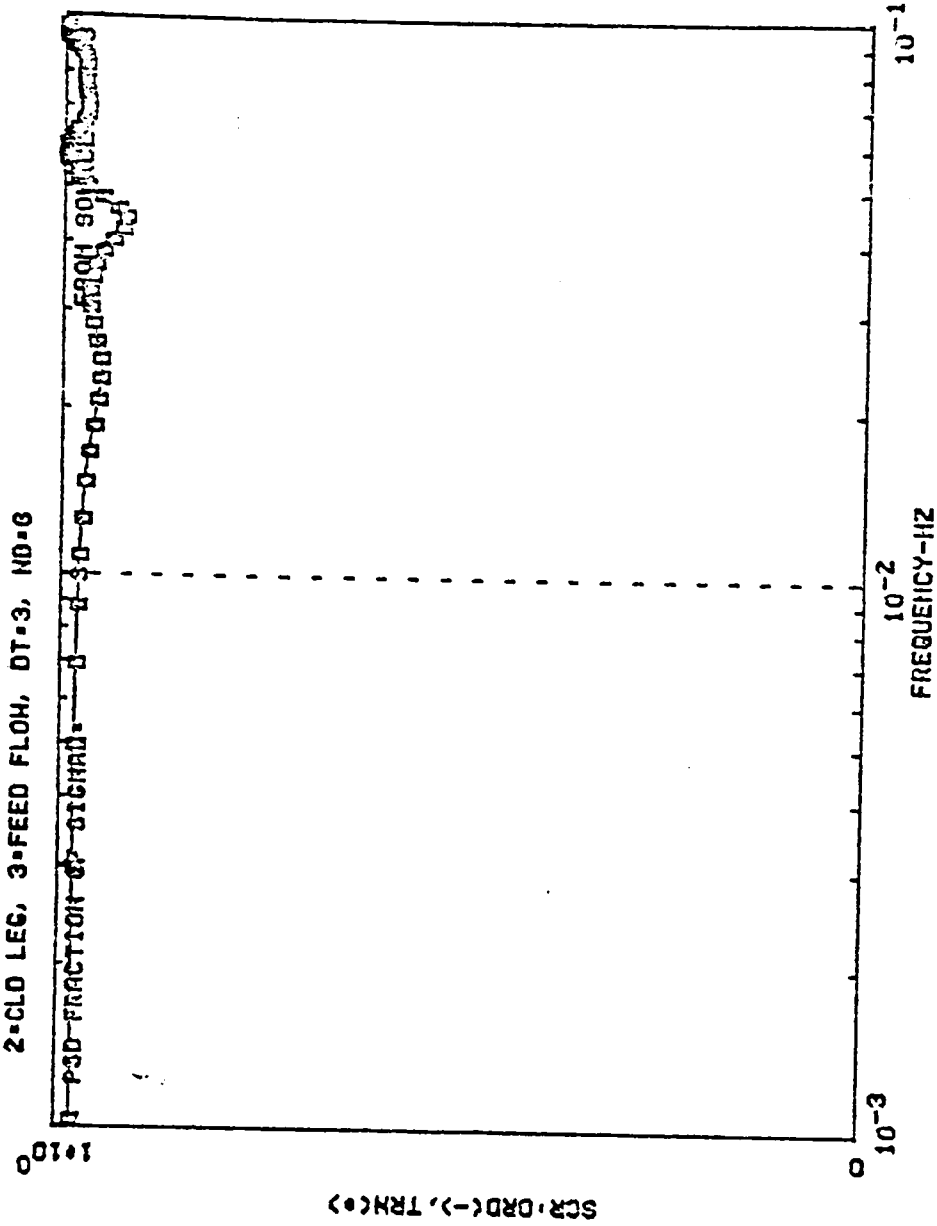


Figure 68. Signal Contribution Ratio from Source Three to Feed Water Flow Rate. (B)

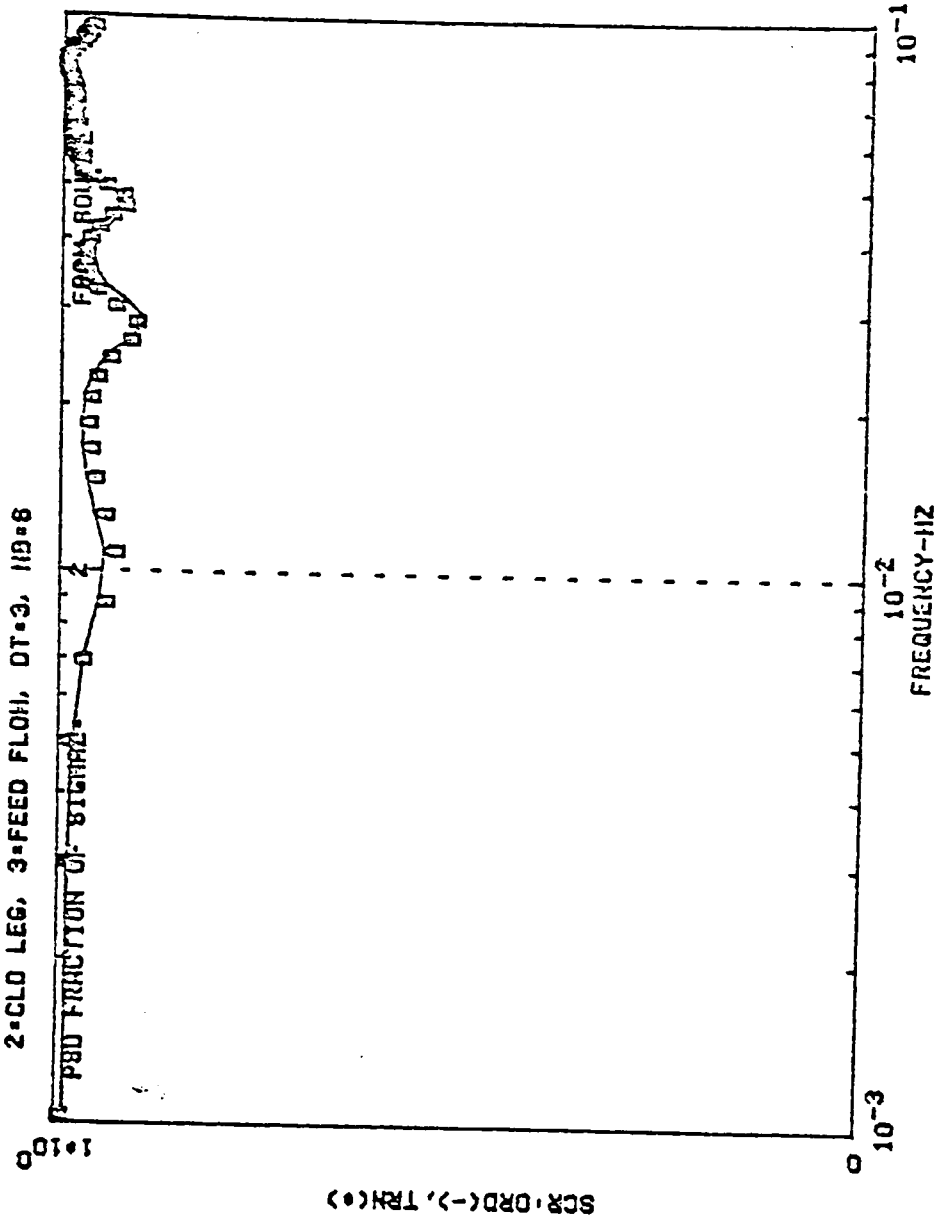


Figure 69. Signal Contribution Ratio From Source Two to Cold Leg Temperature. (B)

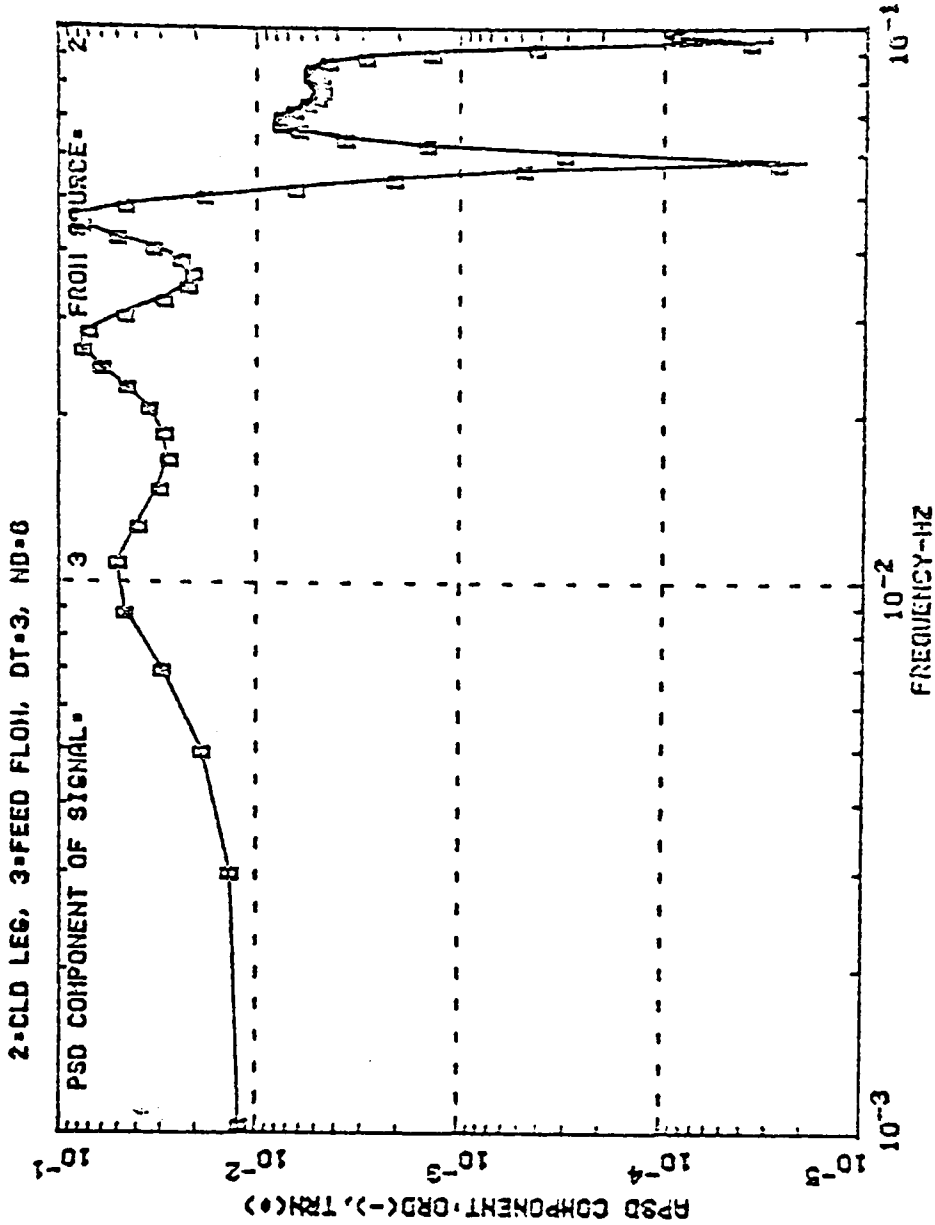


Figure 70. Power Spectrum Component of Feed Water Flow Rate from Source Two.

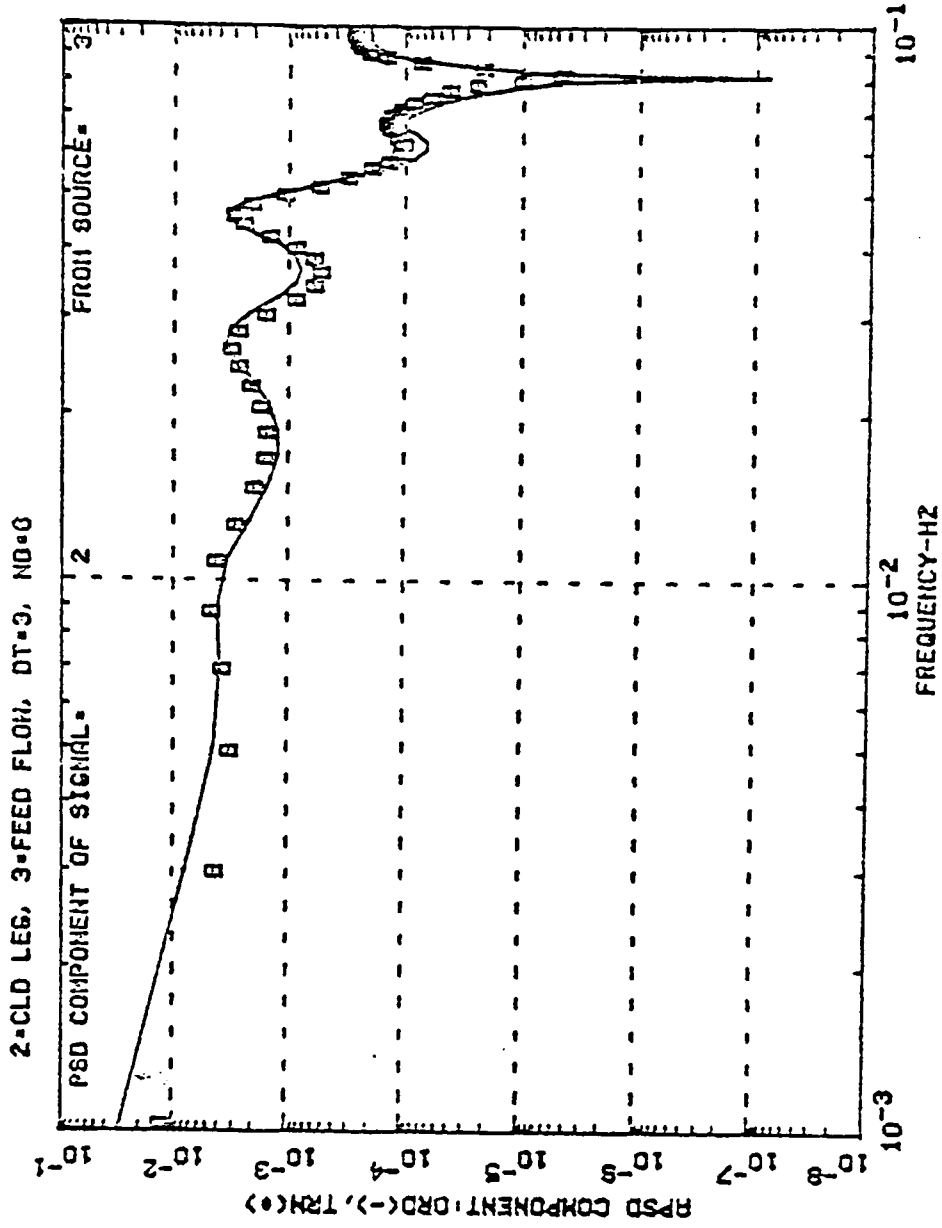


Figure 71. Power Spectrum Component of Cold leg Temperature from Source Three.

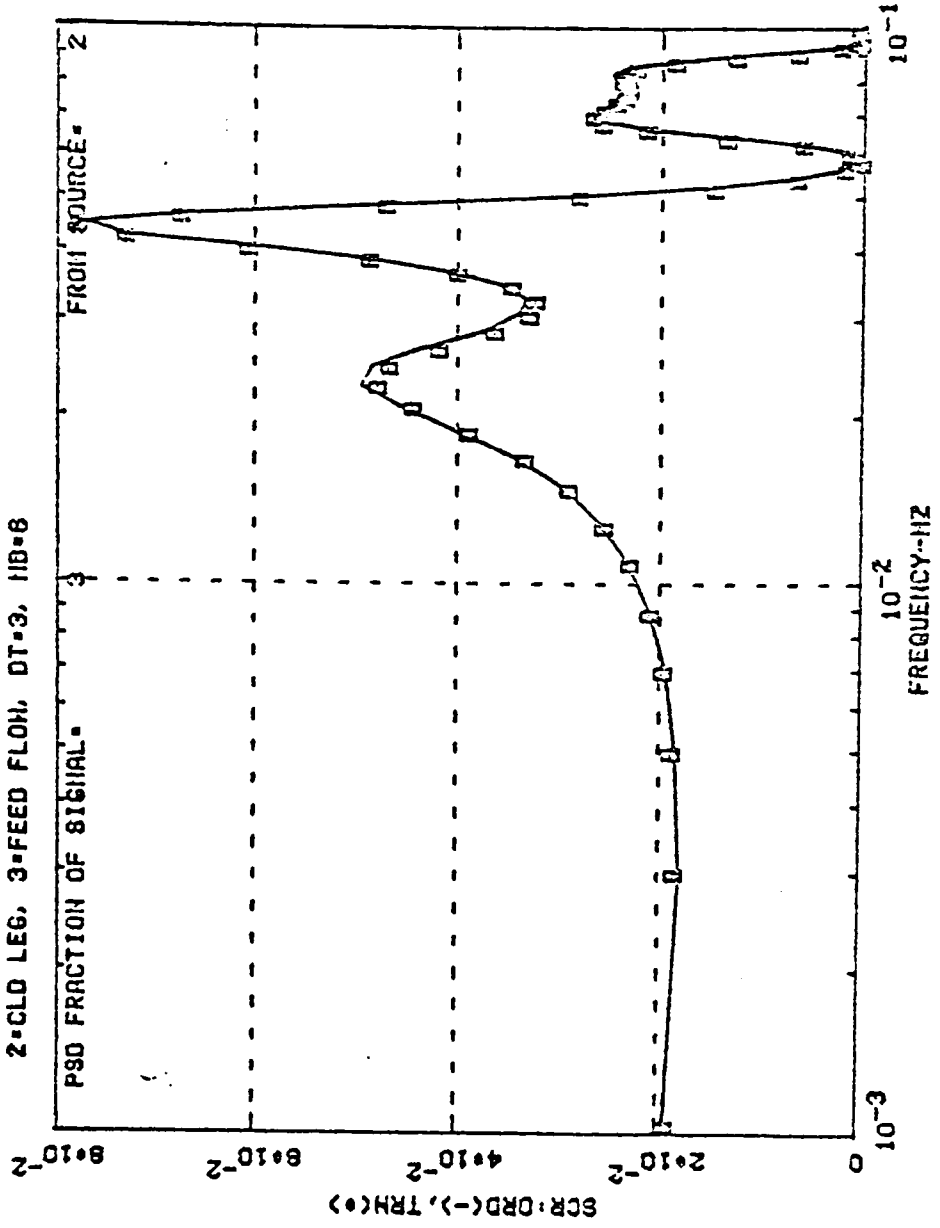


Figure 72. Signal Contribution Ratio from Source Two to Feed Water Flow Rate.

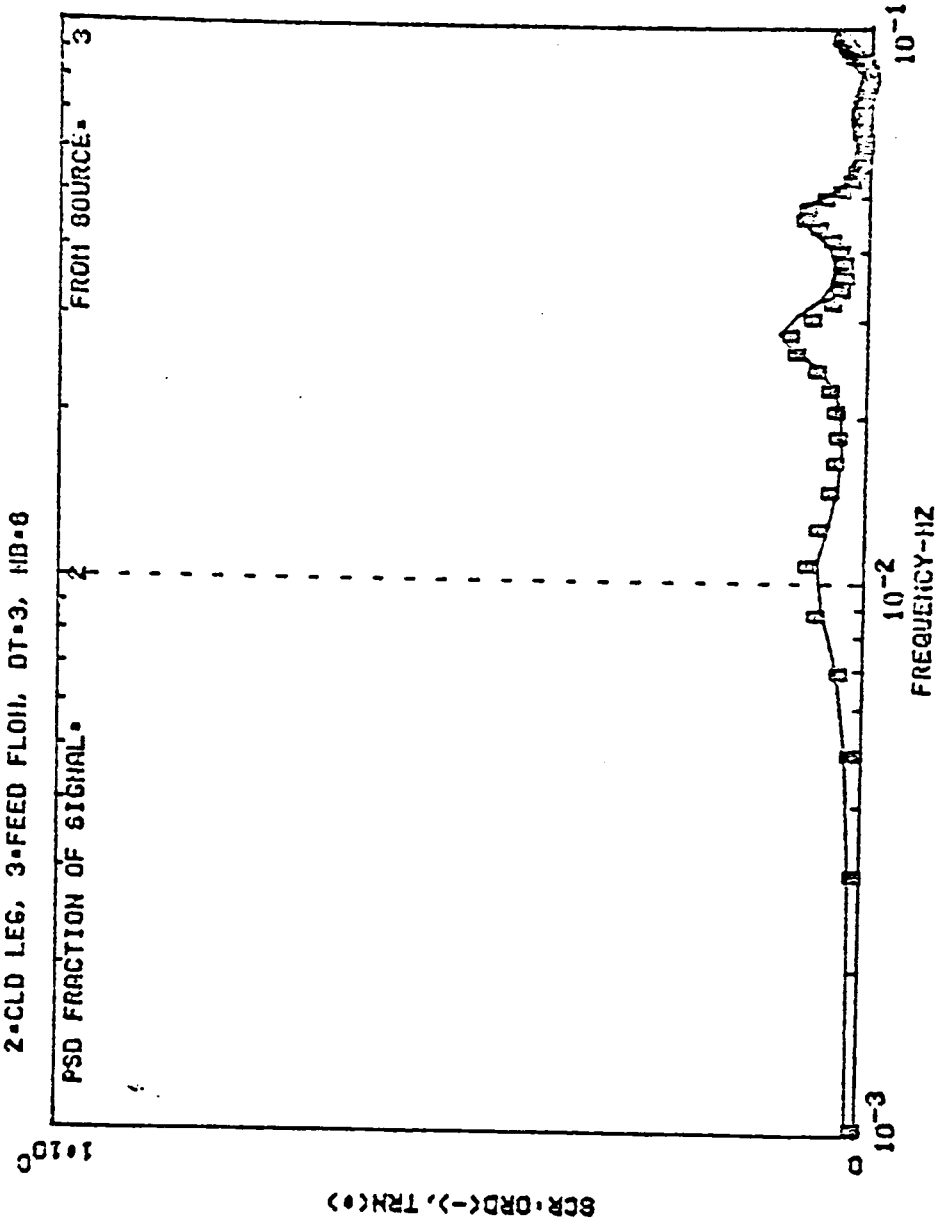


Figure 73. Signal Contribution Ratio from Source Three to Cold Leg Temperature.

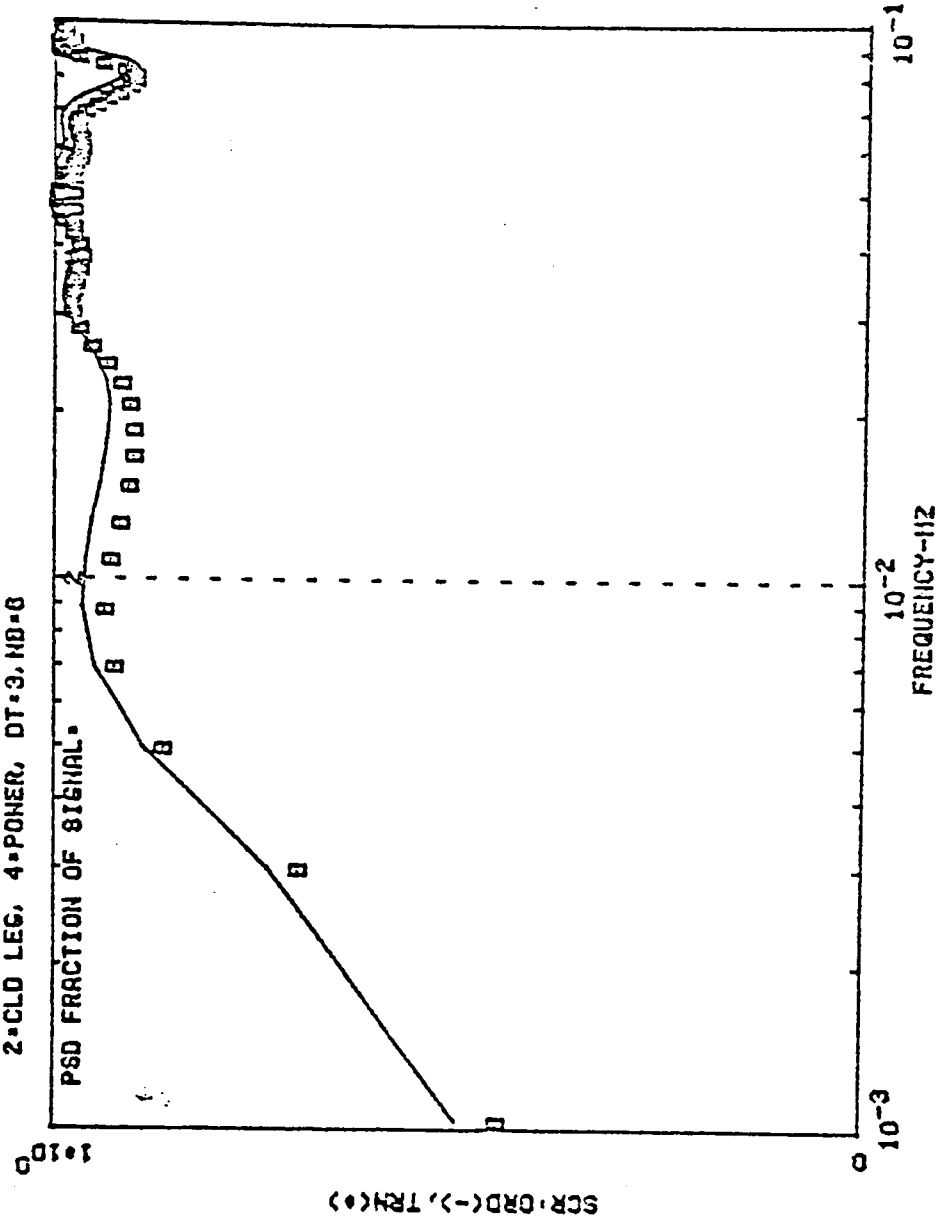


Figure 74. Signal Contribution Ratio from Source Two to Cold Leg Temperature. (C)

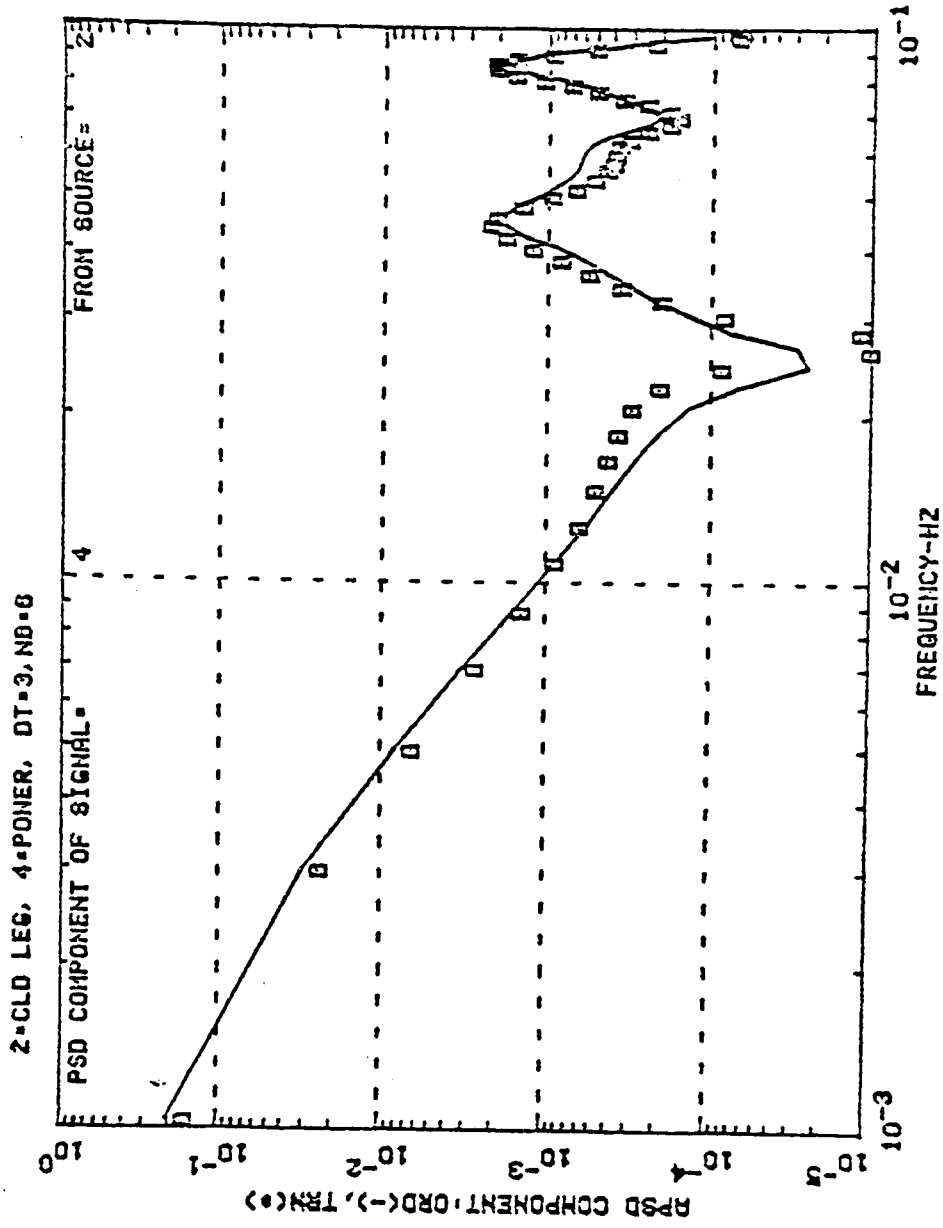


Figure 75. Power Spectrum Component of Power from Source Two.

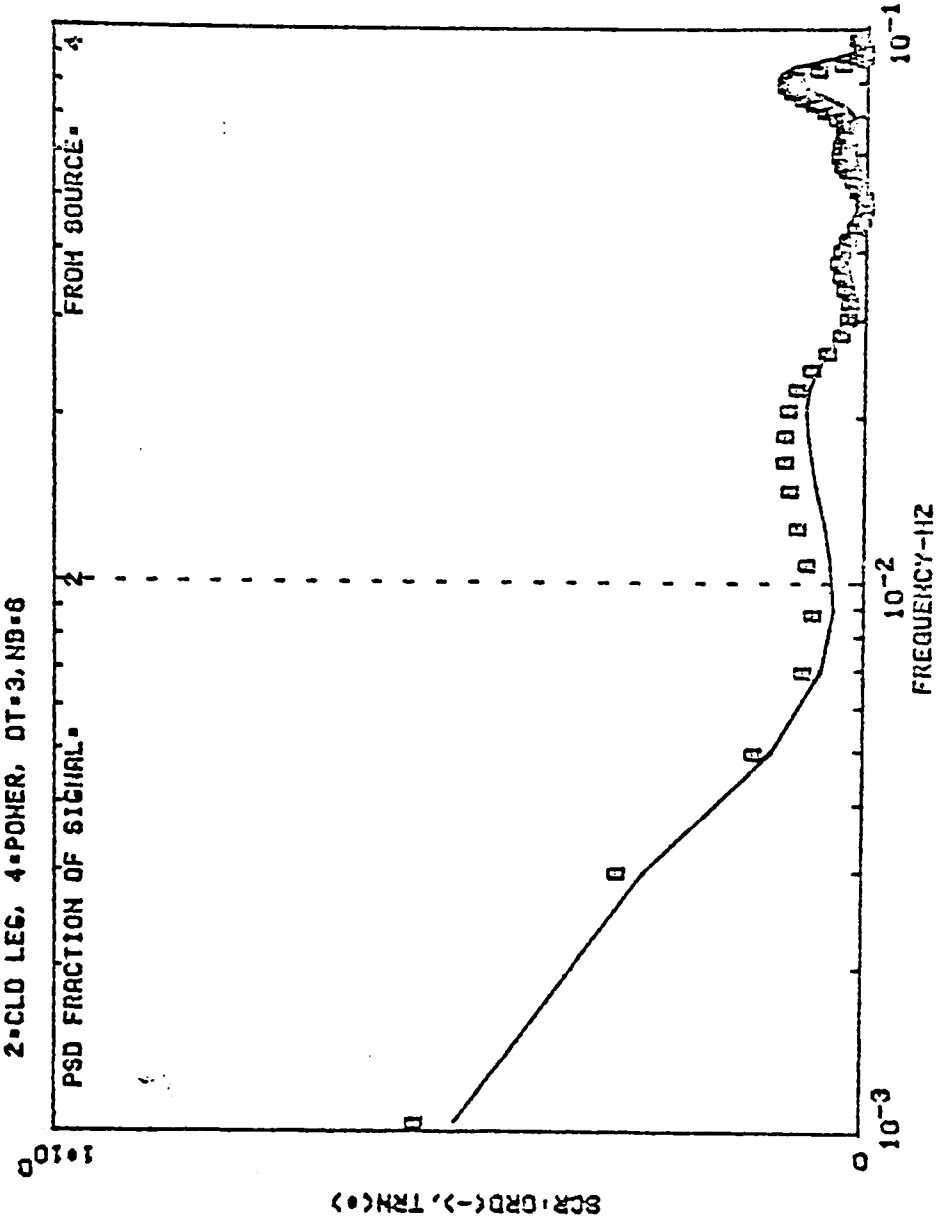


Figure 76. Signal Contribution Ratio from Source Four to Cold Leg Temperature.

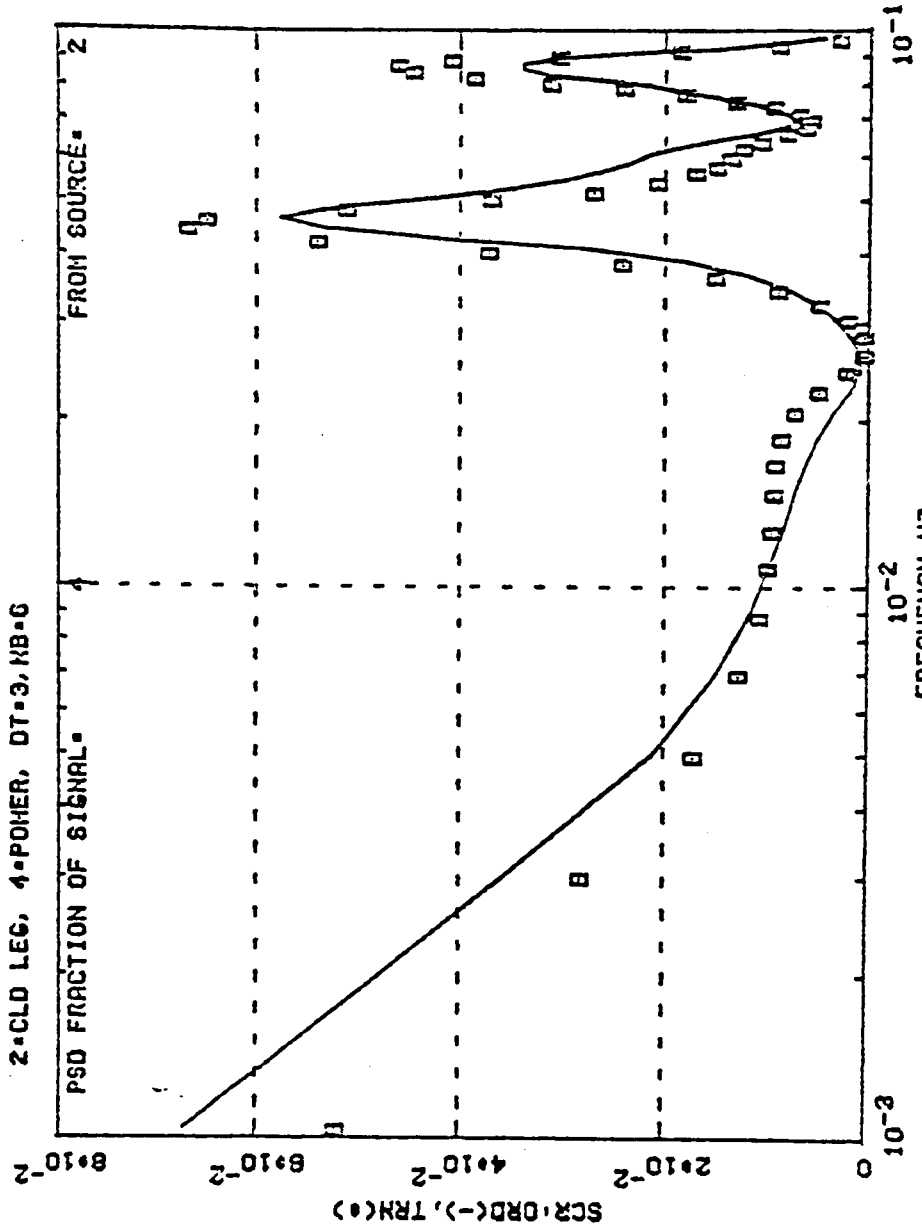


Figure 77. Signal Contribution Ratio from Source Two to Power.

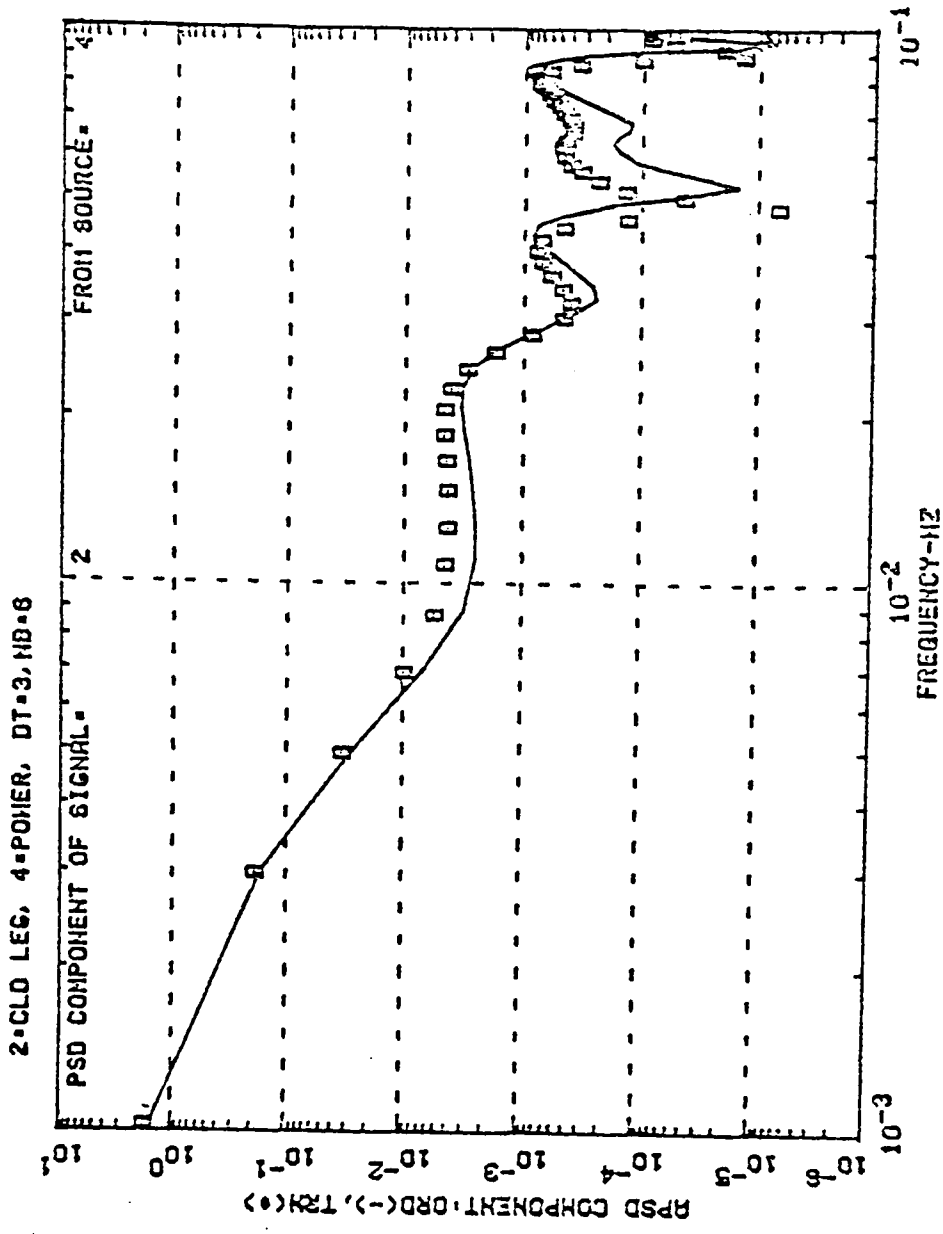


Figure 78. Power Spectrum Component of Cold Leg Temperature from Source Four.

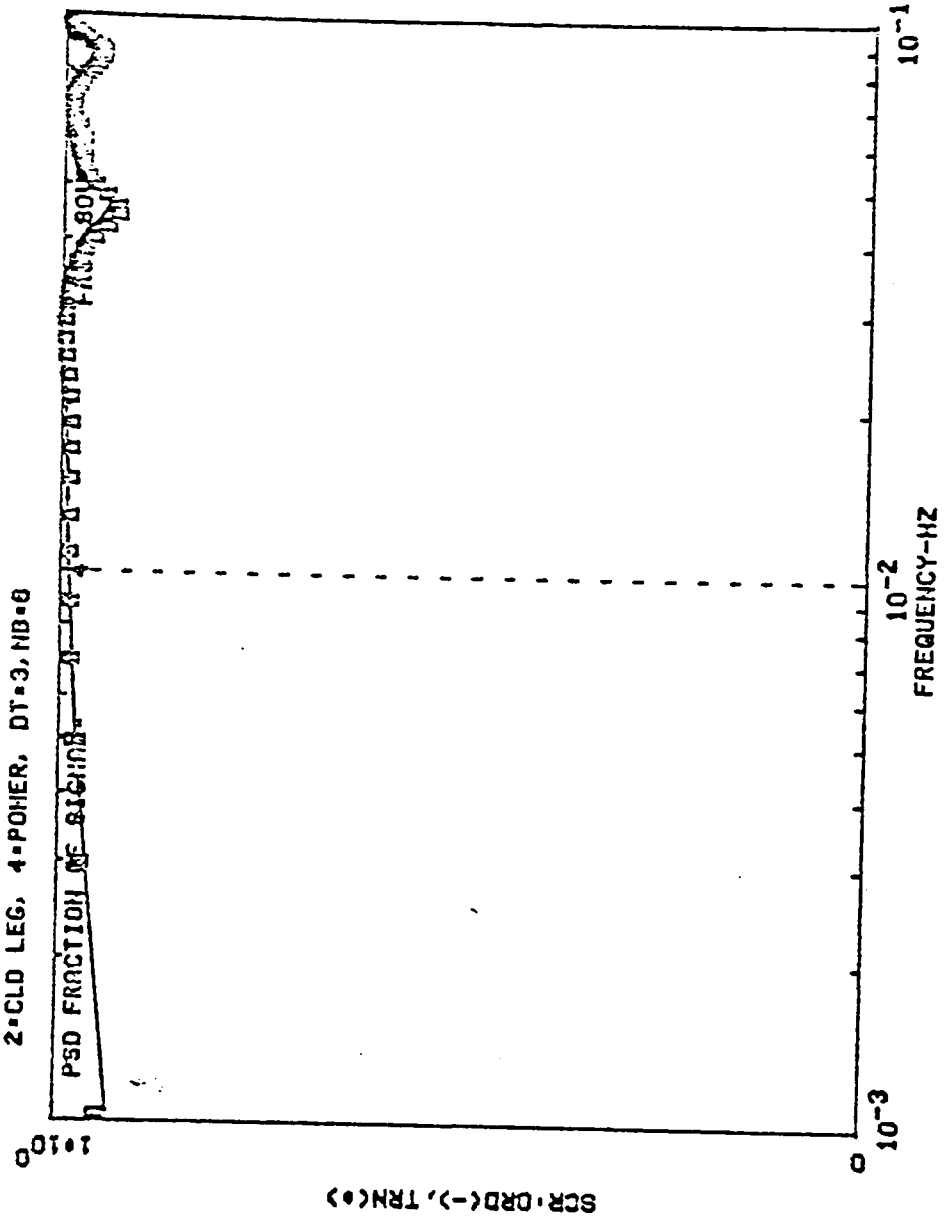


Figure 79. Signal Contribution Ratio from Source Four to Power.
(B)

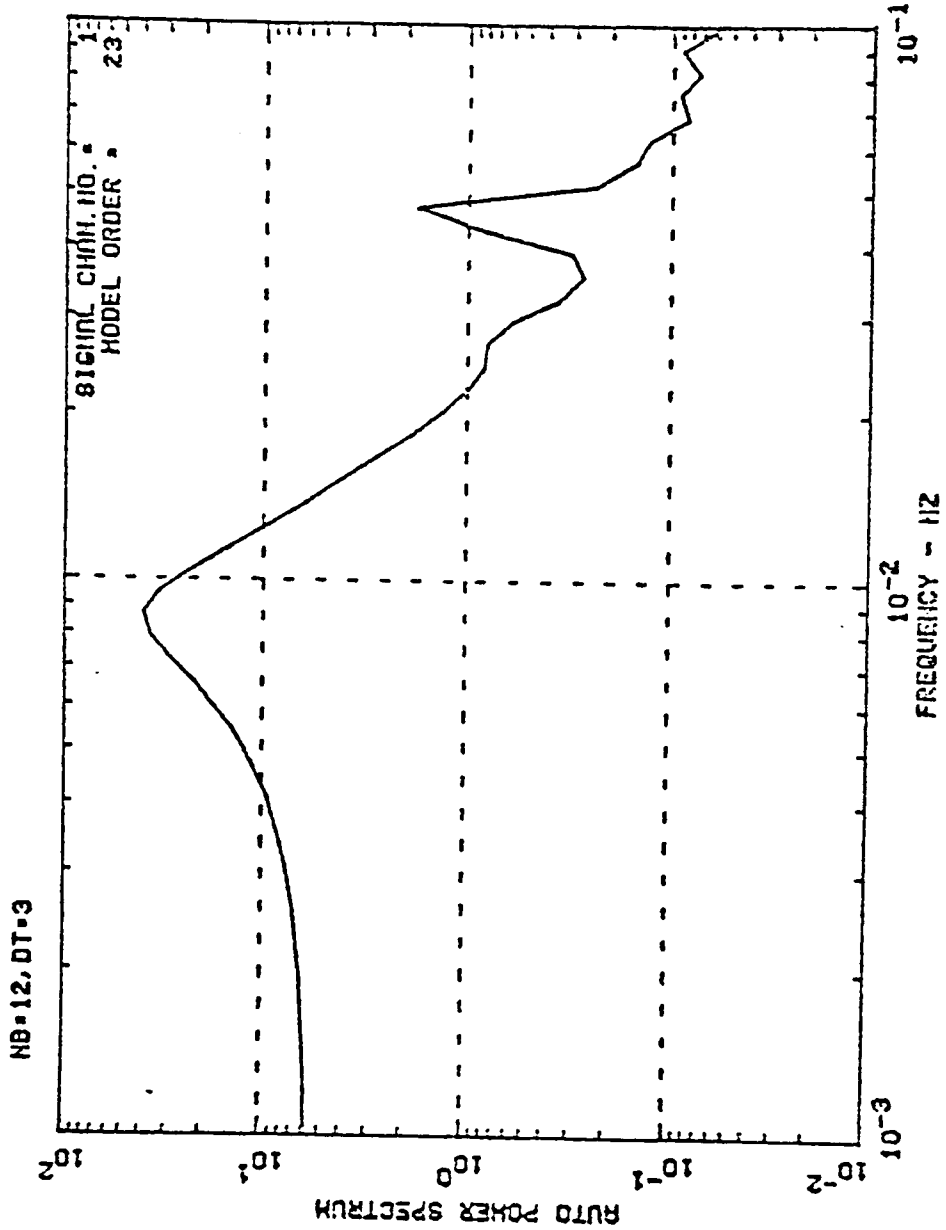


Figure 80. Power Spectrum of Primary Pressure (MAR).

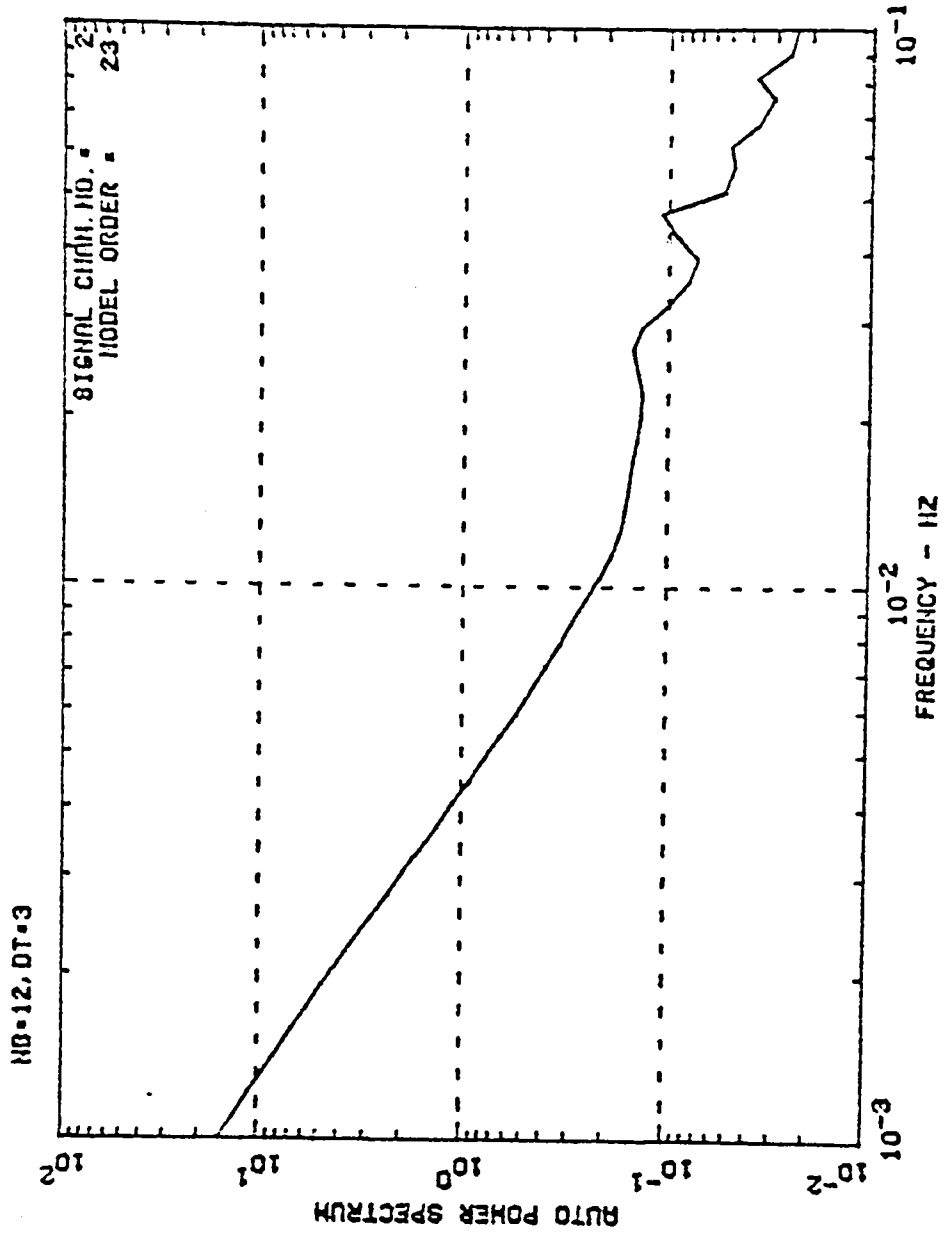


Figure 81. Power Spectrum of Cold Leg Temperature (MAR).

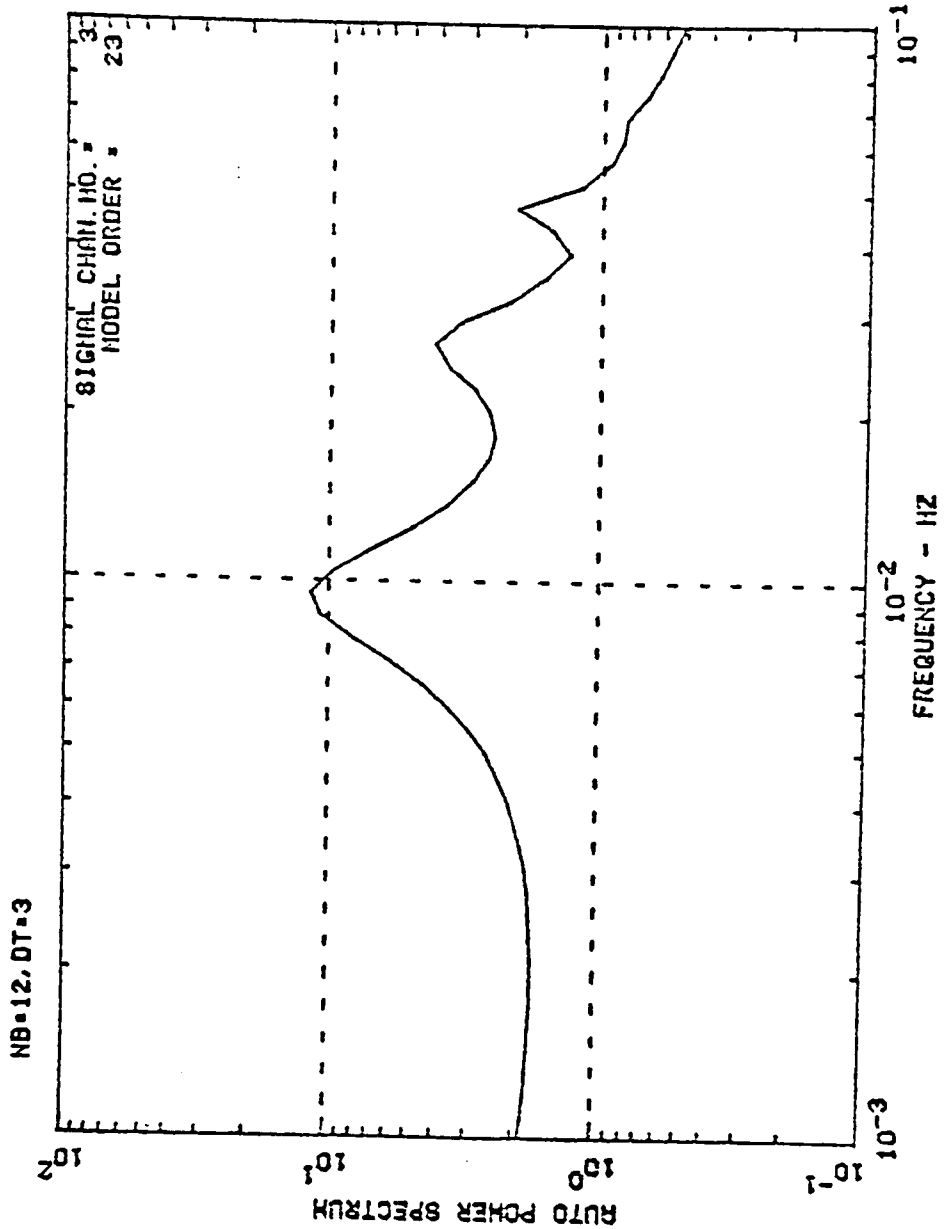


Figure 82. Power Spectrum of Feed Water Flow Rate (MAR).

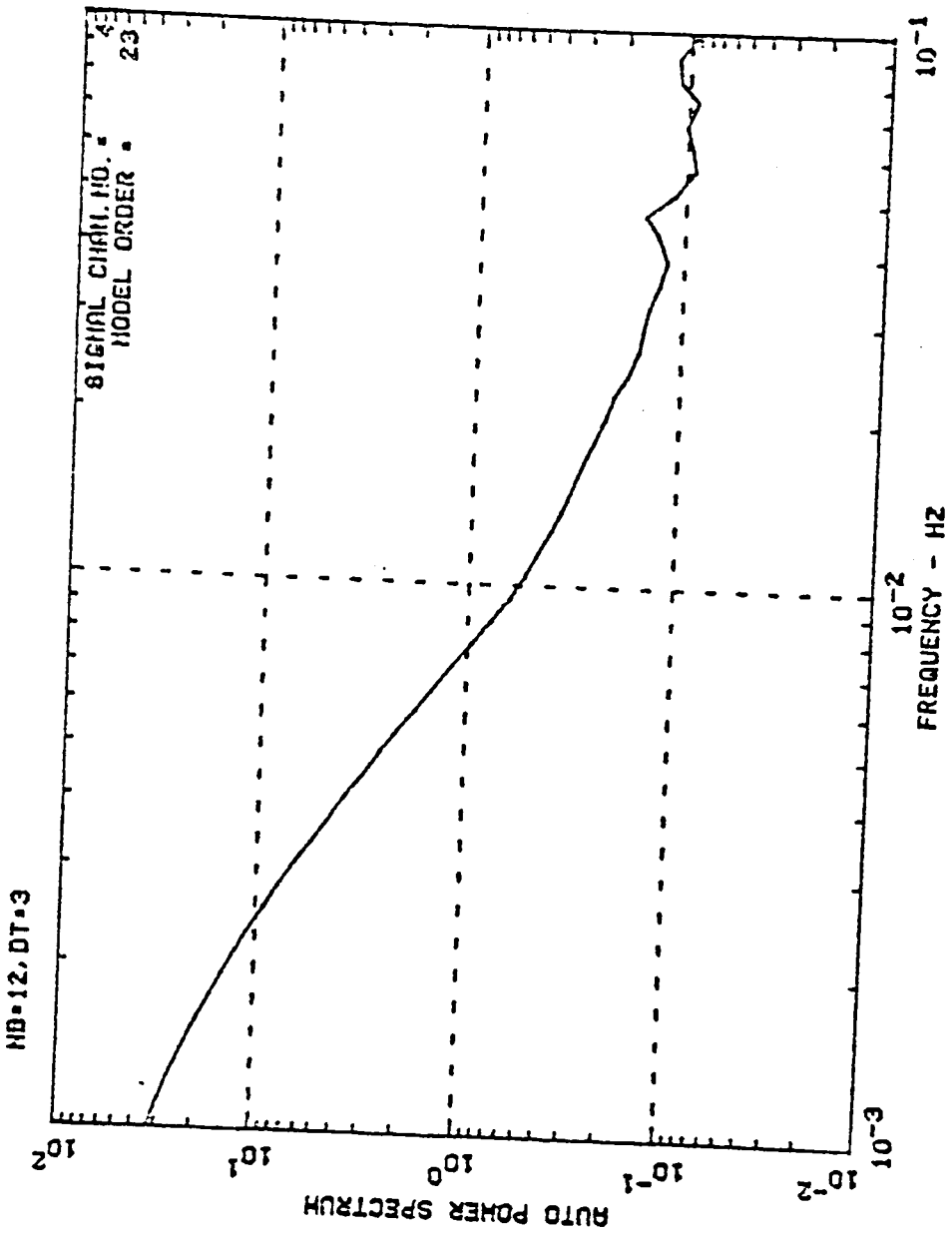


Figure 83. Power Spectrum of Power (MAR).

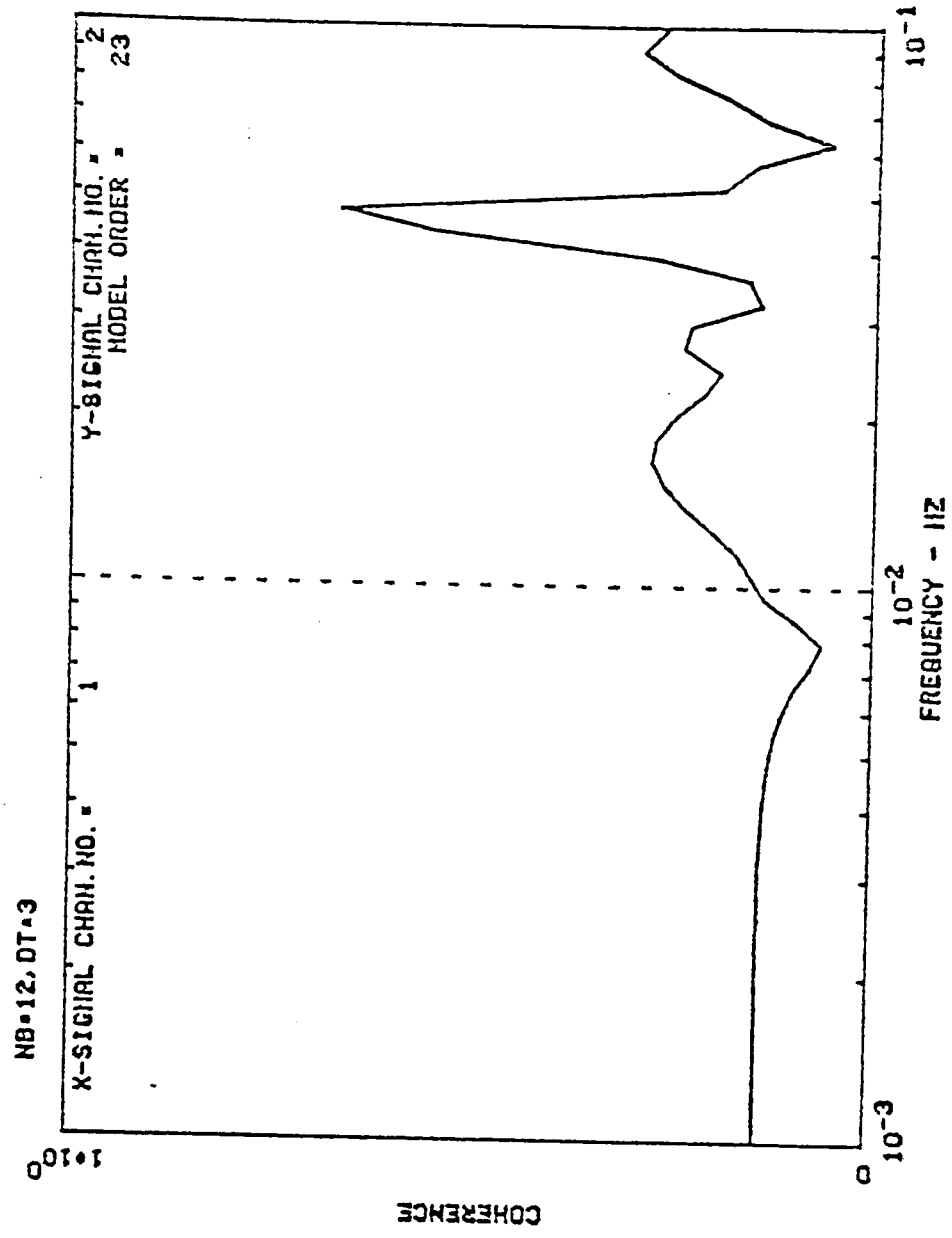


Figure 84. Coherence of Primary Pressure Versus Cold Leg Temperature (MAR).

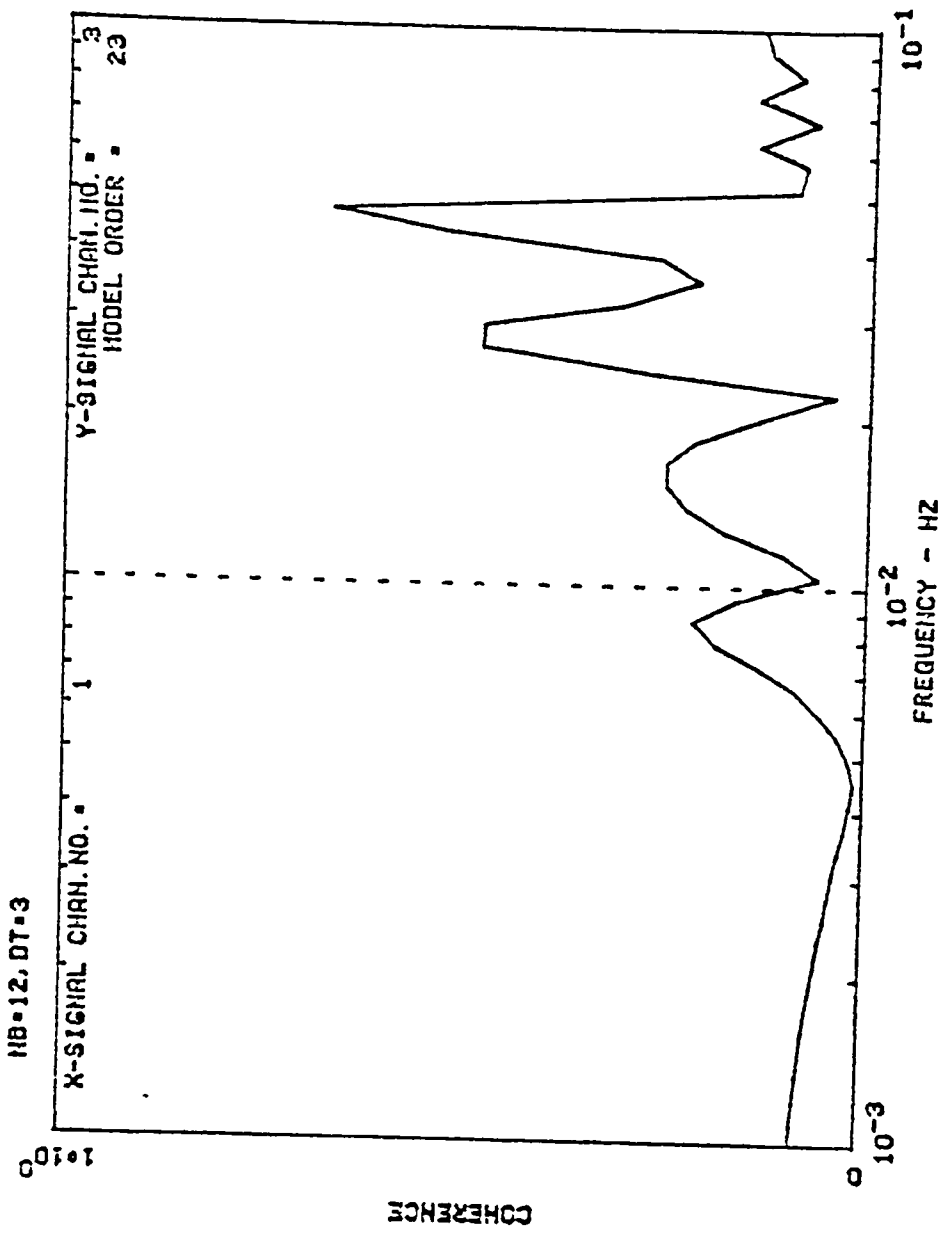


Figure 85. Coherence of Primary Pressure Versus Feed Water Flow Rate (MAR).

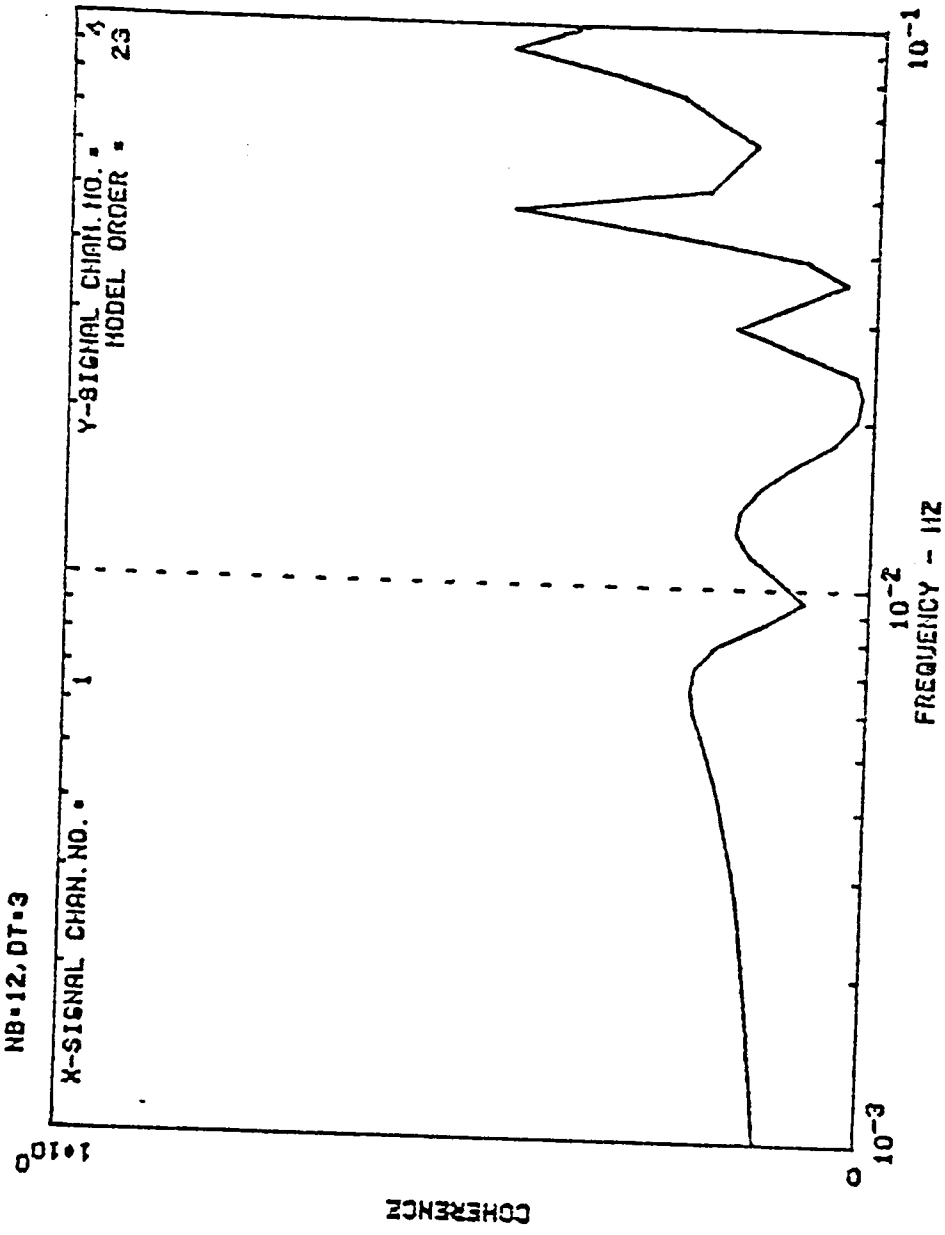


Figure 86. Coherence of Primary Pressure Versus Power (MAR).

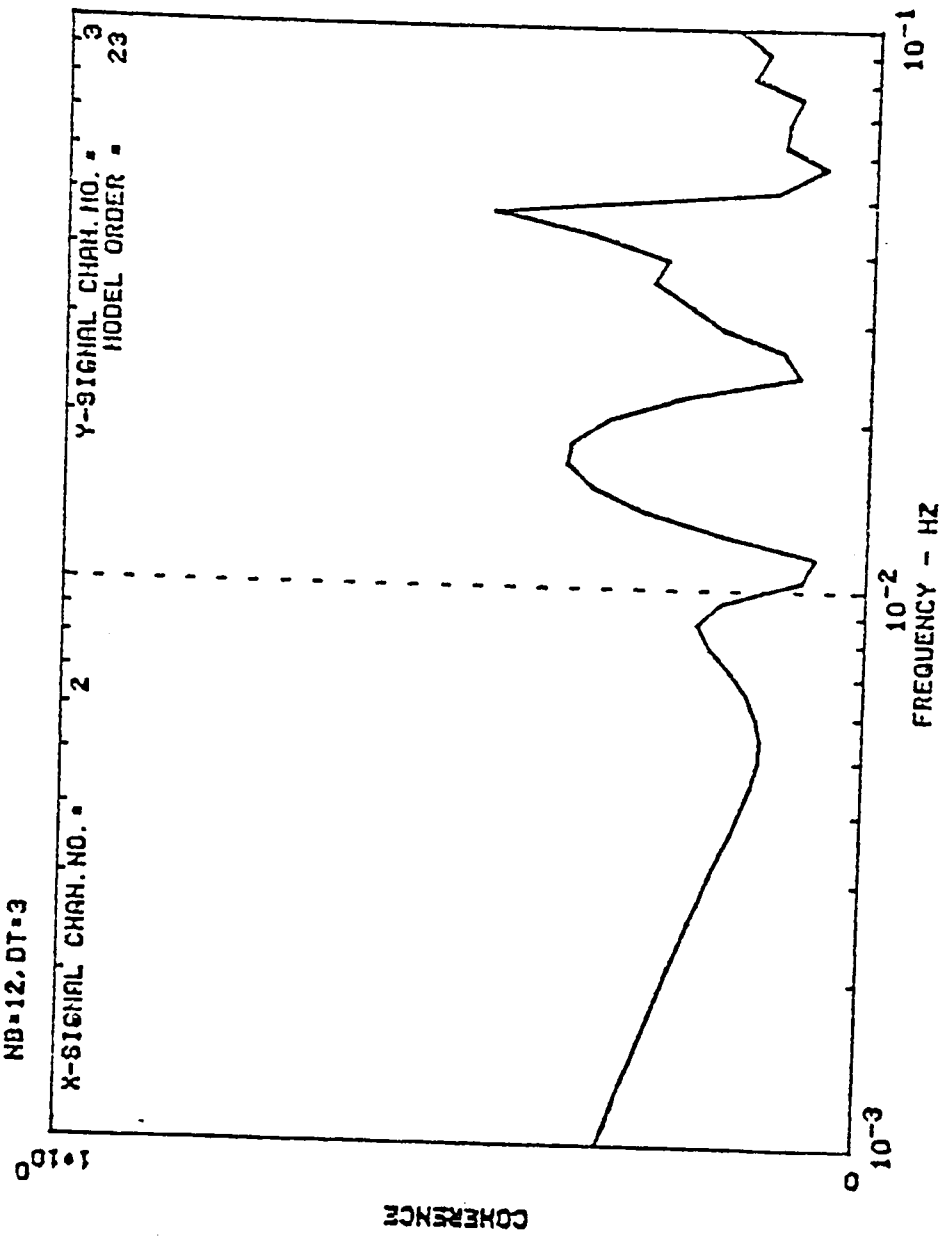


Figure 87. Coherence of Cold Leg Temperature Versus Feed Water Flow Rate (MAR).

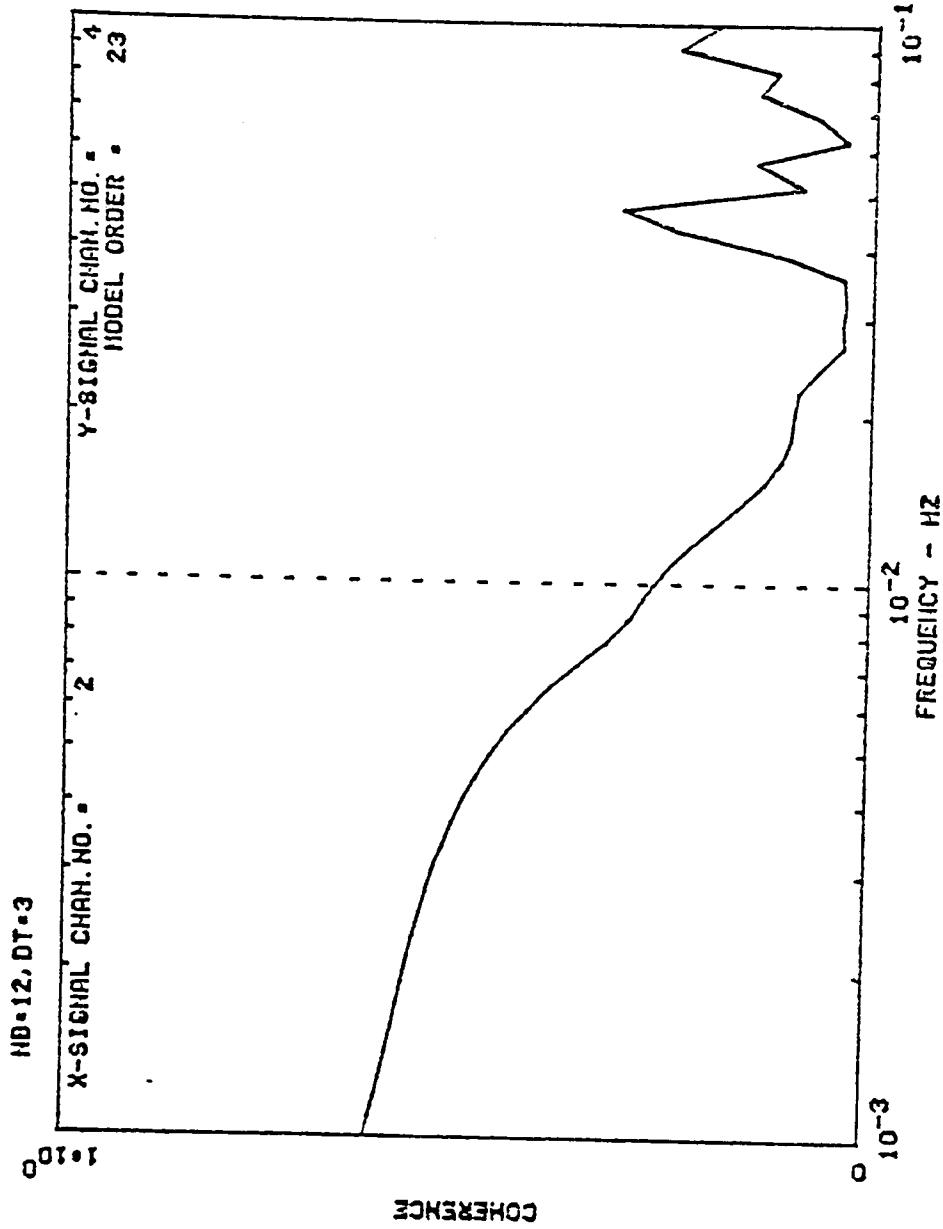


Figure 88. Coherence of Cold Leg Temperature Versus Power (MAR).

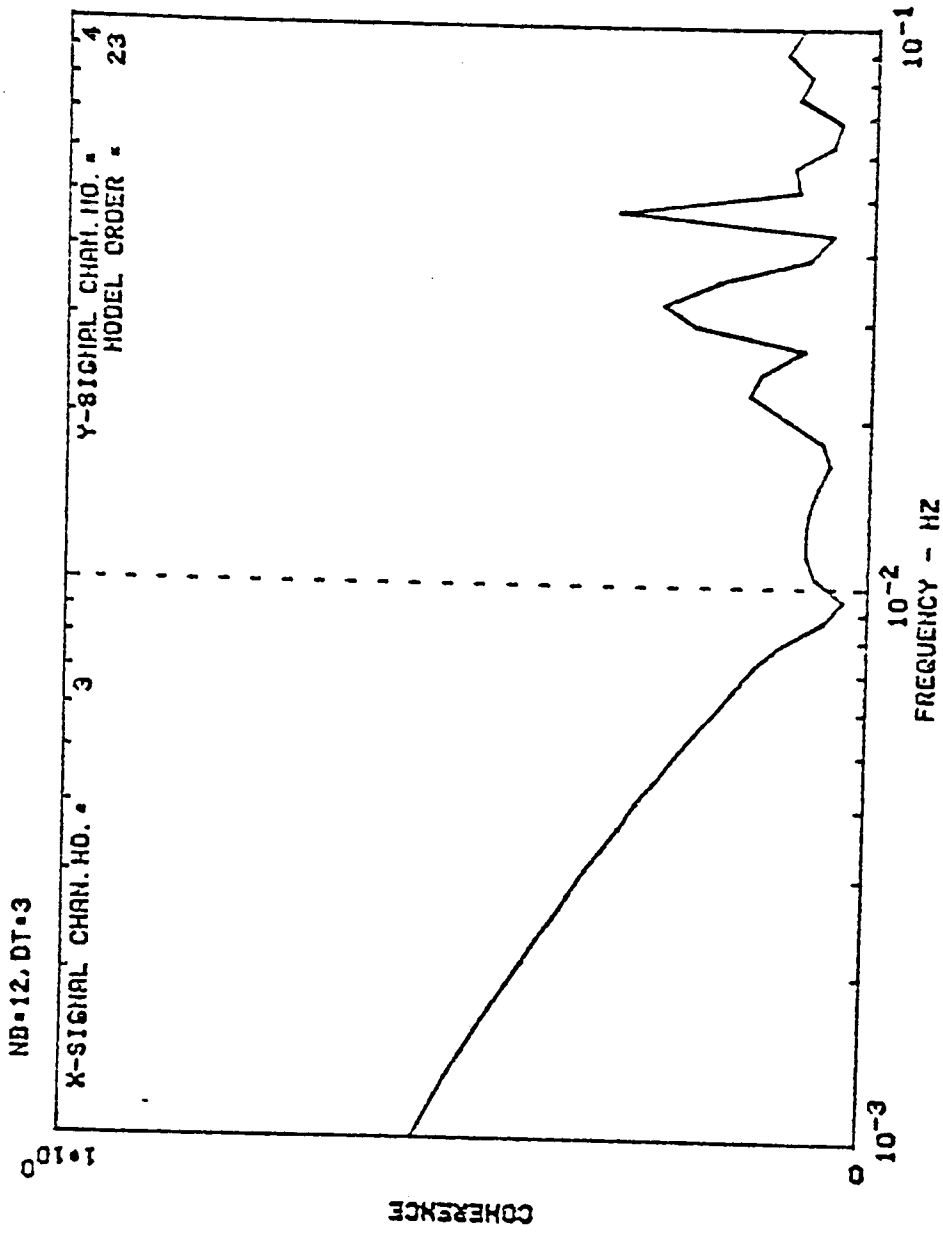


Figure 89. Coherence of Feed Water Flow Rate Versus Power (MAR).

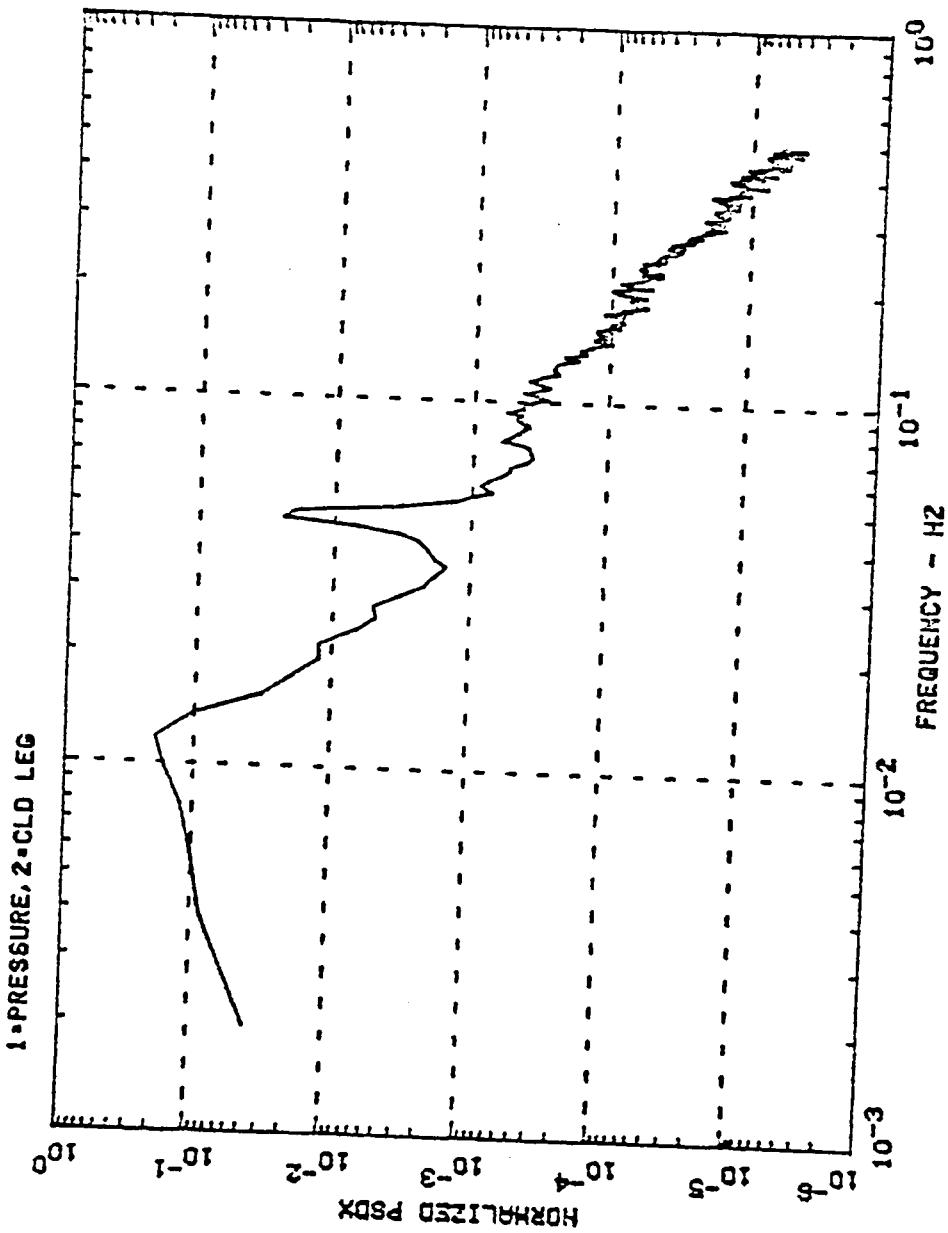


Figure 90. Normalized Power Spectrum of Primary Pressure (FFT).

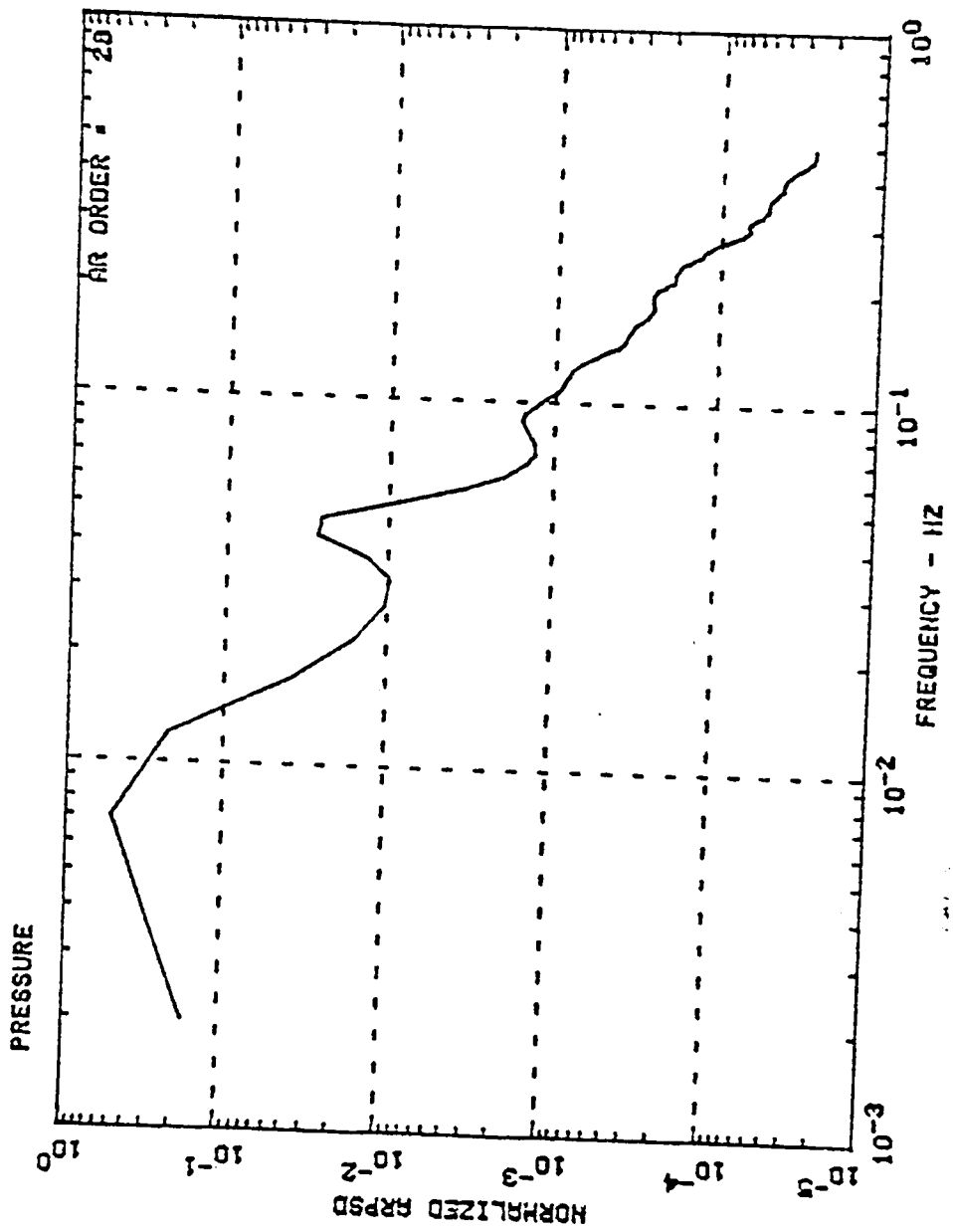


Figure 91. Normalized Power Spectrum of Primary Pressure (AR).

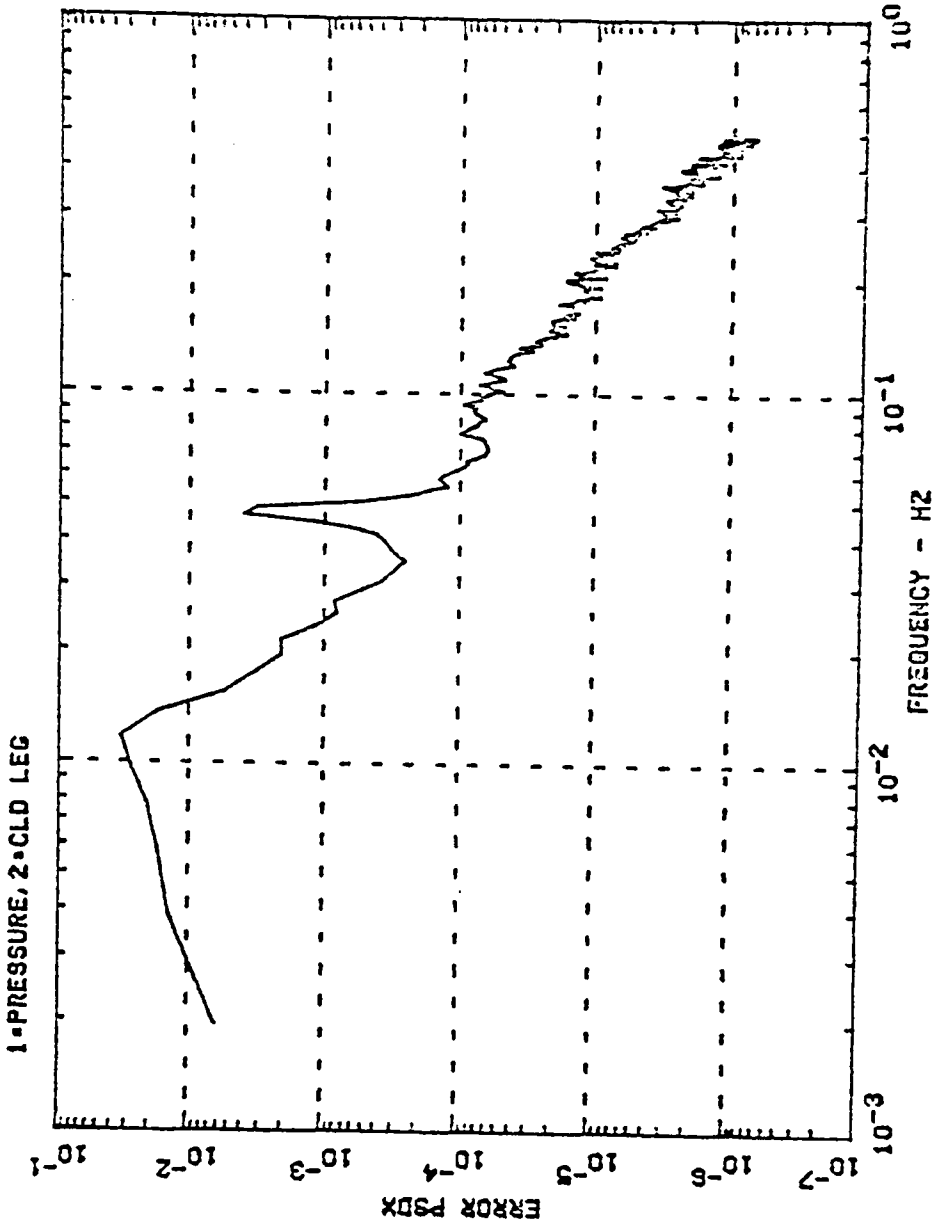


Figure 92. Error Spectrum of Primary Pressure (FFT).

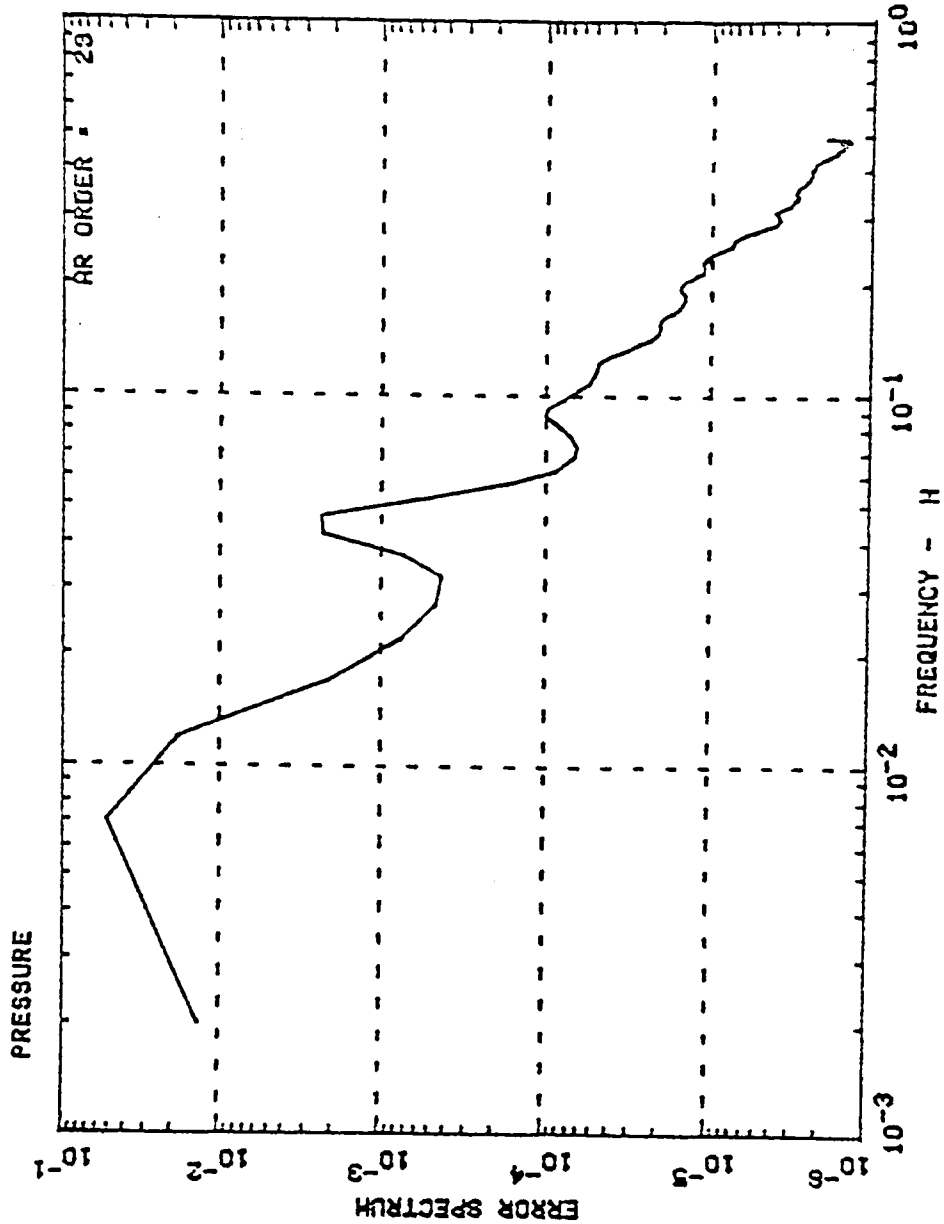


Figure 93. Error Spectrum of Primary Pressure (AR).

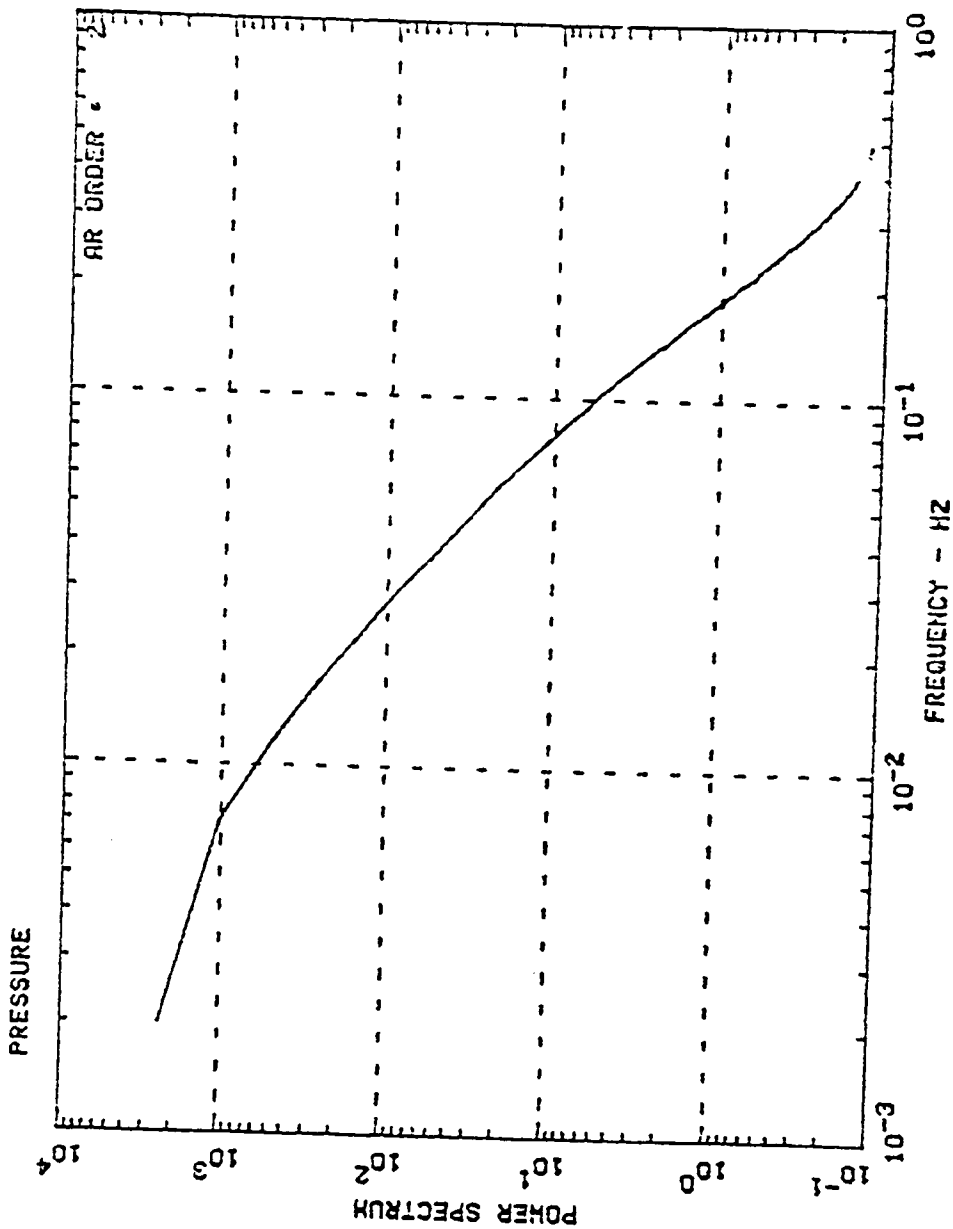


Figure 94. Power Spectrum of Primary Pressure (Order 2).

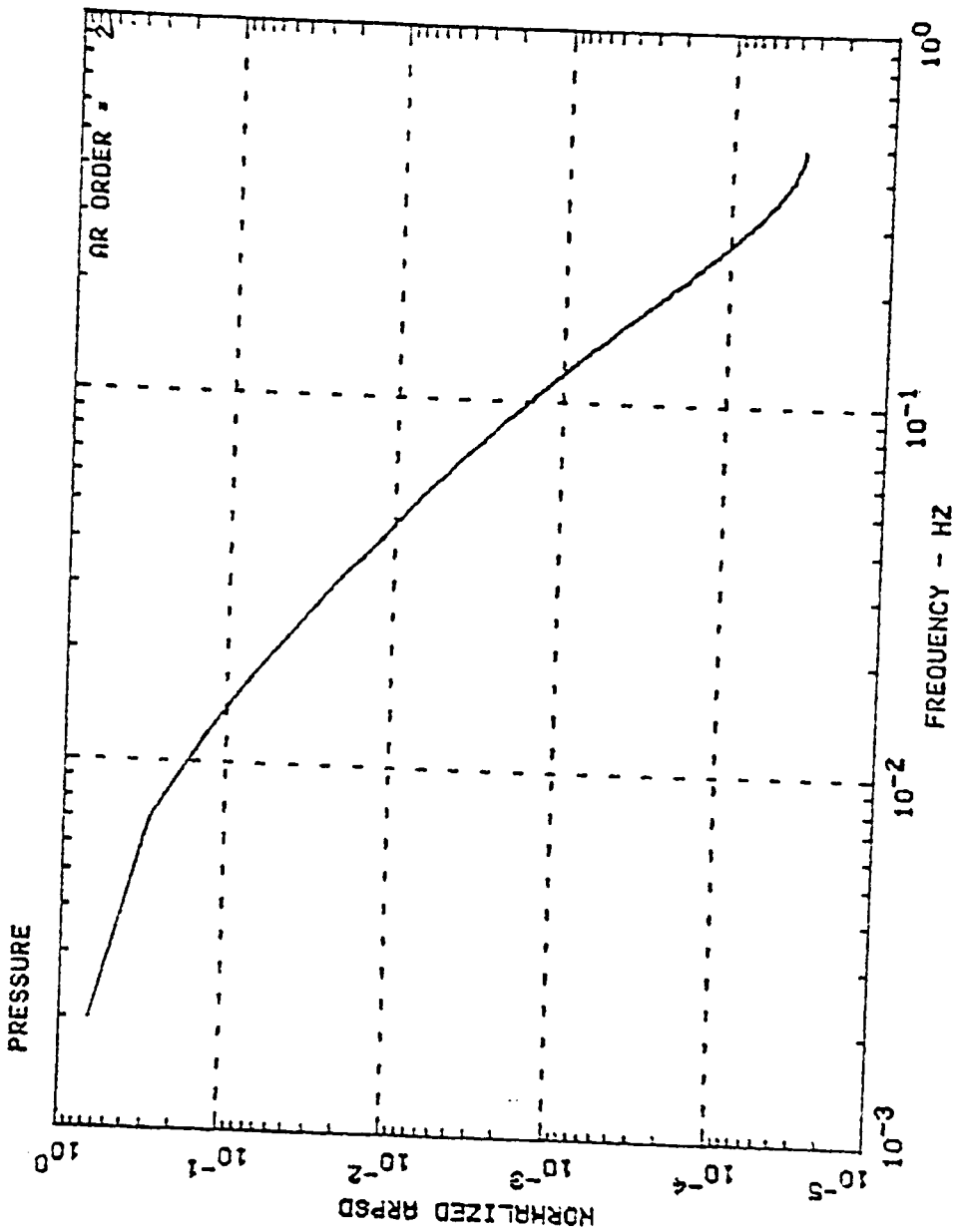


Figure 95. Normalized Power Spectrum of Primary Pressure (Order 2).

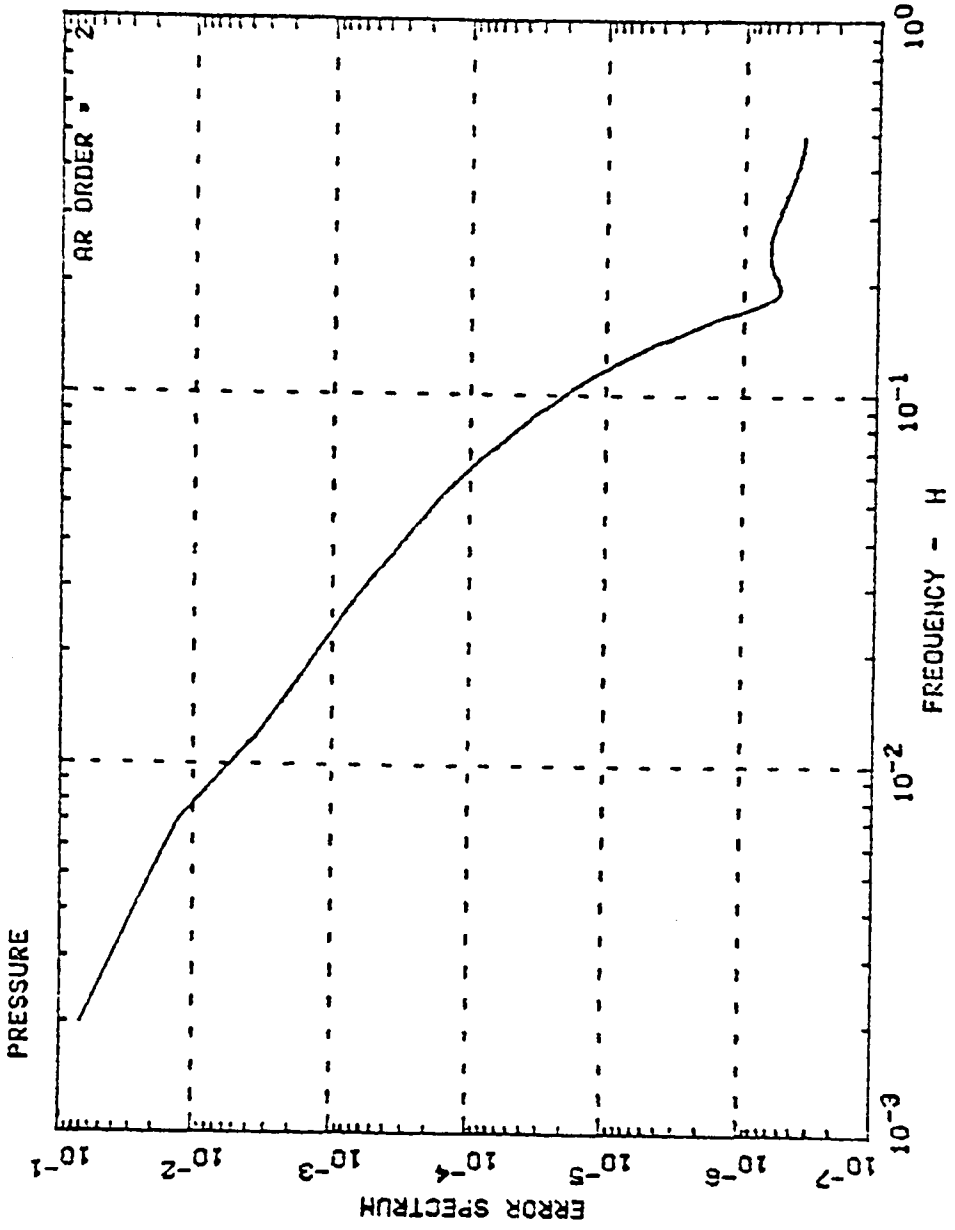


Figure 96. Error Spectrum of Primary Pressure (Order 2).

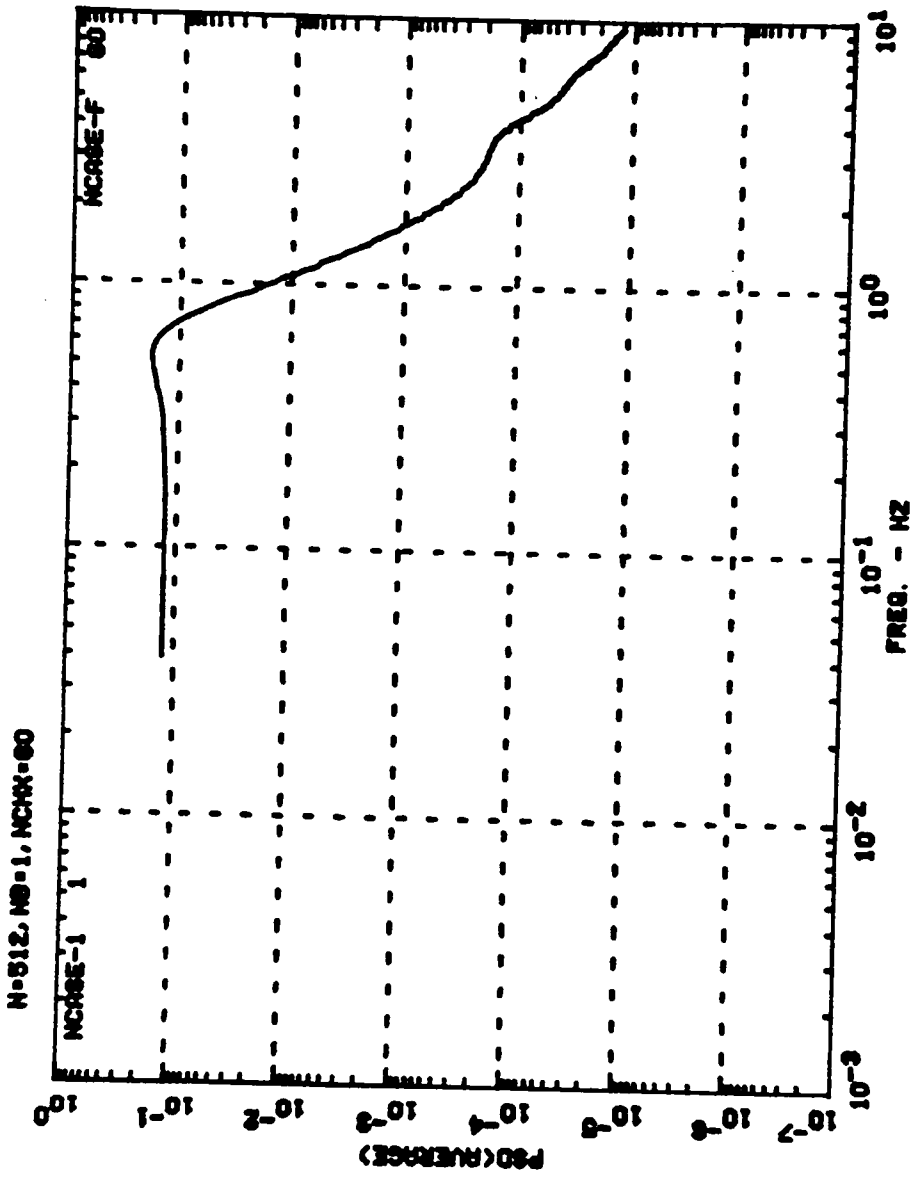


Figure 97. Average Power Spectrum of Case (1) for Order 9.

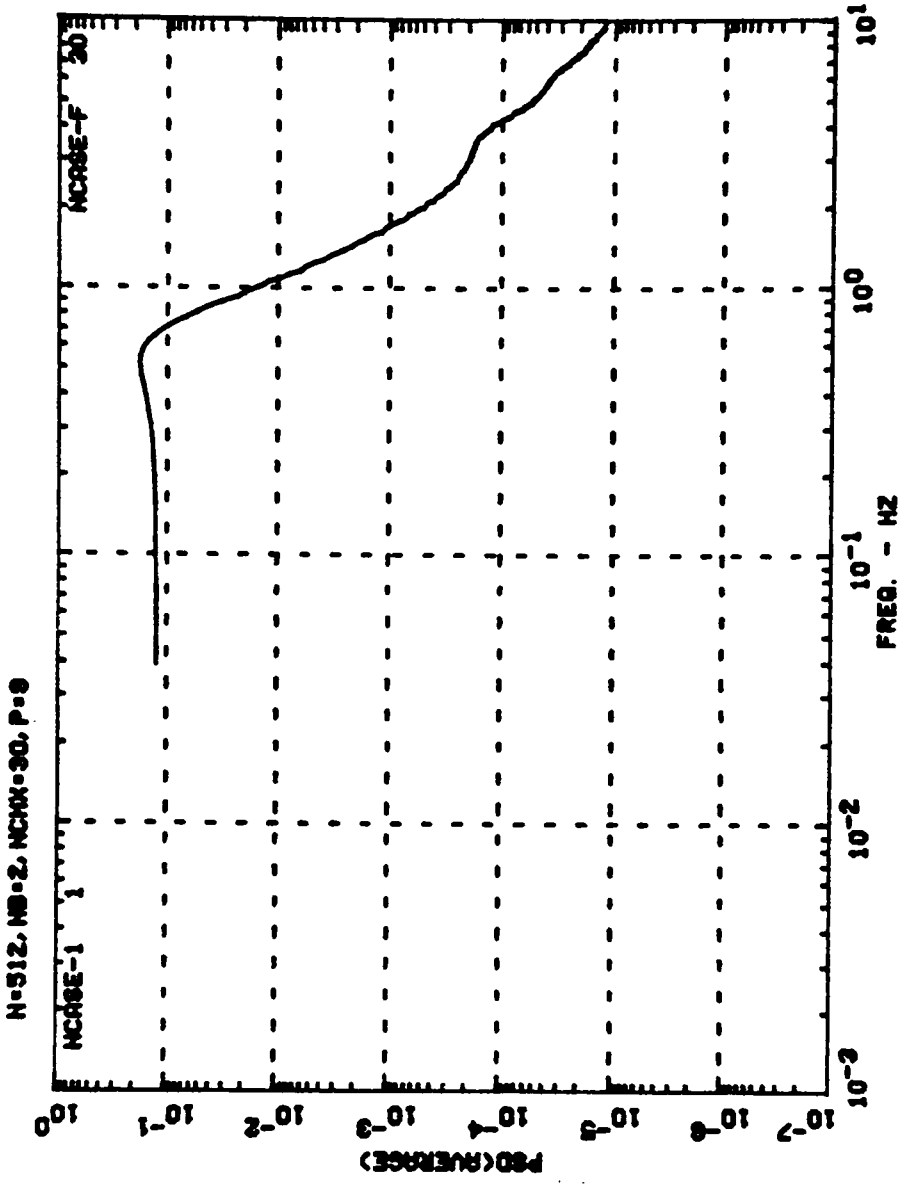


Figure 98. Average Power Spectrum of Case (2) for Order 9.

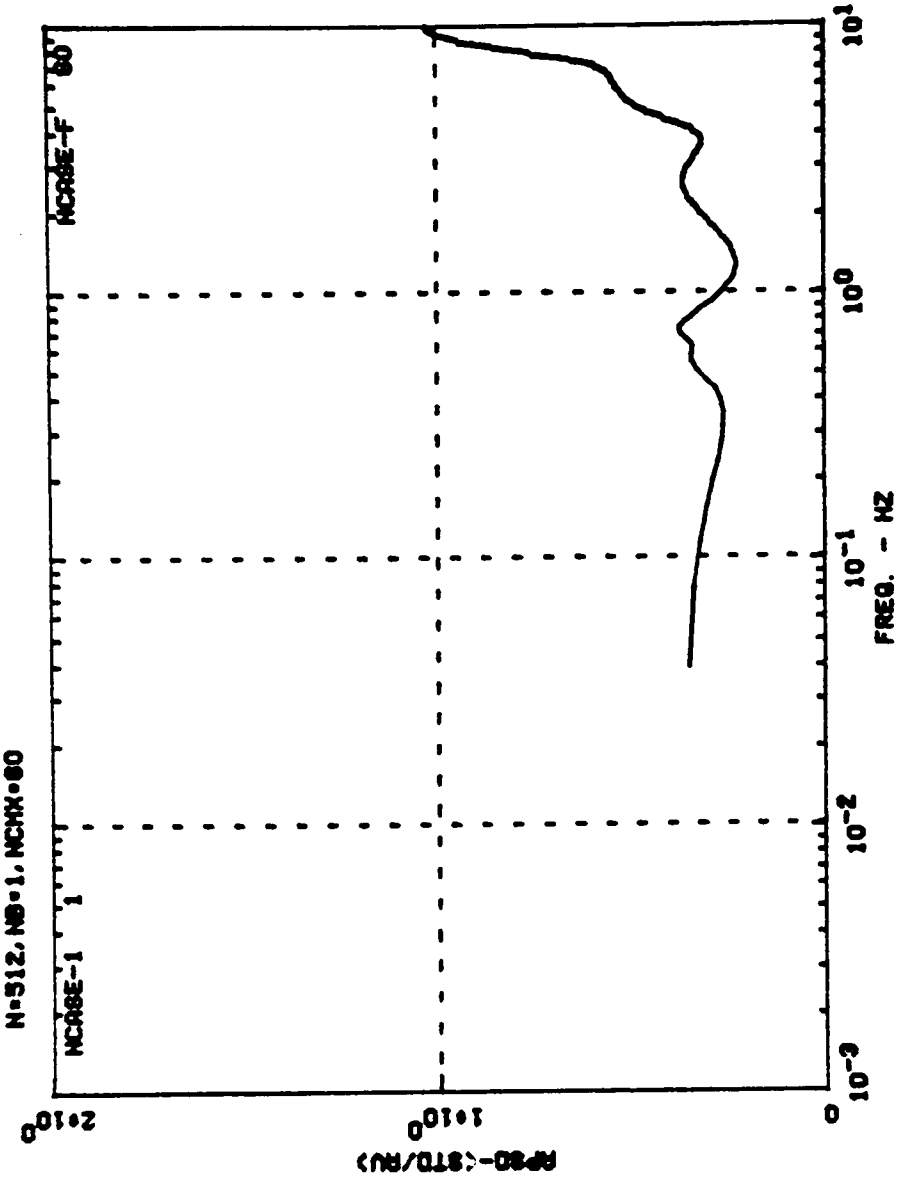


Figure 99. Normalized Standard Deviation of Power Spectrum of Case (1) for Order 9.

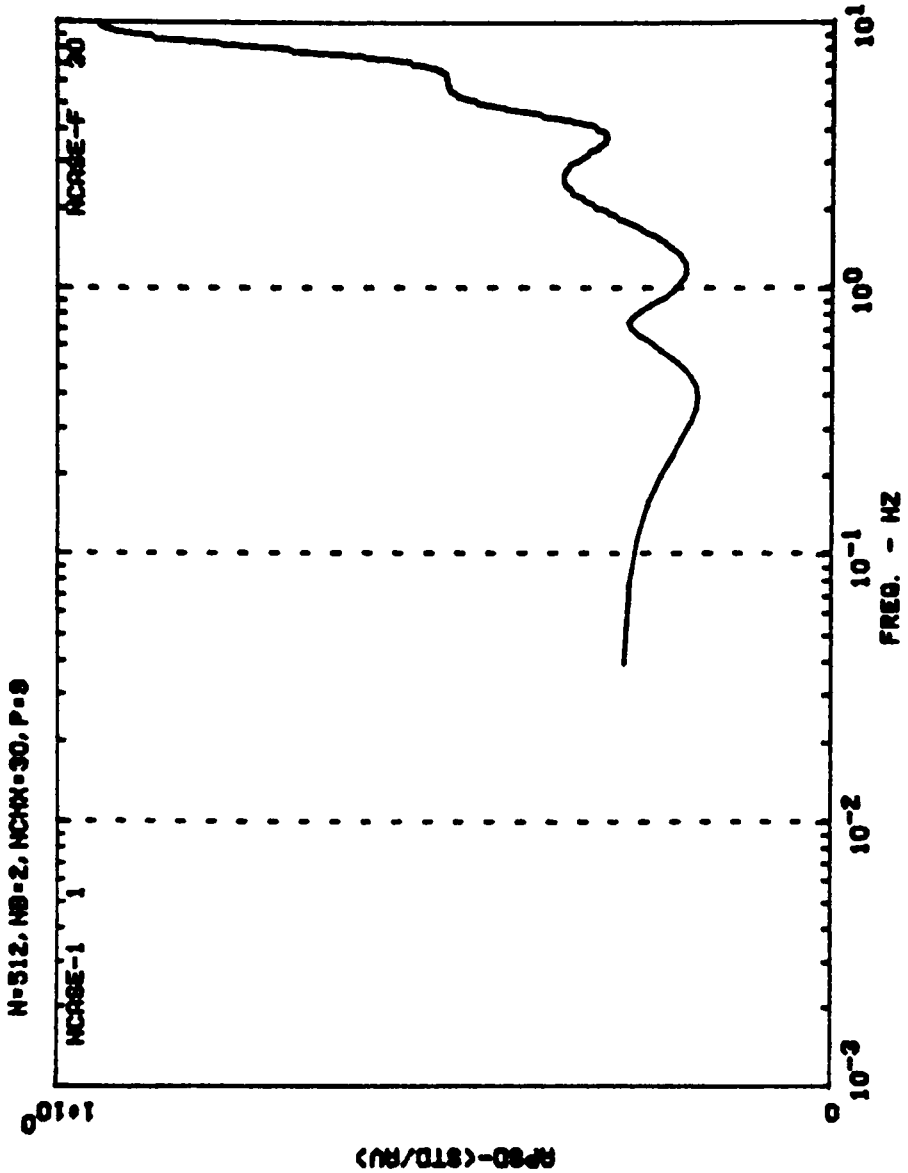


Figure 100. Normalized Standard Deviation of Power Spectrum of Case (2) for Order 9.

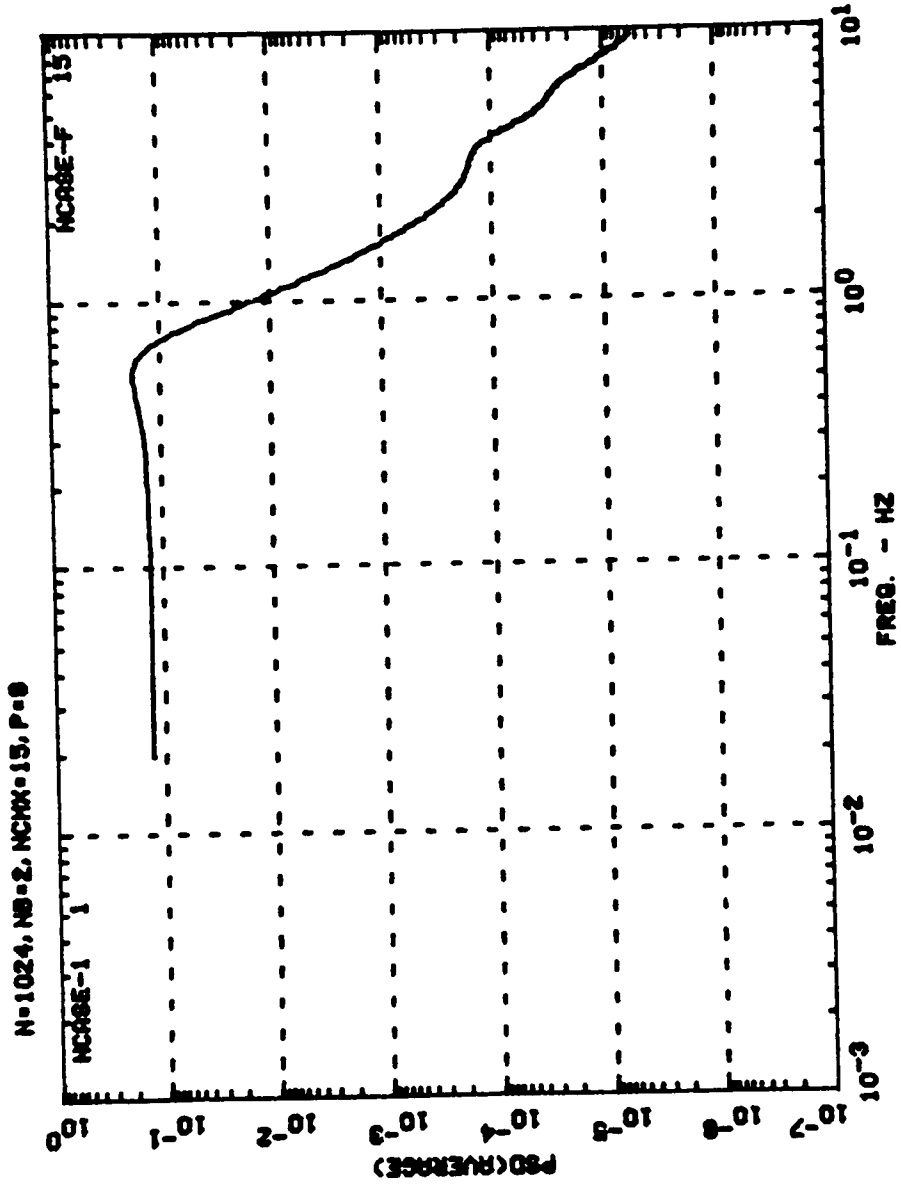


Figure 101. Average Power Spectrum of Case (3) for Order 9.

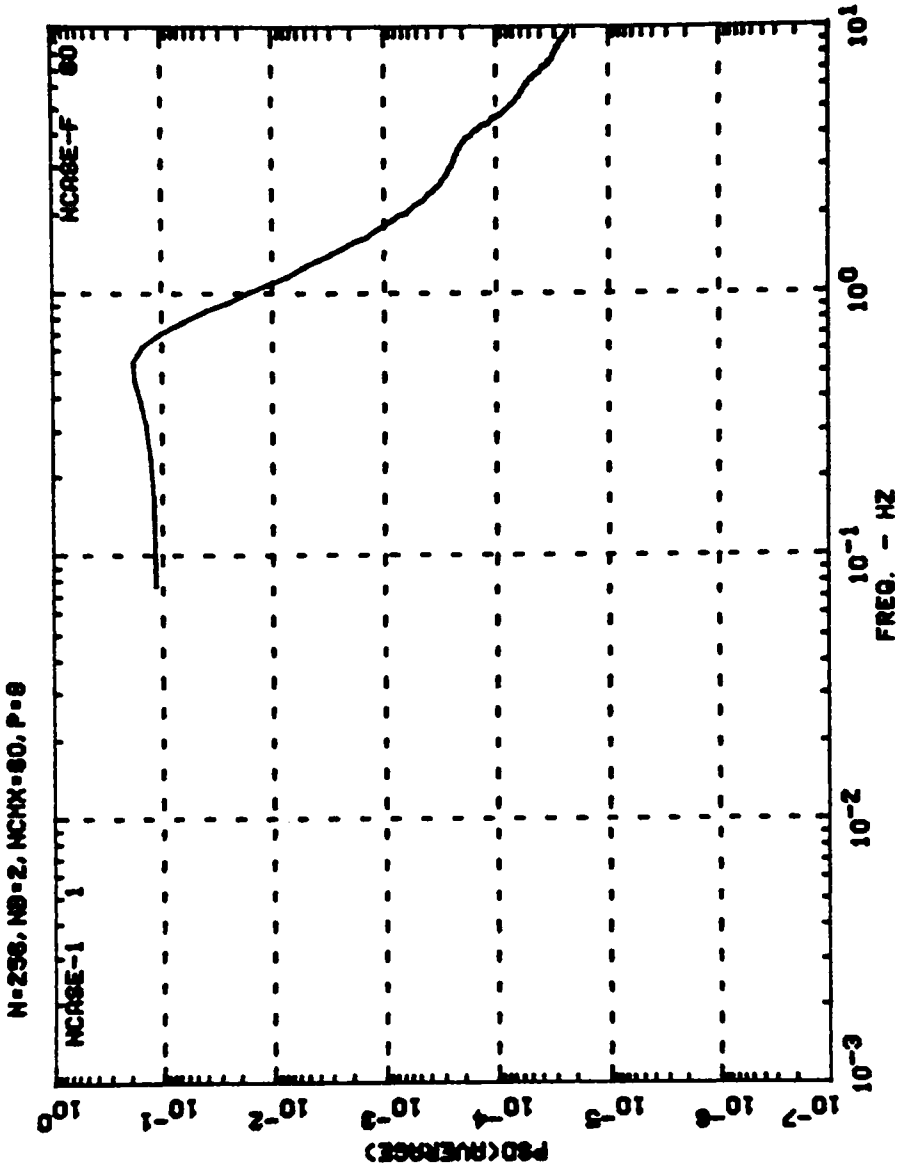
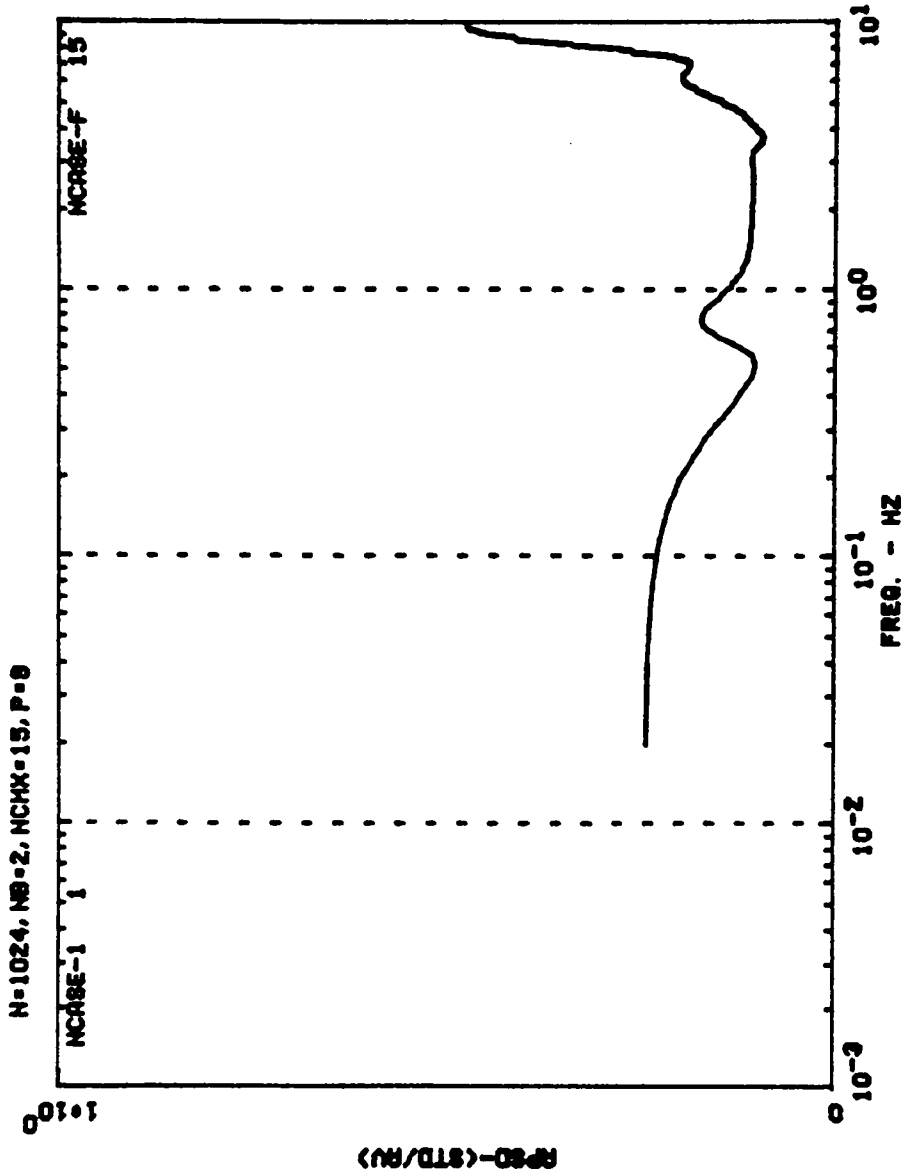


Figure 102. Average Power Spectrum of Case (4) for Order 9.



Page 103. Normalized Standard Deviation of Power Spectrum of Case (3) for Order 9.

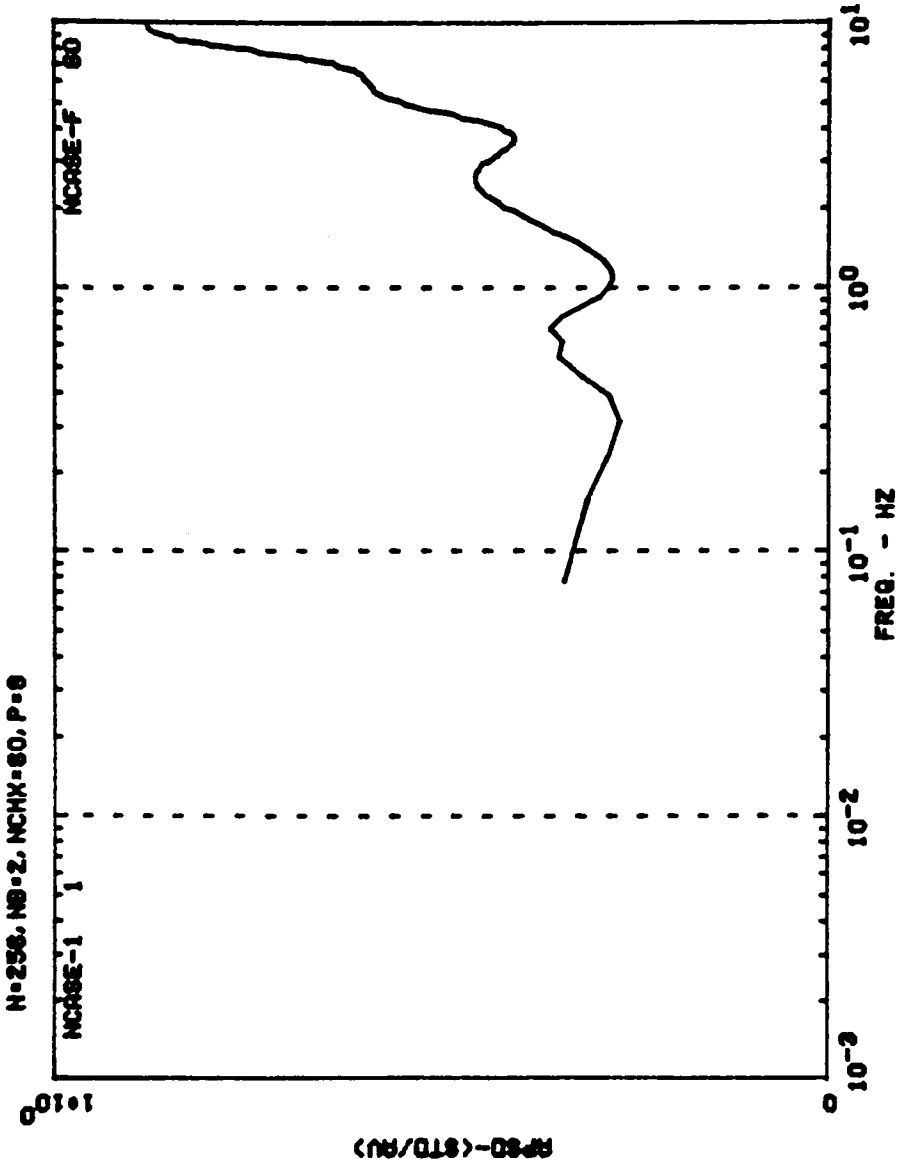


Figure 104. Normalized Standard Deviation of Power Spectrum of Case (4) for Order 9.

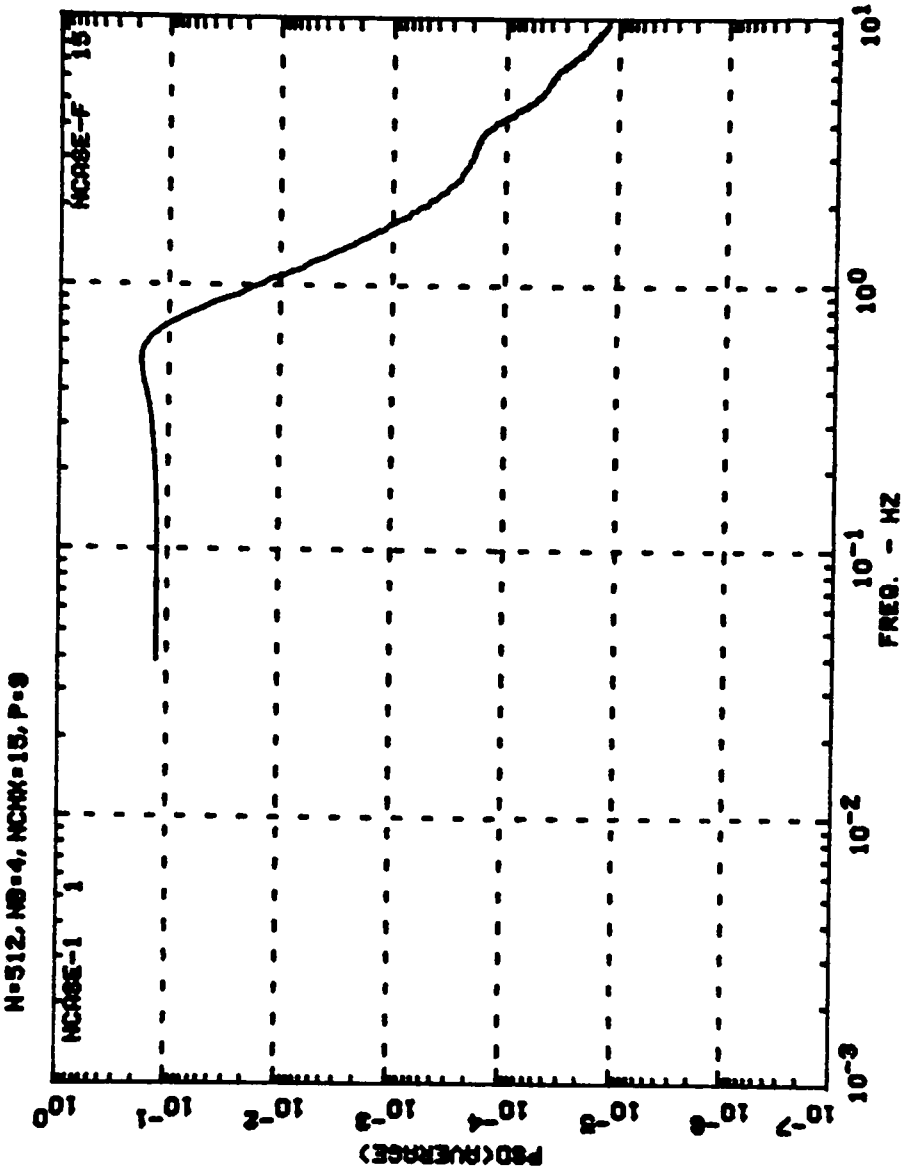


Figure 105. Average Power Spectrum of Case (5) for Order 9.

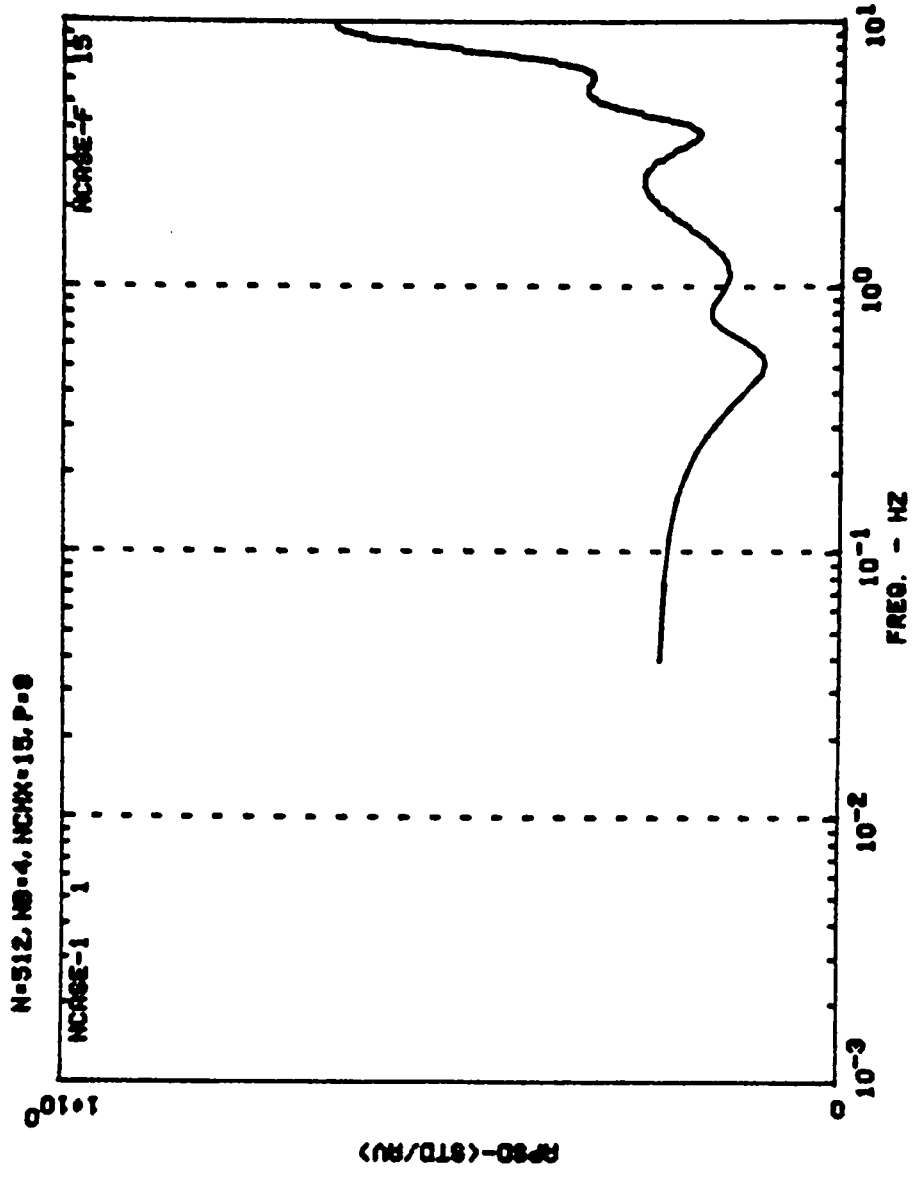


Figure 106. Normalized Standard Deviation of Power Spectrum of Case (5) for Order 9.

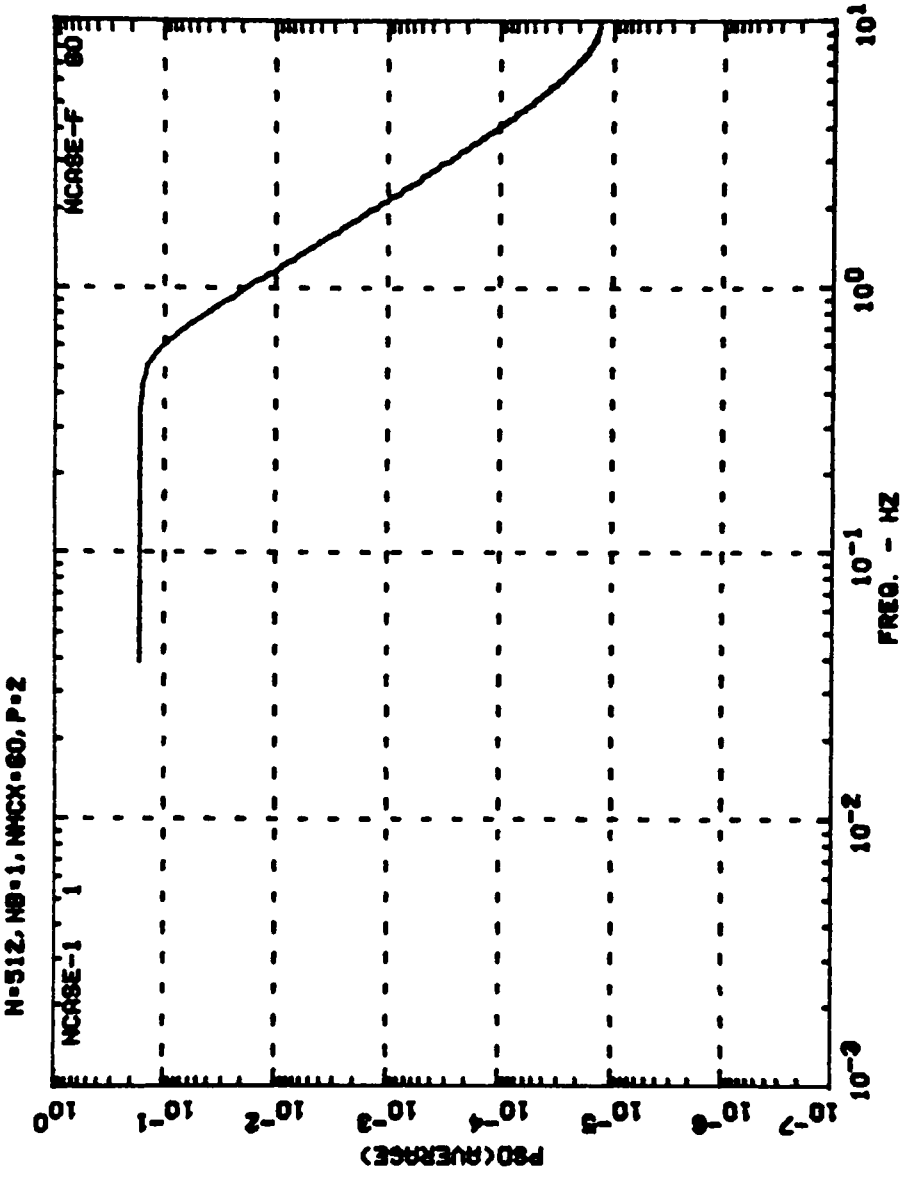


Figure 107. Average Power Spectrum of Case (1) for Order 2.

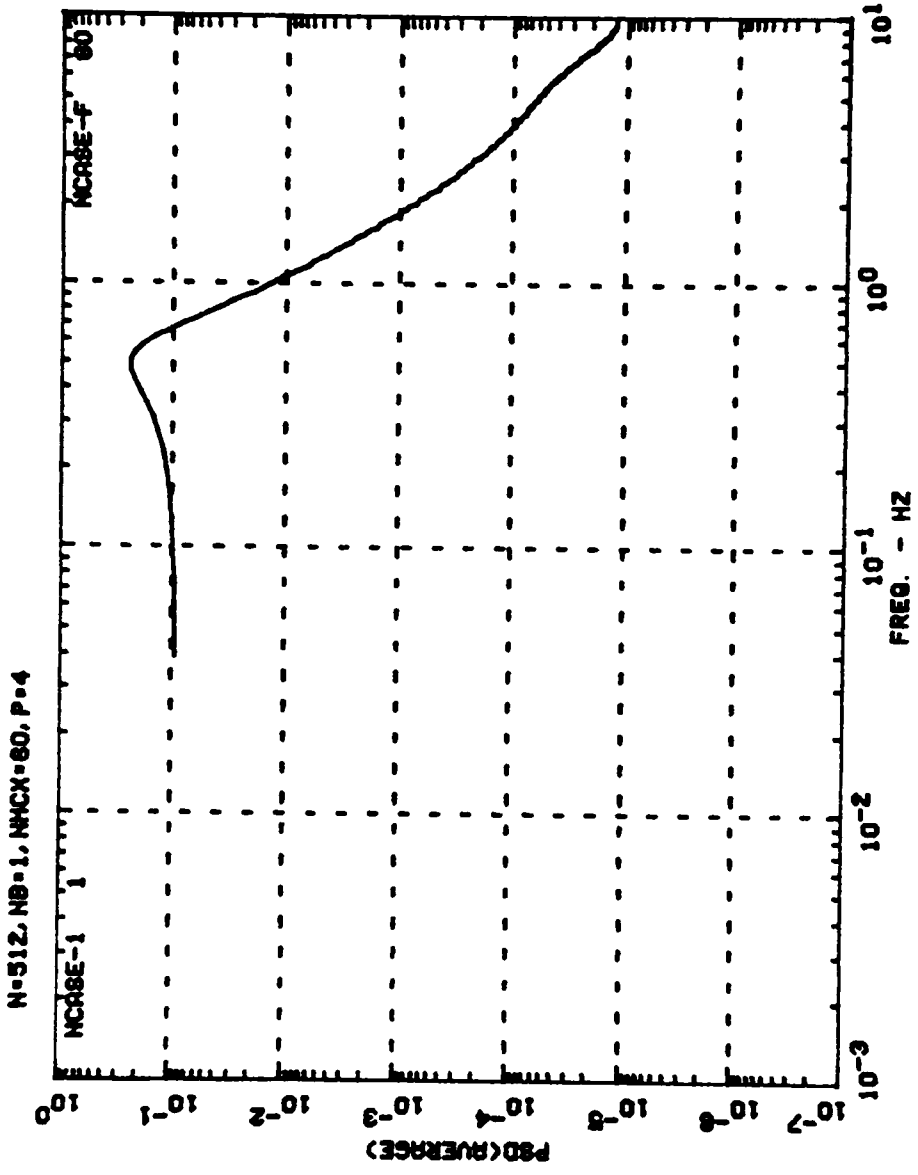


Figure 108. Average Power Spectrum of Case (1) for Order 4.

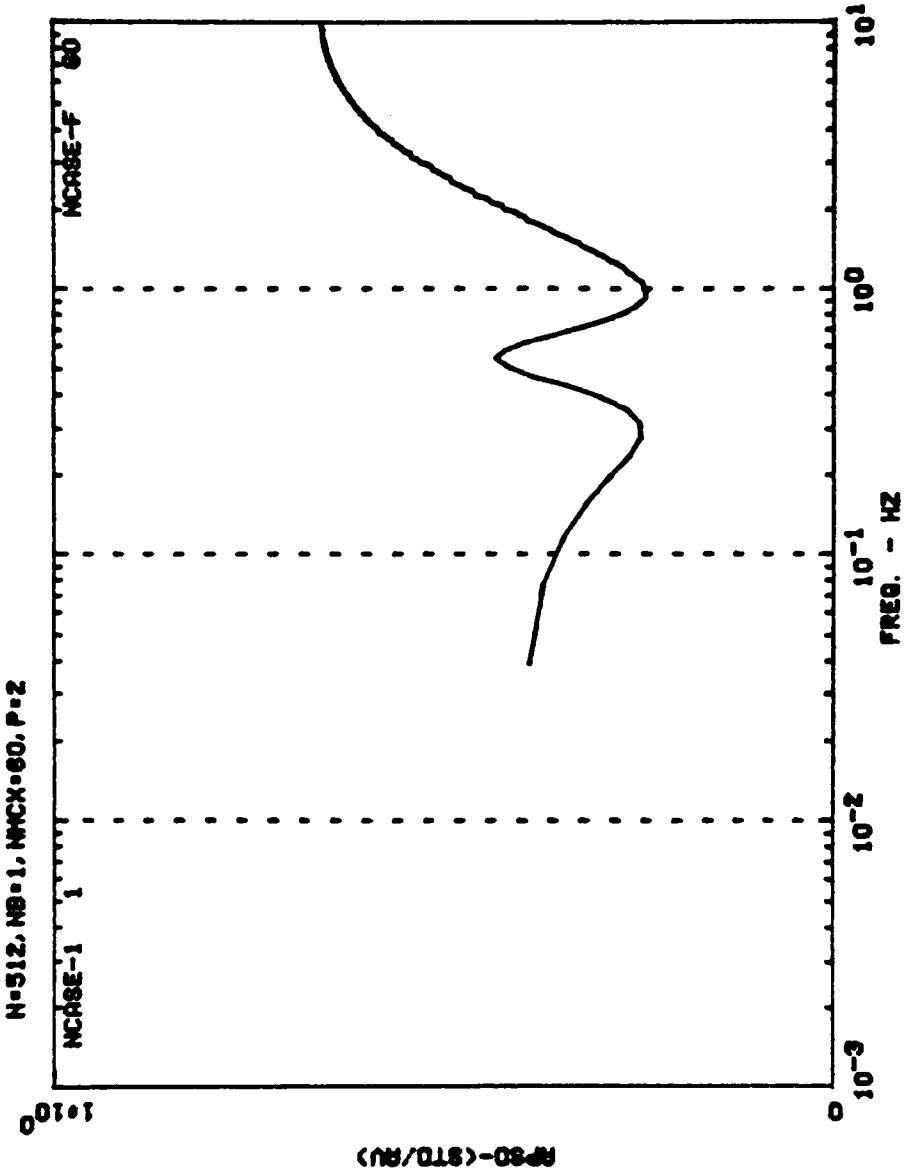


Figure 109. Normalized Standard Deviation of Power Spectrum of Case (1) for Order 2.

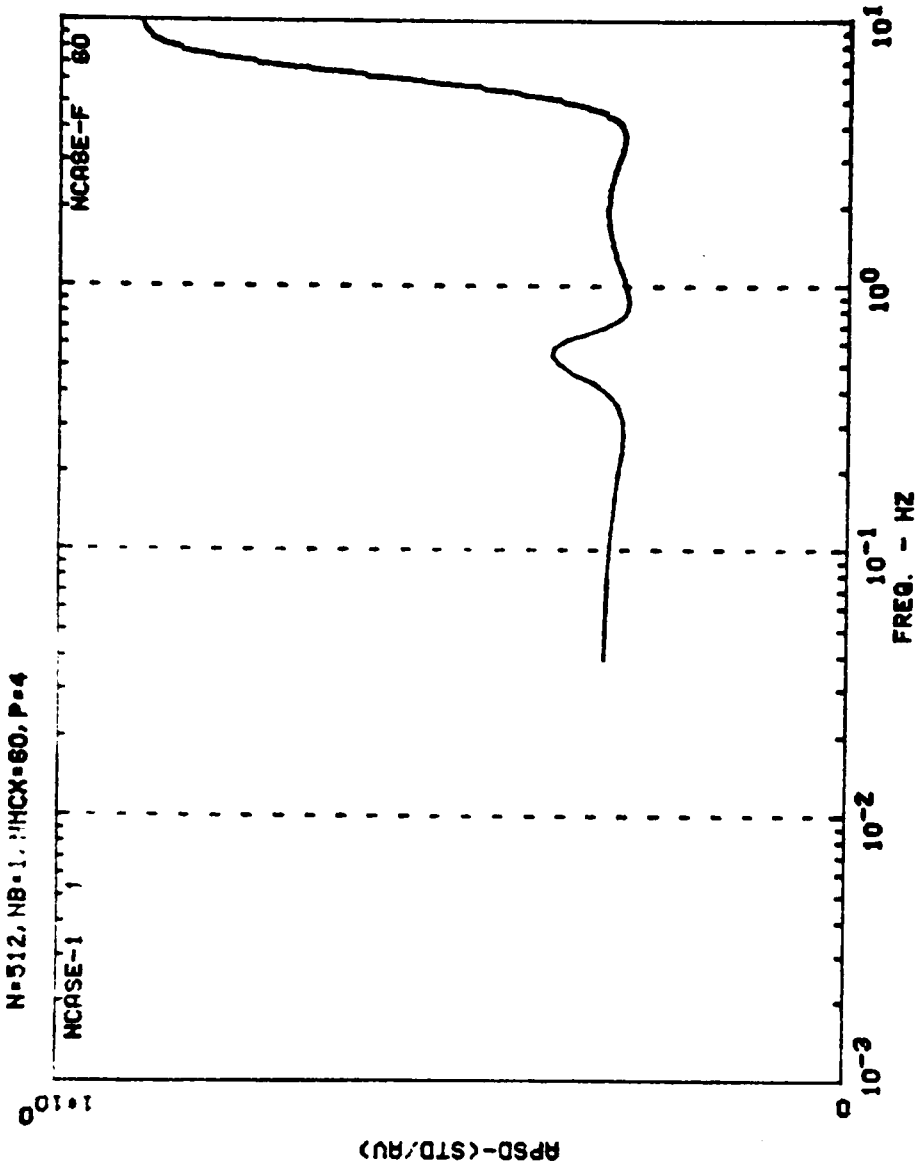


Figure 110. Normalized Standard Deviation of Power Spectrum of Case (1) for Order 4.

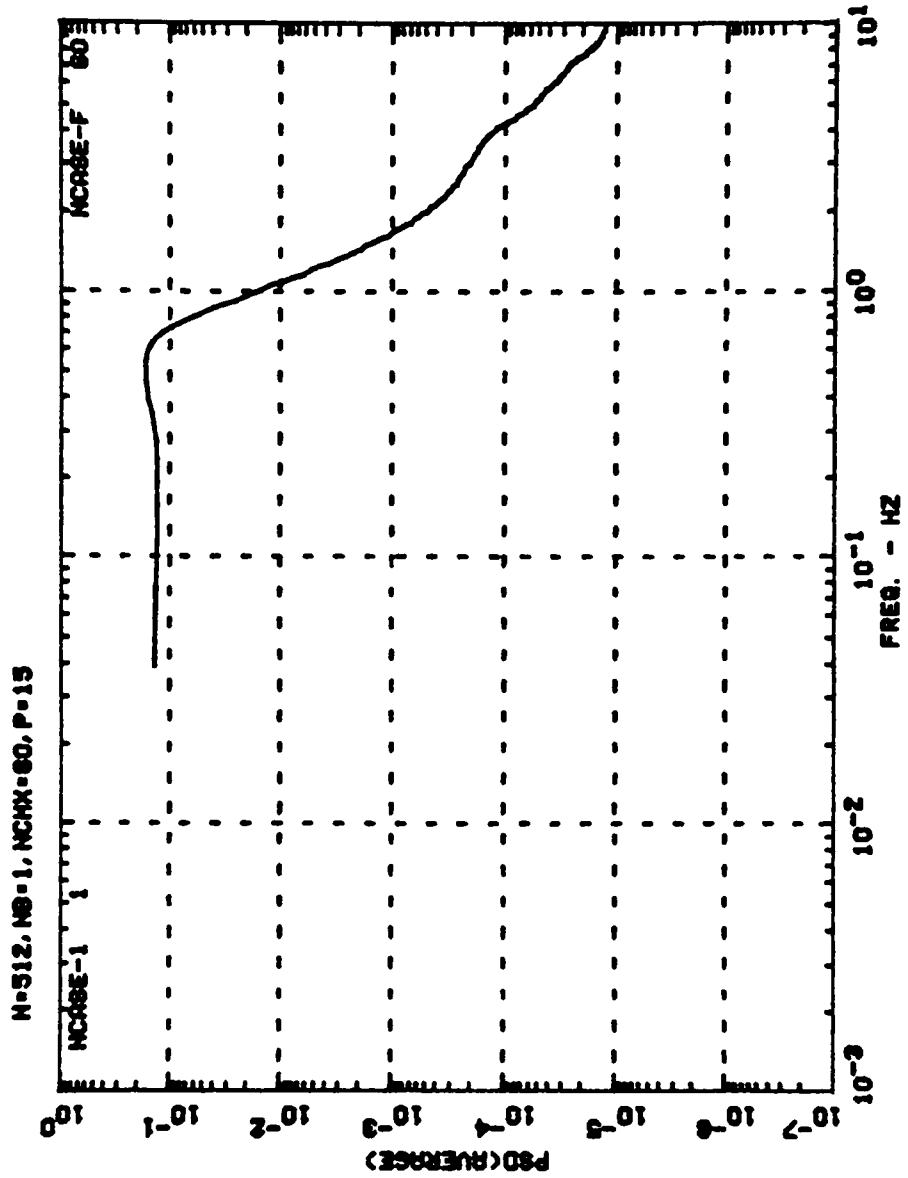


Figure 111. Average Power Spectrum of Case (1) for Order 15.

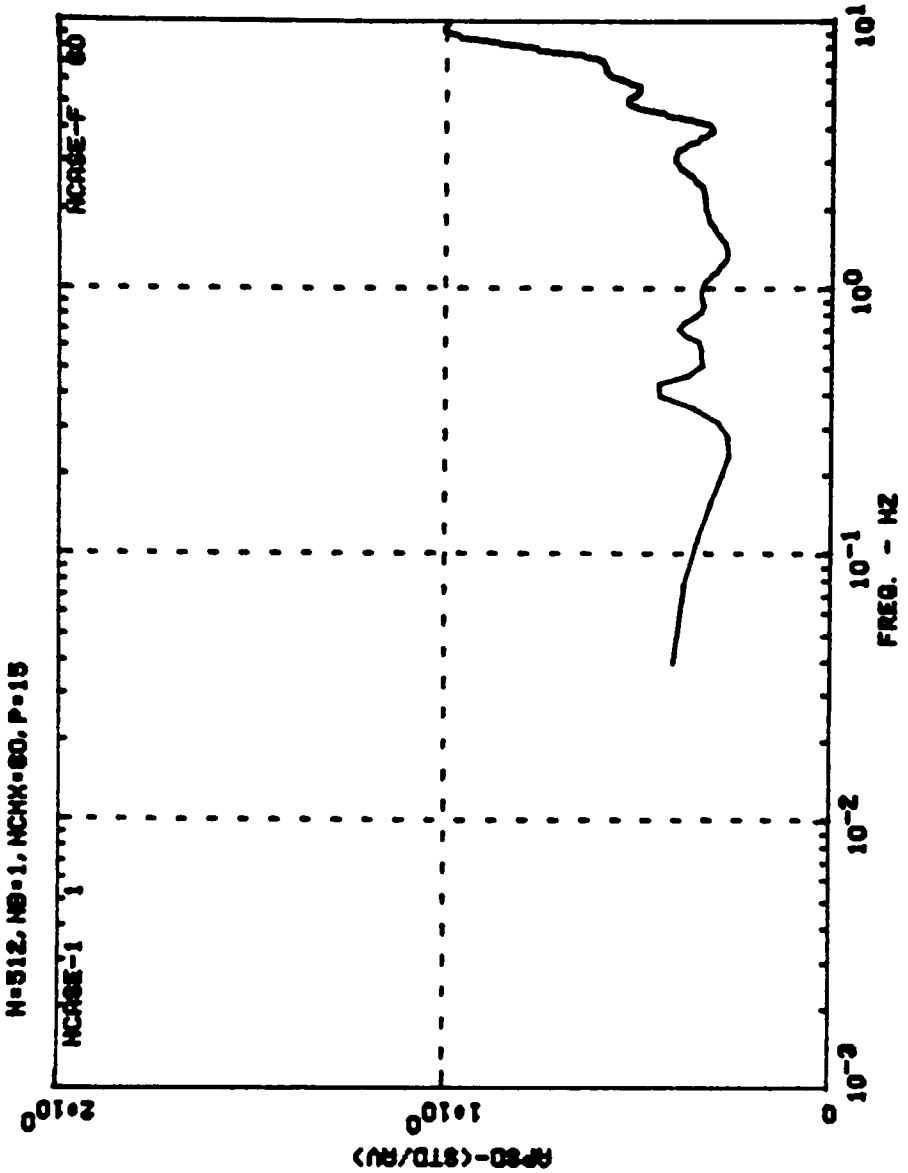


Figure 112. Normalized Standard Deviation of Power Spectrum of Case (1) for Order 15.

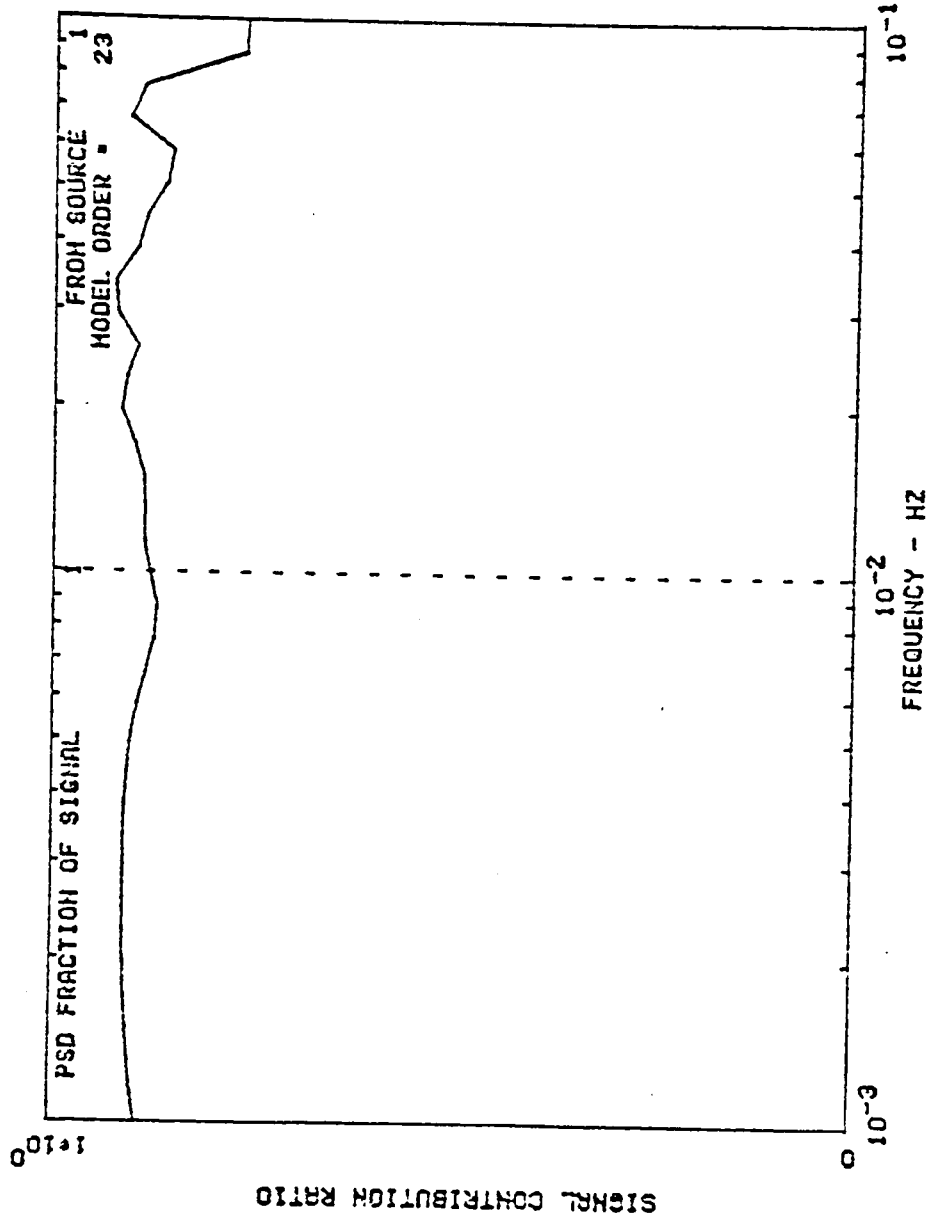


Figure 113. Signal Contribution Ratio from Source One to Primary Pressure (Order 23).

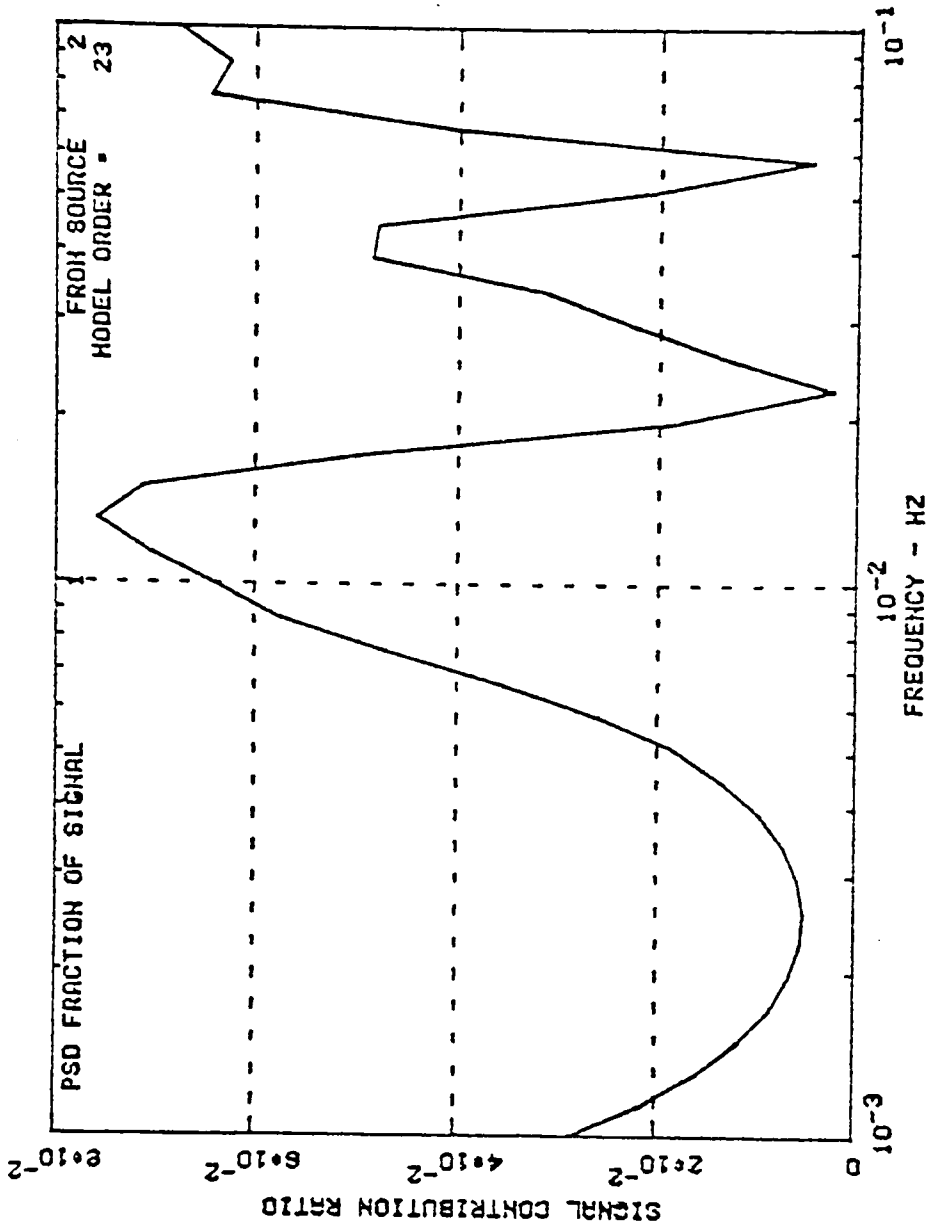


Figure 114. Signal Contribution Ratio from Source Two to Primary Pressure (Order 23).

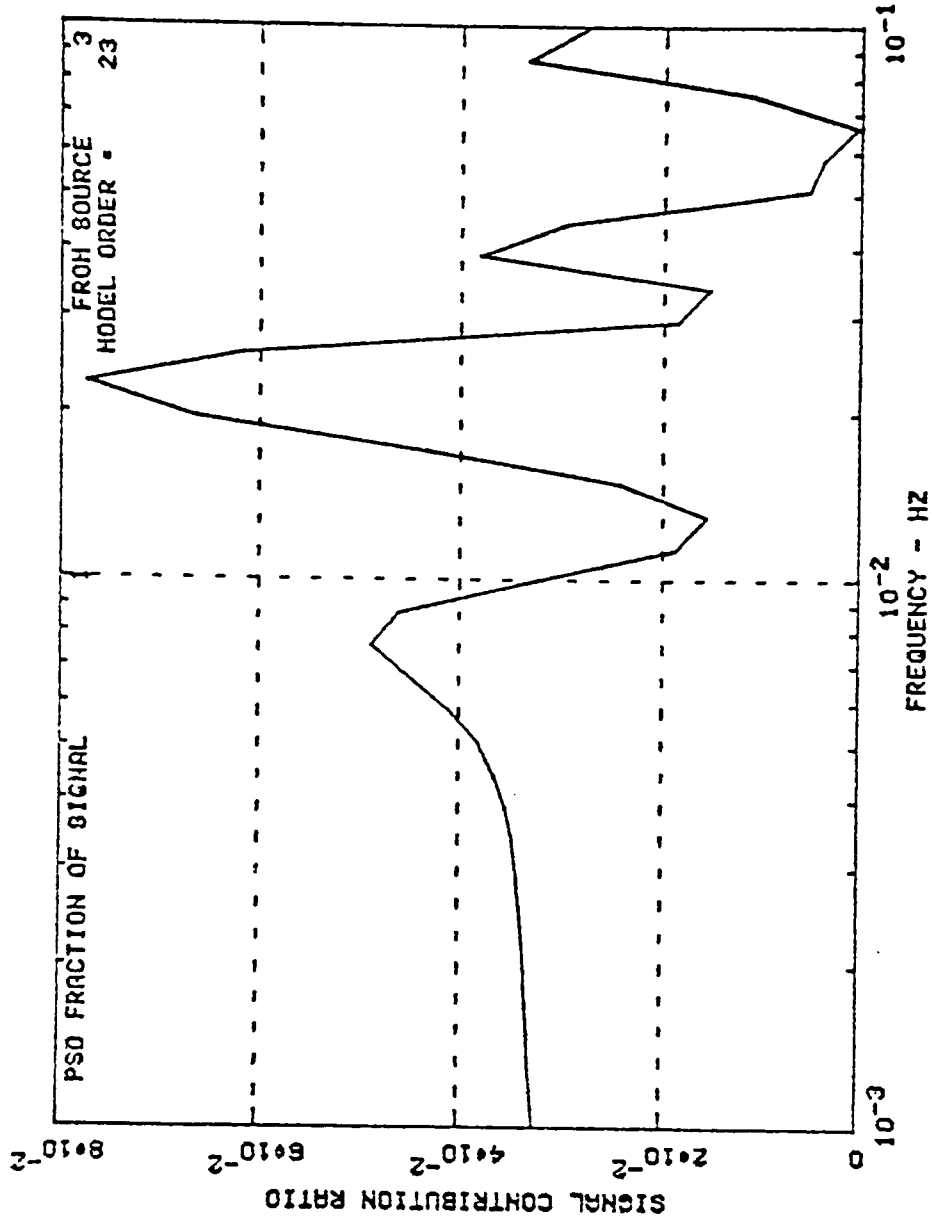


Figure 115. Signal Contribution Ratio from Source Three to Primary Pressure (Order 23).

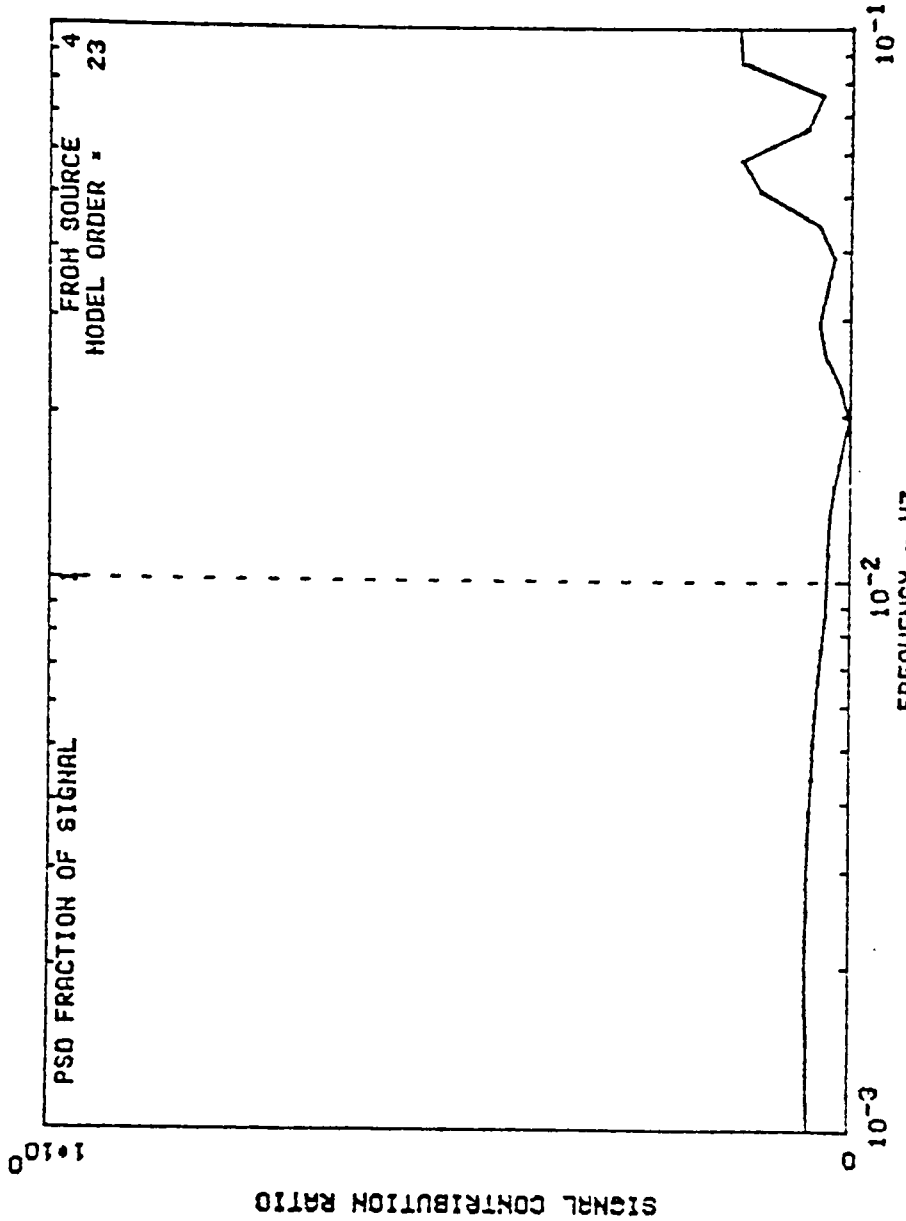


Figure 116. Signal Contribution Ratio from Source Four to Primary Pressure (Order 23).

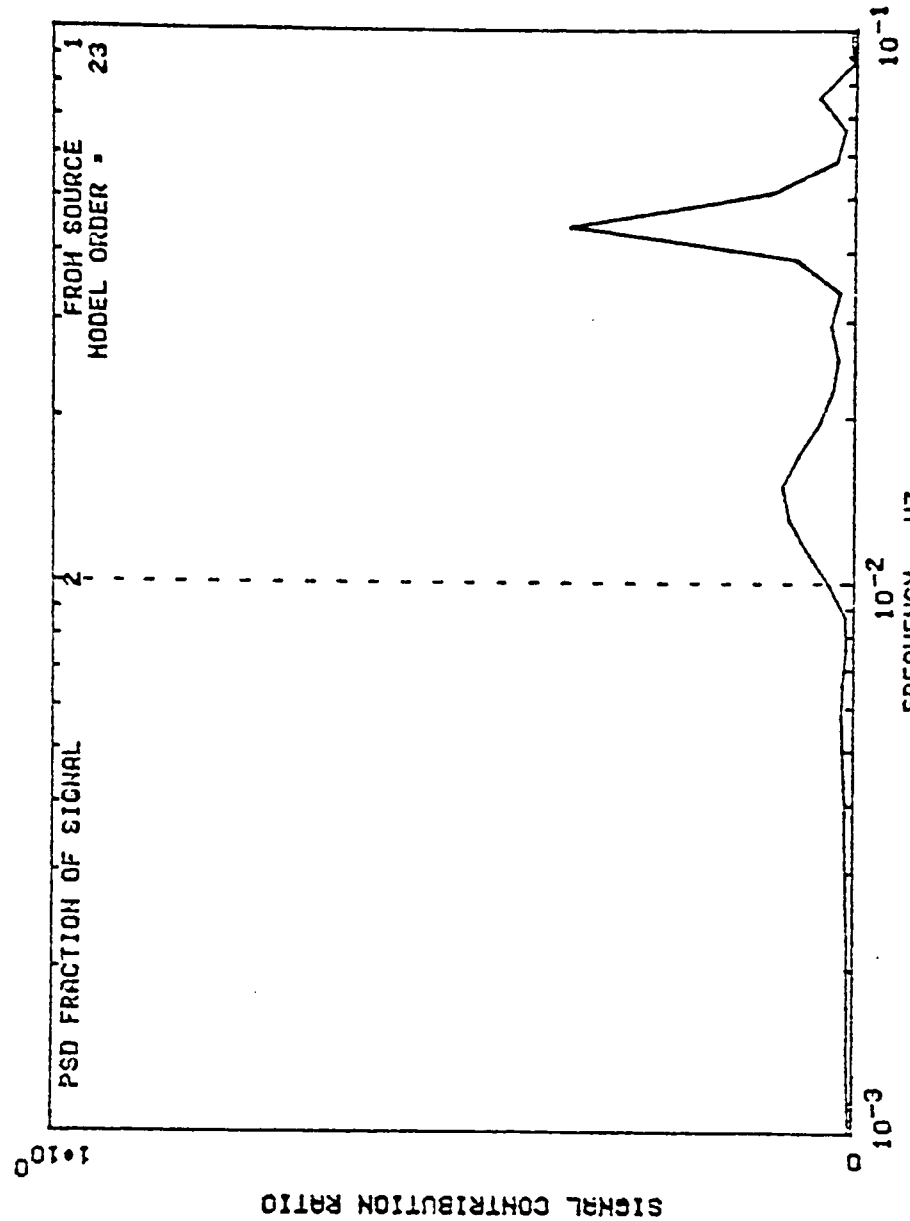


Figure 117. Signal Contribution Ratio from Source One to Cold Leg Temperature (Order 23).

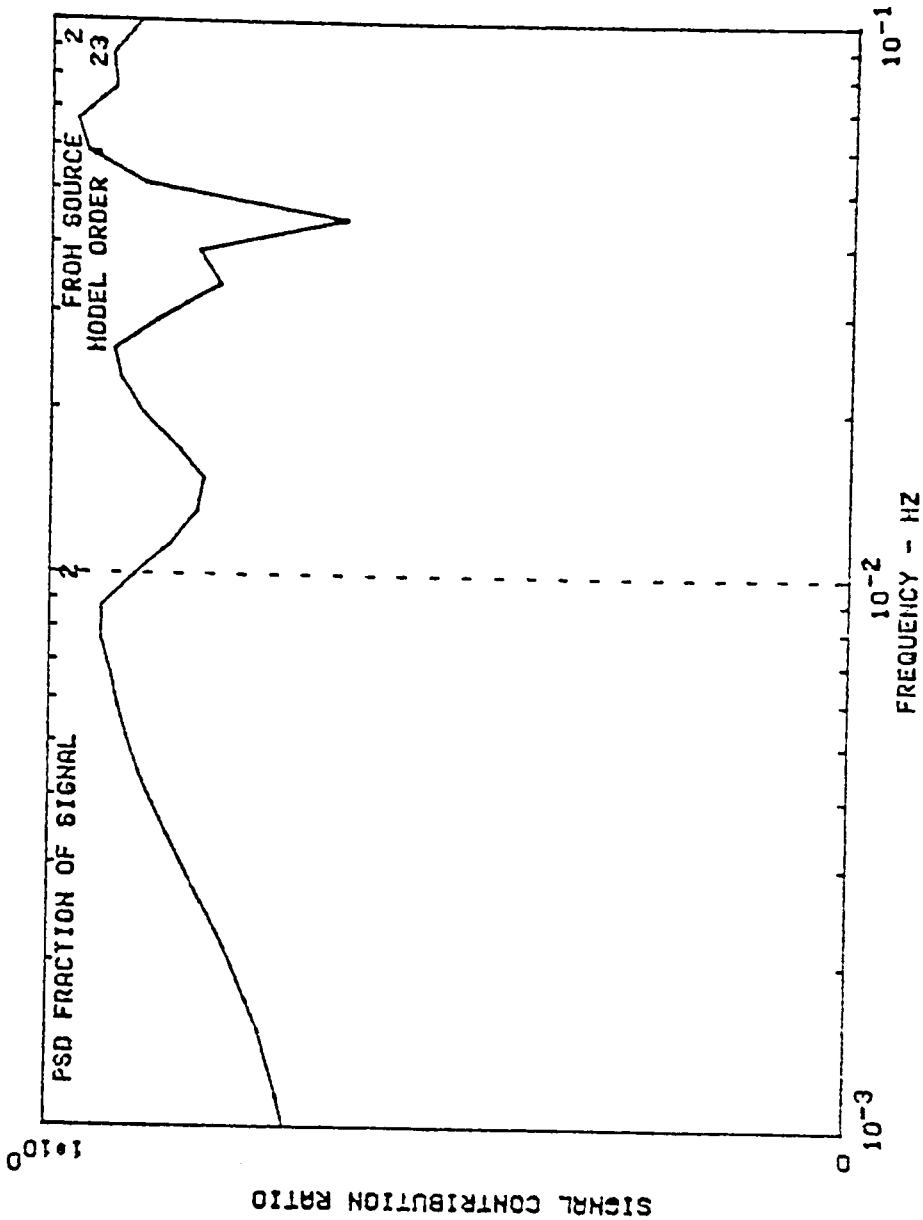


Figure 118. Signal Contribution Ratio from Source Two to Cold Leg Temperature (Order 23).

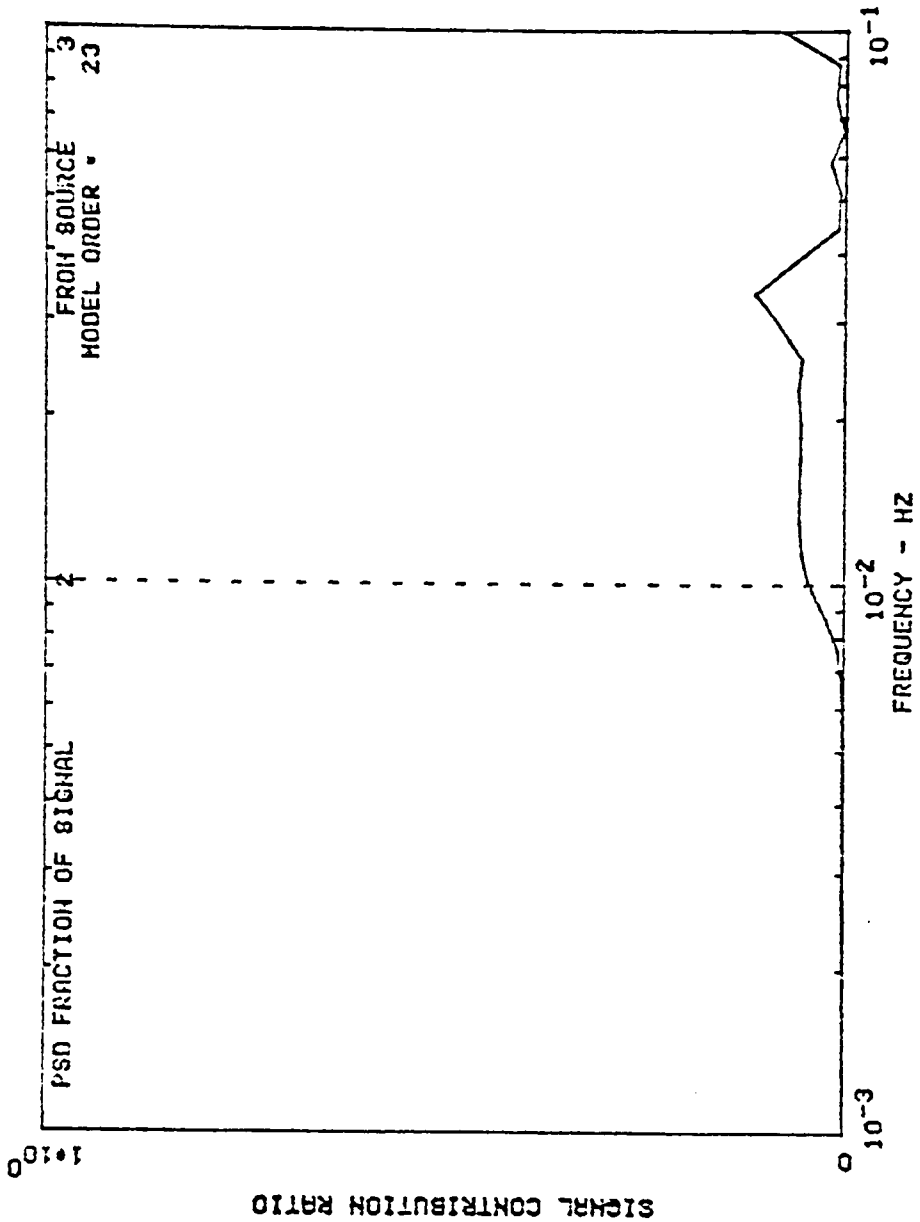


Figure 119. Signal Contribution Ratio from Source Three to Cold Leg Temperature (Order 23).

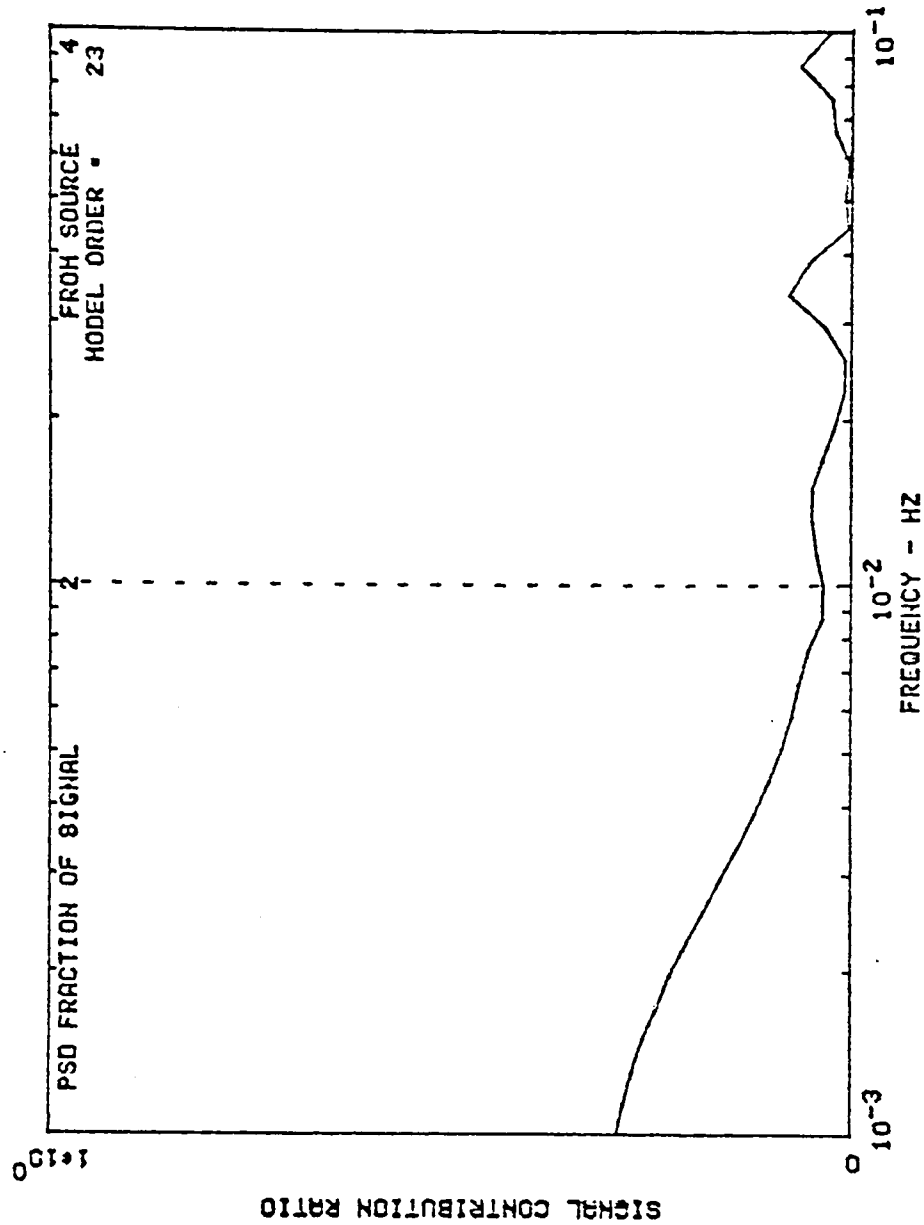


Figure 120. Signal Contribution Ratio from Source Four to Cold Leg Temperature (Order 23).

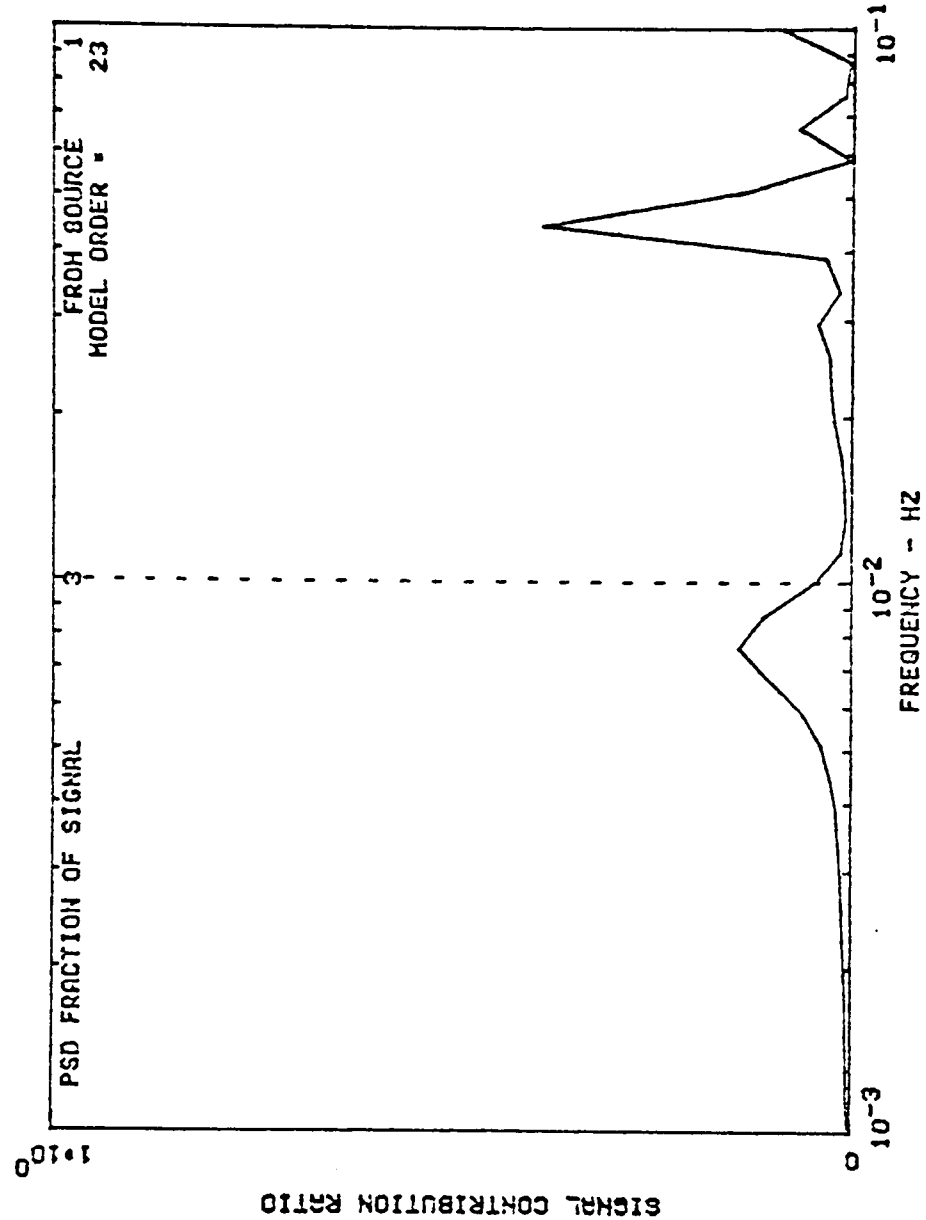


Figure 121. Signal Contribution Ratio from Source One to Feed Water Flow Rate (Order 23).

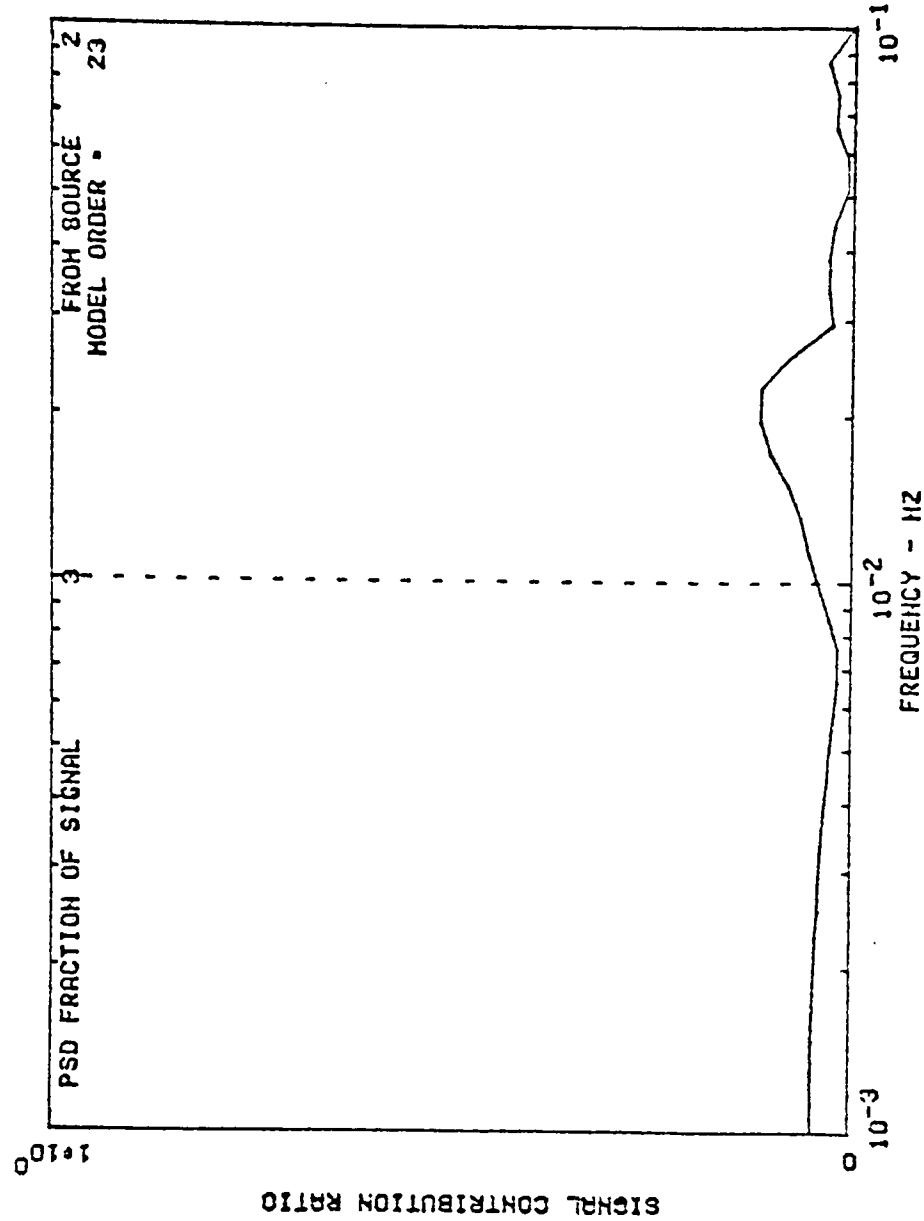


Figure 122. Signal Contribution Ratio from Source Two to Feed Water Flow Rate (Order 23).

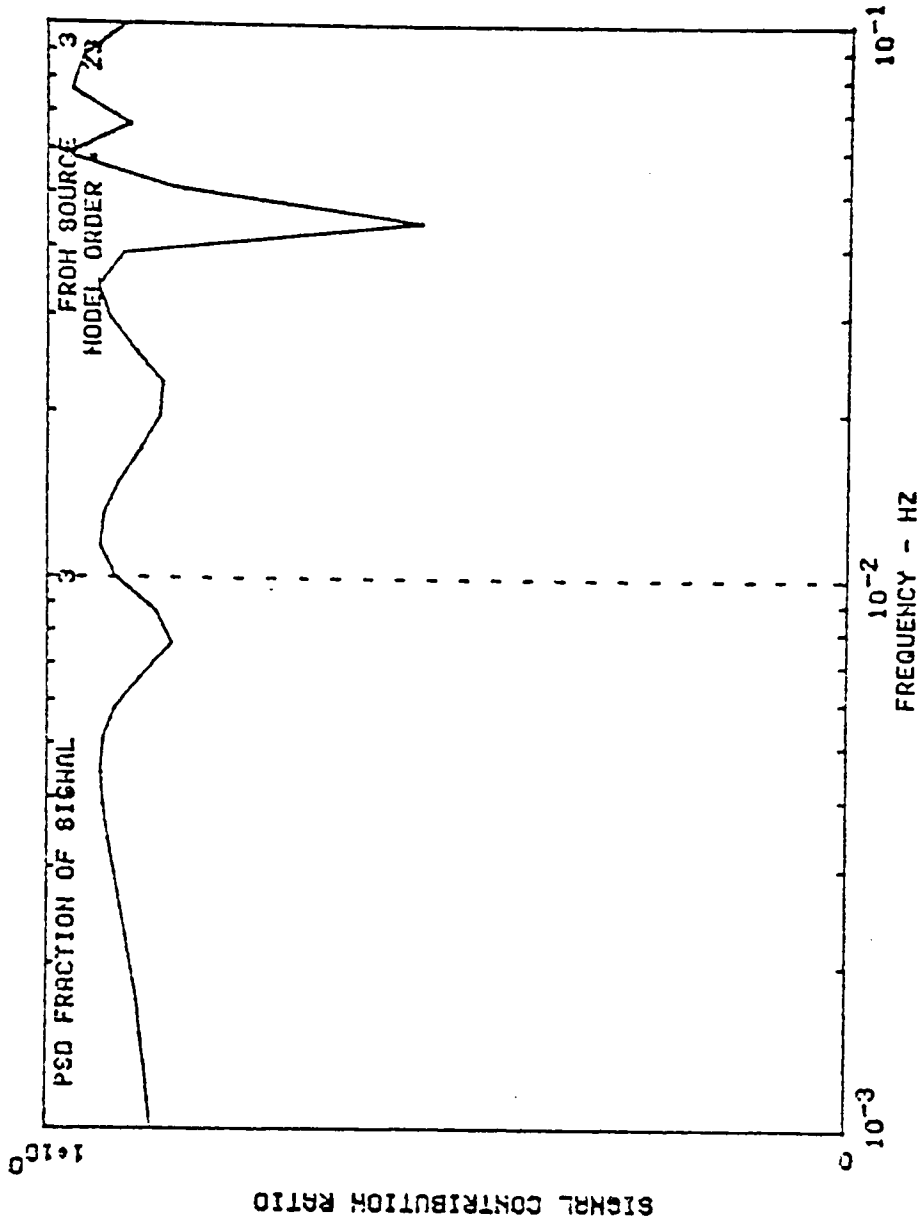


Figure 123. Signal Contribution Ratio from Source Three to Feed Water Flow Rate (Order 23).

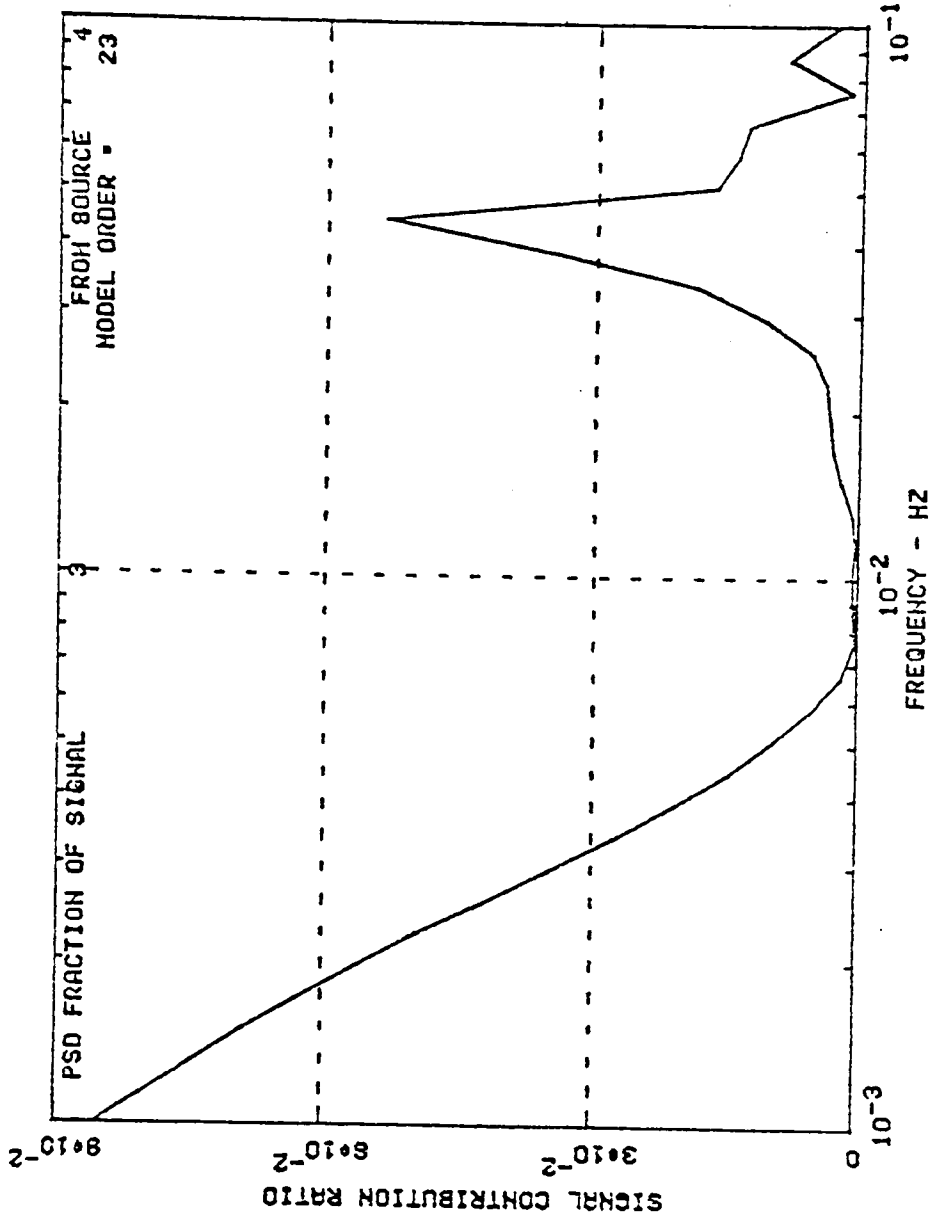


Figure 124. Signal Contribution Ratio from Source Four to Feed Water Flow Rate (Order 23).

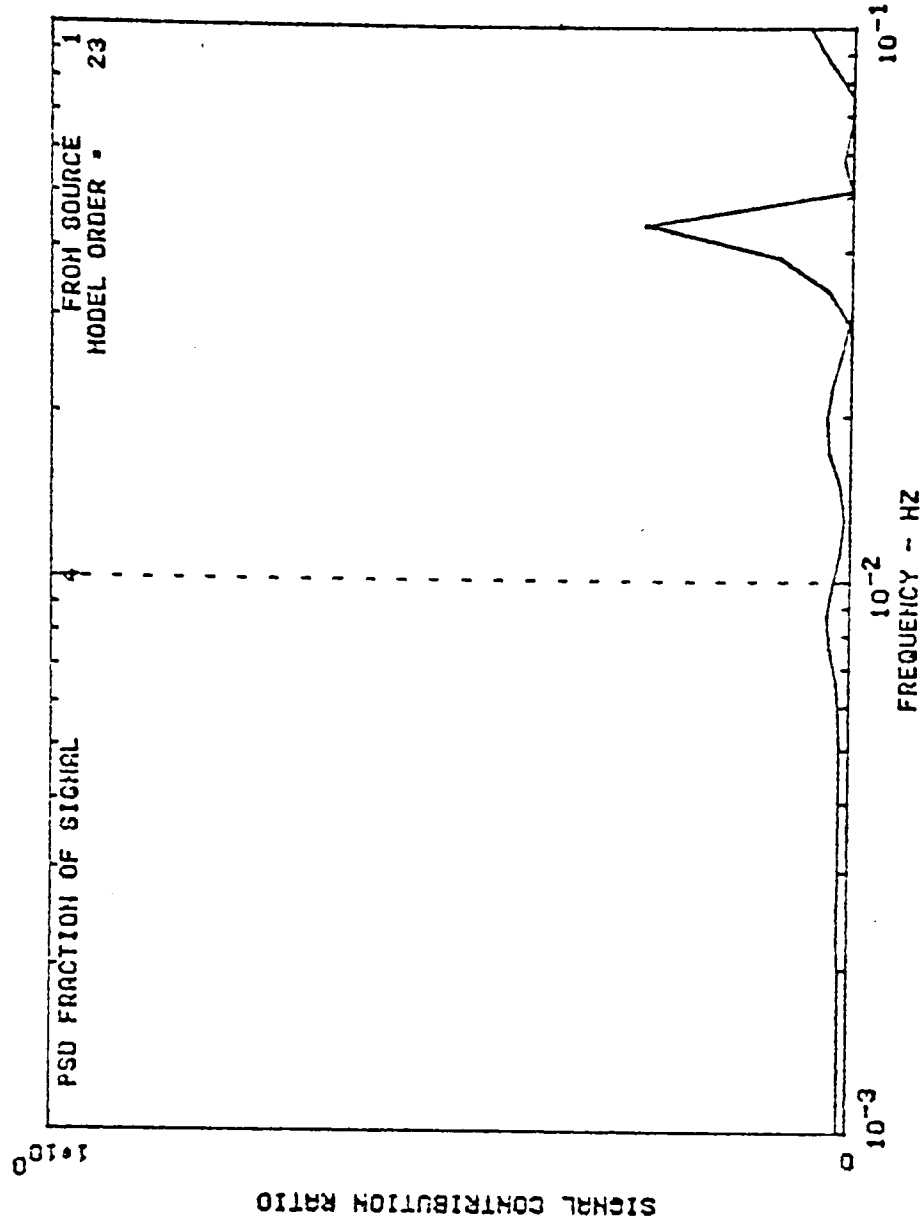


Figure 125. Signal Contribution Ratio from Source One to Power (Order 23).

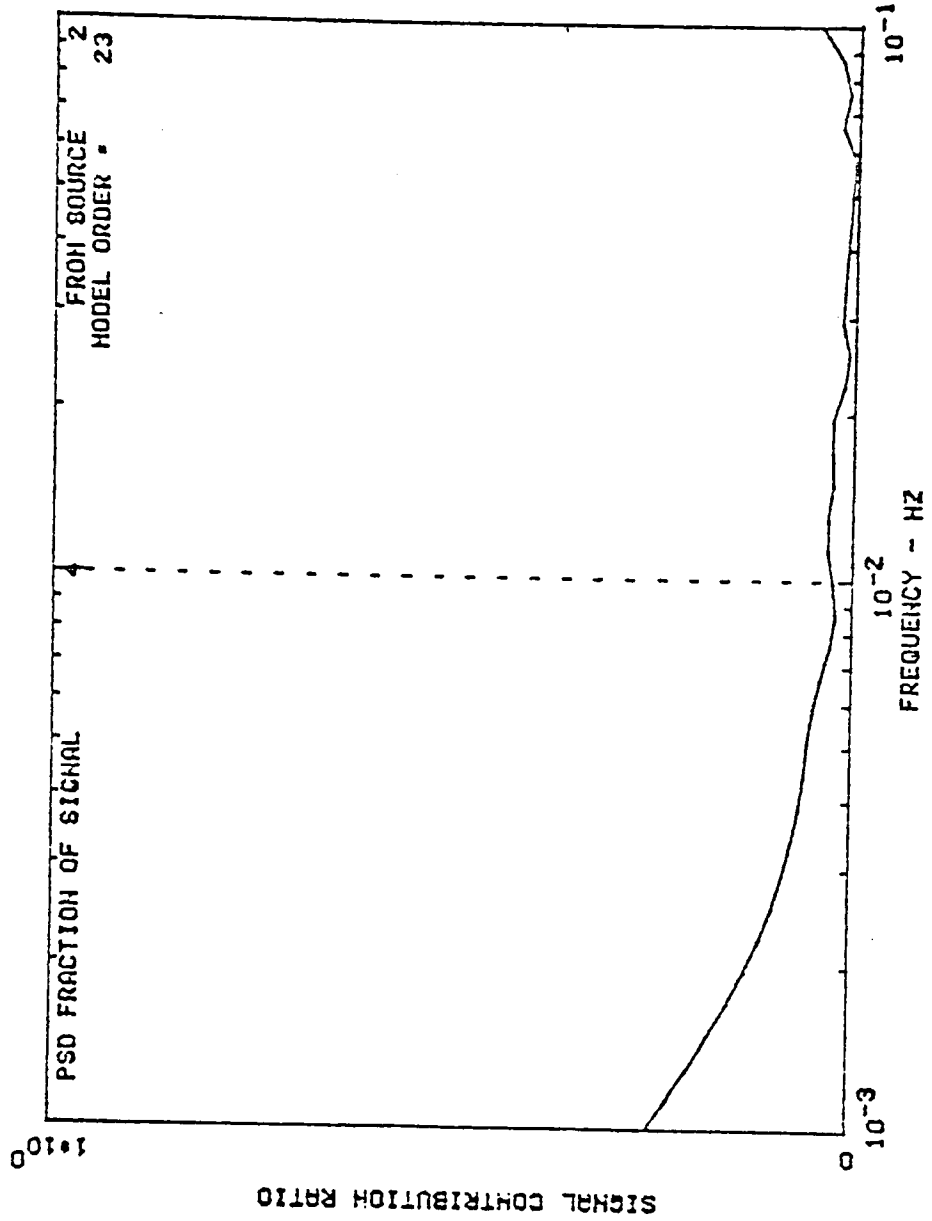


Figure 126. Signal Contribution Ratio from Source Two to Power (Order 23).

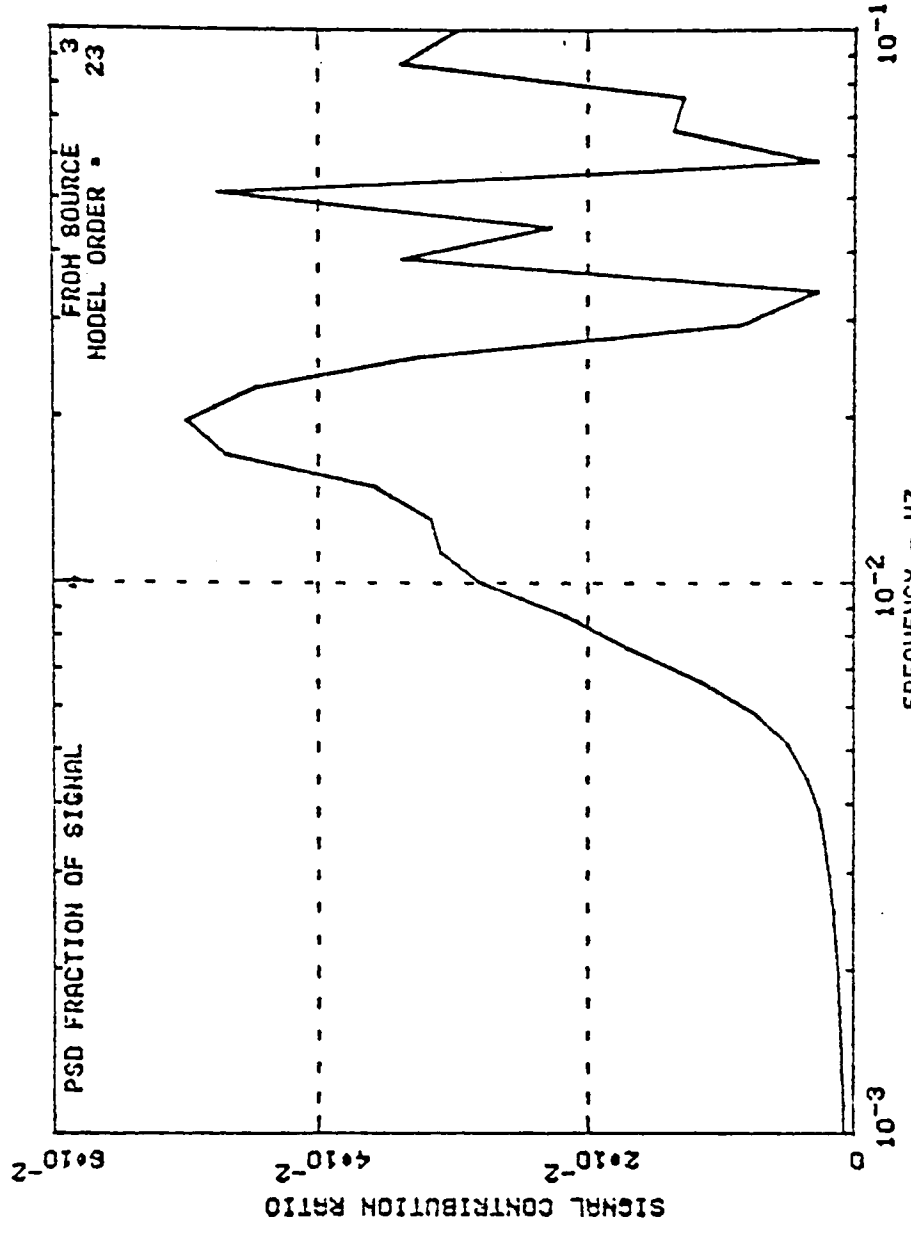


Figure 127. Signal Contribution Ratio from Source Three to Power (Order 23).

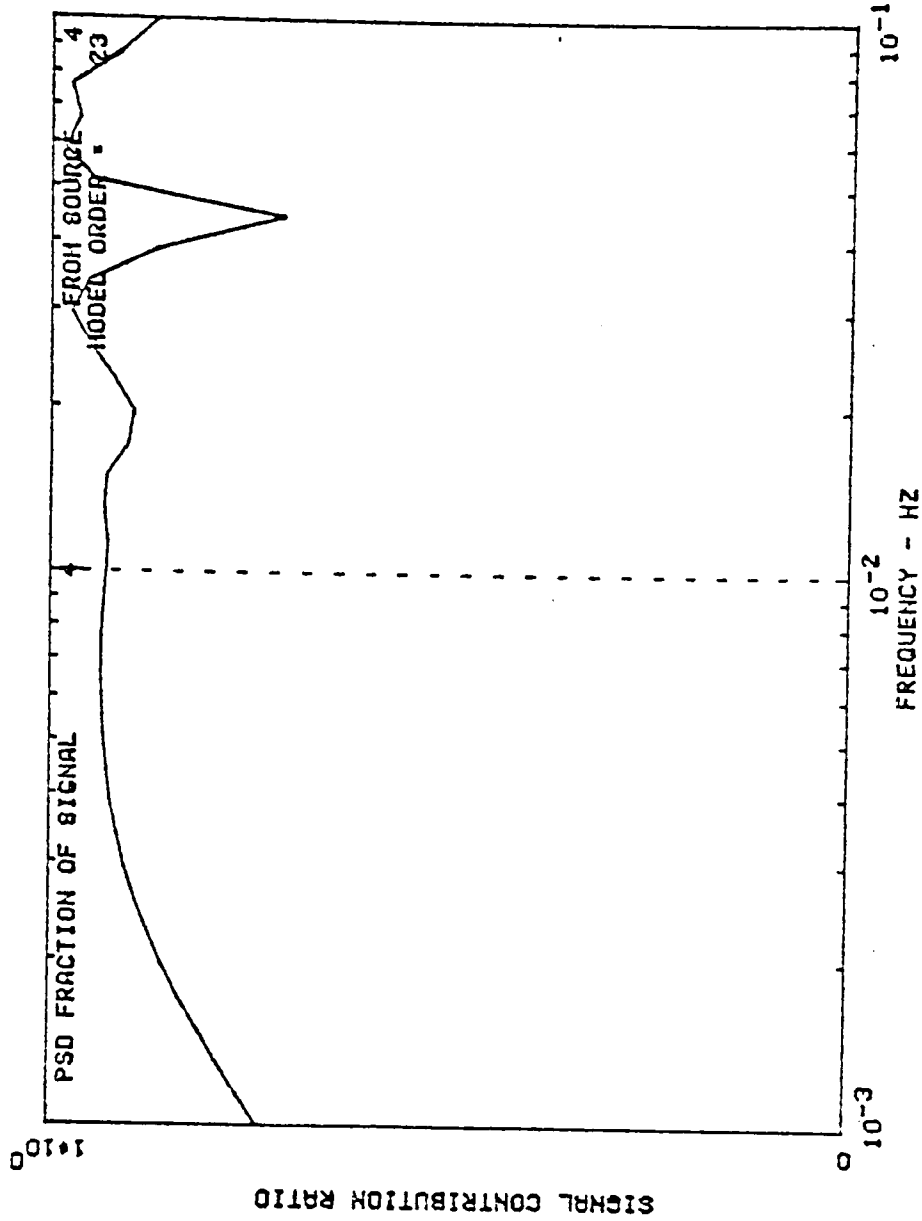
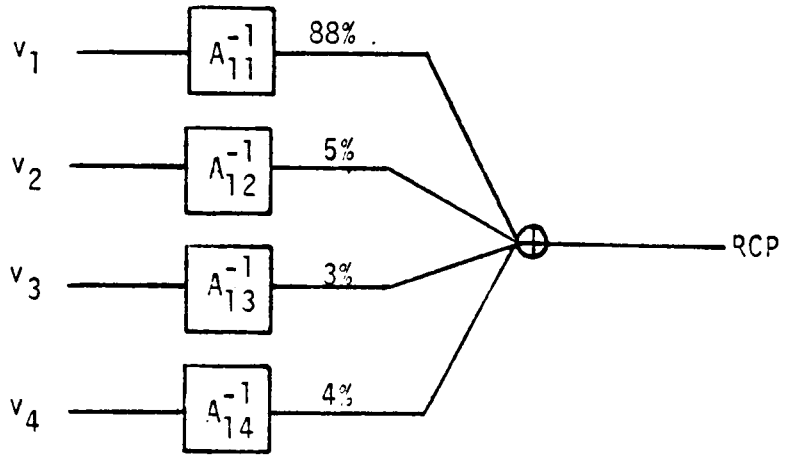
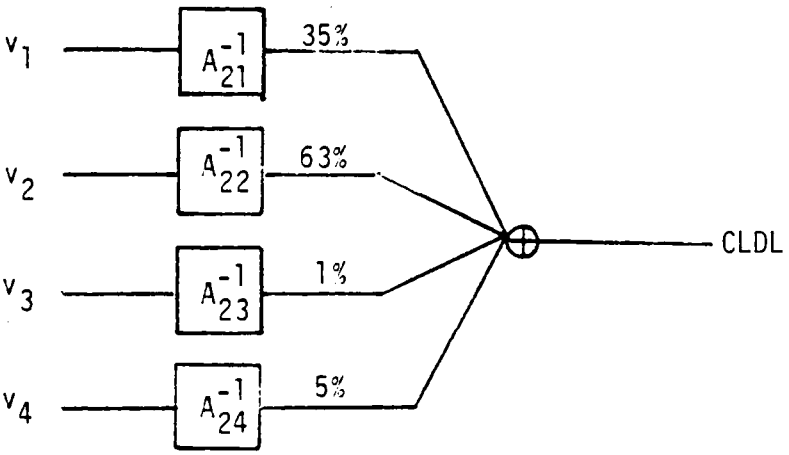


Figure 128. Signal Contribution Ratio from Source Four to Power (Order 23).

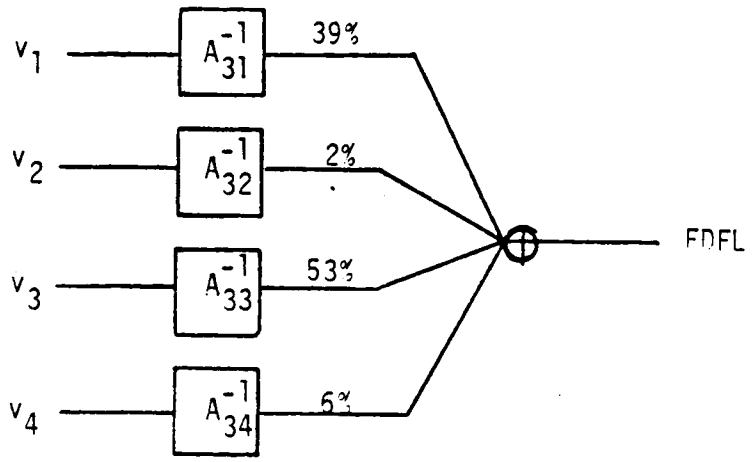


(a) RCP Closed Loop Input-Output Relation

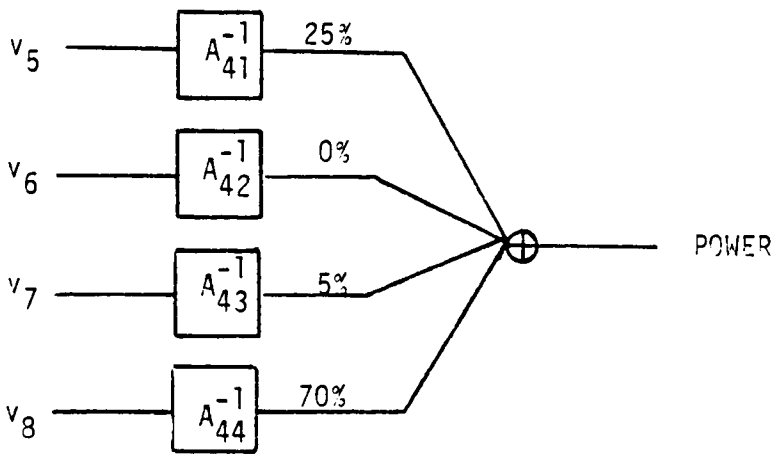


(b) CLDL Closed Loop Input-Output Relation.

Figure 129. Closed Loop Input-Output Relation.



(c) FDFL Closed Loop Input-Output Relation.



(d) Power Closed Loop Input-Output Relation.

Figure 129. (continued)

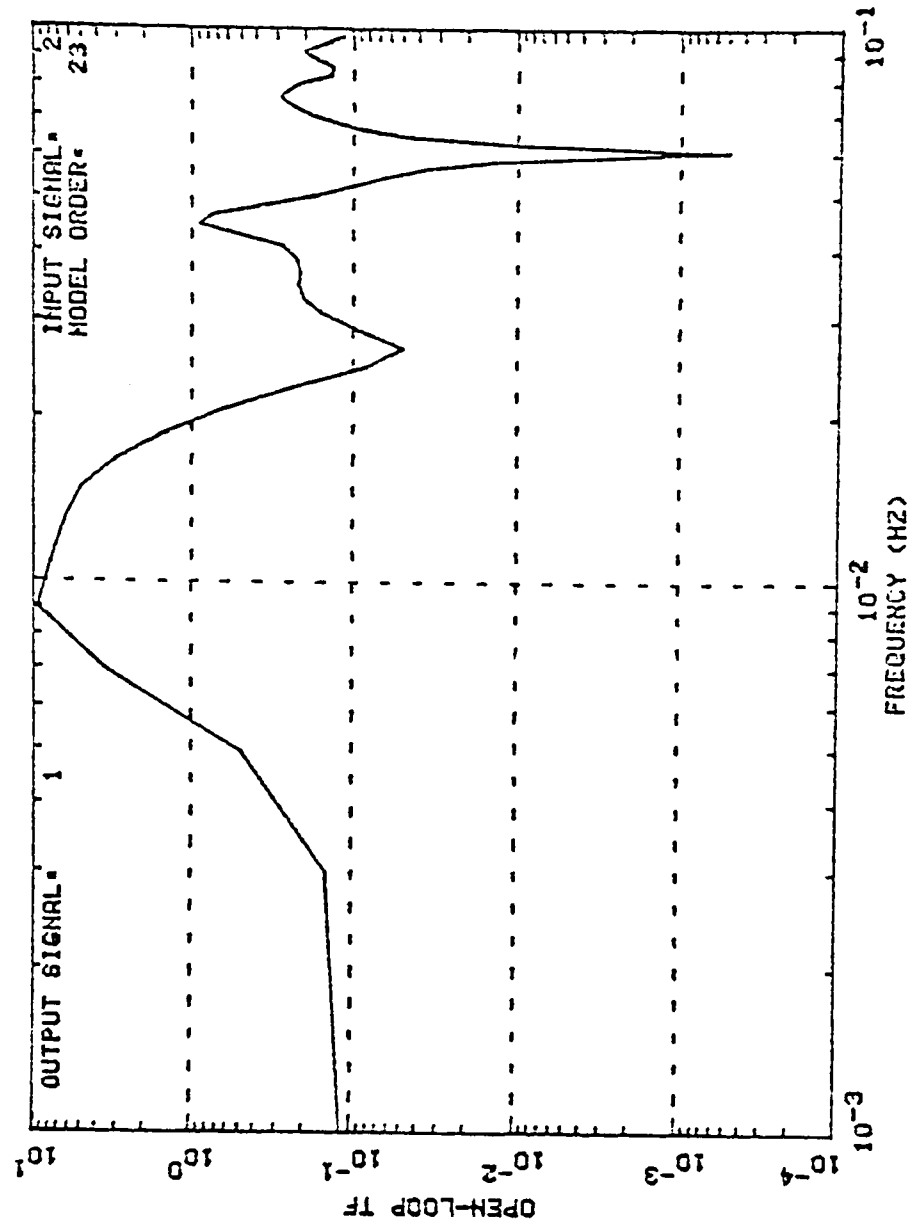


Figure 130. Open Loop Frequency Response of Primary Pressure Versus Cold Leg Temperature.

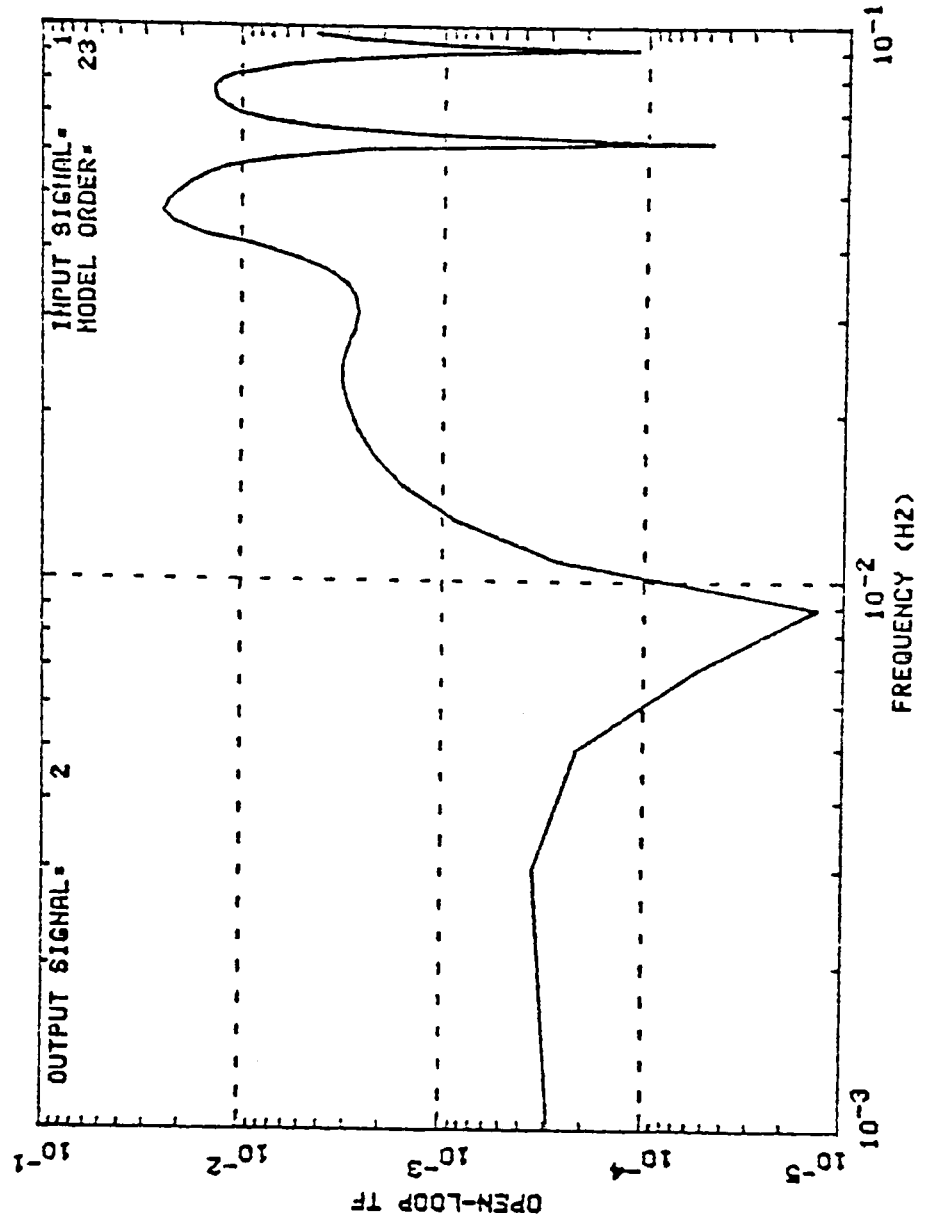


Figure 131. Open Loop Frequency Response of Cold Leg Temperature Versus Primary Pressure.

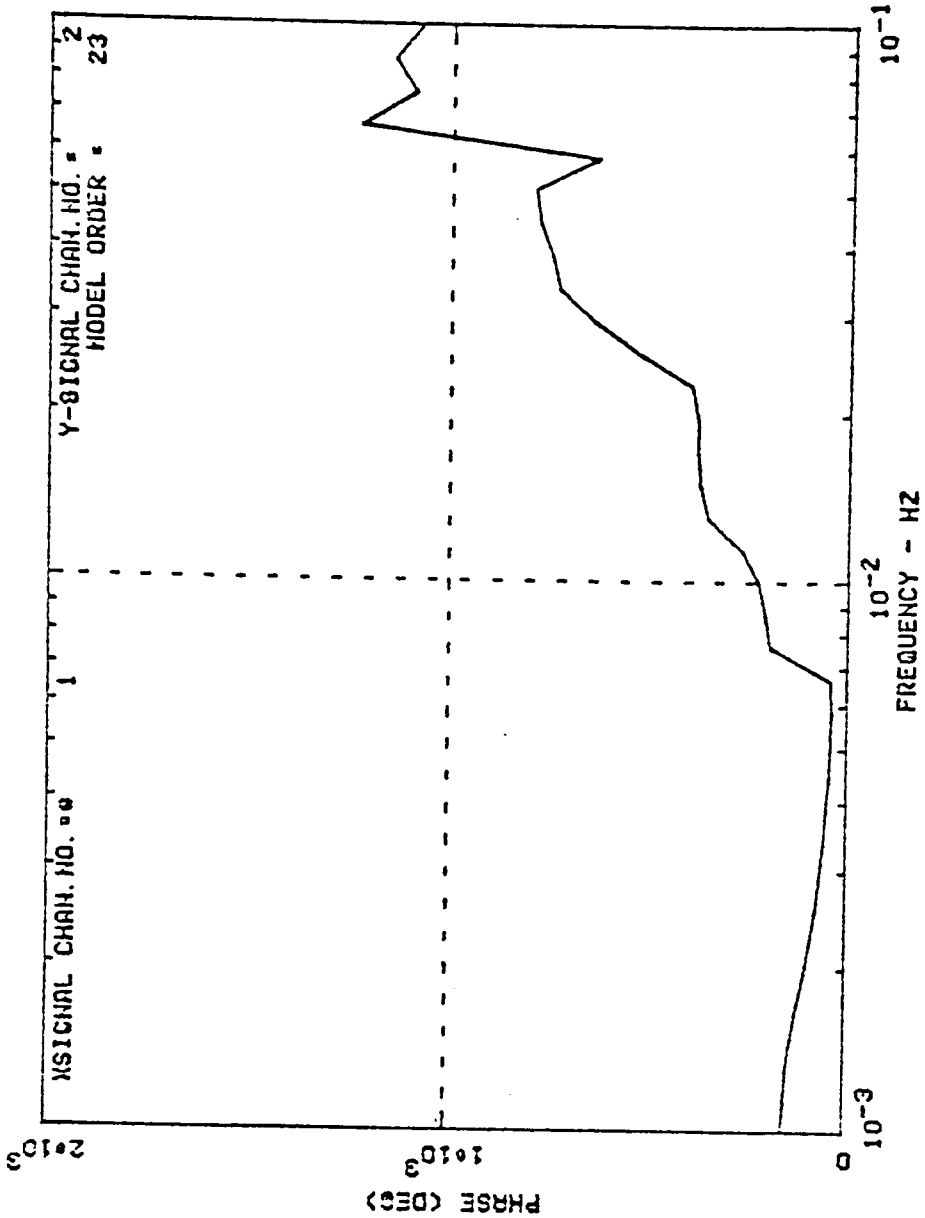


Figure 132. Phase Relation of Primary Pressure Versus Cold Leg Temperature.

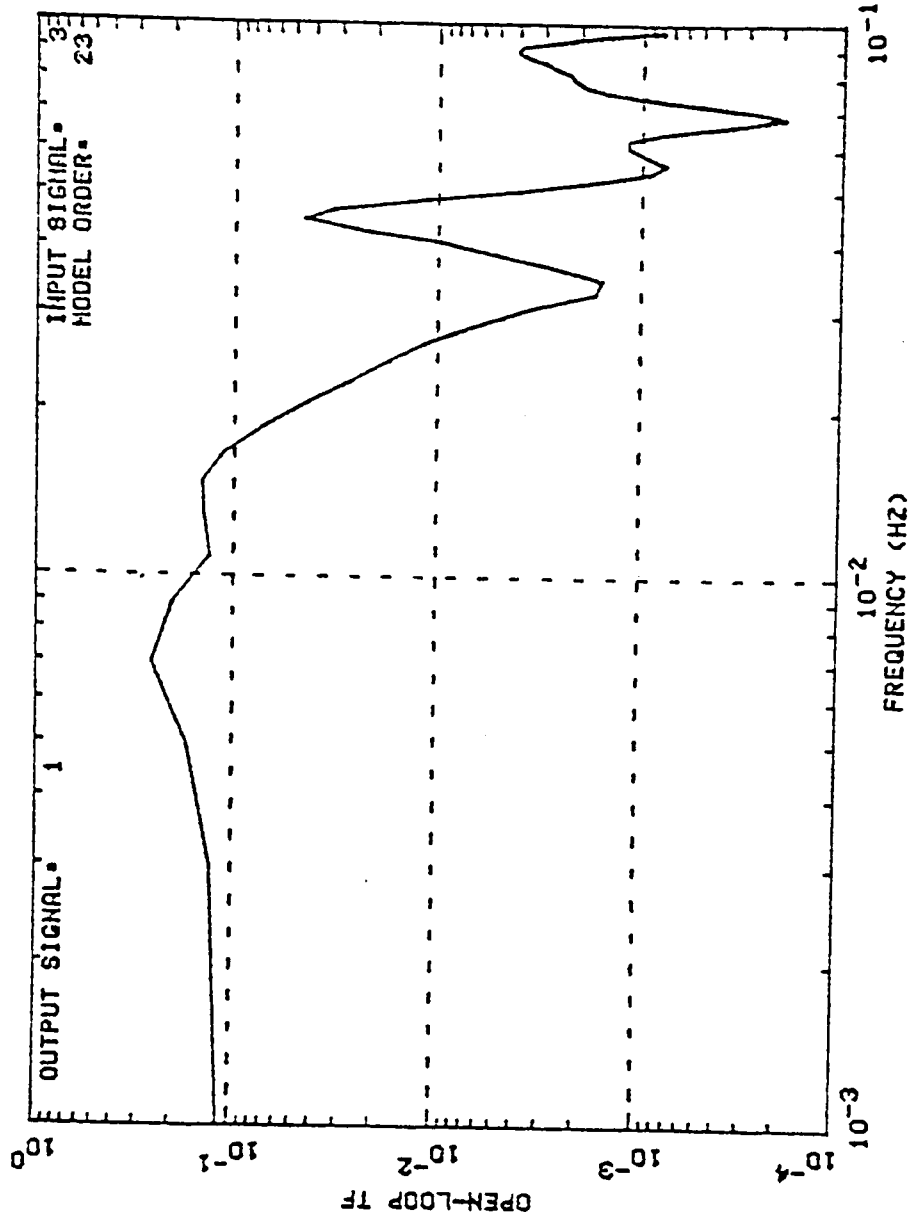


Figure 133. Open Loop Frequency Response of Primary Pressure Versus Feed Water Flow Rate.

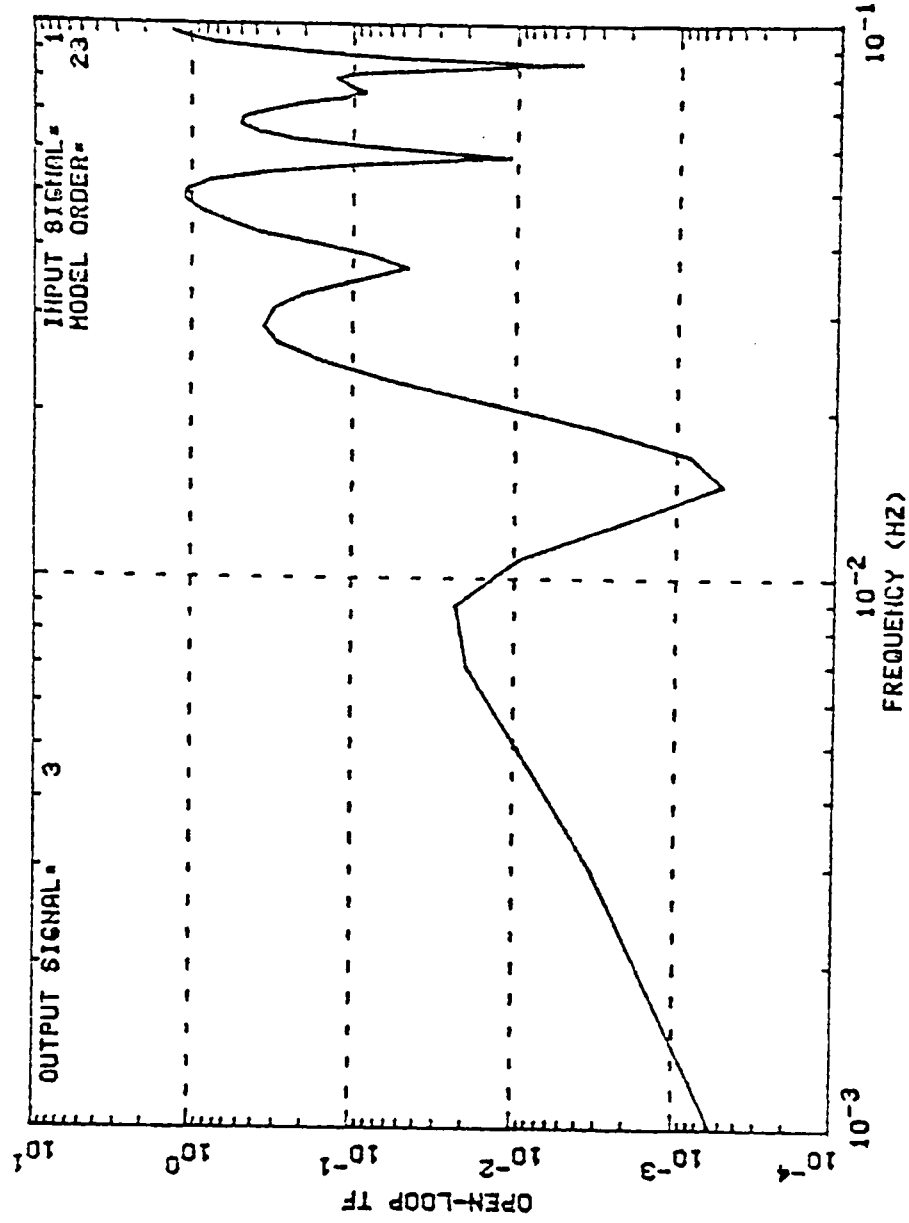


Figure 134. Open Loop Frequency Response of Feed Water Flow Rate Versus Primary Pressure.

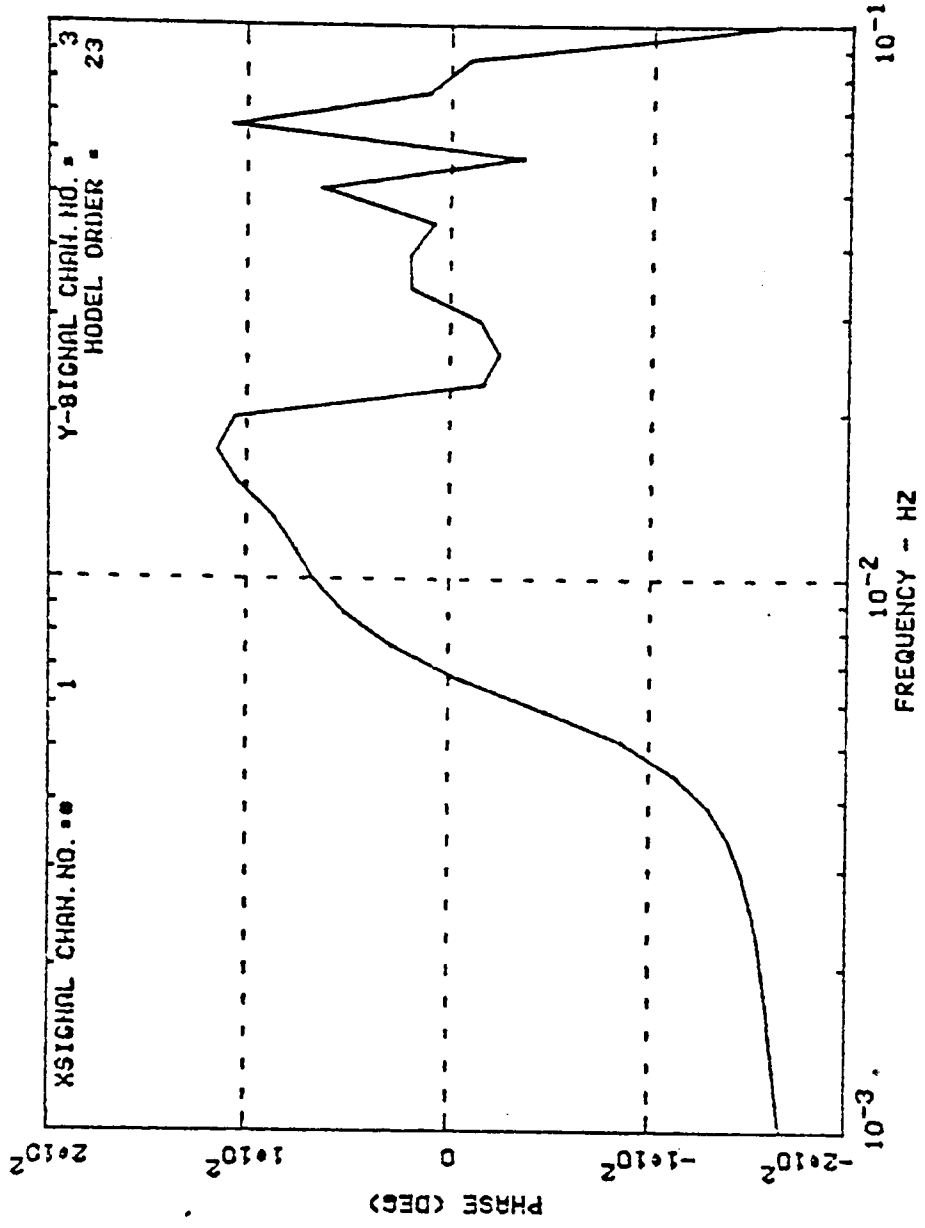


Figure 135. Phase Relation of Primary Pressure Versus Feed Water Flow Rate.

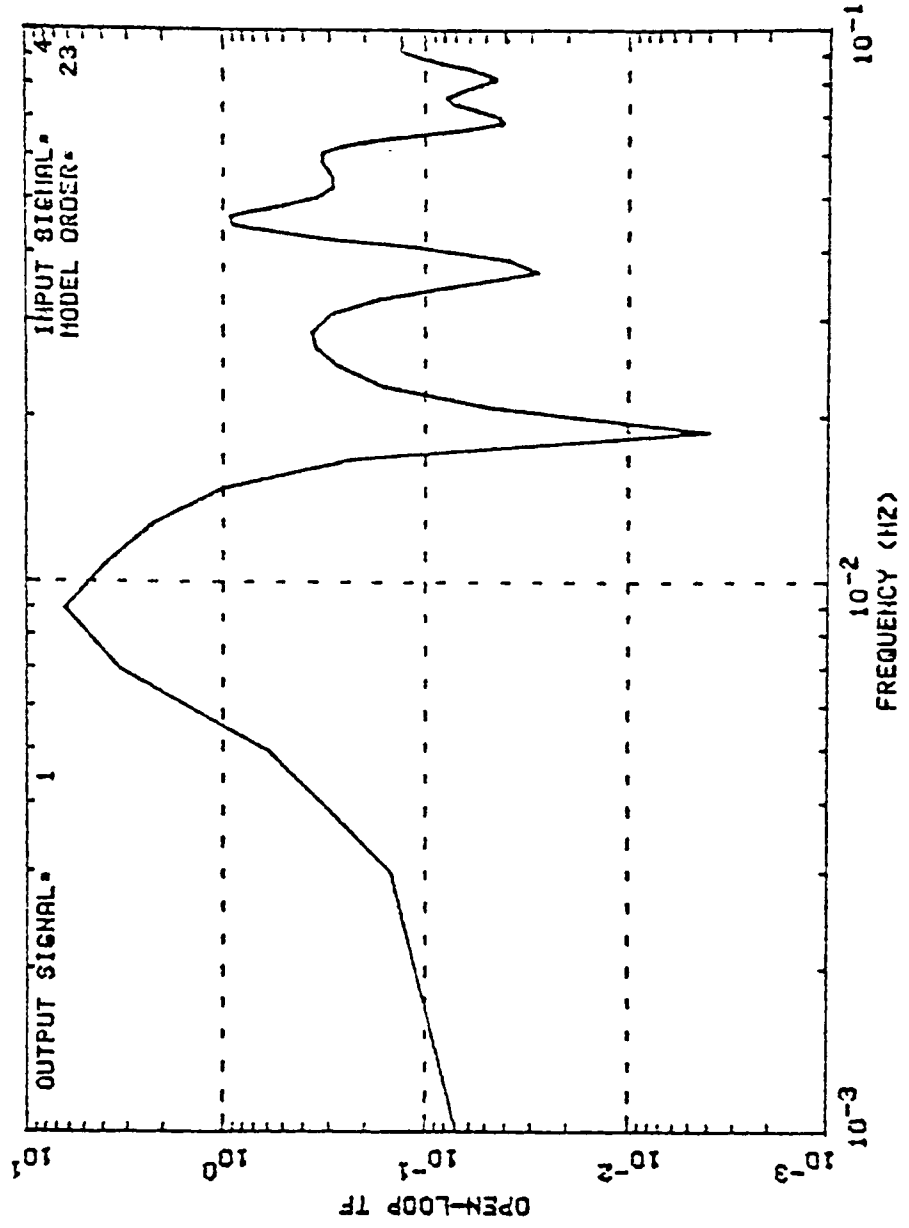


Figure 136. Open Loop Frequency Response of Primary Pressure Versus Power.

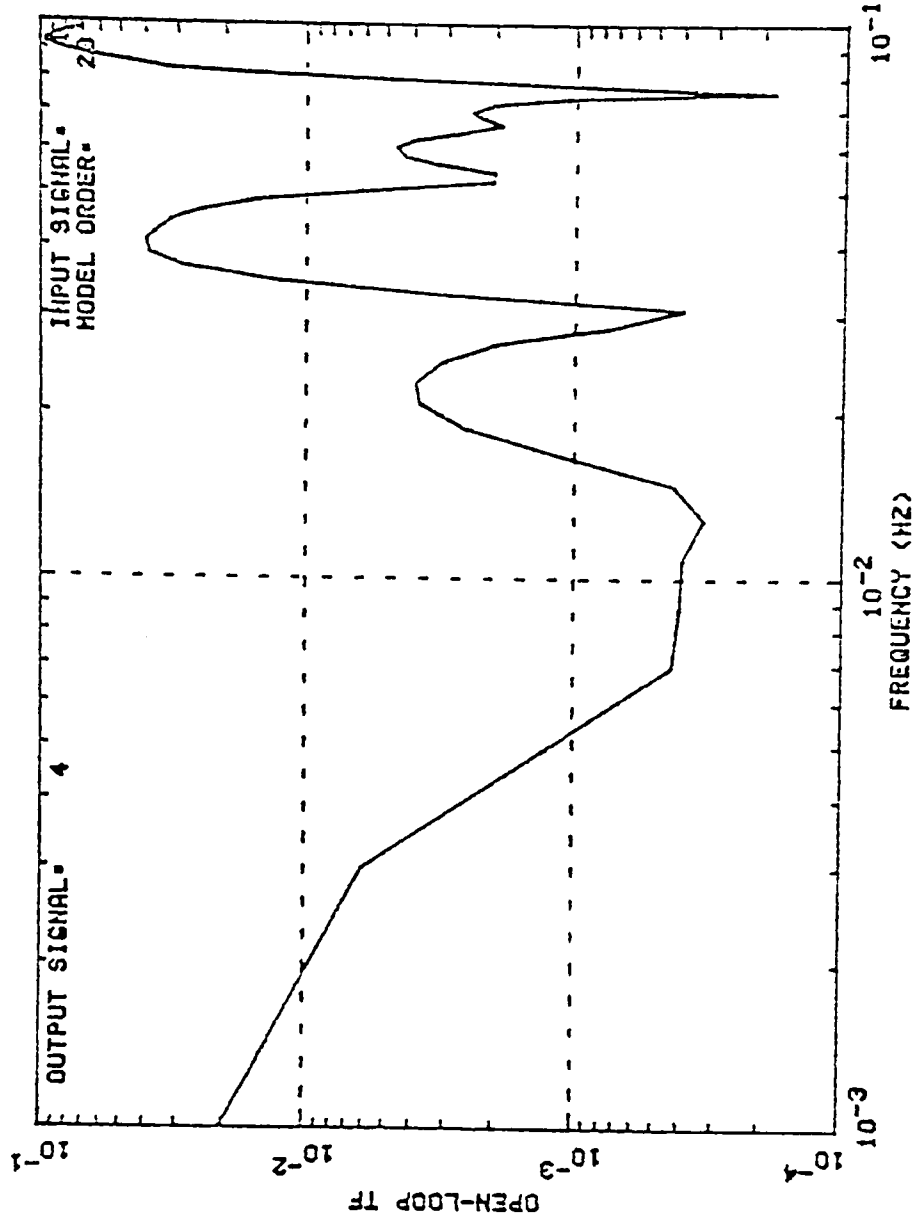


Figure 137. Open Loop Frequency Response of Power Versus Primary Pressure.

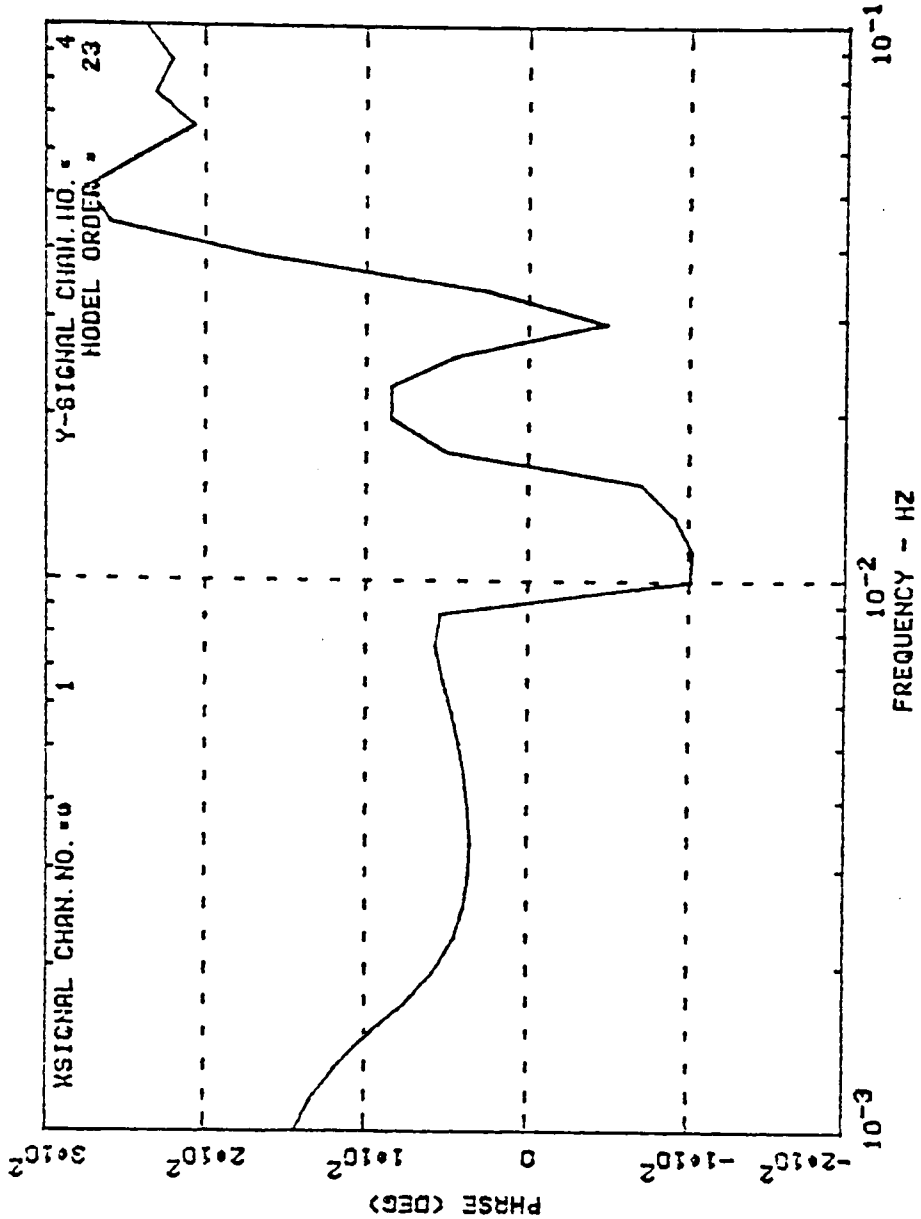


Figure 138. Phase Relation of Primary Pressure Versus Power.

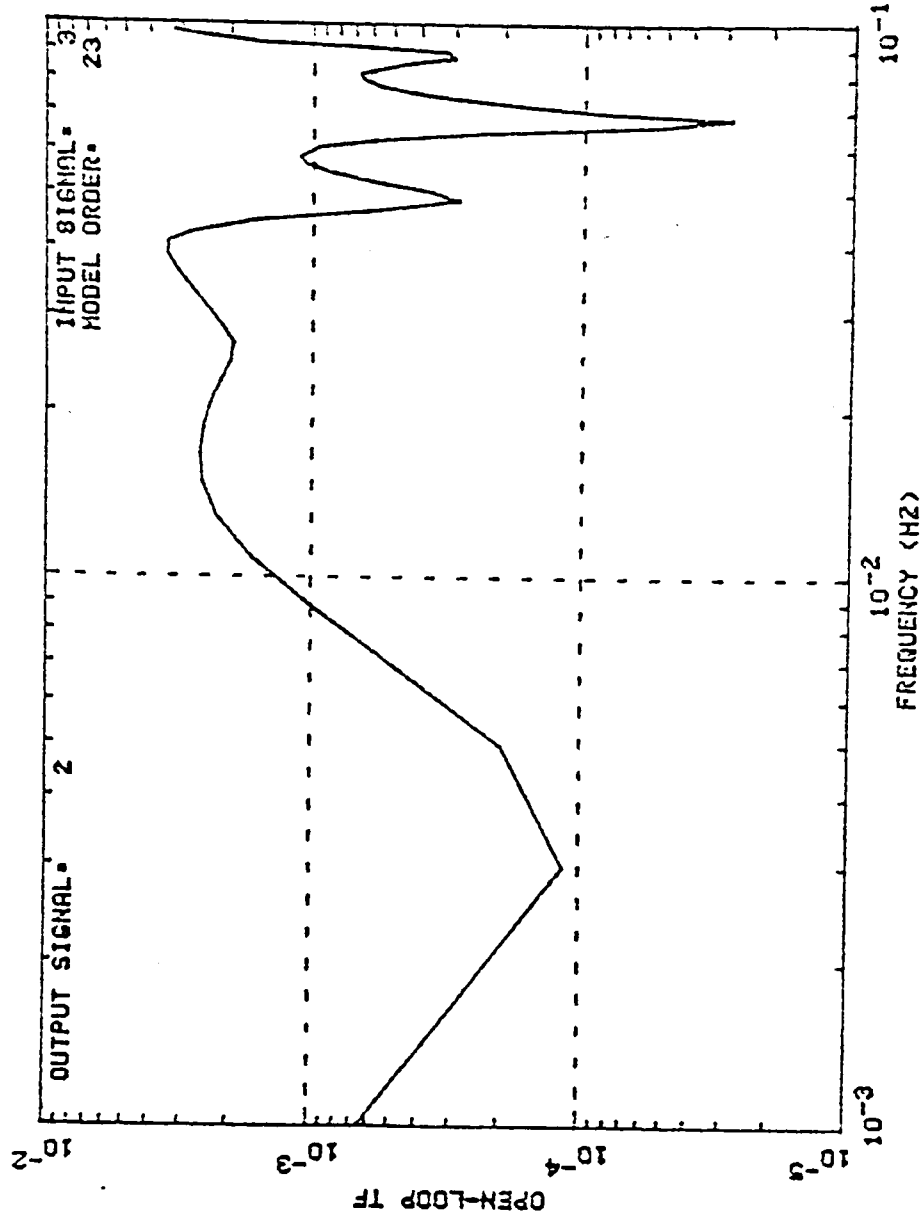


Figure 139. Open Loop Frequency Response of Cold Leg Temperature Versus Feed Water Flow Rate.

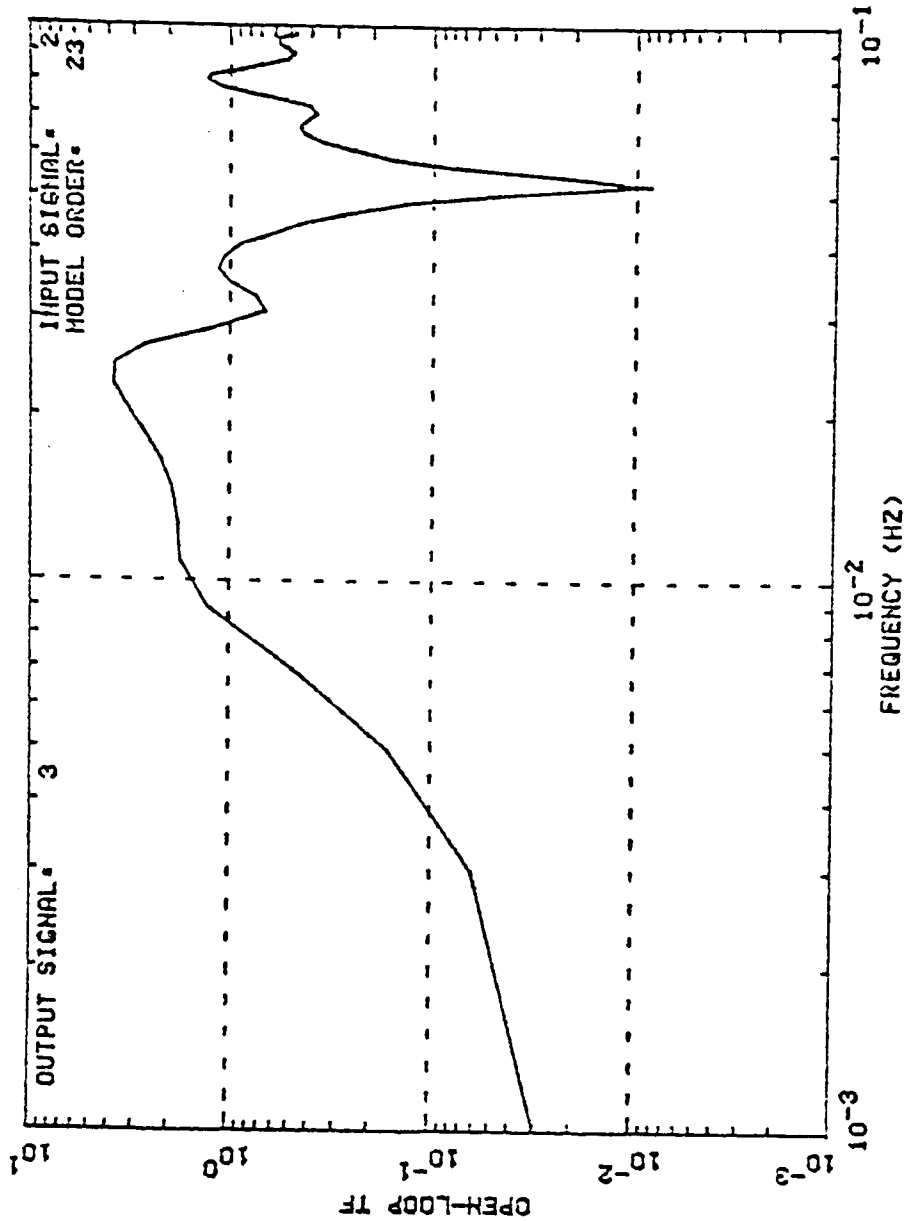


Figure 140. Open Loop Frequency Response of Feed Water Flow Rate Versus Cold Leg Temperature.

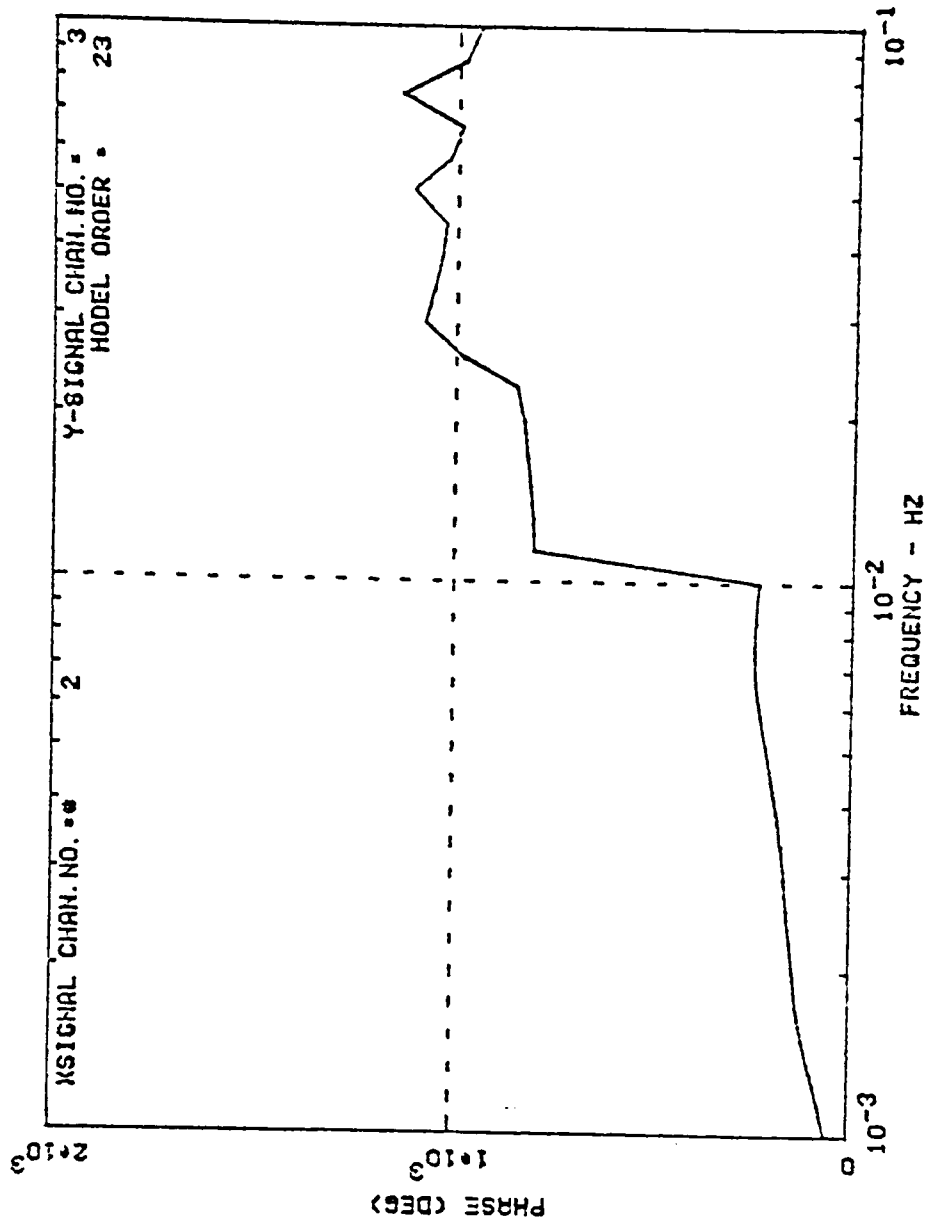


Figure 141. Phase Relation of Cold Leg Temperature Versus Feed Water Flow Rate.

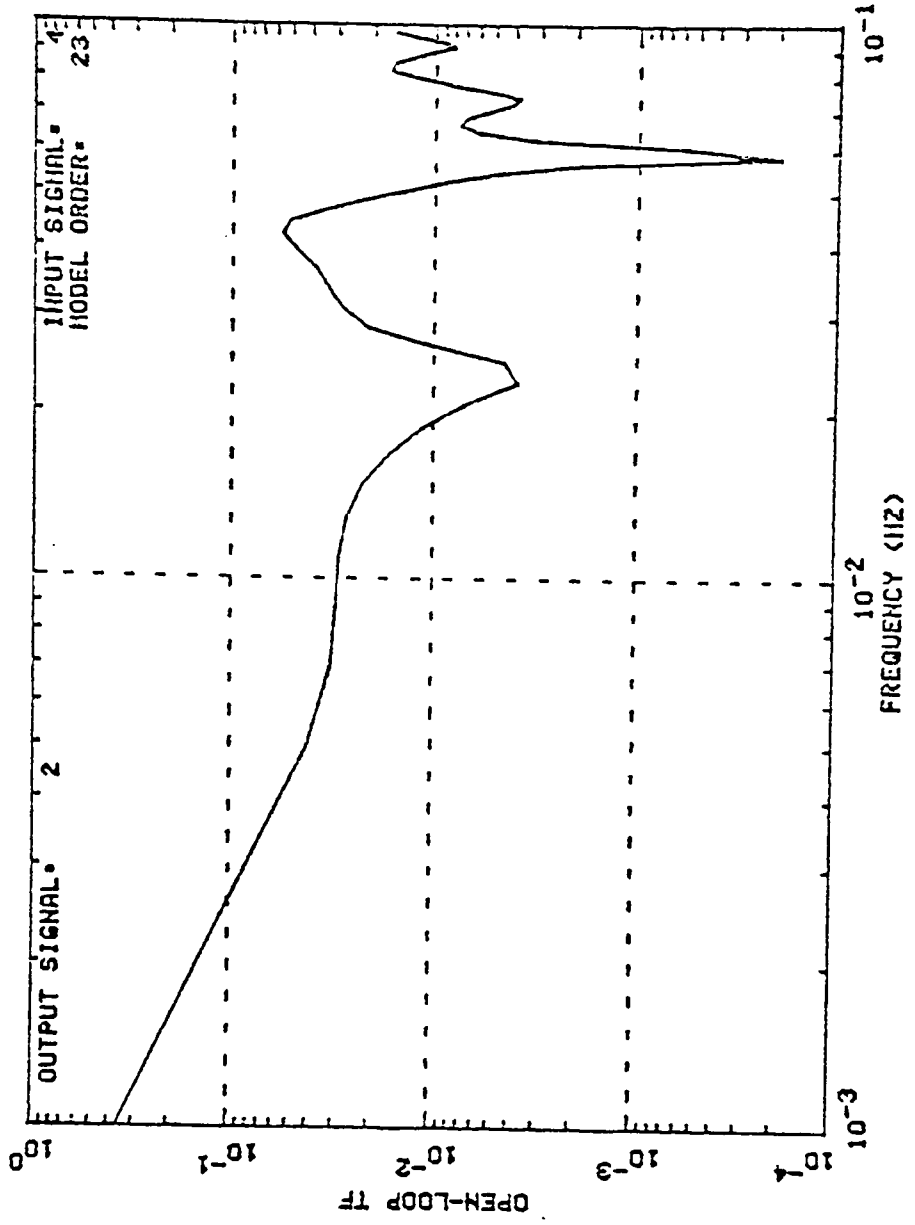


Figure 142. Open Loop Frequency Response of Cold Leg Temperature Versus Power.

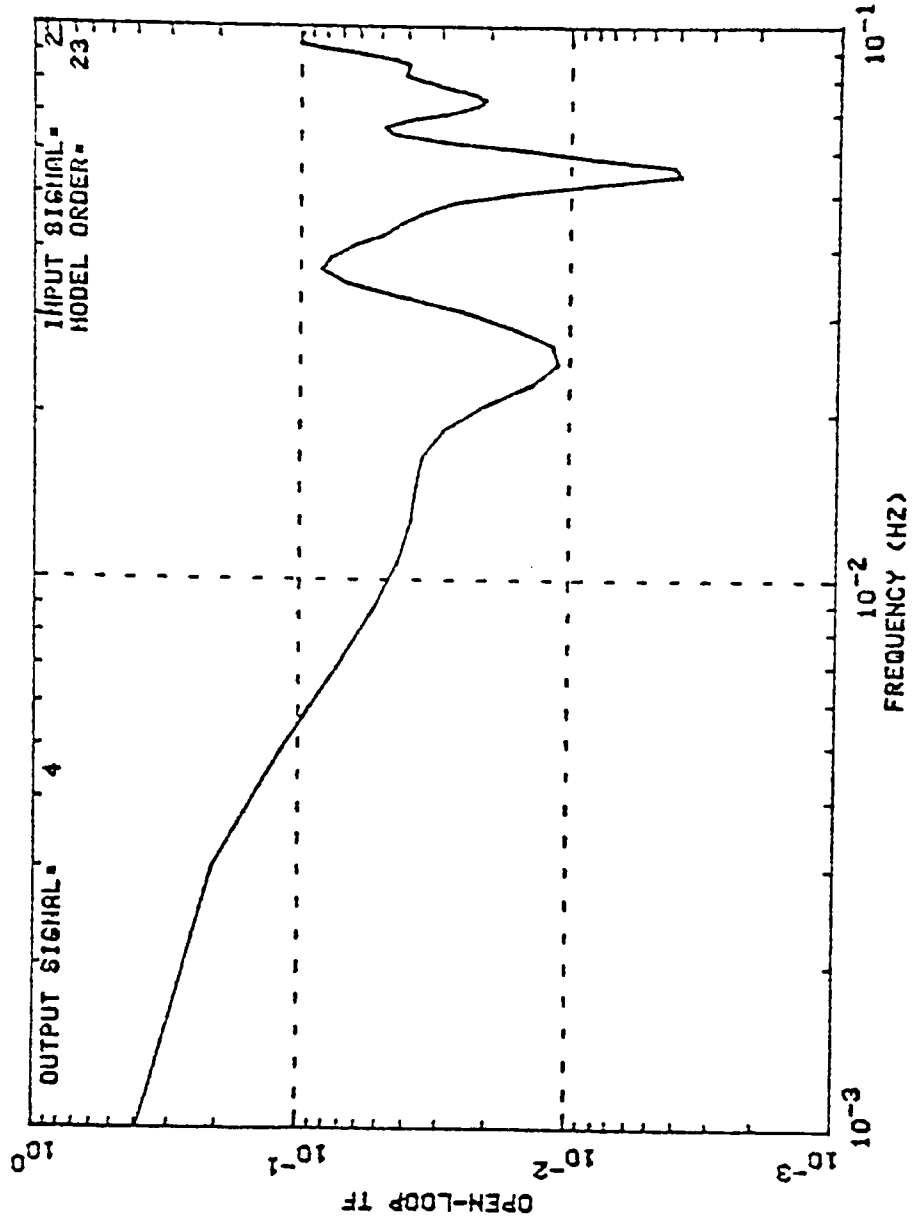


Figure 143. Open Loop Frequency Response of Power Versus Cold Leg Temperature.

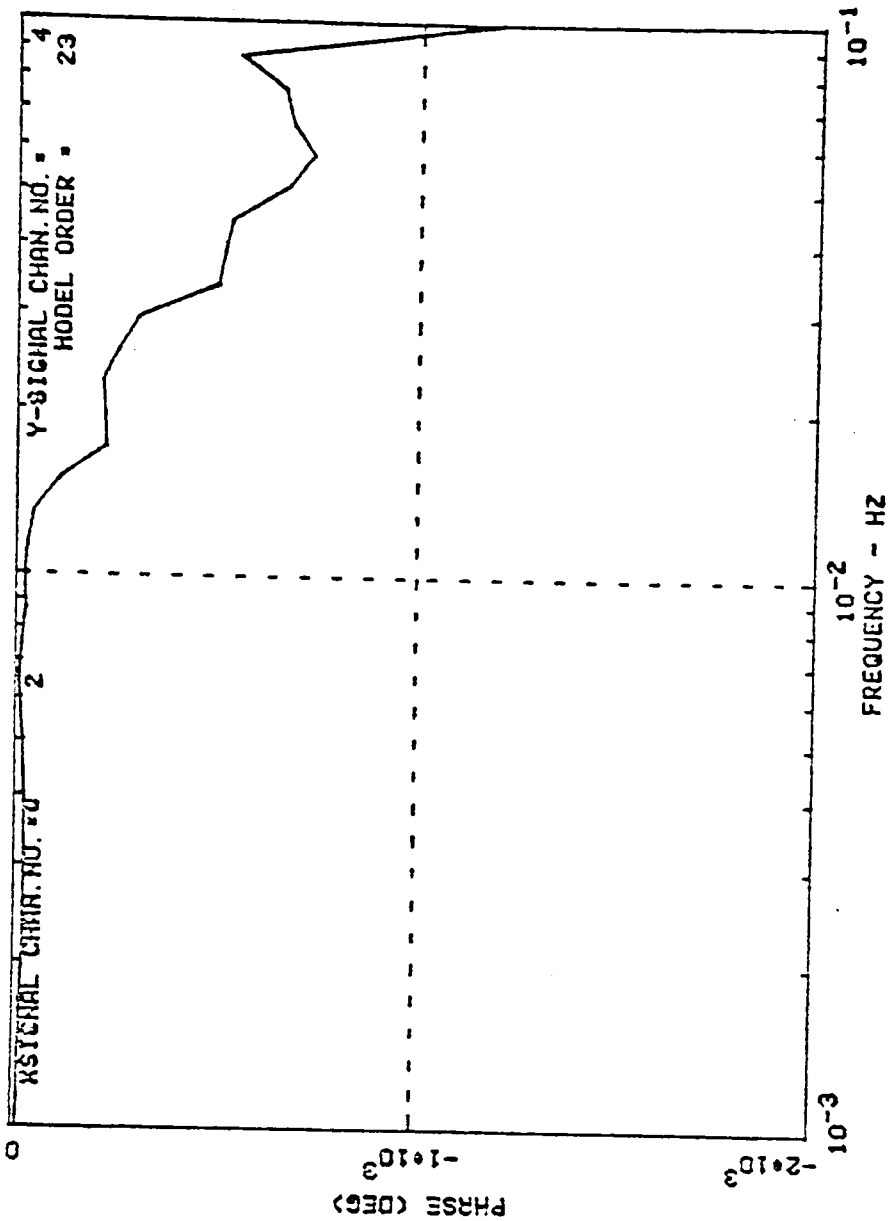


Figure 144. Phase Relation of Cold Leg Temperature Versus Power.

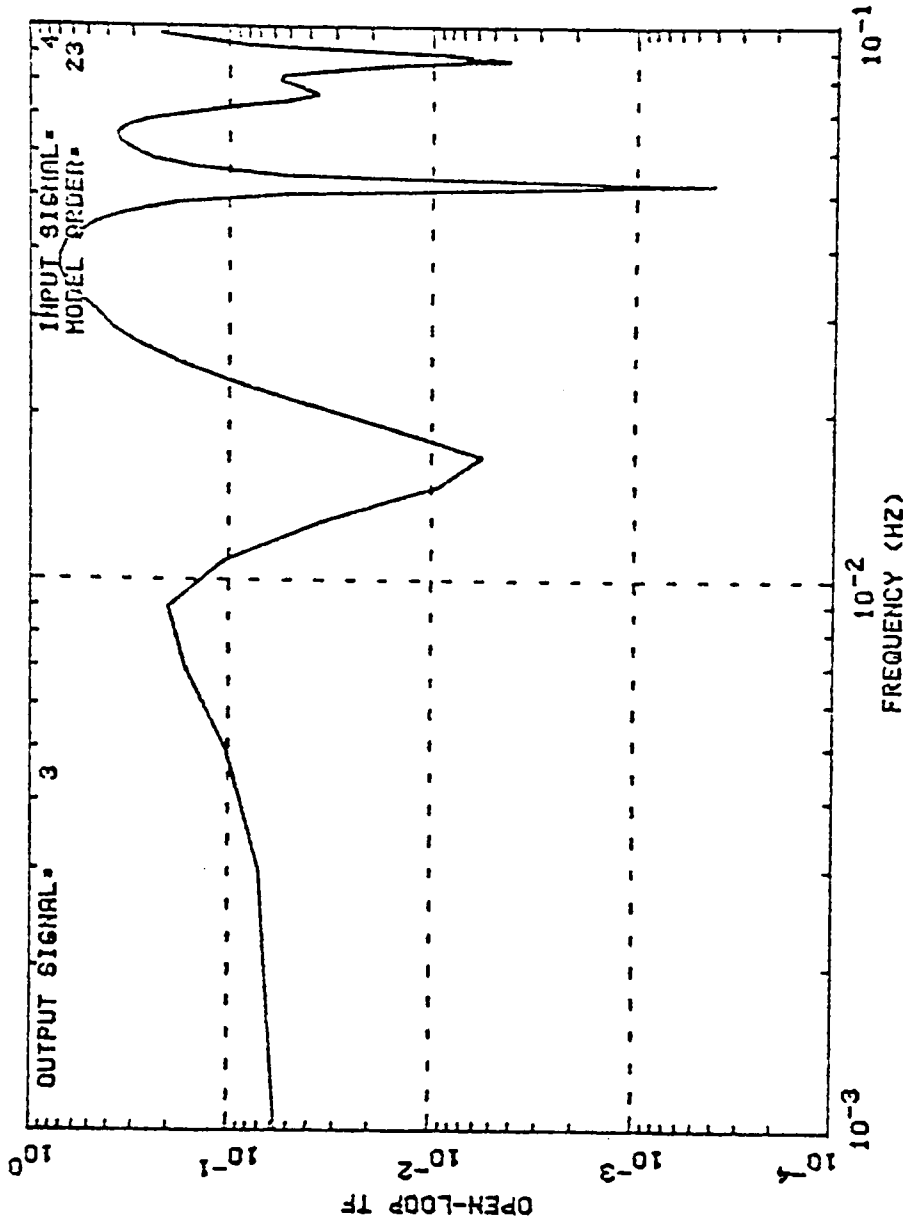


Figure 145. Open Loop Frequency Response of Feed Water Flow Rate Versus Power.

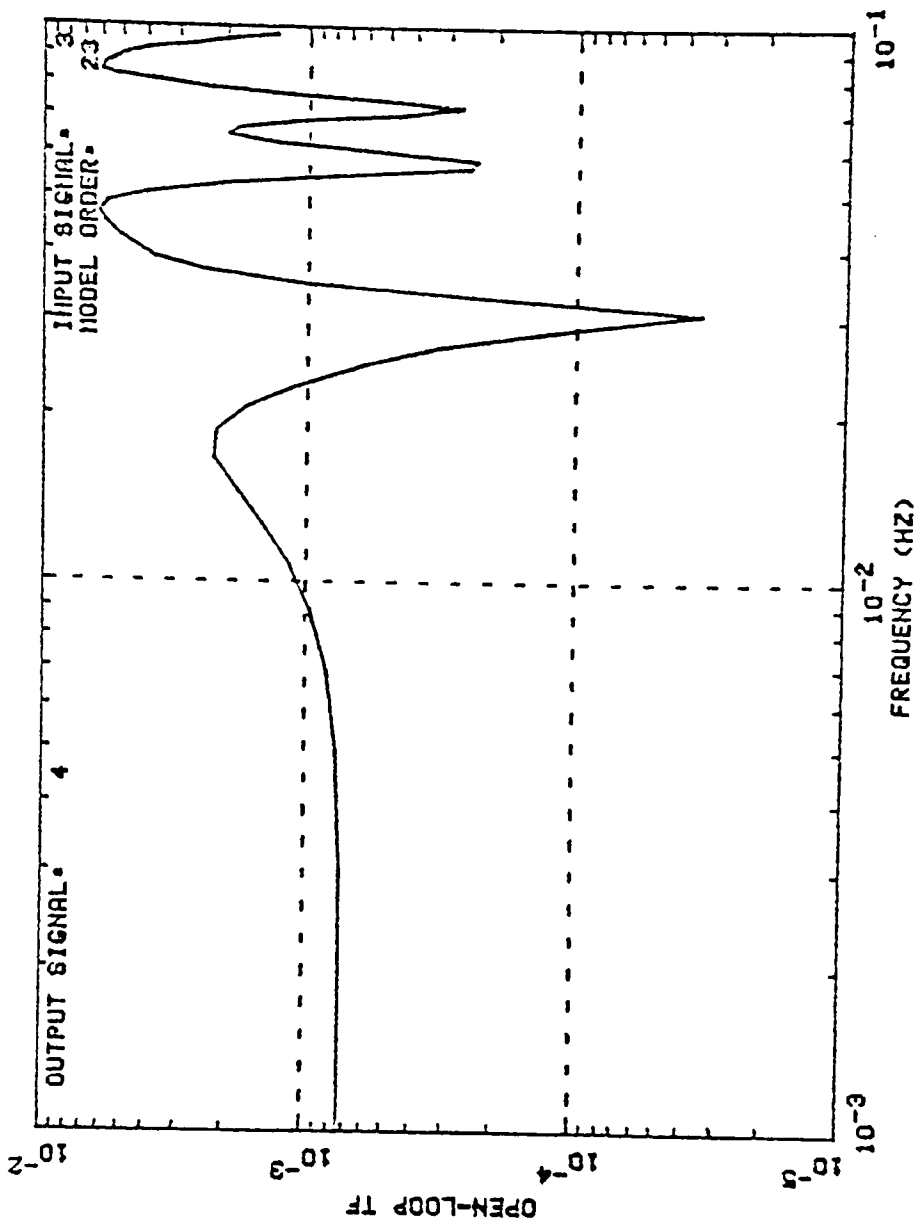


Figure 146. Open Loop Frequency Response of Power Versus Feed Flow Rate.

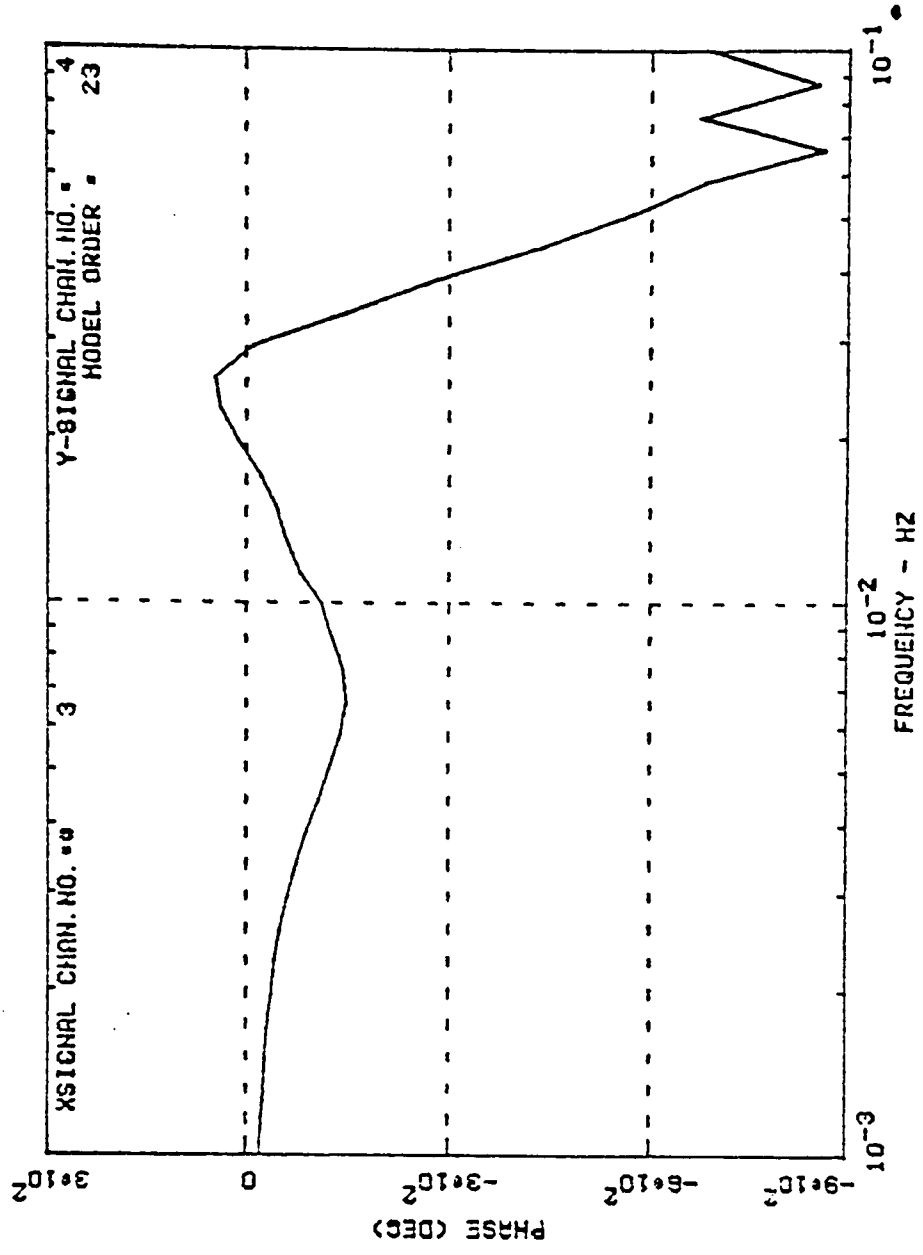


Figure 147. Phase Relation of Feed Water Flow Rate Versus Power.

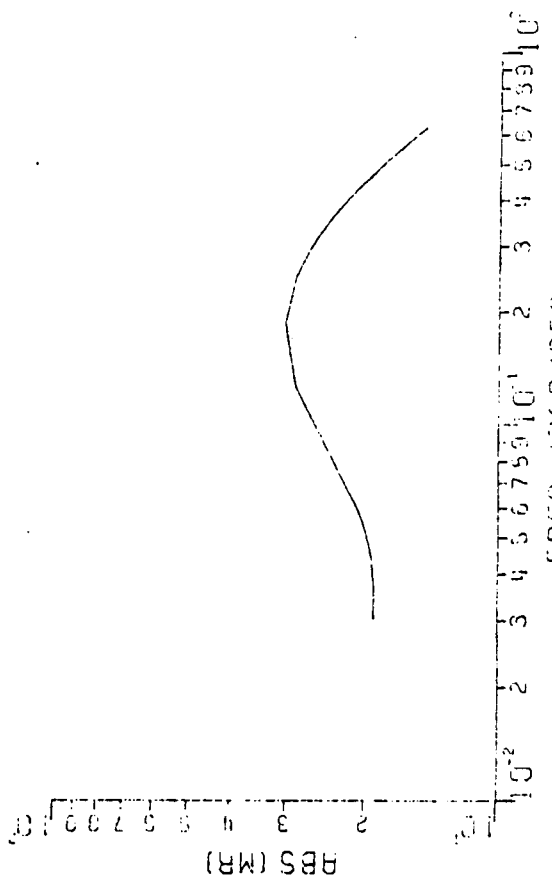


Figure 148. Frequency Response of Feed Water Flow Rate Due to 10% Increase In Inlet Temperature.

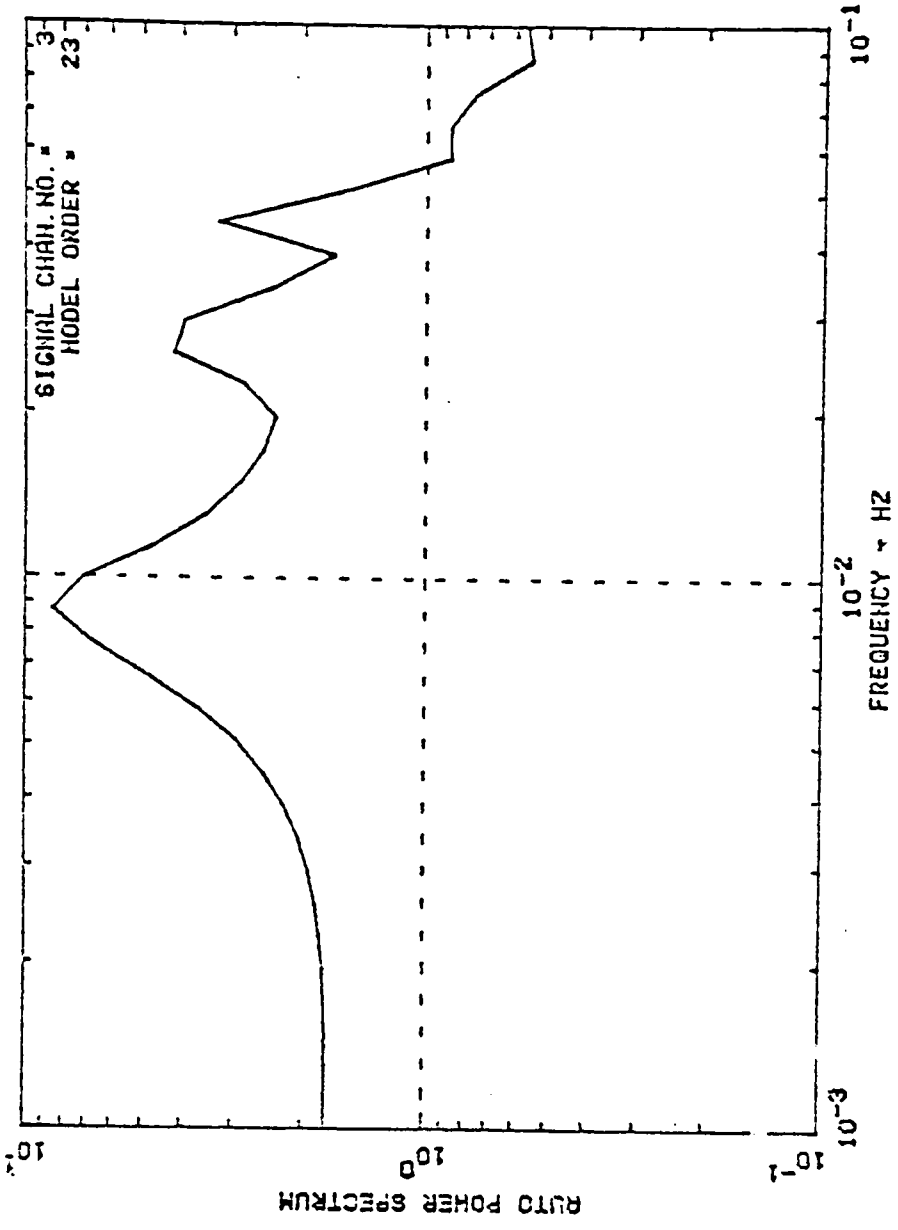


Figure 149. Power Spectrum of Feed Water Flow Rate (Order 23).

VITA

Jeora Melik-Baghdassarians-Fard was born in Tehran, Iran in 1951. He graduated from Armenian High School in Tehran in 1970. He attended Queen Mary College, University of London in London, England in 1972 and graduated with a B. S. degree in Nuclear Engineering in 1975. In 1976 he enrolled in The University of Tennessee Nuclear Engineering Graduate program in Knoxville.

He is married to Arax Martirossian and they have a son, Ara.